

International Atomic Energy Agency

INDC(NDS)-184/GM

---

**INDC**

**INTERNATIONAL NUCLEAR DATA COMMITTEE**

---

**NUCLEAR DATA FOR APPLIED NUCLEAR GEOPHYSICS**

**PROCEEDINGS OF A CONSULTANTS' MEETING  
ON NUCLEAR DATA FOR APPLIED NUCLEAR GEOPHYSICS,  
ORGANIZED BY THE  
INTERNATIONAL ATOMIC ENERGY AGENCY  
HELD IN VIENNA, 7-9 APRIL 1986**

**Edited by V. Piksaikin and A. Lorenz**

**March 1987**

---

**IAEA NUCLEAR DATA SECTION, WAGRAMERSTRASSE 5, A-1400 VIENNA**



**NUCLEAR DATA FOR APPLIED NUCLEAR GEOPHYSICS**  
**PROCEEDINGS OF A CONSULTANTS' MEETING**  
**ON NUCLEAR DATA FOR APPLIED NUCLEAR GEOPHYSICS,**  
**ORGANIZED BY THE**  
**INTERNATIONAL ATOMIC ENERGY AGENCY**  
**HELD IN VIENNA, 7-9 APRIL 1986**

**Edited by V. Piksaikin and A. Lorenz**

**March 1987**

### Abstract

The IAEA Consultants' Meeting on Nuclear Data for Applied Nuclear Geophysics was convened by the IAEA Nuclear Data Section in the IAEA Headquarters, Vienna, Austria, from 7-9 April 1986. The meeting was attended by 13 specialists including nuclear geochemists, nuclear geophysicists, and nuclear data experts from seven countries.

The main objectives of the meeting were to review the status of the requirements for microscopic nuclear cross section needed for the effective implementation of nuclear geophysics methods for the exploration, exploitation and processing of mineral resources, and to develop recommendations for future activities in this field.

The proposed publication contains the text of all the papers prepared especially for this meeting including the conclusions and recommendations worked out during the meeting.

Reproduced by the IAEA in Austria  
March 1987

## Table of Contents

Agenda and List of Papers .....	5
Summary and recommendations .....	7
Subsurface Geochemistry: .....	15
I. Future Applications of Geochemical Data M.M. Herron	
Subsurface Geochemistry: .....	43
II. Nuclear Data for Spectroscopic Analysis J.S. Schweitzer, R.C. Hertzog, P.D. Soran	
Nuclear Ratio Technique Applied to Borehole Exploration for Industrial Metals and Coal F.E. Senftle, J.L. Mikesell	63
Discrete $\gamma$ -Ray Production in (n, $\gamma$ ) reactions for Nuclear Applied Geophysics P. Obložinský, S. Hlaváč	79
Nuclear Data for Elemental Analysis of Geological Samples with 14 MeV Neutrons R. Pepelnik	103
Detection of Na, Mg, Al, and Si in Wells with Reactions Generated by 14 MeV Neutrons R.C. Hertzog, P.D. Soran, J.S. Schweitzer	109
An Example of Nuclear Data Center Services for Geophysics Applications P. Rose, T. Burrows, J. Tuli	119
Fast Neutron Activation Analysis: An Elemental Data Base J.W. McKlveen	131
Bulk Material Analysis Using Energetic Neutrons M.C. Underwood, J.S. Petler	141
Fast Neutron Induced Prompt $\gamma$ -Ray Analysis S. Hlavac, P. Oblozinsky	155
Short Time Activation Analysis in Geoscience F. Grass, G.P. Westphal, T. Kasa	159
Gamma-Rays Production Cross Sections for Al and Si V. Piksaikin, V. Goulo, O. Schwerer	175
List of Participants .....	181



## Agenda and List of Papers

Monday, 7 April 1986

Plenary Session Chairman: J. Schweitzer

Opening remark by J.J. Schmidt

1. Subsurface Geochemistry: I. Future Applications on Geochemical Data. M.M. Herron (presented by J. Schweitzer)
2. Subsurface Geochemistry: II. Nuclear Data for Spectroscopic Analysis. J. Schweitzer and R.C. Hertzog (presented by R.C. Hertzog)
3. Gamma-Rays Production Cross Sections for Al. V. Goulo, V. Piksaikin and O. Schwerer (oral presentation)
4. Field Calibration of Borehole Sonde for Low-Concentration Manganese by Decay Gamma Rays. F.E. Senftle
5. Discrete  $\gamma$ -Ray Production in  $(n, \gamma)$  Reactions for Applied Nuclear Geophysics. P. Oblozinsky and S. Hlavac (presented by P. Oblozinsky)
6. Nuclear Data for Elemental Analysis of Geological Samples with 14 MeV Neutrons. R. Pepelnik
7. Detection of Na, Mg, Al, and Si in Wells with Reactions Generated by 14 MeV Neutrons. R.C. Hertzog and P.D. Soran (presented by P.D. Soran)
8. An Example of Nuclear Data Center Services for Geophysics Applications. P. Rose, T. Burrows and J. Tuli (presented by P. Rose)
9. Fast Neutron Activation Analysis: An Elemental Data Base. J.W. McKlveen

Tuesday, 8 April 1986

Plenary Session (continuation)

10. Bulk Material Analysis Using Energetic Neutrons. M.C. Underwood and J.S. Petler (presented by M.C. Underwood)
11. Fast Neutron Induced Prompt  $\gamma$ -Ray Analysis. S. Hlavac and P. Oblozinsky (presented by P. Oblozinsky)
12. Short Time Activation Analysis in Geoscience. F. Grass, G.P. Westphal, P. Schindler, J. Schmidt

Workshop on "Identification of Microscopic Nuclear Cross Section Requirements for Geochemistry and Geophysics" (Status, Needs, Recommendations)

Chairman: J. Schweitzer

Wednesday, 9 April 1986

Formulation of Conclusions and Recommendations of the meeting.



## Summary and Recommendations

### I. Introduction

A meeting of 13 specialists including nuclear geochemists, nuclear geophysicists, and nuclear data experts from seven countries was held at the International Atomic Energy Agency Headquarters in Vienna, Austria, from 7-9 April, 1986.

Twelve papers were presented which describe the current status of nuclear techniques used in applied nuclear geology (comprising nuclear geophysics and nuclear geochemistry), and the availability of nuclear data for the analysis of measurements. The papers were given by experts who were drawn from academic institutions, Government establishments and from oil producing and oil well logging companies. The discussions following the presentations of the papers identified the areas where additional nuclear data would be needed to improve the nuclear-based assaying techniques.

Direct geological applications, which are based on elemental analysis obtained through neutron-induced gamma-ray spectroscopy have already been established. These include mineralogy, clay typing, volume of clay, well zonation, well-to-well correlation, and enhanced lithology. From these direct applications, indirect quantitative information regarding cation exchange capacity, oil well completion and production rates, rock grain density and porosity, and trace element modelling can be obtained. Furthermore, from the above, information regarding depositional environment, diagenesis, source rock evaluation, oil specific gravity, grain size and rock permeability can be inferred. Identification of elemental concentrations is important not only in geochemical and geophysical applications, but also in mineral explorations. Determination of elemental concentrations using neutron sources requires a detailed knowledge of energy dependent microscopic cross sections for  $(n,p)$ ,  $(n,\alpha)$  and  $(n,n'\gamma)$  reactions from threshold to 15 MeV and a knowledge of the uncertainty in these data to allow calculation of the final elemental concentration uncertainties. Calculation of sub-surface elemental concentrations requires the determination of the neutron flux distribution. At this stage, only macroscopic transport data and covariance information are available for most elements found in bulk media. There is a continuing need for accurate microscopic cross-section data for those nuclides and reactions which are required for the continuous development and improvement of nuclear geophysical and geochemical exploration methods.

While considerable elemental information is currently available, there is an urgent need to collect and evaluate these data to determine what additional information is required to improve and refine the measurement techniques. There are specific instances where existing elemental information needs to be supplemented with isotopic data. There is a need for additional information on interfering reactions, ranges of uncertainties in the data and covariances. The information needs to be consolidated into a handbook and a computerized data base. The data will be useful not only for mineral resource exploration but also for applications in earth sciences, materials sciences, mineralogy, and in other areas.

Implicit in the conclusions of this meeting, the following data scope is recommended to be compiled in a catalogue of microscopic nuclear data for specific use in nuclear geology and stored in an associated computerized data base:

- Data on the following elements are of primary importance for geological consideration: Ca, C, O, Fe, S, Al, Si, Na, Mg, Ti, and V as well as the geologically important elements Zr, Hf, and the rare earth elements.
- Subsurface Ca, C, O, Fe, S, Si, and Ti can currently be detected and determined by neutron-induced prompt gamma-ray spectroscopic techniques, whereas detection of Al, Na, Mg, and V require delayed-activation techniques. Knowledge of the  $(n,p)$ ,  $(n,\alpha)$  and  $(n,n'\gamma)$  reactions for the naturally occurring isotopes of Al, Na, Mg and V are therefore required from threshold to 15 MeV. Uncertainty information is required for the specific microscopic radiative capture data.
- In addition to the elements/isotopes listed above, there are elements of importance to mineral exploration and industrial development. The following elements are amenable to neutron-induced gamma-ray spectroscopic techniques: Cr, Mn, Ni, W, Hg, Cu, Ag, and Au. Other elements which are also of importance but are more difficult to detect, include Co, Mo, Pt, Zn, Rh, Pd, Sn, and Pb.

## II. General comments on data needs and adequacy

In the analysis of bulk media uncertainties due to an inadequate knowledge of the neutron flux distribution, inaccuracies in gamma-ray production cross-sections, isotopic abundances and branching ratios can lead to an inadequate elemental description. In particular, there are large uncertainties in gamma-ray production cross-sections whether experimentally measured or theoretically calculated. Absolute values of gamma-ray production cross sections are required, however, well determined relative values will often suffice. For thermal neutron capture reactions the available cross-section measurements appear to be adequate, but for fast  $(n,x)$  interactions there are both insufficient and inaccurate data. Specifically, discrete gamma-ray production cross sections from  $(n,x\gamma)$  reactions, in the incident neutron energy range from threshold to 15 MeV, are required. This entails that cross-sections must be both measured and calculated from well established nuclear reaction models using an adequate set of parameters. It is important that a consistent description of all reaction channels is achieved when gamma-ray production cross sections are calculated.

In the measurement of  $(n,x\gamma)$  production cross sections the minimum experimental requirements are the use of a high resolution gamma-ray detector, fast timing electronics and, ideally, that the angular distribution of the emitted gamma-rays are determined. However, if the full angular distribution is not available the angle integrated cross-section should be typically obtained from the value measured at 125 degrees. Isotopic rather than elemental cross-sections should be measured. It is clear from the inspection of published data that cross-section determinations are notably sparse in the neutron energy range from threshold to 15 MeV. Measurements and calculations are specifically required in this energy range. Finally the meeting stressed that fast neutron activation cross-sections from threshold to about 15 MeV are inadequately determined and this problem should be addressed.

## III. Proposed Plan to produce the handbook and computerized data base of nuclear data for applied nuclear geophysics

From the discussions at this meeting it is evident that it would be a major long-term effort to produce a full-fledged handbook and an associated data base which would fulfill all nuclear data needs of the nuclear geophysics

and geochemistry community. The meeting participants identified the most pressing requirements, and as a first step towards producing a full-fledged handbook and data base, it is recommended to produce initially interim versions of the handbook from those nuclear data identified as having a high priority at this meeting. This step should be completed in about two to three years.

This near-term effort should be started by the Nuclear Data Section by sending the conclusions and recommendations of this meeting, together with a suggested content list of the interim handbook and illustrations of the format, to other data centres and a selected audience in the nuclear geological community, including selected evaluators and experimentalists.

Concurrent with this, the Nuclear Data Section should review the status and availability of the data and specifically identify:

- the experimental and evaluated data available from existing files;
- discrepancies among experimental data and with respect to evaluated data (e.g. in graphical form); and
- gaps in experimental as well as evaluated data.

The data part of the handbook should be preceded by a concise description of the nuclear analytical techniques currently employed in nuclear geology. The data part of the handbook should be organized in ascending order of atomic weight and the data base should be formatted so as to be immediately usable in analysis calculations by nuclear geologists.

For each of the required isotopes the handbook should contain

- prompt and delayed gamma-ray emission data,
- branching ratios for gamma-ray lines,
- activation cross sections ((n,p), (n, $\alpha$ ), (n,2n) etc.), and
- data for interfering reactions and relative cross sections if needed.

A graphical network-like representation of the activation and interfering reactions should be added. As far as possible, uncertainties should be included with the data. For calculating the neutron flux distributions total cross-sections as well as gamma-ray production cross-sections are needed (see second paragraph below).

For the elements included in the handbook it is required that evaluations for all relevant isotopes be provided including ground and meta-stable state cross-sections. This would be a major long-term effort going beyond the scope of the interim version of the handbook.

For individual reactions and spectral data, tabular as well as graphical representations should be given in the handbook including graphical comparisons of experimental and most commonly used evaluated data. More complete evaluations should be presented in the handbook only in graphical form, and a note added to indicate from which data centres these files would be available. These files should, of course, be included in the nuclear data base for nuclear geology.

A section of the handbook should also be devoted to neutron sources and their parameters including spectra, yields, uncertainties, gamma-ray

calibration standards, spectrum averaged activation and interfering reaction cross sections. The commonly used neutron sources and those which will become useful in the future should be included. The following information should also be included in the interim version of the handbook as an appendix: a timely revised list, ordered by nuclide, of the nuclear data needs of the geophysics and geochemistry community, in WRENDA format, covering discrepant data and those not contained in the handbook.

For the interim version of the handbook data should, as much as possible, be collected from existing experimental data (EXFOR, ENSDF) files and major evaluated data libraries. Gaps and discrepancies should be collected by the Nuclear Data Section as soon as possible so as to be available for the final Research Coordination Meeting of the Coordinated Research Programme on the Measurement and Analysis of 14 MeV Neutron Cross Sections and for the Advisory Group Meeting on Neutron Source Properties in Leningrad. The Nuclear Data Section should avail itself of the assistance of outside experts to measure and evaluate missing or discrepant data and to update existing evaluations. The above state-of-the-art review could lead to a new Coordinated Research Programme (CRP) which would include experimentalists, evaluators and a few scientists with a background in both geology and nuclear physics.

It is suggested that this proposal be considered and possibly recommended at the 15th INDC meeting in Vienna in June 1986. From the discussions and outcome of the present meeting it appears that the area of gamma production data and spectra, particularly at higher neutron energies (15 MeV), is particularly deficient and would need major efforts of experimentalists and evaluators.

#### IV. Specific Objectives

For the elements of interest in geochemical and mineral exploration, the thermal neutron capture cross sections are most important. As there can be large variations in the atomic concentrations and many capture gamma-rays for a specific element resulting in many overlapping interferences, the determination of gamma-ray branching ratios (including many of the weaker branches) to high precision ( $\sim 1\%$ ) is important.

For high energy neutron induced reactions there are two concerns. First there can be several fast neutron reactions (n,p) or (n, $\alpha$ ) on different elements, which commonly occur in geological formations, leading to the same final reaction product which may also be produced by thermal neutron capture. For example, the delayed  $\gamma$ -ray activity of  $^{28}\text{Al}$  produced through thermal neutron capture in  $^{27}\text{Al}$  can be produced prolifically from the (n,p) reaction on  $^{28}\text{Si}$ .

Another important example is the direct interference of the (n,n' $\alpha$ ) reaction on oxygen with inelastic neutron scattering on carbon.

Secondly, some of the elements of specific interest, for example iron, silicon, and calcium, can be detected with acceptable precision through more than one reaction process. It is desirable to link measurements made with delayed-activation, thermal neutron capture, and inelastic neutron scattering techniques in order to derive uniform absolute yields (in atomic concentrations). Therefore, cross sections and branching ratios for a number of "delayed activations" are recommended for several elements which are easily detectable through neutron capture or inelastic neutron scattering reactions.

The following is a list of specific elements and principal reactions and spectral interference data which should be included in the interim handbook and data base.

## Calcium

Calcium is generally detected through the thermal neutron capture reaction. However, calcium is one of the few elements whose capture gamma-rays are subject to significant interferences from the capture gamma-rays of other common sedimentary elements. The most intense capture line from Ca is at 1943 keV, which is close to chlorine capture lines at 1951 and 1958 keV. This line is also close to the Compton edge of the hydrogen capture line, which affects the statistical precision. The second most intense line at 6420 keV is very close to the prominent neutron capture line of titanium at 6418 keV, which is present in many sedimentary environments. Ca can also be determined from the delayed activity produced in the  $^{48}\text{Ca}(n,\gamma)$  reaction. However,  $^{48}\text{Ca}$  has a very low abundance (0.19 %) resulting in generally low count rates unless there is a very high neutron flux. With a sufficiently high flux of high energy neutrons, delayed Ca activity, such as from the  $^{44}\text{Ca}(n,p)^{44}\text{K}$  reaction which is free of contributions from neutron induced reactions on other stable elements, can be used to improve the precision of the analysis of Ca concentration.

## Carbon

The dominant reaction for the detection of carbon is the inelastic neutron scattering to the 4.439 MeV state. In higher carbon concentrations, use of the carbon capture lines is frequently practical. Analyses performed for the evaluation of coal have generally used the capture gamma-ray technique. A direct interference for the inelastic neutron scattering measurement is the  $^{16}\text{O}(n,n'\alpha)^{12}\text{C}$  reaction. This is primarily a concern because of the almost uniformly large O concentration in sediments. For evaluation of this interference, a ratio of gamma-ray intensities needs to be known. For practical considerations, it is necessary to compare the gamma-ray intensities from the inelastic neutron scattering on C to those from O, requiring knowledge of  $^{16}\text{O}(n,n'\gamma)$  gamma-ray production cross sections. In addition one needs to recognize the possible interference of other gamma-rays with energies within 70 keV of the 4.439 MeV carbon gamma-ray. Specifically, the  $\text{Ca}(n,n'\gamma)$  and neutron capture in Ca and Si need to be evaluated as possible interferences.

## Iron

The iron thermal capture gamma-ray spectrum provides the most direct and efficient means for determining iron concentrations that are geochemically relevant. The primary peaks are all free of significant interferences. Iron can also be determined from delayed activity by fast neutrons using the  $^{56}\text{Fe}(n,p)^{56}\text{Mn}$  reaction. However, there are possible interferences which need to be evaluated from the  $^{55}\text{Mn}(n,\gamma)^{56}\text{Mn}$  and the  $^{59}\text{Co}(n,\alpha)^{56}\text{Mn}$  reactions. It should also be noted that Mn has a significant resonance integral which will accentuate the interference from small amounts of Mn.

## Sulfur

The analysis of sulfur is most efficiently performed with the thermal neutron capture reaction. While delayed activity ( $^{37}\text{S}$ ) can be observed in a purely thermal flux, the large yield of  $^{37}\text{S}$  from the  $^{37}\text{Cl}(n,p)^{37}\text{S}$  reaction generally precludes the use of the delayed S activity in borehole applications, regardless of what type of source is used. Possible interference to the 5420 keV capture line of S may be the escape gamma-ray from the Ca capture lines.

For fast neutron activation, sulfur may be detected by the  $^{34}\text{S}(n,p)^{34}\text{P}$  reaction, but some interference may be expected from the presence of chlorine via the  $^{37}\text{Cl}(n,\alpha)$  reaction.

### Chlorine

Chlorine can most efficiently be observed through the thermal neutron capture reaction because of its large neutron capture cross section compared with most sedimentary elements. However, it can also be observed in delayed activation induced through the  $^{37}\text{Cl}(n,\gamma)^{38}\text{Cl}$  reaction (unfortunately, the isotope with the low capture cross section) which is of use when a careful comparison with Na concentration is desired. When the delayed activity is used, some care must be exercised when the K/Cl concentration is large because of the  $^{41}\text{K}(n,\alpha)$  reaction. Chlorine can also be measured by fast neutrons using the  $^{35}\text{Cl}(n,2n)^{34m}\text{Cl}$ ,  $^{37}\text{Cl}(n,p)^{37}\text{S}$  and the  $^{37}\text{Cl}(n,\alpha)^{34}\text{P}$  reactions. It should be noted that the latter reaction has a potential interference from the  $^{34}\text{S}(n,p)^{34}\text{P}$  reaction.

### Sodium

Na concentrations are typically not very high and while detection can occasionally be achieved through thermal neutron capture spectroscopy, the most efficient technique is generally through delayed activation. When using a  $^{252}\text{Cf}$  source, only a minor correction needs to be made for the contribution to the sodium yield from the  $^{24}\text{Mg}(n,p)$  and  $^{27}\text{Al}(n,\alpha)$  reactions. However, if a substantially higher energy neutron source is used, then the corrections are more substantial and require accurate knowledge of the reaction cross sections for energies up to the maximum neutron source energy.

### Magnesium

Mg generally occurs at relatively small concentrations, except in dolomitic rocks. Thus inelastic scattering is usually not useful for determining Mg especially where substantial amounts of  $^{24}\text{Na}$  may be created from the presence of Na and Al in the environment. The low thermal capture cross section makes it difficult to detect Mg through thermal capture spectroscopy over most of its concentration range. The most efficient technique for Mg analysis is through the delayed  $^{27}\text{Mg}$  activity ( $E_\gamma = 844 \text{ keV}, 1014 \text{ keV}, t_{1/2} = 9.5 \text{ min.}$ ). This delayed activity is subject to potential interferences, both from the production of  $^{27}\text{Mg}$  in the  $^{27}\text{Al}(n,p)$  and  $^{30}\text{Si}(n,\alpha)$  reactions and from the delayed activity from  $^{56}\text{Mn}$  which has a strong line at 846 keV which frequently cannot be resolved spectroscopically from the lower energy (and higher intensity)  $^{27}\text{Mg}$  gamma-ray. The latter interference often requires time-dependent spectral analysis to achieve good sensitivity for the analysis of Mg concentration. Magnesium may be measured with fast neutrons via the  $^{24}\text{Mg}(n,p)^{24}\text{Na}$  reaction, but interferences are noted from the  $^{27}\text{Al}(n,\alpha)^{24}\text{Na}$  and the  $^{23}\text{Na}(n,\gamma)^{24}\text{Na}$  reactions.

### Aluminium

Most downhole analyses of Al concentration rely on the delayed activity from  $^{28}\text{Al}$ . This is best achieved with the lowest energy isotopic source. As the energy of the source increases, an increasing contribution to the  $^{28}\text{Al}$  activity is generated by the  $^{28}\text{Si}(n,p)$  reaction. Detection of Al by inelastic scattering is severely complicated by the decay of  $^{27}\text{Mg}$  delayed

activity. It is sometimes desirable to detect Al through the thermal neutron capture reaction, though its low cross section may require lengthy accumulation times. Aluminium may be measured by delayed activity from the  $^{27}\text{Al}(n,p)^{27}\text{Mg}$ , and  $^{27}\text{Al}(n,\alpha)^{24}\text{Na}$  reactions. Interferences can be expected from the  $^{30}\text{Si}(n,\alpha)^{27}\text{Mg}$ ,  $^{26}\text{Mg}(n,\gamma)^{27}\text{Mg}$ ,  $^{24}\text{Mg}(n,p)^{24}\text{Na}$ , and  $^{23}\text{Na}(n,\gamma)^{24}\text{Na}$  reactions.

### Silicon

Si concentrations can most readily be obtained from thermal neutron capture. However, if higher energy neutron sources are used, it will also be seen as delayed  $^{29}\text{Al}$  activity which is needed for correcting the  $^{28}\text{Al}$  activity for determining the concentration of aluminium. Si can also be detected in inelastic scattering, especially through the first excited state, but caution must be exercised as there may be significant yields of this gamma-ray from the decay of  $^{28}\text{Al}$  from the  $^{27}\text{Al}(n,\gamma)$  and  $^{28}\text{Si}(n,p)$  reactions. If phosphorus is present, then the reaction  $^{31}\text{P}(n,\alpha)^{28}\text{Al}$  must be considered in the silicon determination.

### Titanium

Titanium detection is most efficient through thermal capture gamma-rays. However (see discussion under calcium), some care must be exercised because of the interferences between the titanium capture lines and those of other common sedimentary elements. Ti can also be detected through delayed activity from the  $^{50}\text{Ti}(n,\gamma)^{51}\text{Ti}$  reaction. For this delayed activity, the potential contributions to the delayed activity from the  $^{51}\text{V}(n,p)$  reaction and the  $^{54}\text{Cr}(n,\alpha)$  reaction are generally negligible because of the relatively small concentrations of V and Cr as compared to Ti under most circumstances.

### Vanadium

The only practical mode for determining the concentration of vanadium is through the delayed activity from the thermal neutron capture reaction on  $^{51}\text{V}$ . Some care is needed in using this technique for borehole analysis since the  $^{52}\text{V}$  delayed activity can also be created by the  $^{52}\text{Cr}(n,p)^{52}\text{V}$  and  $^{55}\text{Mn}(n,\alpha)^{52}\text{V}$  reactions. Mn is frequently present in greater abundance than vanadium. Furthermore, all of these elements are likely to be contained in steels, so that when logging in cased holes or when a portion of the logging instrument near the detector is exposed to the neutron flux, interference becomes a major problem. However, with proper techniques, excellent sensitivity can be obtained for vanadium analyses. Vanadium may also be measured with fast neutrons using the  $^{51}\text{V}(n,p)^{51}\text{Ti}$  reaction. Cr and Ti are potential interferences via the  $^{54}\text{Cr}(n,\alpha)^{51}\text{Ti}$  and  $^{50}\text{Ti}(n,\gamma)^{51}\text{Ti}$  reactions.

### Chromium

The most practical method to measure chromium is by thermal capture gamma-rays. Delayed gamma-rays via the  $^{50}\text{Cr}(n,\gamma)^{51}\text{Cr}$  reaction may also be used, but interferences from the reactions  $^{54}\text{Fe}(n,\alpha)^{51}\text{Cr}$  and  $^{50}\text{Ti}(n,\gamma)^{51}\text{Ti}$  can be expected. If fast neutron activation is used, the  $^{52}\text{Cr}(n,p)^{52}\text{V}$  reaction is the most important, but potential interferences from the  $^{51}\text{V}(n,\gamma)^{52}\text{V}$  and  $^{55}\text{Mn}(n,\alpha)^{52}\text{V}$  reactions are anticipated. Fast neutron inelastic scattering on  $^{52}\text{Cr}$  also leads to a 1434 keV excitation which is contaminated by the delayed activity.

## Manganese

Manganese can generally be detected through the delayed activation from the  $^{55}\text{Mn}(n,\gamma)^{56}\text{Mn}$  reaction. With a well thermalized source, the only spectral interference is from the  $^{27}\text{Mg}$  delayed activity, which will generally require a half-life analysis to separate the dominant peak. However, this delayed activity also contains other peaks that permit a quantitative analysis, even if the 846 keV line is impractical to use. When using higher energy neutron sources, a significant interference is produced from the  $^{56}\text{Fe}(n,p)^{56}\text{Mn}$  reaction. Resolution of the relative contributions from Mn and Fe requires the use of flux-integrated cross sections and the iron concentration as determined through neutron capture reactions, or by the analysis of additional activities, such as that from  $^{54}\text{Mn}$  which will have different relative production rates from Mn and Fe than will the  $^{56}\text{Mn}$  activity. However, this latter activity has a very long half-life ( $t_{1/2} = 312.5$  days) requiring very intense, high energy sources for practical analyses. Manganese can be measured by capture gamma-rays but because of the relatively low yield, this type of measurement will be practical only in high grade ores. Fast neutrons lead to the reaction  $^{55}\text{Mn}(n,\alpha)^{52}\text{V}$  with interferences from the  $^{51}\text{V}(n,\gamma)^{52}\text{V}$  and  $^{52}\text{Cr}(n,p)^{52}\text{V}$  reactions.

## Nickel

Capture gamma-ray analysis is the most suitable method for nickel analysis, and the highest energy line is free of interference. Alternatively, the gamma-ray at 1454 keV produced by neutron inelastic scattering on  $^{58}\text{Ni}$  may be used. Fast neutron activation is not a satisfactory method because of relatively poor sensitivity.

## Copper

Copper can be determined by thermal decay gamma-rays via the  $^{65}\text{Cu}(n,\gamma)^{66}\text{Cu}$  reaction with possible interference from  $^{27}\text{Mg}$  produced from  $^{27}\text{Al}$  or  $^{26}\text{Mg}$ . Copper can also be measured by thermal neutron capture, although the sensitivity is substantially lower than by the decay gamma method. An inelastic neutron reaction yielding a gamma-ray of 962 keV can be measured, but again the sensitivity is substantially lower than for the decay gamma method. Fast neutron reactions lead to annihilation radiation and these reactions may be used in those cases where there are no additional significant positron emitters.

## Tungsten

Tungsten analysis is best determined by delayed gamma-rays using the  $^{186}\text{W}(n,\gamma)^{187}\text{W}$  reaction. While there are copious gamma-rays produced by inelastic scattering, the intensities are relatively low and the method is not recommended because of poor sensitivity.

## Gold

For rapid borehole analysis, the best method for gold is the  $^{197}\text{Au}(n,n'\gamma)^{197}\text{Au}$  reaction yielding a 279 keV gamma-ray with a 7.8 sec half-life. If long activation times are permissible, the delayed gamma-rays from the reaction  $^{197}\text{Au}(n,\gamma)^{198}\text{Au}$  are substantially more sensitive. Other fast neutron activations are less sensitive, and not recommended.

# Subsurface Geochemistry: I. Future Applications of Geochemical Data

Michael M. Herron  
Schlumberger-Doll Research, Ridgefield, CT 06877-4108

## Abstract

Chemical measurements currently play a very small role in subsurface formation evaluation in the petroleum industry. However, new advances in interpretation of such data, combined with new measurement capabilities indicate that the role of geochemistry will expand rapidly in the future. Applications can be conveniently divided into two general classes relating to the fluids and to the solids. In the case of the fluids, the major applications are the direct detection of hydrocarbons and of soluble impurities in subsurface water. These impurities not only interfere with the detection of hydrocarbons by geophysical techniques, but may also impact the production techniques to be used. New applications have been developed for the use of inorganic chemical data in evaluating subsurface solids. These include a new normative analysis which permits a quantitative estimation of the minerals which make up the rock. This geochemical mineralogy permits a significantly enhanced rock description beyond that available from geophysical data alone. In addition, the geochemically-derived mineralogy has applications in such areas as the interpretation of depositional environment and diagenesis, and the estimation of such parameters as cation exchange capacity, grain size, and even permeability.

## INTRODUCTION

In considering the status and future of nuclear geochemistry in the petroleum industry, two questions should be considered. First, why should we be interested in the chemical concentrations of subsurface earth formations? Second, what elements are most important for both the current and future applications of subsurface geochemistry? The first question focuses on the driving force behind large-scale use of, and demand for, high quality geochemical data. The second question addresses a prioritization of data types from an end-user's point of view; the end user is a sedimentary geochemist. It is hoped that such a prioritization from a user's perspective can help in the rapid acquisition of the most urgently needed physics measurements which will ultimately result in the highest quality geochemical data.

Applications of nuclear geochemistry data can be conveniently divided into three groups: direct, indirect, and inferred. Direct applications are defined here as those which relate raw data, elemental concentrations, directly to the chemical source, i.e. the fluids and minerals which comprise a formation. Indirect applications, on the other hand, utilize the output of the direct application, such as the mineralogy, to calculate formation properties such as total clay content or cation exchange capacity (CEC). Finally, inferred applications use the direct and indirect outputs to deduce or infer something about the history of the formation. The inferred applications can cover topics ranging from interpretation of the sedimentary depositional environment to estimation of the fluid transport properties.

## DIRECT APPLICATIONS

### Petroleum Hydrocarbon Detection

The most important direct application of nuclear geochemistry is the determination of carbon in sedimentary formations. This is done in practice by measuring the carbon/oxygen ratio using prompt gamma ray spectrometry following a pulse of neutrons (Lock and Hoyer, 1974; Westaway et al., 1980). The C/O ratio varies from zero in a water-filled sandstone with no carbon sources, to a maximum that depends on the porosity and hydrocarbon saturation. In carbonate rocks such as limestones and dolomites, a substantial fraction of carbon is contained in the minerals, which complicates the interpretation of hydrocarbon saturation. This technique is hampered by the interpretation ambiguities, low sensitivity, and consequent slow logging requirements; as a result, C/O logging is largely restricted to measurement behind casing. Nevertheless, the need exists for a good measure of hydrocarbon content that is independent of the salinity of formation waters.

### Source Rock Evaluation

A related application of carbon determination is the evaluation of petroleum source rocks for their carbon content (S. Herron, 1986). In essence, the oxygen contents of the formation and fluids are modeled from geological information and used to convert the bulk C/O ratio to the total carbon content of the formation. In non-carbonate samples, the total carbon equals the total organic carbon (TOC) which is the most fundamental measure of source rock quality. In carbonate-bearing rocks, the carbonate fraction, and therefore the inorganic carbon contribution, can be estimated from log measurements of the Ca concentration. The TOC can then be determined as total carbon minus inorganic carbon.

### Fluid Impurities

Another direct application of nuclear geochemistry concerns the impurities present in formation fluids. The most important impurities are  $\text{Na}^+$  and  $\text{Cl}^-$ , but the fluids can also contain significant  $\text{Mg}^{2+}$ ,  $\text{Ca}^{2+}$ ,  $\text{K}^+$ ,  $\text{HCO}_3^-$ , and  $\text{H}_2\text{S}$ . These impurities may significantly affect completion and production operations, as well as safety, but they are most universally important for their impact on electrical measurements which are used to deduce hydrocarbon volumes. The electrical conductivity of a formation depends on the conductivity of the fluids, which, in turn, depends on the impurity concentrations. The formation conductivity also depends on the water saturation,  $S_w$ , which is the fraction of pore space occupied by water. Current evaluation techniques require an estimation or external knowledge of the water

conductivity in order to infer  $S_w$  from the measured resistivity. An improved determination of  $S_w$ , and thereby the hydrocarbon saturation, should be available from the combination of resistivity data and impurity concentrations determined from geochemical measurements.

## Mineralogy

Although the applications listed above relate to the fluids and hydrocarbons in sedimentary formations, the more general applications are directed at the minerals. This is due to the fact that for most of the elements which have been detected in the subsurface, concentrations in the solid phase far outweigh those in the fluid phases. Direct applications have been made which approximate the mineralogy of subsurface samples from the chemical content (e.g. Everett et al., 1983; Peverraro and Russell, 1984; M. Herron, 1986; Mellor and Underwood, 1985). These represent a significant advance over previous log interpretation techniques where only the general rock type, or lithology, as opposed to the constituent minerals, could be inferred from geophysical log responses. Geophysical responses are relatively insensitive to the mineralogy and only large changes in the type of rock can be firmly interpreted. In contrast, small changes in mineralogy can produce large changes in chemical concentrations, without a change in overall lithology. For example, the transition from a pure quartz sandstone to a sandstone with high potassium feldspar concentrations could reduce the matrix density from  $2.65 \text{ g/cm}^3$  to  $2.63 \text{ g/cm}^3$ , an almost insignificant amount. But the aluminum or potassium concentrations could simultaneously increase by an order of magnitude, even though both formations are classified as sandstones.

The foundations of the element-to-mineral transformation are the assumptions that the amount of each detected element in each mineral phase is constant and that all mineral phases present have been considered. A series of simultaneous linear equations can be constructed relating the total quantity of each element to the amount of each mineral and the elemental concentration in that mineral. Although this is similar to any generalized inverse problem, application of the principle has met with only limited success in practice. This is most frequently due to insufficient geochemical data being available for the number of minerals.

The number of minerals in sedimentary formations is in the several hundreds, which might seem to preclude a general element-to-mineral transform from working. Fortunately, as few as ten minerals constitute over 95% of sedimentary formations. Many formations contain as few as 4 to 6 minerals, which makes mineral identification from geochemistry far more feasible. However, it must be stressed that in order to determine mineralogy accurately, the geochemical data must contain sufficient elements to describe the system and these elements must be diagnostic, i.e. they must have a significant contrast in concentration in the minerals of

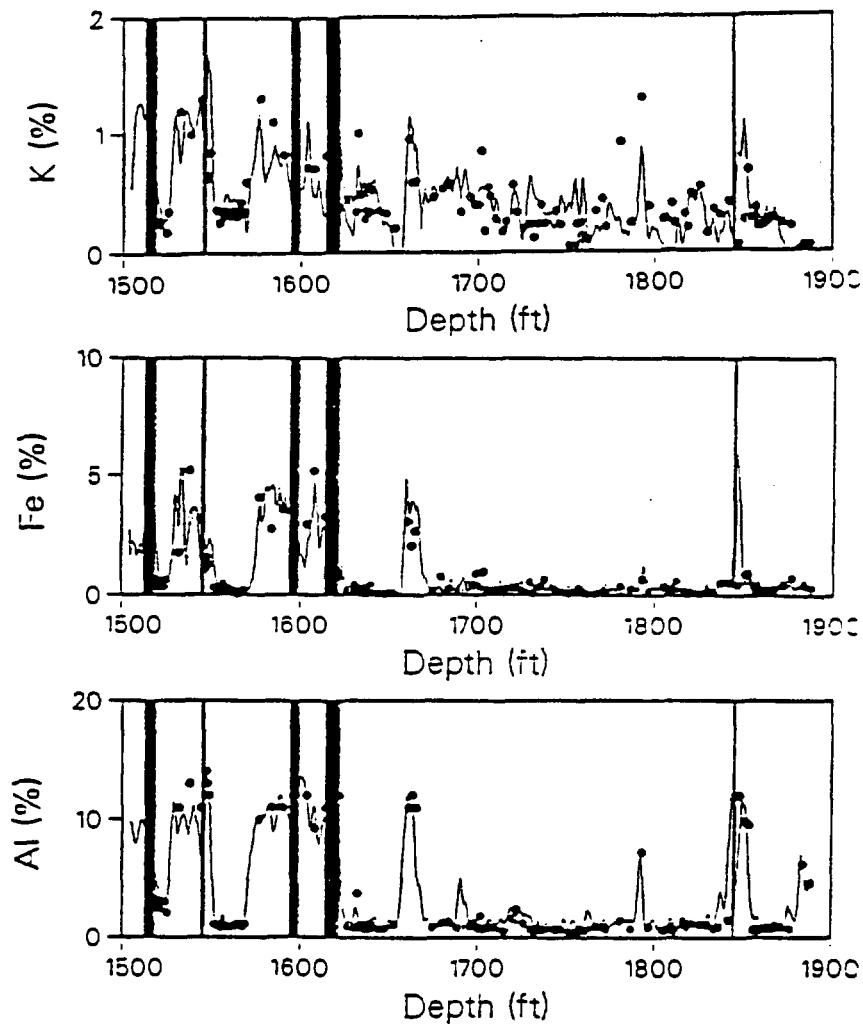
interest. Previous attempts to use Th, U, and K concentrations from natural gamma-ray spectroscopy to derive clay mineral types have been hampered by the limited number of elements and the fact that these elements are not generally diagnostic for the clay minerals.

Many minerals have very well defined chemical compositions. Quartz, for example, is well characterized by its formula of  $\text{SiO}_2$ . For other minerals, the chemical composition is a simplification of the true composition. The formula for the common heavy mineral zircon is  $\text{ZrSiO}_4$ , and there is always a substitution of Hf for Zr in natural zircons to the extent that the Hf content is about 1% by weight. Thus the formula and true composition are not always exactly the same.

A further complication regarding the stability of composition involves the clay minerals. These minerals are widely believed to have highly variable compositions due to substitution of one element for another in the lattice and to adsorption of elements on the clay surfaces. To the extent that this compositional variability exists, of course, it invalidates the assumptions involved in the element-to-mineral transformation. Recently, however, it has been suggested that the compositional variability of many clays is largely governed by the type of clay and the degree of lattice order of the clay (M. Herron, 1986). Variations due to the origin of the sediments appear to be relatively small. The degree of order in the lattice may also reflect the clay's origin as detrital or as authigenic. Such a possibility is exciting because authigenic clays generally exert a more negative impact on such important formation properties as permeability than do detrital clays. If clay mineral compositions can be described by the type of clay and lattice order, then the assumptions for element-to-mineral transformations will not be violated.

### **An Example of Log-Derived Geochemical Mineralogy**

Mineralogy was successfully derived from geochemical log data from a well in Venezuela (Everett et al., 1983; M. Herron, 1986). In this well, there are four dominant minerals: the clay minerals kaolinite and illite; potassium feldspar; and quartz. The mineral abundances of three of these minerals, kaolinite, illite, and potassium feldspar, were estimated from concentrations of the elements Al, Fe, and K measured either on core or remotely by geochemical logging tools. The Al abundances were determined from the Enhanced Resolution (ERT\*) log; Fe concentrations were determined from the Gamma-Ray Spectrometry (GST\*) log; K concentrations were measured by the Natural Gamma-Ray Spectrometry (NGS\*) log. The comparison between concentrations determined from logs with those measured on sidewall core samples using neutron activation analysis is shown in Figure 1. Lignite zones, which can interfere with the measurements, are shown as black bands. As is always the case in such



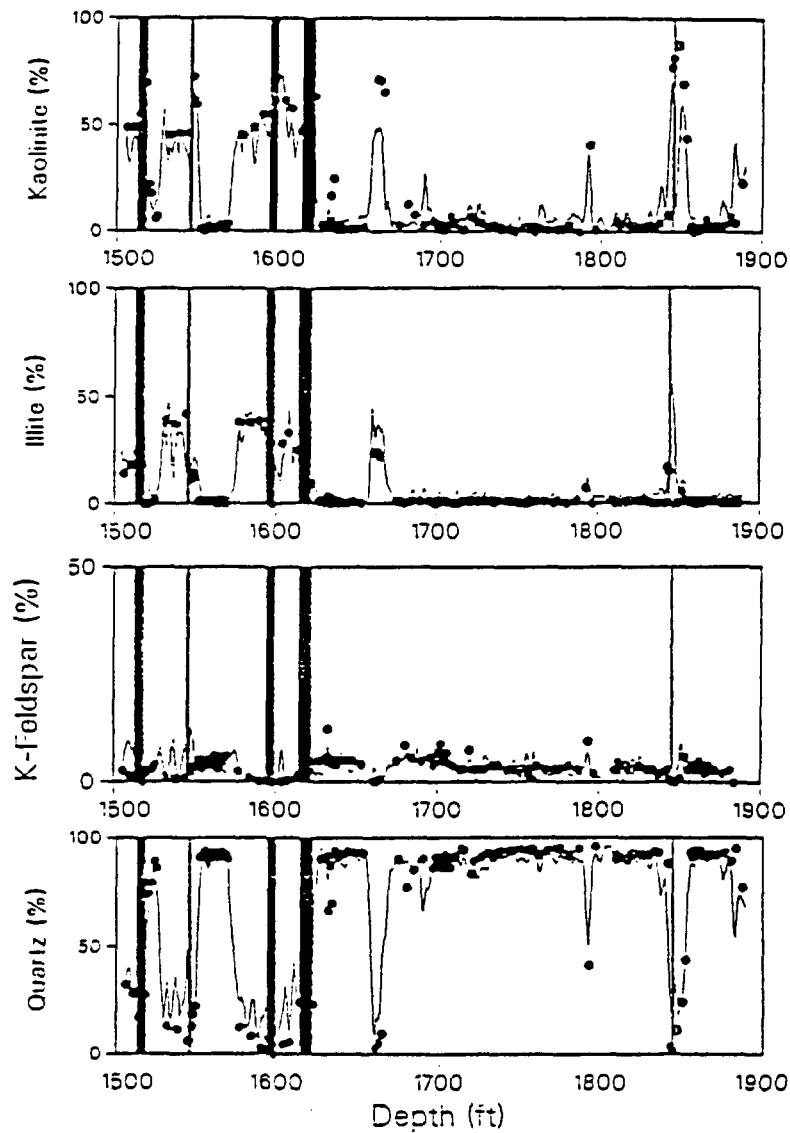
1. Elemental concentrations in a Venezuelan well determined by geochemical logs (lines and on sidewall core samples by instrumental neutron activation analysis (points). Log data are from the Enhanced Resolution (ERT) log for Al, the Gamma-Ray Spectroscopy (GST) log for Fe, and the Natural Gamma-Ray Spectroscopy (NGT) log for K.

comparisons, there is a large difference in formation volume sampled by the two techniques that leads to occasional discrepancies. Only one gram of sample was analyzed by neutron activation, while the logs are sensitive to a formation

• Mark of Schlumberger

volume that is orders of magnitude greater. Nevertheless, there is a remarkably good agreement between the core data and concentrations from the geochemical logs.

The log-derived concentrations were used as inputs into a set of simultaneous linear equations relating elemental concentrations, mineral abundances, and end-point compositions. Solving the simultaneous equations results in continuous logs of mineral abundances, as shown in Figure 2. The remainder term, i.e. 100% minus the sum of kaolinite, illite, and feldspar abundances, is assumed to be quartz, which contains none of the input elements. Also shown are



2. Mineral abundances in the Venezuelan well derived from the log chemical concentrations (lines) and as measured on the sidewall cores by x-ray diffraction (points).

the mineral abundances determined by x-ray diffraction on each of the sidewall core samples; these have an estimated uncertainty of  $\pm 20$  relative percent. Clearly there is good agreement between the two means of estimating mineral abundances.

The degree of agreement between the mineralogy measured by x-ray diffraction and that estimated from the geochemical logs should allay some of the concerns about the element-to-mineral transformations, at least for this well and perhaps on a broader scale as well. The same transform used for the Venezuelan well has been successfully applied to sediment samples from Long Island, New York (M. Herron, 1986). Similar transformations have been attempted in the past (e.g. Pevraro and Russell, 1984), using geophysical as well as limited geochemical log data. Geochemical inputs have the advantage of being more diagnostic of minerals present, although they generally have greater statistical fluctuation in the data.

It is important to note that such models will fail if all minerals are not accounted for. More generally applicable models will require more elemental inputs and more mineral outputs than the simple three element/four mineral model used above. It is possible to include Si and Ca as inputs to the model, elements which are measurable with the GST and/or ERT logs, allowing quartz and calcite to be calculated as output minerals. The future will undoubtedly show that other elements can be detected by wireline methods, and these will lead to a dramatic increase in our ability to characterize subsurface earth formations.

## INDIRECT APPLICATIONS

Information on the types and quantities of minerals present in sedimentary formations could significantly affect many aspects of the petroleum industry. The basic reason for this is that mineralogy is inherently more detailed descriptive information than is simple lithological classification. Once the mineralogy of a well has been determined from geochemical data, a whole host of applications can be derived from that information. Several possible applications for log-derived mineralogy are listed in Table 1, and some of these are discussed below.

Table 1. Current and future applications of wireline geochemistry		
Direct	Indirect	Inferred
Mineralogy	CEC	Depositional Environment
Clay Typing	Completion Risk	Diagenesis
Volume of Clay	Production Risk	Source Rock Evaluation
Well Zonation	Grain Density	API Gravity
Well-to-Well Correlation	Porosity	Grain Size
Enhanced Lithological Description	Trace Element Modeling	Permeability

## Well-to-Well Correlation

In well-to-well correlation, the object is to identify a given sedimentary unit in two or more wells. This is usually done by comparing the raw responses of geophysical logs or the total gamma ray signature in the wells and looking for similar curve character. Of course, two zones may have similar curve character and magnitude, despite being unrelated genetically. The reliability of this correlation can be significantly enhanced if mineralogies, rather than raw data, can be directly compared. Similarly, the zonation of similar intervals in a single well can be improved if the mineral assemblage is available.

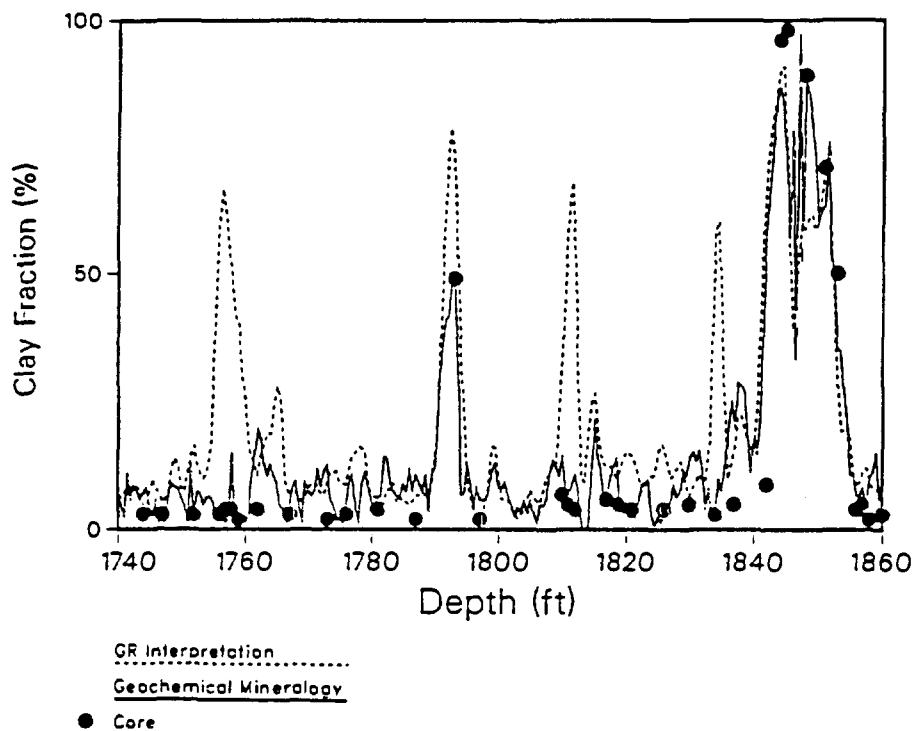
## Volume of Clay

If the mineralogy is completely known, then the total quantity of clay is an immediate sum of each of the individual clay abundances. This term, also known as  $V_{Cl}$ , is critical for the evaluation of geophysical log responses because the clay minerals have a significant impact on virtually every log measurement. Consequently, attempts to approximate the clay content have been formulated for several types of geophysical log data. These estimations are imprecise and frequently unreliable. In contrast, the estimations based on geochemical data are much more fundamentally sound.

One of the most commonly used logs for estimating clay content is the gamma ray (GR) log. Clay content is obtained by scaling the minimum and maximum GR readings over an interval to correspond to 0% and 100% clay, respectively. An example of the clay content estimated from GR is shown in Figure 3 along with the clay mineral content determined from x-ray diffraction analysis of core samples. Also shown in Figure 3 are the sum of clay mineral abundances determined from the geochemical logs. Clearly, the GR-derived estimate shows good agreement with the core data over certain intervals. On the other hand, there are three zones where the GR-derived estimates far exceed both the core data and the geochemically-derived values: 1760 ft, 1810 ft, and 1840 ft. Presumably, in these intervals there are non-clay sources of Th, U, and/or K that are responsible for the gamma ray activity spikes. A likely set of candidates are heavy minerals such as zircon and monazite, which contain high concentrations of Th and/or U. Figure 3 clearly illustrates the improved accuracy obtained by estimating clay content directly from geochemical data.

## Cation Exchange Capacity

A second important indirect application of geochemical mineralogy concerns the cation exchange capacity (CEC) of the formation, usually expressed as milliequivalents per 100 g.

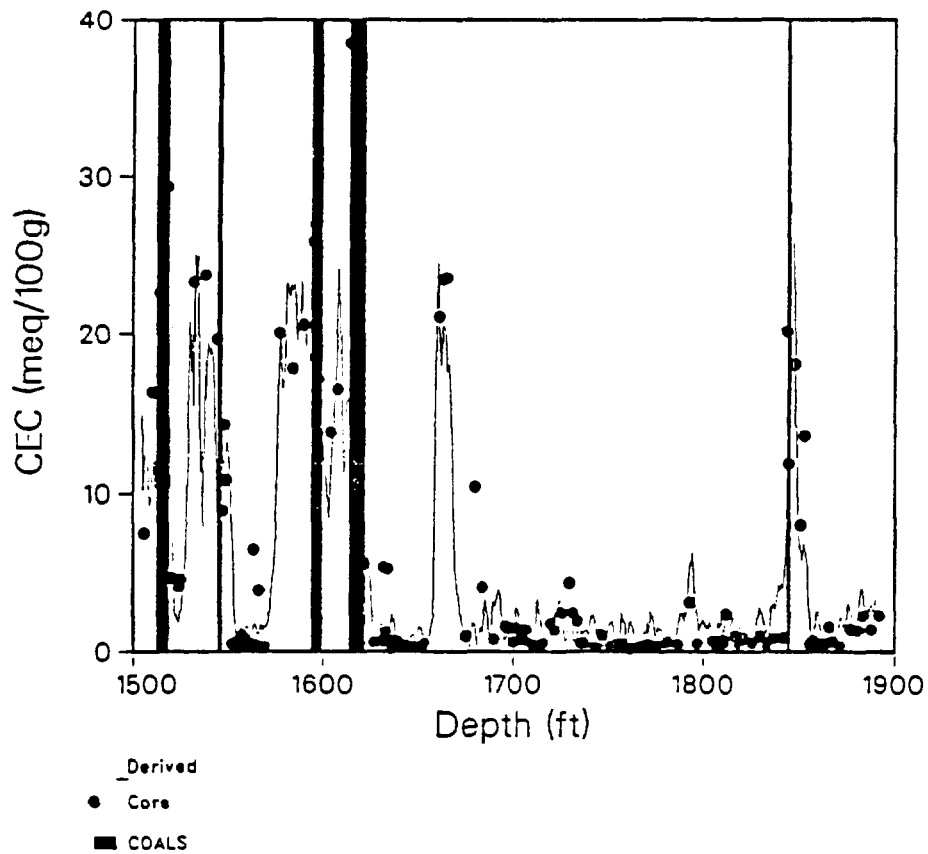


3. Estimates of total clay minerals in the Venezuelan well from the geochemical mineralogy (solid curve), from the Gamma Ray log (dashed curve), and as measured on sidewall cores by x-ray diffraction.

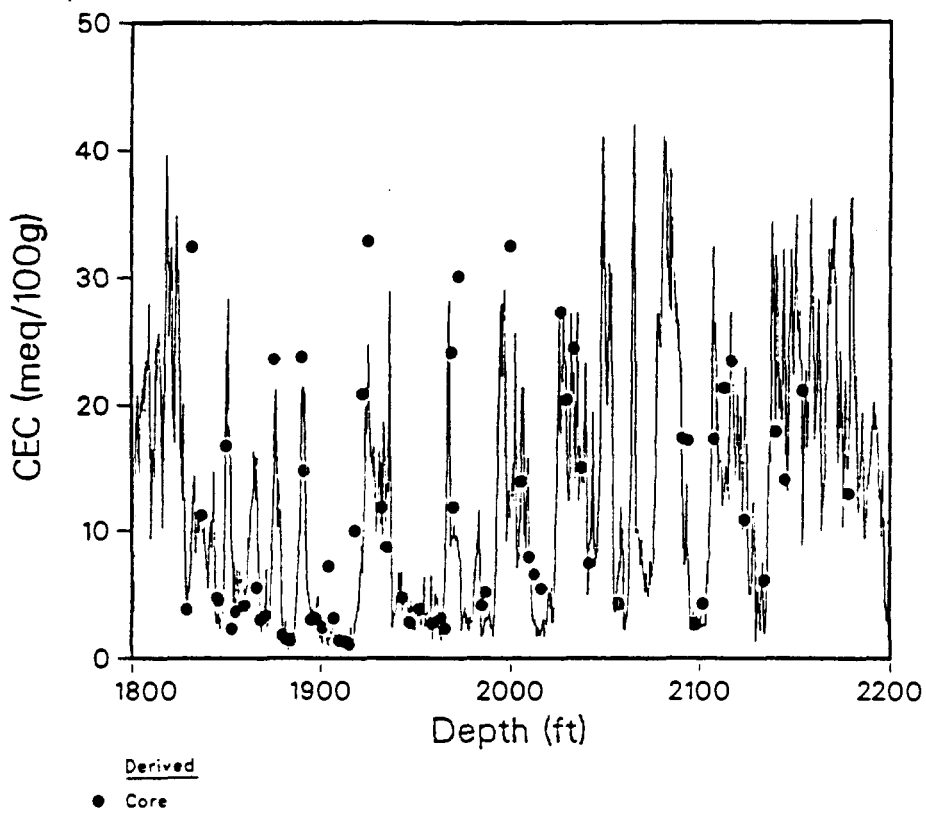
Interpretation of the electrical response in formations containing clay minerals is complicated by the fact that the clays, unlike most other common minerals, can conduct electricity. The direct impact of the clay minerals on the resistivity logs has been modeled according to the CEC of the formation (Waxman and Smits, 1968). The CEC of the formation, in turn, is controlled by the CEC of the constituent clays. Kaolinite and chlorite have relatively low CEC's and only a minor impact on the resistivity. Illite, and particularly smectite, exert a much more pronounced effect and have correspondingly higher CEC's. Obviously, it is important to understand the type of clays at least as much as the total clay content that was derived earlier.

The CEC of the formation can be estimated as a linear combination of the abundances of each clay mineral multiplied by the CEC of that clay. Figure 4 compares the CEC estimated from the geochemically-derived mineralogy with values measured in the laboratory on the sidewall cores (M. Herron, 1986). There is overall remarkably good agreement between the derived and measured CEC values, despite a few discrepancies. Note particularly the interval at 1793 ft, which has a low CEC of only 3 meq/100g despite being composed of 40% clay. Because this interval is identified as essentially containing only kaolinite, the derived CEC is as low as the measured CEC. Virtually any other procedure would be unable to provide as accurate a CEC log as that shown in Figure 4.

A second example of a log-derived CEC compared to core measurements is shown in Figure 5. This well is located in Kern County, California and penetrates very feldspar-rich sands and



4. Cation exchange capacity estimated from the geochemical mineralogy (line) and as measured on sidewall cores (points) for the Venezuelan well.



5. Cation exchange capacity estimated from geochemical mineralogy (line) and as measured on core plugs (points) for a California well. The highest CEC values reflect the presence of the swelling clay, smectite.

shales. A six-element/seven-mineral model, expanded to include quartz, calcite, and smectite, was used to derive the mineralogy. The additional inputs are Si and Ca from the GST and excess H beyond that contained in the pore fluids but part of the clays. Smectites have the largest CEC values of any clays, and so the derived CEC is heavily dependent on the accuracy of the derived smectite abundance. Clearly, the agreement between log-derived and measured CEC values shows that the geochemical model is estimating the smectite abundance fairly well.

### **Completion and Production Risk Assessment**

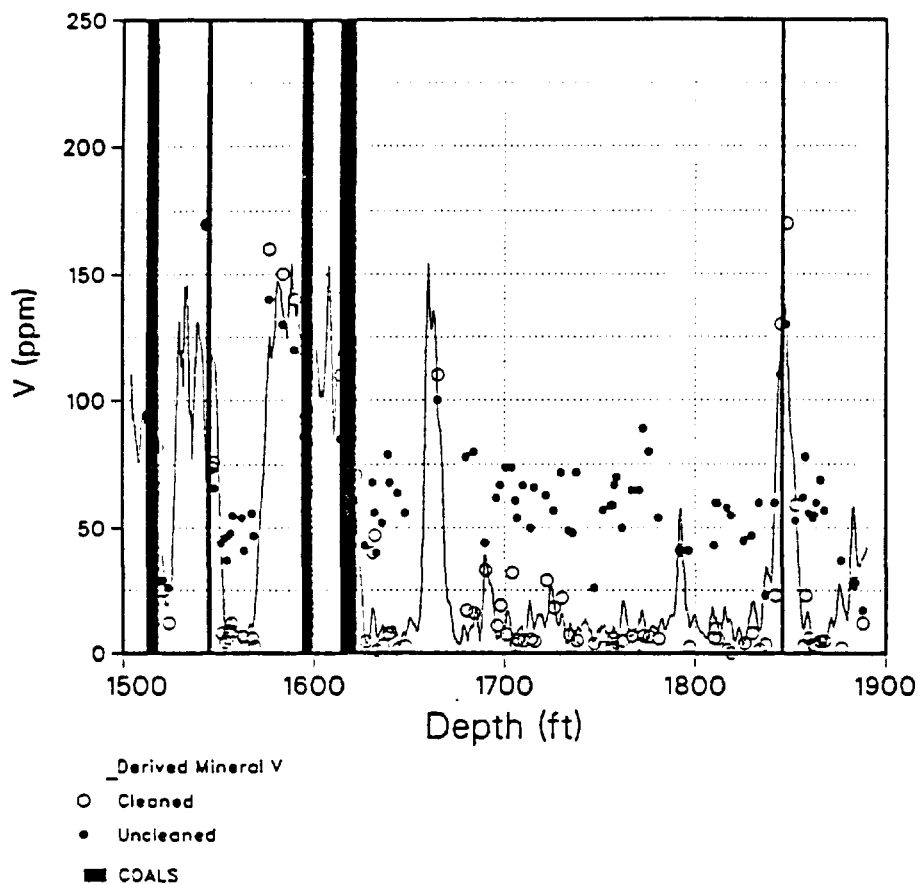
Completion and production operations are significantly affected by the presence of clay minerals, especially smectites. Smectite refers to a family of clay minerals that have the ability to absorb quantities of fresh water and then swell in size. This swelling behavior causes a variety of problems in the near-borehole environment that are generalized as formation damage. An additional problem relates specifically to heavy oil operations where steam is added to heat the oil and reduce its viscosity. The well shown in Figure 5 is just such a well. When steam is introduced to layers containing smectite, a significant fraction of the added steam energy is absorbed by the high water content of the clay thus reducing the efficiency of the operation. Ordinary geophysical log measurements are unable to establish the smectite content of the formation. As indicated above, expanded geochemical models have the ability to quantitatively estimate the smectite content, thus providing valuable data to the reservoir and production engineers.

### **Grain Density and Porosity**

One of the most important answers needed in formation evaluation is the porosity, the fraction of the total volume that is occupied by pore space. Density tools, gamma-ray attenuation devices, measure the bulk density of a formation. The bulk density can be exactly related to the porosity if the average matrix density is known. In practice, the average matrix density is rarely known, and it is therefore set to a constant value. However, the average matrix density can be computed from the mineral abundances which geochemical data permit to be accurately estimated. Experience has shown that porosities determined in this manner agree better with core measurements than other, more conventional log-based estimates of porosity.

### **Elemental Modeling**

The foundation of the element-to-mineral transformation is that common sedimentary minerals have fixed chemical concentrations, provided the degree of lattice order is taken into account. Thus far, elements that have been considered include only the major elements. Recent work has indicated that trace elements can also be modeled as if they are present in sedimentary



6. Vanadium concentrations in the Venezuelan well estimated from the geochemical mineralogy (line), and as measured by INAA on cleaned (open circles) and uncleaned (filled circles) sidewall samples. The excess V in some of the uncleaned samples represents the contribution of the heavy oil.

minerals at fixed, albeit very low, concentrations (M. Herron, 1986). Many trace elements can also be detected in subsurface formations by geochemical tools. Figure 6 shows a synthetic log of vanadium concentrations, modeled by taking the derived mineralogy in Figure 2 and assigning discrete V concentrations to each mineral. For comparison, Figure 6 also shows the V concentrations measured on the sidewall core samples before and after the heavy oil was removed. The synthetic log agrees well with the V concentrations in the cleaned samples and in uncleaned shaly samples where the minerals are the only source of vanadium. Hydrocarbon-bearing samples, on the other hand, show an excess of V due to the presence of heavy oil. Vanadium was also measured downhole using the ERT log and concentrations showed good agreement with the uncleaned sidewall data. The excess V, normalized to the fraction of oil present determined from other logs, is calculated at about 400 ppm, which compares favorably to the 390 ppm measured on an oil sample.

Such a calculation of excess V would be impossible without being able to estimate the mineral vanadium contribution. Indeed, the highest absolute V concentrations are in the shales, not in the oil-rich sands. The vanadium content of heavy oils has been related to the viscosity of the oil (e.g. Kapo, 1978) and is of use in classifying crude oil families and in establishing original

source rock characteristics (Premovic, 1984; Hitchon and Filby, 1984; Lewan, 1984). Vanadium has also been linked to organic matter in oil shales (Desborough et al., 1974; Riley and Saxby, 1982; Leventhal and Hostermann, 1982). Studies such as these are enhanced if the mineral contributions of trace, as well as major, elements can be quantified.

## **INFERRED APPLICATIONS**

Several applications of geochemical data to subsurface earth formations relate to the history of the formation and require an integration of the geochemically-derived mineralogy with geologic knowledge. These applications infer past properties and processes related to the formation, and are not direct applications of the data.

### **Depositional Environment**

Establishing the environment of deposition of a subsurface formation is a critical step in the petroleum business. The interpretation of depositional environment is often the key information for deciding where to drill adjacent wells that are most likely to intercept formations of interest. In the past, several investigators have attempted to develop relationships between depositional environment and elemental data (e.g., Adams and Weaver, 1958; Cody, 1971; Carson and Arcaro, 1983; Lonnie, 1982; Couch, 1971; Furst, 1981). Similarly, sedimentologists have long considered the relationship between mineralogy, grain size, and depositional environment (Blatt et al., 1972; Davies and Ethridge, 1975).

The availability of Th and U concentrations from natural gamma ray spectroscopy tools led Adams and Weaver (1958) to investigate the relationship between the Th/U concentration ratio and depositional environment. They concluded that the total abundances of Th and U in sediments are largely controlled by the presence of clay minerals and resistate minerals, such as zircon; the relative abundances of Th and U are determined by the extent to which U has been oxidized and leached from the parent material. These characteristics permit a classification of material by Th/U ratio and total Th content into regimes that correspond broadly to depositional environment.

Several authors have noted a relationship between clay mineral type and depositional environment, particularly in deltaic systems (e.g. Parham, 1966; Lonnie, 1982). It has been observed that in the river portion of both modern and ancient deltas, kaolinite is the dominant clay. Marine deposits are dominated by illite and mixed-layer illite-smectite clays, while transitional, near-shore environments are intermediate in composition. These observations also follow for the Venezuelan well data in Figure 2. The lowest shale intervals are nearly free

of illite, but contain abundant kaolinite. The deposits in the lower half of the well have been identified as being river channel deposits. The upper shales, particularly at 1530 ft and 1590 ft, are more illitic, consistent with the interpretation that these represent an estuarine, moderate salinity environment. This is an example of the great power mineralogy has for enhancing depositional environment interpretations.

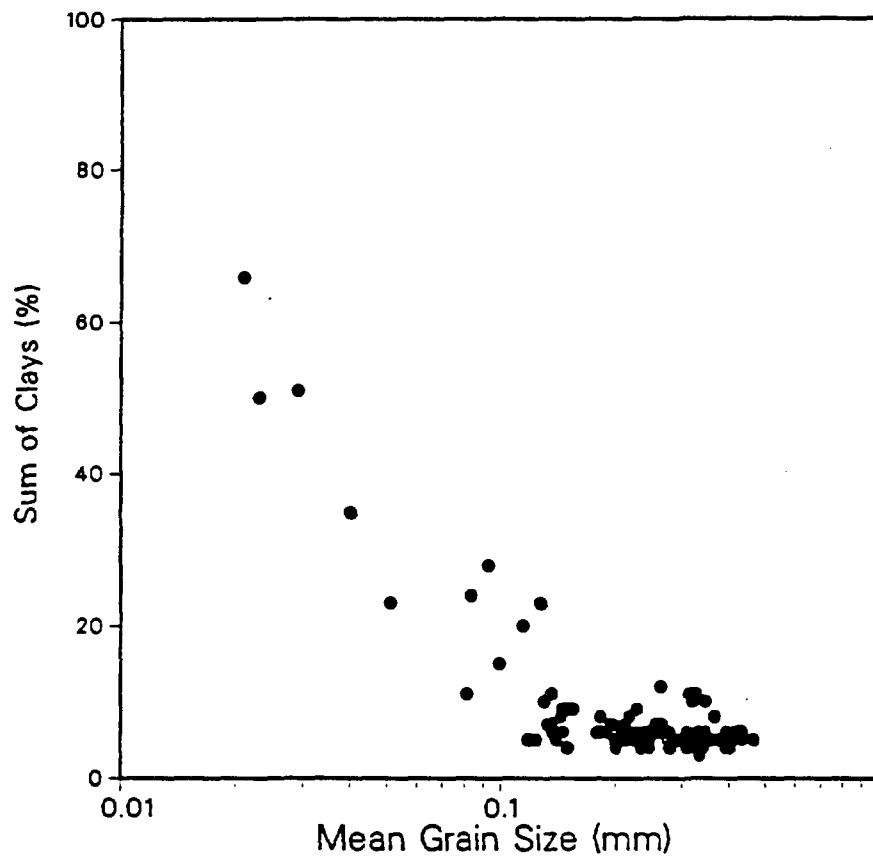
## Grain Size

The size of sedimentary grains, as well as the distribution of sizes, is important for several reasons. Size and degree of sorting reflect the original sediment size and the hydrodynamic conditions, both during transportation and at the time of deposition. These are key factors in interpretations of geologic history, including the depositional environment. Grain size and sorting are also important ingredients in the production of hydrocarbons. Larger grains tend to produce larger flow channels for fluids, and greater permeability. Similarly, poorly sorted sands have lower porosities and permeabilities than do well sorted sands.

A qualitative, general relationship between mineralogy and grain size has been suspected for a long time. Blatt et al. (1972) give a plausible picture of how the important sedimentary minerals may have characteristic grain size distributions. For example, clay minerals are inherently very fine, commonly smaller than 0.002 mm in diameter. Quartz and feldspar, on the other hand, are rarely that small. It follows that the average size of a sediment which is clay-free is likely to be larger than the average size of a sediment composed of 30% clay minerals. Similarly, Davies and Ethridge (1975) showed that the average size of quartz grains increased as the percentage of quartz in the sediment increased.

Two additional clues to the size of detrital sediments come from the feldspar content and the heavy mineral content. Odom et al. (1976) showed that, for clay-free sandstones, the fine grained fraction (<0.125 mm) increased with the potassium feldspar content. We have observed this phenomenon in many other samples using multivariate statistical analysis. We have also observed a similar connection between the Zr or Hf content, due to the resistive mineral zircon, and the percentage of fine to very fine sand. Because zircons are fairly restricted in size to about 0.060 mm diameter (von Englehardt, 1977), they can be powerful indicators of very fine grained quartz, which has a similar hydrodynamic diameter. Pirkle et al. (1984) analyzed the size distribution of heavy mineral-rich sands and found them to be extremely well sorted and with a mean grain size of .125 mm. It seems likely that such information can be successfully integrated into a chemically-derived estimate of the detrital grain size.

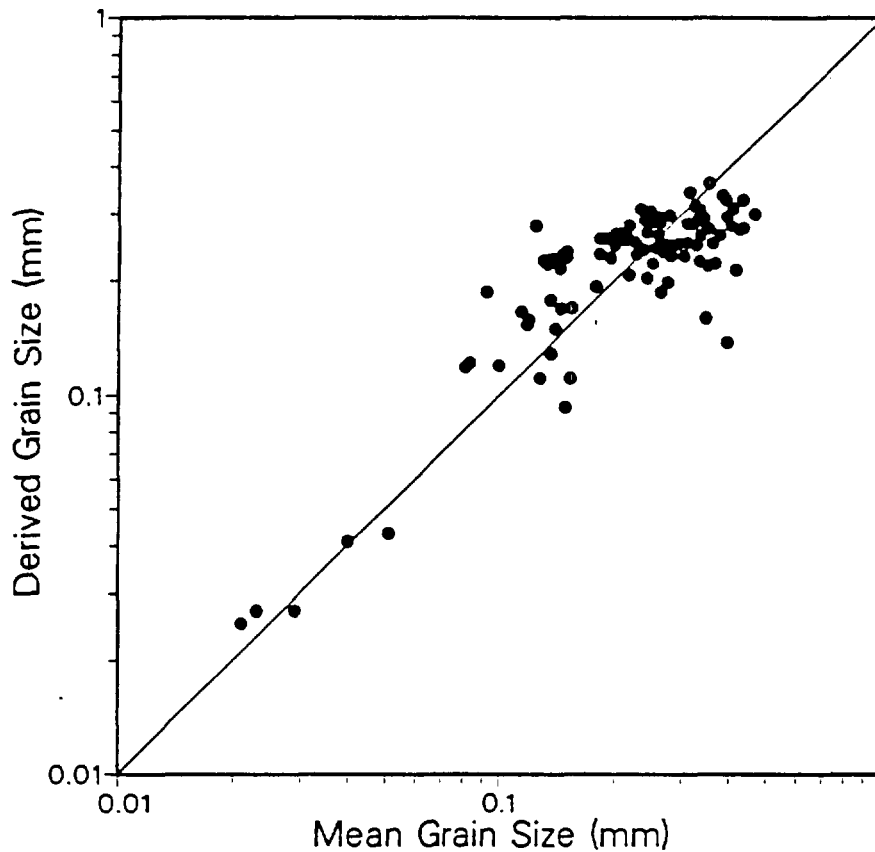
Figure 7 shows mean grain size data for the Venezuelan well discussed earlier (Everett et al., 1985) and total clay content. In the shaliest of these sand samples, the impact of increasing clay



7. Mean grain size in the Venezuelan samples and clay content. For clay-rich samples, there is a clear tendency for increasing clay content to result in a smaller mean size. For the sands containing about 5% clay, however, there is a wide range of mean sizes that are unrelated to clay content.

content is to decrease the mean size as mentioned earlier. For most of the samples, however, there is no clear relationship between size and clay content. Considering the relationships between mineralogy and grain size discussed above, a transformation has been constructed using the major mineral and zircon (estimated from Hf) abundances to estimate the grain size relationships in this well. Figure 8 is a best fit of measured mean grain size and a mean size estimated from the kaolinite, illite, feldspar, and Hf contents. It is clear that the inclusion of the feldspar and zircon information produces a much better estimate of grain size than does the reliance on clay content alone. A similar estimate is available from currently available log data, with the substitution of non-clay uranium (M. Herron, 1986) for the hafnium.

The grain size information thus far included in the description of Figure 8 relates only to the depositional process. That is, there are sound hydrodynamic reasons which explain the relationship between sediment deposition and mineral sorting. For example, in a high energy environment, coarse material is deposited while clay minerals remain in suspension; conversely, under quiet conditions, sand grains are not being transported and clay minerals are preferentially deposited. Two factors which must be included in a general model are the original grain size of the parent material, and the changes during sediment transport. Fortunately, these

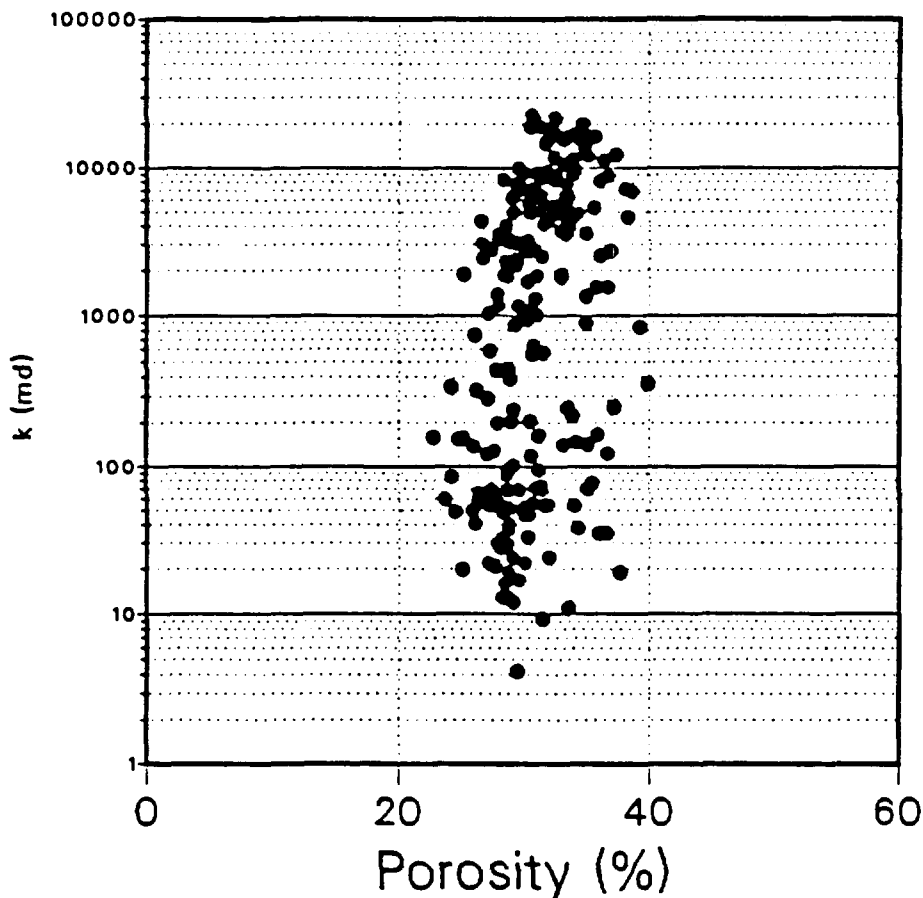


8. Mean grain size in the Venezuelan samples fit linearly to the concentrations of Al, K, and Hf. Much of the grain size variance that was unaccounted for solely by the clay content (or Al) is accounted for by changes in the K and Hf concentrations, reflecting K-feldspar and zircon, respectively.

parameters are also mirrored in the finally deposited material composition reflecting the "chemical maturity" of the sediment. The California well, for example, contains abundant feldspar in the sand units, indicating relative immaturity of the sediment when compared to the Venezuela well which contains at most 10% feldspar. This immaturity also extends to grain size, as the coarsest California samples are significantly coarser than any of the Venezuelan samples.

### Permeability

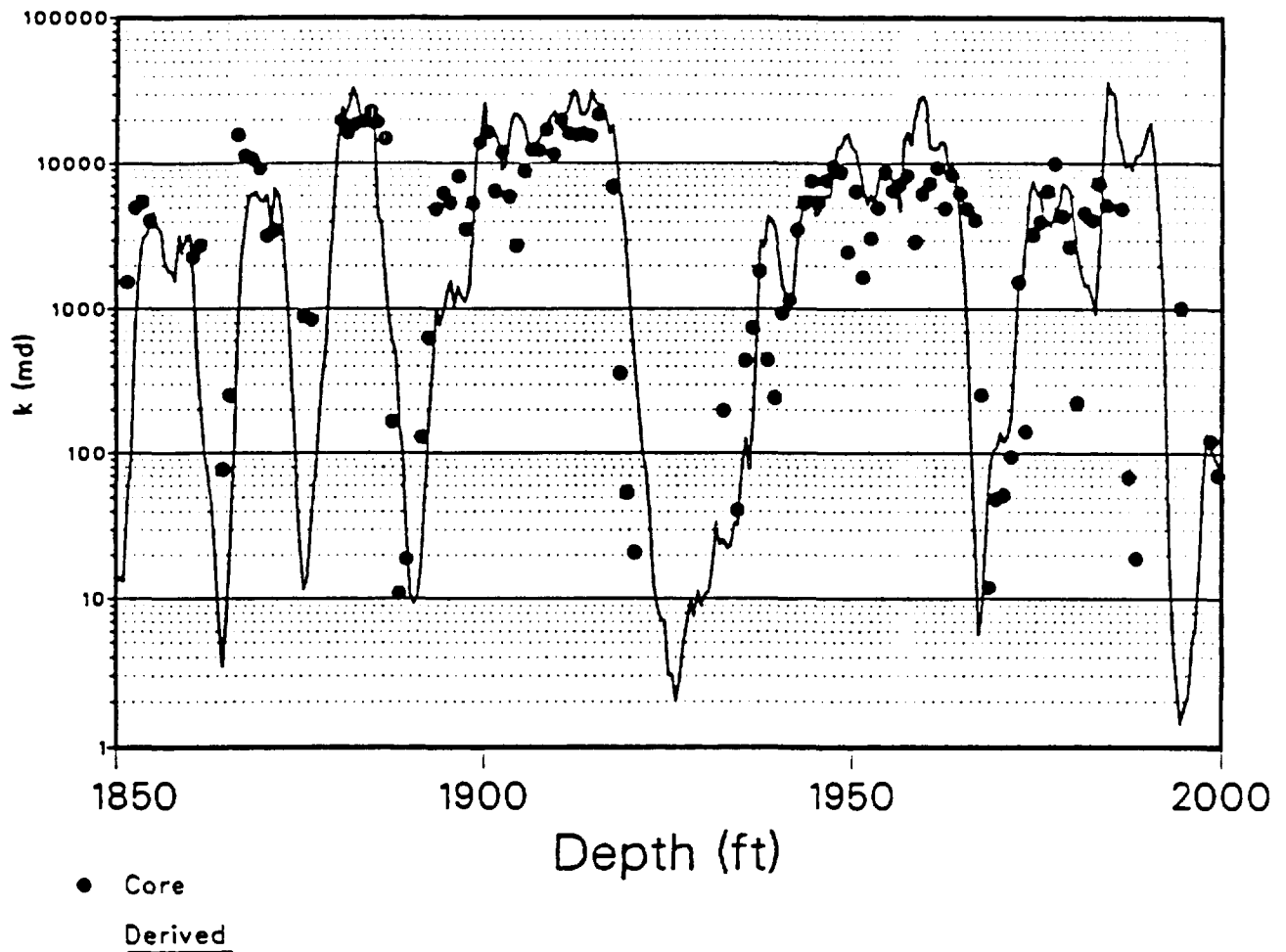
Permeability is, in some respects, the most important parameter in petroleum exploration and production because the commercial viability of a well is determined by the rate of return, and this depends on the flow rate of the well. Despite its importance, there are no satisfactory and reliable means of estimating permeability from currently available log data. As a result, geologists frequently seek a second measurement that shows some degree of correlation with permeability. It is sometimes found in some reservoirs that a correlation exists between the logarithm of permeability and porosity. When such a correlation is found, it is of great interest



9. Porosity and permeability measured on core plug samples from the California well. Note that for a given porosity, permeability varies over about four orders of magnitude.

because porosity can be determined on a continuous basis from logs. Most often, however, the correlations are poor and not transferable from zone to zone or from field to field. As an example, Figure 9 shows measured porosity and permeability to air in core samples from the California well. In this well, samples of a given porosity can vary in permeability by about four orders of magnitude. Thus, a different means of estimating permeability is required.

From a physics point of view, it is clear that the permeability of a porous medium is largely independent of the composition of the solid. Permeability, like porosity, is a function of the pore system, not the solid matrix. All else being equal, the permeability of a glass bead pack will not change if all the glass is replaced by, for example, aluminum. From an earth sciences point of view, however, all else is rarely, if ever, equal. As has been demonstrated, when one property of a natural formation changes, other properties, including composition, usually change as well. Changes in depositional environment and provenance are paralleled by changes in mineralogy. Changes in mineralogy are accompanied by changes in particle size, shape, morphology, and location. Consequently, changes in mineralogy accompany changes in the pore system geometry, and this directly impacts the permeability.



10. Permeability estimated from the geochemical mineralogy and porosity and as measured on the plug samples for the California well. Most of the permeability variation is caused by changes in clay content and in grain size, factors that are not reflected in the porosity variations. Compare the difference between estimated and measured permeabilities with Figure 9.

Figure 10 shows the core permeability for the California well as a function of depth. Also shown is a transform that uses the geochemically-derived mineral abundances as inputs to estimate a likely permeability in shaly sand environments. The transform and its derivation will be published elsewhere. Some of the core data are slightly off-depth, and there are significant differences in formation volume sampled between logs and core. It is clear, however, that the inclusion of log-derived mineralogy has permitted a far better estimate of permeability than that possible from the porosity alone. There is good agreement not only regarding the absolute magnitude of the permeability, but also the trends within units, between the derived and core data.

## ELEMENT PRIORITIZATION

Since the geochemical models of the future have not been invented yet, and indeed, will depend on analytical methodology development, it is a bit presumptuous to consider a full prioritization of the most important elements. Nevertheless, the spectrum of elements that may be commercially measurable in the next ten to twenty years is limited. Despite the limit of model development, some elements can be regarded as more important than others in the determination of mineralogy. Some minerals exert a stronger impact on the applications, such as permeability, than do others. Minerals and applications which can be extremely important in surficial geochemistry and mining, but which are rarely important in the petroleum industry, are purposefully omitted.

### 1. Calcium

Calcium is perhaps the most valuable diagnostic element for all the sedimentary world. The overwhelming majority of sedimentary calcium is contained in the carbonate minerals calcite ( $\text{CaCO}_3$ ), aragonite ( $\text{CaCO}_3$ ), and dolomite ( $\text{CaMg}(\text{CO}_3)_2$ ), though important quantities are present in ferroan dolomites, ankerite ( $\text{CaFe}(\text{CO}_3)_2$ ), and in the clastic minerals calcic plagioclase, biotite mica, and some smectites. Carbonate rocks account for 10-15% of the sedimentary world, and about half of the petroleum is in carbonate reservoirs. Porosity in such reservoirs is low, commonly less than 20%. Dolomitization, complete or partial replacement of calcite with dolomite, is common. Grain densities are, in  $\text{g/cm}^3$ , 2.71 for calcite and 2.87 for dolomite. Thus, a bulk density of 2.68 would be interpreted, assuming no other minerals and a fluid density of 1  $\text{g/cm}^3$ , as ranging between 2% porosity if the matrix is calcite to 10% if the matrix is dolomite! Clearly, the estimate of reserves is quite sensitive to the mineralogy. For the two mineral system of calcite and dolomite, however, the inclusion of the Ca concentration allows a solution of the mineral abundances, a suitable grain density, and porosity.

In clastic rocks, calcite is an important post-depositional cementing agent. The impact of the cement is to reduce porosity and permeability, while adding to the overall strength of the rock. Dolomite is also a common secondary mineral in clastic reservoirs and its abundance may be interpreted in terms of diagenetic history. The use of Ca for interpreting other clastic minerals is probably not very important.

### 2. Carbon

Carbon is of fundamental importance in hydrocarbon exploration and development. At the present time, however, estimates of hydrocarbon volumes by resistivity techniques are

generally more reliable, more accurate, and certainly faster than estimates using the neutron bombardment and prompt gamma-ray detection technique. This, of course, does not imply that a need for a fast, accurate carbon measurement does not exist. The need may be strongest in wells which have been cased, where zones containing hydrocarbons may have been overlooked in the past, and where resistivity devices are inappropriate due to the conductive steel casing. Carbon is also important, as previously mentioned, for source rock evaluation.

### 3. Iron

Iron is most important in subsurface formations in clay minerals, glauconite, siderite, pyrite, and some carbonates such as ankerite. Although one usually associates Fe with such common minerals as siderite and pyrite, in the Venezuelan well Fe was a diagnostic indicator of the clay mineral illite (M. Herron, 1986) and this may be an important, overlooked residence. The presence of glauconite in cores provides strong, non-fossil evidence of a marine depositional environment. Similarly, the distinction between siderite and pyrite in shales is an important clue to diagenetic history (e.g. Berner, 1984). Evidence suggests that the Fe content of kaolinites is related to the degree of structural disorder or crystallinity (Mestdagh et al., 1978), and similar relationships may exist for other clay minerals. If so, iron may be critical in establishing whether subsurface clays are detrital or authigenic.

### 4. Sulfur

Sedimentary sulfur resides in the sulfate form as gypsum or anhydrite, in the sulfide form, mainly as pyrite, and as native sulfur. Because of the multitude of naturally occurring valence states, sulfur is diagnostic of oxidizing and reducing conditions of the past. Berner and Raiswell (1984) have suggested that the ratio of carbon to pyrite sulfur in sediments may distinguish marine from fresh water sediments. In addition, S is an important constituent of many heavy oils and may be linked to the viscosity of the oil.

### 5. Potassium

The major potassium bearing minerals in sedimentary rocks are potassium feldspar and the clay minerals illite and mixed-layer illite/smectite. Micas such as muscovite and biotite contain abundant K but are only locally important. Because illite and K-feldspar are such major constituents of sediments, their identification and quantification are of great importance. In addition, there are many reports that smectite diagenetically alters to illite and the greater potassium content of older shales compared to more recent ones corresponds to this. This alteration has been cited as a probable cause for some cases of overpressuring, a dangerous

occurrence if unforeseen. It has been suggested that the conditions for this alteration may be somewhat similar to the conditions for oil generation from kerogen.

## 6. Chlorine

As described earlier, one of the key elements of formation evaluation is the estimation of water saturation from resistivity measurements. The resistivity depends strongly on the porosity, the water saturation, the conductivity of the water (related to its impurity content), and less strongly on the conductivity of clay minerals. If a measure of the impurity content were available from geochemical logs, and particularly if that measurement investigated deeply into the formation, it would significantly enhance the interpretation of resistivity data.

## 7. Sodium

Sodium has three important sources in the subsurface: fluids, the mineral halite, and the mineral albite. Less common, but locally important mineral forms include trona, borax, and analcite. The comments on fluid chlorine also pertain to sodium. Albite, the sodium end member of plagioclase, is a common mineral in sediments, both as detrital material and as an important authigenic mineral.

## 8. Magnesium

The major mineral forms of Mg are dolomite and certain clay minerals, especially chlorite and smectites. Additional Mg is found in solid solution with many Ca minerals and in some evaporites. The comments above relating to the importance of establishing the degree of dolomitization hold for Mg as well.

## 9. Aluminum

Aluminum is the third most abundant element in the earth's crust and is a major component of all of the clay minerals, feldspars, and micas. The Al content of these minerals varies over about a factor of 3 from low Al chlorites (ca. 7%) to kaolinite (20%), while it is absent in quartz. Thus, Al is a very diagnostic element for sedimentary geochemistry.

## 10. Thorium

Thorium is a trace element, with crustal abundances averaging only about 10 ppm, yet it has significant diagnostic power and can be routinely determined in the subsurface from the

gamma-ray emissions of daughter radionuclides. The major sources of Th are the clay minerals and heavy minerals. Th concentrations in feldspars are quite low. Thus, Th is an excellent adjunct element for aluminum. Indeed, Th shows a strikingly high correlation with Al in samples without much feldspar or heavy minerals. The thorium content of the clay minerals is ill-defined at present, with wide ranges often quoted (Fertl, 1979). However, it has been suggested that the Th content of some clay minerals may be directly related to their degree of lattice disorder (M. Herron, 1986). If this proves correct, it might prove possible to determine the crystallinity as well as the abundance of some clays.

## 11. Hydrogen

Hydrogen is an important constituent of all pore fluids, but the hydrogen content of water and oil is so similar as to be non-diagnostic in logging, and there are already geophysical means of estimating the total porosity. However, the hydrogen content that is not part of the fluids is of great diagnostic value. Common hydrous minerals include all clays, micas, gypsum, and opal. The total hydrogen minus the pore hydrogen can be a valuable input for diagnosing clay mineralogy.

## 12. Silicon

Silicon is the second most abundant element in the earth's crust, behind oxygen, and is a major component of sands and shales, which comprise about 85-90% of sediments. Its major role in so many minerals, however, limits the diagnostic power of the element somewhat. Many common minerals have Si concentrations between 20 and 30%, while the Si content of pure quartz is only increased to 47%. Proper identification of the quartz content in a sediment would be enhanced by an accurate Si determination, but it would still require other supplementary elemental data.

## 13. Boron

Boron is also a trace element in the earth's crust. Its major sources are clay minerals, some evaporites such as borax, and some heavy minerals such as tourmaline. As with other heavy minerals, tourmaline is concentrated in environments that remove very fine grained material. Boron is found in clay minerals most strongly associated with illite and related glauconite, so it has some diagnostic power for clay mineralogy. Boron has been used in the past as a paleosalinity indicator, the theory being that the adsorption of B by illite was related to the boron content of the water, which in turn reflects the salinity (Reynolds, 1965).

#### 14. Zirconium & Hafnium

The source of these elements is overwhelmingly the heavy mineral zircon. Because of this, these elements, though occurring in trace quantities, do not have the complications for heavy mineral interpretation that Ti, B, the REE, Th, and U have. Because the two elements invariably occur together, they are equally diagnostic and are not listed separately.

#### 15. Uranium

Uranium, like thorium, is present in most formations at only trace abundances. However, the Th/U ratio has been shown to be diagnostic of certain depositional environments, and this increases the value of subsurface U measurements. The major sources of subsurface U are the clay minerals, organic matter, and some heavy minerals. Th and U in tetravalent states have very similar chemical properties and thus covary in many igneous mineral suites with a Th/U ratio generally close to their abundance ratio of 3.5. However, in oxidizing environments, U can be converted to a mobile +6 valence and be leached from the formation while Th remains inert, resulting in an increased Th/U ratio. In marine reducing environments containing abundant organic matter, U is apparently adsorbed on or complexed to the organic matter resulting in a low Th/U ratio and, frequently, a correlation between U and organic carbon. Uranium is also an important element for source rock and oil shale evaluation.

#### 16. Titanium

Titanium is a minor element in sediments, typically occurring at levels less than 1% by weight. The major sources of titanium in sediments are clays and heavy minerals, especially rutile and anatase. Since many heavy minerals show strong correlations, non-clay Ti may be correlated to other heavy minerals.

#### 17. Rare Earth Elements

The rare earth elements (REE) occur in trace abundances in common sediments. The major sources are the clays, feldspars, and certain phosphate minerals such as the common heavy mineral monazite. Light rare earth elements (LREE) are typically adsorbed by clays and removed quickly from seawater. Heavy rare earth elements (HREE), on the other hand, can form stable hydroxide complexes and remain soluble in seawater. Thus, deep ocean shales have a lower LREE/HREE ratio than do nearshore shales. Again, this may prove to be valuable information for depositional environment reconstruction. The REE elements also have very large thermal neutron capture cross sections, impacting both the direct measure of cross

section, and also other neutron measurements, such as 'neutron porosity.' Modeling of these parameters is greatly hindered by an absence of information about the concentrations of effective thermal neutron absorbers.

#### 18. Vanadium

Vanadium is a trace element whose major sources are clay minerals and certain organic matter such as heavy oil, the organics in some oil shales, and kerogens. V has a strong tendency to replace the Mg in certain porphyrin compounds typically found in the asphaltene fraction of organic matter. During processes which remove or destroy the light hydrocarbon fraction, the asphaltenes may be relatively unaffected and thus comprise a larger fraction of the total hydrocarbon. In some heavy crudes, the V content has frequently been linked to the viscosity of the oil, higher V indicating greater viscosity. Vanadium may also be important in source rock evaluation, particularly when combined with other information.

## CONCLUSIONS

This has been a brief tour through some important current and future applications of geochemical data in the subsurface. The critical point for all of the applications of geochemical data is not that all of the transforms are known or even that absolutely universal transforms exist, but rather that there is great potential for expanding and enhancing formation evaluation through the use of geochemical data. Applications are being developed and tested using geochemical data and the ground truth provided by laboratory measurements. Some of these applications have been attempted in the past using specific elemental concentrations or non-specific chemical data such as the total natural gamma-ray activity. In certain cases, the use of elemental data to derive mineralogical properties without first deriving the mineral abundances can be legitimate. Properties that can be expressed as linear combinations of some minerals, such as the cation exchange capacity or the total volume of clay minerals, can also be expressed as linear combinations of some elements. This follows from the fact that the mineral abundances themselves can be expressed as linear combinations of the elements. In general, however, applications based on only one or two elements will have very limited application and low reliability.

The ability to detect more diagnostic elements, and the reduction of measurement uncertainty, will permit the development of models capable of interpreting more minerals and perhaps even the degree of crystallinity of the clay minerals. As larger models are developed, the question of widespread or even world-wide applicability can be more fully addressed and the role of

adsorption more carefully considered. While there are far more naturally-occurring minerals than elements, the number of significant minerals is small enough as to be approachable using these techniques. The timely development of models will go hand in hand with the development of downhole analytical techniques for elemental analysis. Clearly, the ultimate usefulness of geochemical information in the petroleum industry will strongly depend on our ability to quantify the raw measurements in terms of elemental concentrations. The examples presented here clearly show the immense potential of geochemical measurements for providing abundant, vitally important information that will eventually result in a significant enhancement in the evaluation of sedimentary formations.

## References

- Adams, J. A. S. and Weaver, C. E. (1958) "Thorium-to-uranium ratios as indicators of sedimentary processes: Example of concept of geochemical facies," *Bulletin of the American Association of Petroleum Geologists*, 42, 387-430.
- Berner, R. A. (1984) "Sedimentary pyrite formation: An update," *Geochimica et Cosmochimica Acta*, 48, 605-615.
- Berner, R. A. and Raiswell, R. (1984) "C/S method for distinguishing freshwater from marine sedimentary rocks," *Geology*, 12, 365-368.
- Carson, B. and Arcaro, N. P. (1983) "Control of clay-mineral stratigraphy by selective transport in Late Pleistocene-Holocene sediments of Northern Cascadia Basin - Juan de Fuca Abyssal Plain: Implications for studies of clay-mineral provenance," *Journal of Sedimentary Petrology*, 53, 395-406.
- Cody, R. D. (1971) "Adsorption and the reliability of trace elements as environment indicators for shales," *Journal of Sedimentary Petrology*, 41, 461-471.
- Couch, E. L. (1971) "Calculation of paleosalinities from boron and clay mineral data," *Bulletin of the American Association of Petroleum Geologists*, 55, 1829-1837.
- Davies, D. K. and Ethridge, F. G. (1975) "Sandstone composition and depositional environment," *American Association of Petroleum Geologists Bulletin*, 59, 239-264.
- Desborough, G. A., Pitman, J. K., and Huffman, C., Jr. (1976) "Concentration and mineralogical residence of elements in rich oil shales of the Green River Formation, Piceance Creek Basin, Colorado, and the Uinta Basin, Utah - A preliminary report," *Chemical Geology*, 17, 13-26.
- Dypvik, H. and Eriksen, D. Ø. (1978) "Natural radioactivity of clastic sediments and the contributions of U, Th, and K," *Journal of Petroleum Geology*, 5, 409-416.
- Everett, R. V., Herron, M. M., and Pirie, G. (1983) "Log responses and core evaluation case study technique: Field and laboratory procedure," *Transactions of 24th Society of Professional Well Log Analysts Annual Meeting, Calgary*.
- Everett, R. V., Herron, M. M., Pirie, G., Schweitzer, J. and Edmundson, H. (1985) "Faja case study results on a single well - MFM-7S," *60th Annual Fall Technical Conference of the Society of Petroleum Engineers of AIME, Las Vegas, September 22-25, SPE 14176*.

- Fertl, W. (1979) "Gamma ray spectral data assists in complex formation evaluation," Transactions, 6th European Formation Evaluation Symposium, Society of Professional Well Log Analysts, London, March 1979; also Log Analyst, Nov-Dec 1979.
- Furst, M. (1981) "Boron in siliceous materials as a paleosalinity indicator," *Geochimica et Cosmochimica Acta*, 45, 1-13.
- Garrels, R. M. and Lerman, A. (1981) "Phanerozoic cycles of sedimentary carbon and sulfur," Proceedings of the National Academy of Science of the USA, 78, 4652-4656.
- Gromet, L. P., Dymek, R. F., Haskin, L. A., and Korotev, R. L. (1984) "The 'North American shale composite': Its compilation, major and trace element characteristics," *Geochimica et Cosmochimica Acta*, 48, 2469-2482.
- Herron, M. M. (1986) "Mineralogy from geochemical well logging," *Clays and Clay Minerals*, in press.
- Herron, S. L. (1986) "A total organic carbon log for source rock evaluation," Transactions of Twenty-Seventh Annual Society of Professional Well Log Analysts Annual Meeting, Houston.
- Hilton, J. and Gibbs, M. M. (1985) "The horizontal distribution of major elements and organic matter in the sediment of Esthwaite Water, England," *Chemical Geology*, 47, 57-83.
- Hitchon, B. and Filby, R. H. (1984) "Use of trace elements for classification of crude oils into families - Example from Alberta, Canada," *American Association of Petroleum Geologists Bulletin*, 68 (7), 838-849.
- Kapo, G. (1978) "Vanadium: Key to Venezuelan fossil hydrocarbons," in 'Bitumens, asphalts and tar sands' (Chilingarian and Yen, eds.), Elsevier, New York, pp. 213-241.
- Kralik, M. (1984) "Effects of cation-exchange treatment and acid leaching on the Rb-Sr system of illite from Fithian, Illinois," *Geochimica et Cosmochimica Acta*, 48, 527-533.
- Leventhal, J. S. and Hosterman, J. W. (1982) "Chemical and mineralogical analysis of Devonian black-shale samples from Martin County, Kentucky; Carol and Washington Counties, Ohio; Wise County, Virginia; and Overton County, Tennessee," *Chemical Geology*, 37, 239-264.
- Lewan, M. D. (1984) "Factors controlling the proportionality of vanadium to nickel in crude oils," *Geochimica et Cosmochimica Acta*, 48, 2231-2238.
- Lock, G. A. and Hoyer, W. A. (1974) "Carbon/Oxygen (C/O) log: Use and interpretation," *Journal of Petroleum Technology*, Sept.
- Lonnie, T. P. (1982) "Mineralogic and chemical composition of marine, nonmarine, and transitional clay beds on south shore of Long Island, New York," *Journal of Sedimentary Petrology*, 52, 529-536.
- Mellor, D. W. and Underwood, M. C. (1985) "Formation properties from high resolution neutron activation gamma-ray spectra," Transactions of Twenty-Sixth Society of Professional Well Log Analysts Annual Meeting, Dallas.
- Mestdagh, M. M., Vielvoye, L., and Herbillon, A. J. (1980) "Iron in kaolinite: II. The relationship between kaolinite crystallinity and iron content," *Clay Minerals*, 15, 1-13.
- Mosser, Ch., Leprun, J. C., and Blot, A. (1985) "Les éléments traces des fractions <math><2\mu\text{m}</math> à kaolinite et smectite formées par altération de roches silicatées acides en Afrique de l'Ouest (Sénégal et Haute-Volta)," *Chemical Geology*, 48, 165-181.

- Murali, A. V., Parthasarathy, R., Mahadevan, T. M., and Sankar Das, M. (1983) "Trace element characteristics, REE patterns and partition coefficients of zircons from different geological environments - A case study on Indian zircons," *Geochimica et Cosmochimica Acta*, 47, 2047-2052.
- Peveararo, R. C. A. and Russell, K. J. (1984) "Interpretation of wireline log and core data from a mid-Jurassic sand/shale sequence," *Clay Minerals*, 19, 483-505.
- Pirkle, E. C., Pirkle, F. L., Pirkle, W. A., and Stayert, P. R. (1984) "The Yulee heavy mineral sand deposits of northeastern Florida," *Economic Geology*, 79, 725-737.
- Premovic, P. I. (1984) "Vanadyl ions in ancient marine carbonaceous sediments," *Geochimica et Cosmochimica Acta*, 48, 873-877.
- Reynolds, R. C. (1965) "The concentration of boron in Precambrian seas," *Geochimica et Cosmochimica Acta*, 29, 1-23.
- Riley, K. W. and Saxby, J. D. (1982) "Association of organic matter and vanadium in oil shale from the Tootlebut Formation of the Eromanga Basin, Australia," *Chemical Geology*, 37, 265-275.
- Scott, H. D. and Smith, M. P. (1973) "The aluminum activation log," *Transactions of Fourteenth Society of Professional Well Log Analysts Annual Meeting, Houston*.
- Snyder, D. D. and Fleming, D. B. (1985) "Well logging - A 25-year perspective," *Geophysics*, 50, 2504-2529.
- Tardy, Y. (1975a) "Element partition ratios in some sedimentary environments. I- Statistical treatments," *Sci. Géol. Bull.*, 28, 59-73.
- Tardy, Y. (1975b) "Element partition ratios in some sedimentary environments. II - Studies on North American black shales," *Sci. Géol. Bull.*, 28, 75-95.
- von Englehardt, W. (1977) *The origin of sediments and sedimentary rocks*, Halsted Press, 359 pp.
- Waxman, M. H. and Smits, L. J. M. (1968) "Electrical conductivities in oil-bearing shaly sands," *Society of Professional Engineering Journal*, 243, 107-122.
- Weber, K. J. (1971) "Sedimentological aspects of oil fields in the Niger Delta," *Geologie en Mijnbouw*, 50, 559-576.
- Westaway, P., Hertzog, R., and Plasek, R. E. (1980) "The gamma spectrometer tool inelastic and capture gamma-ray spectroscopy for reservoir analysis," *Annual Fall Technical Conference of the Society of Petroleum Engineers of AIME, Dallas, SPE 9461*.



## Subsurface Geochemistry: II. Nuclear Data for Spectroscopic Analysis

J. S. Schweitzer  
Schlumberger-Doll Research, Ridgefield, CT 06877-4108, and

R. C. Hertzog and P. D. Soran  
Schlumberger Well Services, Houston, TX 77210-4594

### ABSTRACT

Geochemical analyses of subsurface formations can provide significant information about the minerals and the fluids contained in the rock. While most previous work has been based on the analyses of cores, significant advances have been made to provide such analyses from gamma ray spectroscopy data obtained in a well. Previous work on spectroscopic measurements in a well has largely concentrated on qualitative analysis or the detection of ore-grade minerals. A nuclear geochemical analysis, however, requires the quantitative measurement of elemental concentrations of trace elements, as well as major elements in widely varying concentrations. This requirement places extreme demands on the quality of the spectroscopic measurements, data rates, and relating observed gamma ray intensities to the original elemental concentration. The relationship between gamma ray intensities and elemental concentration is critically dependent on the specific  $(n,x\gamma)$  cross sections and their uncertainties. The elements of highest priority for geochemical analysis are considered with respect to the importance of competing reactions and the neutron energy regions that are most significant.

### INTRODUCTION

Historically, measurements made in subsurface formations have been oriented towards the identification of bulk properties of the rock or the identification of specific ore deposits. These measurements placed only limited demands on the nuclear cross sections needed to interpret the measurements. Geochemical analyses on subsurface formations tended to rely only on the laboratory analysis of cores retrieved from a well. However, because of heterogeneities, small cores are frequently unrepresentative of the rock as a whole,<sup>1,2)</sup> and the recovery of cores from deep wells or unconsolidated sands is both expensive and frequently unsuccessful.<sup>3)</sup> As a result of the difficulties associated with core retrieval and analysis, the ability to obtain accurate measurements from within a well continuously, as a function of depth, would contribute much to the quantitative analysis of subsurface formations. Recent advances in geochemical research<sup>4-8)</sup> have also shown how mineralogy of the rock and an analysis of the fluids in the rock could be obtained from an accurate elemental analysis of the subsurface formations. From the mineralogical analysis, many important properties of the geological strata can be obtained. It is obvious that such detailed analyses can also be used to evaluate specific coal or ore bodies.<sup>9-11)</sup> Except for the naturally occurring radioactive elements, Th, U, and K, all other elements can only be detected by induced radioactivity. The vast majority of attempts at determining elements in rocks have been based on neutron-induced reactions and the detection of gamma rays produced in the reaction. The gamma rays may be prompt, from  $(n,n'\gamma)$ ,  $(n,\gamma)$ , or  $(n,x\gamma)$  reactions, where  $x$  is typically  $\alpha$  or  $p$ . Occasionally  $(n,2n)$  reactions or  $(n,n'p)$

or (n,n' $\alpha$ ) reactions may be significant. Delayed gamma rays from unstable nuclear ground states or isomeric states may be produced in any of the above reactions. Therefore, spectroscopic measurements needed to obtain reliable elemental concentrations from subsurface measurements place severe demands on the nuclear cross sections required to convert gamma ray peak count rates to an elemental concentration.

Because of the nature of measurements in a well, certain fundamental constraints must be recognized. Borehole geometry tends to be long, narrow cylinders with severe constraints on the maximum diameter for any equipment lowered into a well. Thus, large diameter crystals, whether scintillators or semiconductors, cannot be used. Similarly, all sources must be restricted to the constraints on diameter. This is not too severe a problem for chemical neutron sources, such as  $^{252}\text{Cf}$  or AmBe, but is a severe problem when attempting to use an accelerator to produce neutrons such as with the d,t reaction ( $E_n \approx 14$  MeV). In addition, in deep wells the problems are further compounded by the high pressures and temperatures ( $T > 150$  °C). There are many descriptions in the literature<sup>6, 8, 9, 12-19</sup> of spectrometers that can be used under such conditions and the specifics of such spectrometers will not be discussed here. While many of the earliest spectrometers were based on NaI(Tl) detectors, the evaluation of many ore-grade minerals and general mineral and fluid analysis requires the energy resolution provided by Ge detectors. In all the following discussions, we will deal only with the question of gamma ray analysis when Ge detectors are used.

A further complication in obtaining accurate elemental analysis of the rock is the presence of the borehole itself, which frequently contains elements that are also present in the rock. Correcting for the presence of material in the hole is not a trivial problem.<sup>20-23</sup> It can be solved generally only through accurate cross section data or extensive calibrations. We will not be concerned here with this problem, though many features of the problem will be addressed in the context of understanding the relationship between gamma ray spectral yields and the concentration of elements in the minerals and the fluid.

Finally, it should be clear that these types of measurements correspond to a neutron point source in an almost infinite medium. Thus the neutron flux has both a spatial and an energy dependence, resulting in a complicated source distribution for any particular gamma ray. While a number of attempts have been made to address this problem,<sup>10, 11, 24-26</sup> successfully relating gamma ray intensities to elemental source contributions still requires significant research.

## **GAMMA RAY CROSS SECTIONS FOR SIGNIFICANT ELEMENTS**

The main elements of interest for a geochemical analysis, such as shown in Table 1, are the dominant elements in the earth's crust as well as a few of the trace elements as noted by Herron.<sup>5</sup> Obviously, when logging for particular minerals as ores, the elements in the ore take on a singular importance. Many of the problems specific to mineral logging, such as the lack of any fluid in the rock, have been reviewed by Senftle,<sup>9</sup> and are atypical of the situation in general geochemical analyses of the subsurface. We shall concentrate on the the general problems associated with the analysis of subsurface formations using nuclear geochemical logging.

### **Neutron Capture Reactions**

Before considering specific elements and reaction cross sections, it would be useful to review certain basic features of downhole measurements of neutron-induced gamma ray spectroscopy. Many elements can be detected through thermal neutron

Table 1. Geologically significant elements.

ELEMENT	PRINCIPAL GEOCHEMISTRY
H	H <sub>2</sub> O, hydrocarbons, clays, micas
O	silicates, carbonates, clays, ...
Si	silicates, clays, micas, ...
Al	some silicates, feldspars, clays, micas
Fe	some silicates, siderites, hematite, chlorite, feldspars, micas
Ca	carbonates, phosphates, smectite, anhydrite
Na	feldspars, smectite, NaCl
K	K-feldspars, illite, micas
Mg	some silicates, dolomite, chlorite, smectite, micas

capture reactions. The detection of thermal neutron capture gamma rays can be accomplished through either time gating of a d,t accelerator source or through the use of chemical sources. The best source for this purpose is <sup>252</sup>Cf since it has the lowest mean energy (2 MeV) of commonly available neutron sources, and its flux will be easily thermalized, without the accompanying fast neutron induced reactions. For example, compare source neutron spectra from <sup>241</sup>AmBe<sup>(27)</sup> and <sup>252</sup>Cf<sup>(28)</sup> as shown in Figures 1 and 2. The relationship between the element concentration and the yield of the capture gamma ray will be proportional to:

$$Y_i(\gamma) \sim \frac{\eta_i \sigma(i)}{\Sigma}$$

The macroscopic cross section  $\Sigma$  can be determined either in a separate measurement<sup>(29-31)</sup> or simultaneously<sup>(32)</sup> while obtaining neutron capture spectra. The uncertainty on the elemental concentration will be directly related to the uncertainty in the microscopic thermal capture cross section  $\sigma(i)$  and the uncertainty in the measurement of  $\Sigma$  (typically ~ 5%). If timing with a pulsed neutron source is used to separate out the thermal neutron capture reactions, then no other reaction uncertainties affect the final elemental uncertainty. If the capture reactions are observed with a continuous source, such as a chemical source, certain gamma ray lines must be used with care as they may also be produced in competing (n,p) or (n, $\alpha$ ) reactions. The lower the energy of the neutron source, the less the competing reactions are a problem, thus making the <sup>252</sup>Cf source the best one for this purpose.

### Inelastic Neutron Induced Reactions

Prompt gamma rays produced by (n,n') reactions are also useful for determining elemental concentrations of the more abundant elements. All the fast neutron reaction cross sections tend to be proportional to the target nuclear size. There are no strong resonance behaviors that enhance the fast reaction rates significantly. Therefore, the

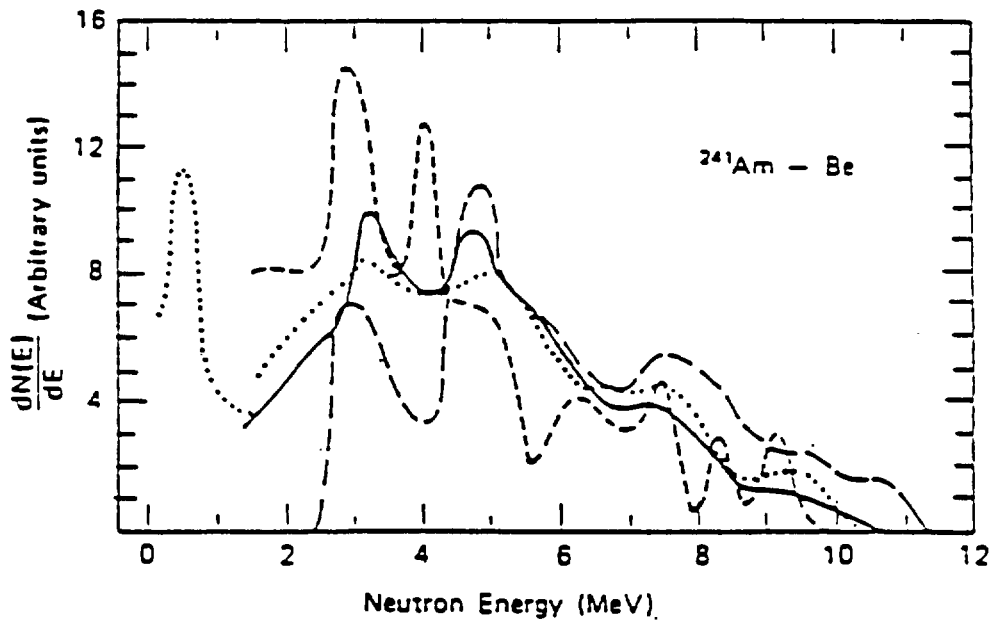


Figure 1.  $^{241}\text{Am}$ -Be spectrum.

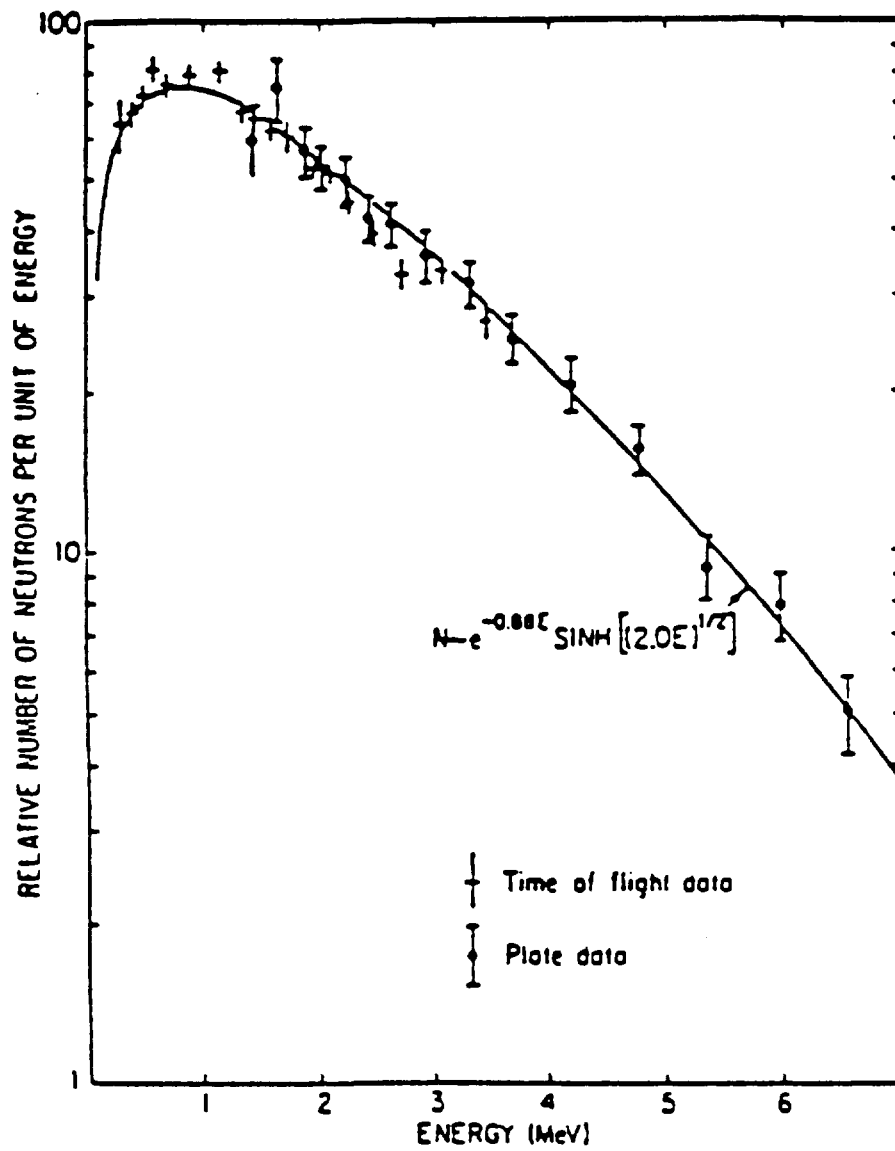


Figure 2.  $^{253}\text{Cf}$  spectrum.

relative gamma ray excitations are usually simply proportional to the elemental atomic concentrations in the formations. To minimize the background from neutron capture reactions, it is generally desirable to detect inelastic neutron induced (prompt) gamma radiation during the burst of a pulsed accelerator. However, a number of the important inelastic neutron scattering gamma rays are also produced by competing  $(n, x\gamma)$  reactions on other elements. With a 14 MeV neutron source, the 4.439 MeV gamma ray from  $(n, n')$  on  $^{12}\text{C}$  can also be produced from the  $(n, n'\alpha)$  reaction on  $^{16}\text{O}$ . Since there is generally much more O (typically over 3 times more oxygen than carbon) in the environment than C (with the exception of coal), the accuracy with which the C concentration can be determined is related to the accuracy with which the 4.439 MeV gamma ray production from O can be determined. Another problem that can exist when using inelastic reactions, especially for the less abundant elements, is the contamination from delayed activity which could produce the same gamma ray. This is most important where the abundance of the element, weighted by the appropriate flux-averaged cross section, is significantly larger than for the primary reaction. An example of such a case would be attempting to determine the aluminum concentration in a dolomitic rock ( $\text{CaMg}(\text{CO}_3)_2$ ) through the inelastic scattering to the first and second excited states of  $^{27}\text{Al}$  at .844 and 1.014 MeV. Both of these states are populated in the  $\beta^-$  decay of  $^{27}\text{Mg}$  produced in the  $^{26}\text{Mg}(n, \gamma)^{27}\text{Mg}$  reaction. In this case, it would be necessary to use only the lower intensity gamma rays from inelastic scattering to higher excited states. As before, in all inelastic reactions, the effective flux-averaged cross section needs to be determined. This requires a good knowledge of the high energy portion (above 1 MeV) of the neutron flux, which is determined by the details of the high energy neutron cross sections for all the elements present in the environment.

### Delayed Activation Reactions

The determination of elemental concentrations through neutron activation reactions and the observation of delayed activity has become a routine technique.<sup>33)</sup> When small samples are used in the thermal flux of a reactor, precise results can be obtained, since the small sample does not significantly perturb the neutron flux. In addition, the essentially completely thermal energy of the spectrum allows a direct identification of the element which captured a neutron to produce the observed gamma ray. In subsurface measurements, however, there is never a perfectly thermal energy distribution. Even with  $^{252}\text{Cf}$ , there is a sufficiently significant high energy component to the spectrum that the detection of small concentrations of a particular element can be significantly affected by the presence of a larger amount of neighboring ( $Z+1$ , and/or  $Z+2$ ) competing elements. Such an example would be the measurement of a small amount of Al through the delayed activity from the  $^{27}\text{Al}(n, \gamma)^{28}\text{Al}$  reaction when a significant fraction of this activity may actually be created from the  $^{28}\text{Si}(n, p)^{28}\text{Al}$  reaction. Figure 3 shows delayed activation spectra following irradiations with a  $^{252}\text{Cf}$  source and a 14 MeV source. The chlorine lines in both spectra are due to thermal capture. The increased intensity of the  $^{28}\text{Al}$  activity, relative to the chlorine activity, is due to the yield from the  $^{28}\text{Si}(n, p)^{28}\text{Al}$  reaction. The problem has increased from the level of a complication to a severe difficulty if a high energy neutron source is used<sup>34)</sup> to produce the delayed activity of primary interest. This is often desirable since there is a fixed maximum intensity that can be used with any chemical source because of safety considerations when handling the source at the surface. An accelerator based neutron source is only limited in intensity by the power available and the quality of the accelerator itself. Thus, one may be able to generate a number of orders of magnitude more neutron intensity and subsequently increased primary delayed activity by using an accelerator. This is a particular

26.4 pu SANDSTONE  
LABORATORY FORMATION  
10" BOREHOLE

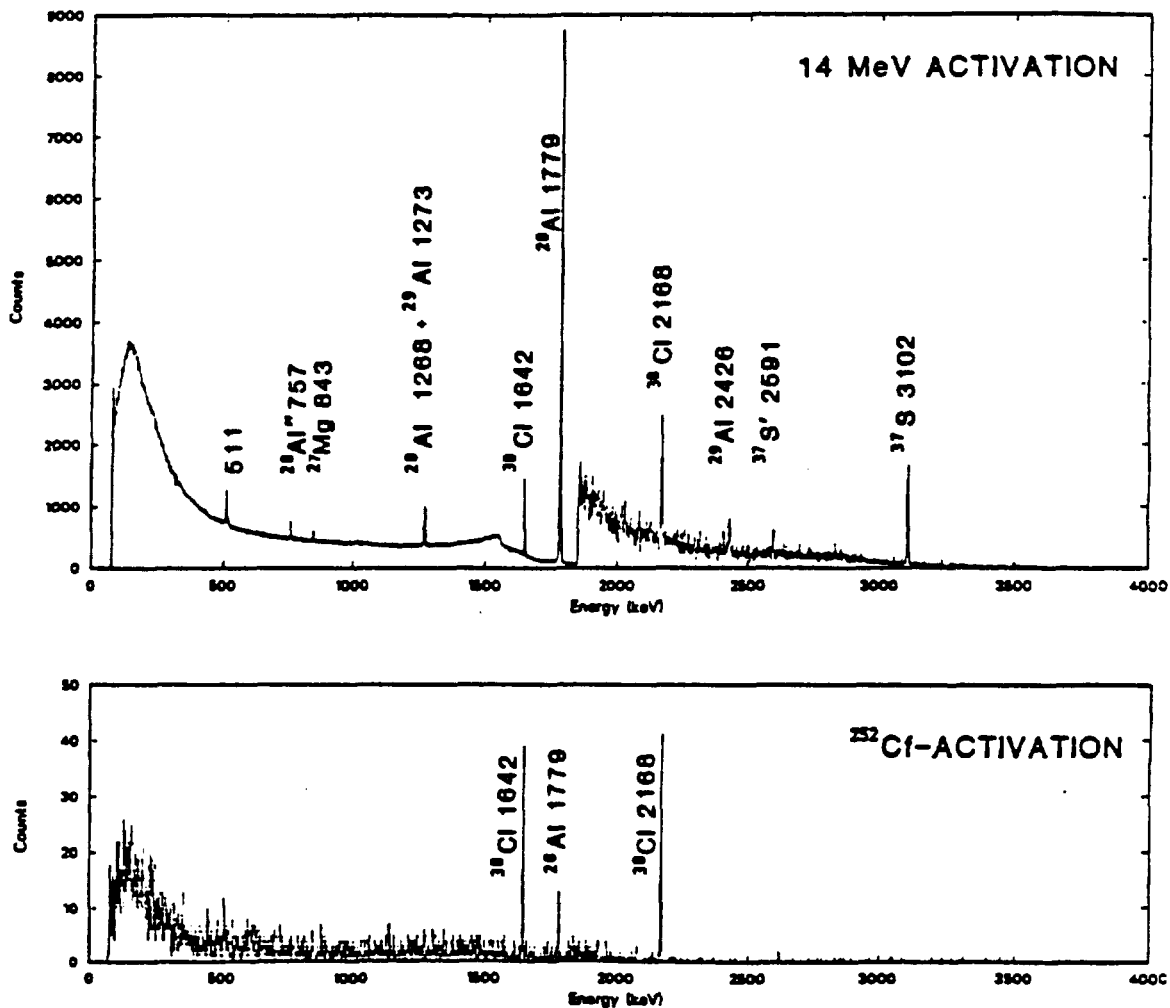


Figure 3. Delayed activation spectra following irradiation with a 14 MeV source and following irradiation with a  $^{252}\text{Cf}$  source.

advantage since time for measurements is always very restricted. However, the high energy neutrons create secondary (interfering) delayed activity which is often attributable to more than one element initially present in the region being analyzed. To make use of the increased primary activity requires accurate cross section data to resolve the relative contributions to a particular delayed gamma ray activity.

### Cross Section Uncertainties

In recent years many groups have begun modeling the evolution of neutron fluxes through extended media and the detection of radiation from such an extended source.<sup>35)</sup> All neutron cross sections are necessary for these calculations from the source energy to thermal energies. Frequently, for even simple problems the uncertainties in currently evaluated cross section libraries result in an uncertainty that is completely unacceptable. A recent study has shown that the  $^{28}\text{Al}$  activity created by the thermal capture of  $^{27}\text{Al}$  must be corrected for the  $^{28}\text{Si}(n,p)^{28}\text{Al}$  reaction, especially when a 14 MeV neutron source is used. When the  $^{28}\text{Si}$  concentration is determined from the  $^{29}\text{Si}(n,p)^{29}\text{Al}$  delayed activity, an error of  $\pm 100\%$  could typically be obtained

in the derived aluminum concentration, when there are uncertainties of about  $\pm 20\%$  in the two Si (n,p) cross sections.<sup>34)</sup> A more severe problem is present when more than two delayed activities must be coupled to derive a set of elemental concentrations.<sup>36)</sup> Studies such as these can also be used to determine the most important energy regions for improved precision in cross sections.

When discussing uncertainties in cross sections, it is important to realize which uncertainties are actually important. As an illustration we consider the case of delayed activity of  $^{28}\text{Al}$  and  $^{29}\text{Al}$  created from the presence of both Al and Si in the rock under study. To simplify the discussion, assume that the relevant activities at the end of irradiation have been determined. The amount of  $^{28}\text{Al}$  created will be given by:

$$Y(^{28}\text{Al}) = I_{\text{Al}} \eta_{\text{Al}} + I_{\text{Si}} \eta_{\text{Si}} + I_{\text{P}} \eta_{\text{P}}$$

where  $\eta_i$  represents the concentration of the elements in the measurement volume.  $I_i$  represents the flux integrated production cross section

$$I_i = \int_E \int_V \sigma_i(E) \Phi_n(E, \mathbf{r}) dE dV$$

where  $\sigma_i$  is the energy dependent cross section for producing  $^{28}\text{Al}$  from element  $i$  and  $\Phi_n(E, \mathbf{r})$  is the energy dependent neutron flux distribution. The amount of  $^{29}\text{Al}$  will be given by:

$$Y(^{29}\text{Al}) = I_{\text{Si}} \eta_{\text{Si}}$$

The uncertainty on the Si concentration determined by this method will be governed by the absolute error in the  $^{29}\text{Si}(n,p)^{29}\text{Al}$  cross section. However, if we solve these equations for the Al concentration:

$$I_{\text{Al}} \eta_{\text{Al}} = \text{Yield}(1.779 \text{ MeV}) - K \cdot \text{Yield}(1.273 \text{ MeV})$$

where

$$K = \frac{(\text{abundance } ^{28}\text{Si}) \cdot (\text{reaction rate } ^{28}\text{Si})}{(\text{abundance } ^{29}\text{Si}) \cdot (\text{reaction rate } ^{29}\text{Si})}$$

We find that the uncertainty on the Al concentration is governed by the absolute uncertainty in the thermal capture cross section, but only the relative error in the two Si (n,p) cross sections. Naturally, these considerations assume that there are no uncertainties in the neutron flux distributions  $\Phi_n(E, \mathbf{r})$  which, in turn, is based on the assumption that there are no uncertainties in the neutron scattering and reaction cross sections.

For a source in which  $E_n(\text{average}) > \text{few MeV}$ , the energy region near  $E_n(\text{average})$  is always important for determining the uncertainty in the total reaction rate. Other regions are important where either the specific cross sections are strongly varying or the neutron flux has a local maximum. These considerations led to the conclusion that the Si (n,p) cross sections needed to be more precisely determined in the energy regions between 6 and 8 MeV and 11 and 14 MeV when measurements are performed with 14 MeV neutrons.<sup>34)</sup>

### Spectroscopic Interferences

Interfering reactions can be thought of as two types. The type discussed above involves interfering contributing parent nuclei that lead to the actual production of the same nuclear state from different reactions involving different initial elements. An example of this type of interference is the 4.439 MeV carbon gamma ray produced from both carbon and oxygen or the delayed  $^{28}\text{Al}$  activity produced from either Al or

Si. The other type of interference is spectral interference, which occurs when entirely different nuclear states produce gamma rays that are too close in energy to distinguish with a given system resolution, e.g.  $\sim 3$  keV for Ge, such as the 843.8 keV gamma ray from the decay of the first excited state of  $^{27}\text{Al}$  and the 846.8 keV gamma ray from the decay of the first excited state of  $^{56}\text{Fe}$ . This problem occurs most frequently in  $(n,\gamma)$  reactions, but it is generally not too important as there are usually many other gamma rays produced which can be used to determine the concentration of the element. In addition, armed with good information on branching ratios, one can use isolated peaks (non-interfered) to compute the contributions in the competing portions of the spectra leading to a separation of the relative components.

However, it is crucial to know the possible interferences to ensure that the gamma rays used for determining the elemental concentrations are indeed only from one element. When such interferences occur in delayed activity, it is frequently possible to separate out the components by taking time-dependent spectra and performing a half life analysis on the observed summed intensity.

Many of the factors which govern the spectroscopic analysis in boreholes can be most easily seen by discussing the methods for detection of particular elements. The actual cross section data, uncertainties, and identifiable additional needs will be discussed in a later section, though an overall picture will evolve from the discussions of particular elements. There is frequently more than one way to observe a particular element. The choice of an optimum technique will frequently depend on the elemental concentration, details of the spectrometer, and the total set of elements which are needed for a particular application. However, general guides can be established for particular circumstances<sup>37)</sup> to compare sensitivities for particular spectrometer configurations.

## SPECIFIC ELEMENTS

For general geochemical analysis, there can be different opinions of whether a particular element is important. However, we have selected as a starting point the elements mentioned by Herron<sup>3)</sup> which have a broad applicability not dependent on the particular circumstances. For each element, the primary reaction mechanisms will be reviewed and the significant interferences will be discussed to provide the information needed to determine the needs for particular cross section data and improved uncertainties. Without discussing the cross section implications specifically, the determination of the flux distribution  $\phi_n(E,r)$  requires both scattering and reaction cross sections for all energies  $E_n \leq E_s$  where  $E_s$  is the maximum neutron energy from the source. For fission type source spectra, the needs for data at the highest energies is not as critical as for line or more strongly structured neutron sources. In addition to total cross sections, angular distributions are particularly important for scattering cross sections.

### Hydrogen

Hydrogen can only be detected spectroscopically through the neutron capture reaction. There are no significant interfering reactions under normal geological conditions.

### Boron

When boron can be detected, it would be through the prompt  $^{10}\text{B}(n,\alpha)^7\text{Li}$  reaction to the first excited state with the production of a 478 keV gamma ray. The main

difficulty for the quantitative analysis of B is the large background in this region of the prompt spectrum relative to the typical concentrations of B in the environment. In addition, some Ge crystal assemblies contain B which provides a constant background rate, which must be corrected in the observed spectra.

### Carbon

The dominant reaction for the detection of carbon is through the inelastic scattering to the 4.439 MeV state. In higher carbon concentrations, use of the carbon capture lines is frequently practical. Analyses performed for the evaluation of coal<sup>10, 11)</sup> have been the ones which have generally used the capture gamma ray technique. The only significant interference for the inelastic measurement is the  $^{16}\text{O}(n,n'\alpha)^{12}\text{C}$  reaction. This is primarily a concern because of the almost uniformly large O concentration in sediments.<sup>32, 38)</sup>

### Oxygen

While oxygen can readily be detected through the  $^{16}\text{O}(n,p)^{16}\text{N}$  reaction delayed activity ( $E_\gamma = 6.13$  MeV,  $t_{1/2} = 7$  sec.), it is more generally detected through the inelastic scattering to the first excited state at 6.13 MeV. This is due to the general interest in determining the concentration of other elements in addition to O, which is essentially impossible through the delayed activity approach (though the oxygen signal will often still be present in longer delayed activity measurements, it is usually desirable to minimize the amount of background which would be introduced by the  $^{16}\text{N}$  delayed activity).

### Sodium

Na concentrations are typically not very high and while detection can occasionally be achieved through thermal neutron capture spectroscopy, the most efficient technique is generally through delayed activation. When using a  $^{252}\text{Cf}$  source, only a minor correction needs to be made for the contribution to the sodium yield from the  $^{24}\text{Mg}(n,p)$  and  $^{27}\text{Al}(n,\alpha)$  reactions. However, if a substantially higher energy neutron source is used,<sup>36)</sup> then the corrections are more substantial and require accurate knowledge of the reaction cross sections for energies up to the maximum neutron source energy.

### Magnesium

Mg generally occurs at relatively small concentrations, except in dolomitic rocks. Thus inelastic scattering is usually not useful for determining Mg especially where substantial amounts of  $^{24}\text{Na}$  may be created from the presence of Na and Al in the environment. The low thermal capture cross section makes it difficult to detect Mg through thermal capture spectroscopy over most of its concentration range. The most efficient technique for Mg analysis is through the delayed  $^{27}\text{Mg}$  activity ( $E_\gamma = 844$  keV, 1014 keV,  $t_{1/2} = 9.5$  min.). This delayed activity is subject to potential interferences, both from the production of  $^{27}\text{Mg}$  in the  $^{27}\text{Al}(n,p)$  and  $^{30}\text{Si}(n,\alpha)$  reactions and from the delayed activity from  $^{56}\text{Mn}$  which has a strong line at 846 keV which frequently cannot be resolved spectroscopically from the lower energy (and higher intensity)  $^{27}\text{Mg}$  gamma ray. The latter interference often requiring time-dependent spectral analysis to achieve good sensitivity for the analysis of Mg concentration.

## Aluminum

Most downhole analyses of Al concentration rely on the delayed activity from  $^{28}\text{Al}$ .<sup>6, 39, 40)</sup> This is best achieved with the lowest energy chemical source. As the energy of the source increases, an increasing contribution to the  $^{28}\text{Al}$  activity is generated by the  $^{28}\text{Si}(n,p)$  reaction.<sup>34)</sup> Detection of Al by inelastic scattering is severely complicated by the decay of  $^{27}\text{Mg}$  delayed activity. It is sometimes desirable to detect Al through the thermal neutron capture reaction, though its low cross section may require lengthy accumulation times.

## Silicon

Si concentration can most readily be obtained from thermal neutron capture. However, if higher energy neutron sources are used, it will also be seen as delayed  $^{29}\text{Al}$  activity which is needed for correcting the  $^{28}\text{Al}$  activity<sup>34)</sup> for determining the concentration of aluminum. Si can also be detected in inelastic scattering, especially through the first excited state, but caution must be exercised as there may be significant yield of this gamma ray from the decay of  $^{28}\text{Al}$  from the  $^{27}\text{Al}(n,\gamma)$  and  $^{28}\text{Si}(n,p)$  reactions.

## Sulfur

The analysis of sulfur is most efficiently performed with the thermal neutron capture reaction. While delayed activity ( $^{37}\text{S}$ ) can be observed in a purely thermal flux, the large yield of  $^{37}\text{S}$  from the  $^{37}\text{Cl}(n,p)^{37}\text{S}$  reaction generally precludes the use of the delayed S activity in borehole applications, regardless of what type of source is used.

## Chlorine

Chlorine can most efficiently be observed through the thermal neutron capture reaction because of its large capture cross section compared with most sedimentary elements. However, it can also be observed in delayed activation induced through the  $^{37}\text{Cl}(n,\gamma)^{38}\text{Cl}$  reaction (unfortunately, the isotope with the low capture cross section) which is of use when a careful comparison with Na concentration is desired. When the delayed activity is used, some care must be exercised when the K/Cl concentration is large because of the  $^{41}\text{K}(n,\alpha)$  reaction.

## Potassium

The determination of potassium is almost always performed through the detection of the naturally radioactive  $^{40}\text{K}$ .<sup>41, 42)</sup>

## Calcium

Calcium is generally detected through the thermal capture reaction. However, calcium is one of the few elements whose capture gamma rays are subject to significant interferences from the capture gamma rays of other common sedimentary elements. The most intense capture line from Ca is at 1943 keV, which is close to chlorine capture lines at 1951 and 1958 keV. This line is also close to the Compton edge of the hydrogen capture line, which affects the statistical precision. The second most intense line at 6420 keV is very close to a prominent capture line of titanium<sup>11, 43)</sup> at 6418 keV, which is present in many sedimentary environments. Ca can also be determined from the delayed activity produced in the  $^{48}\text{Ca}(n,\gamma)$  reaction. However,  $^{48}\text{Ca}$  is very low abundance (0.19%) resulting in generally low count rates unless there is a very high neutron flux. With a sufficient flux of high energy neutrons, delayed Ca activity, such as from the  $^{44}\text{Ca}(n,p)^{44}\text{K}$  reaction<sup>44)</sup> which is free of contributions from

neutron-induced reactions on other stable elements, can be used to improve the precision of the analysis of Ca concentration.

### Titanium

Titanium detection is most efficient through the thermal capture gamma rays. However, as previously discussed, some care must be exercised because of the interferences between the titanium capture lines and those of other common sedimentary elements. Ti can also be detected through delayed activity from the  $^{50}\text{Ti}(n,\gamma)^{51}\text{Ti}$  reaction. For this delayed activity, the potential contributions to the delayed activity from the  $^{51}\text{V}(n,p)$  reaction and the  $^{54}\text{Cr}(n,\alpha)$  reaction are generally negligible because of the relatively small concentrations of V and Cr as compared to  $\text{Ti}^{51}$  under most circumstances.

### Vanadium

The only practical mode for determining the concentration of vanadium is through the thermal capture reaction on  $^{51}\text{V}$ . Some care is needed in using this technique for borehole analysis since the  $^{52}\text{V}$  delayed activity can also be created by the  $^{52}\text{Cr}(n,p)^{52}\text{V}$  and  $^{55}\text{Mn}(n,\alpha)^{52}\text{V}$  reactions. Mn is frequently present in greater abundance than the vanadium. Furthermore, all of these elements are likely to be contained in steels, so logging in cased holes or when the portion of the logging instrument near the detector can receive any neutron flux become major problems. However, with proper techniques, excellent sensitivity can be obtained<sup>43)</sup> for vanadium analyses.

### Chromium

Like many elements in this mass region, Cr has diagnostic high energy capture gamma rays<sup>46, 47)</sup> which are not subject to significant interferences. Thermal capture delayed activity is very weak, especially for the times that are practical for borehole observations. High energy neutron-induced delayed activities can be used,<sup>48, 49)</sup> but like most elements in this region, the delayed activities are subject to interferences from adjacent elements, requiring precise cross section data and complete analysis for all the elements in this group.

### Manganese

Manganese can generally be detected through the delayed activation from the  $^{55}\text{Mn}(n,\gamma)^{56}\text{Mn}$  reaction. With a well thermalized source, the only spectral interference is from the  $^{27}\text{Mg}$  delayed activity, which will generally require a half life analysis to separate the dominant peak. However, this delayed activity also contains other peaks that permit a quantitative analysis, even if the 846 keV line is impractical to use. When using higher energy neutron sources, a significant interference is produced from the  $^{56}\text{Fe}(n,p)^{56}\text{Mn}$  reaction. Resolution of the relative contributions from Mn and Fe requires the use of flux-integrated cross sections and the iron concentration as determined through neutron capture reactions, or by the analysis of additional activities, such as that from  $^{54}\text{Mn}$  which will have different relative production rates from Mn and Fe than will the  $^{56}\text{Mn}$  activity. However, this latter activity has a very long half life ( $t_{1/2} = 312.5$  days) requiring very intense, high energy sources for practical analyses.

### Iron

The iron thermal capture gamma ray spectrum provides the most direct and efficient means for determining iron concentration at all concentrations that are geochemically relevant. The primary peaks are all free of significant interferences.

## Heavier Elements

The heavier elements generally occur in low concentrations as compared with the elements previously discussed. Other than for U and Th, this condition, with a few exceptions,<sup>47)</sup> implies that detection is almost always through the analysis of delayed activation, whether induced by thermal capture or high energy reactions. U and Th have traditionally been analyzed by the naturally occurring radiation<sup>41, 42)</sup> (of daughter products in the decay series), and techniques have been developed to deal also with the disequilibrium problem in the uranium<sup>17)</sup> analysis.

## CROSS SECTION DATA

Accurate cross section data, both for reactions and scattering, are needed for two reasons. Before the reaction rates can be determined, it is necessary to generate the neutron flux distributions,  $\phi_n(E,r)$ , (an example of which is shown in Figure 4) throughout the geological formation.<sup>50)</sup> Once the flux has been determined, the reaction cross sections are then necessary to determine the reaction rates.

To perform neutron activation analysis calculations (growth and interference) it is necessary to have neutron cross section data and covariance information. For natural elements there is a reasonable data base for thermal, inelastic, and threshold reactions.<sup>51)</sup> Table 2 illustrates the thermal elastic and radiative capture cross sections

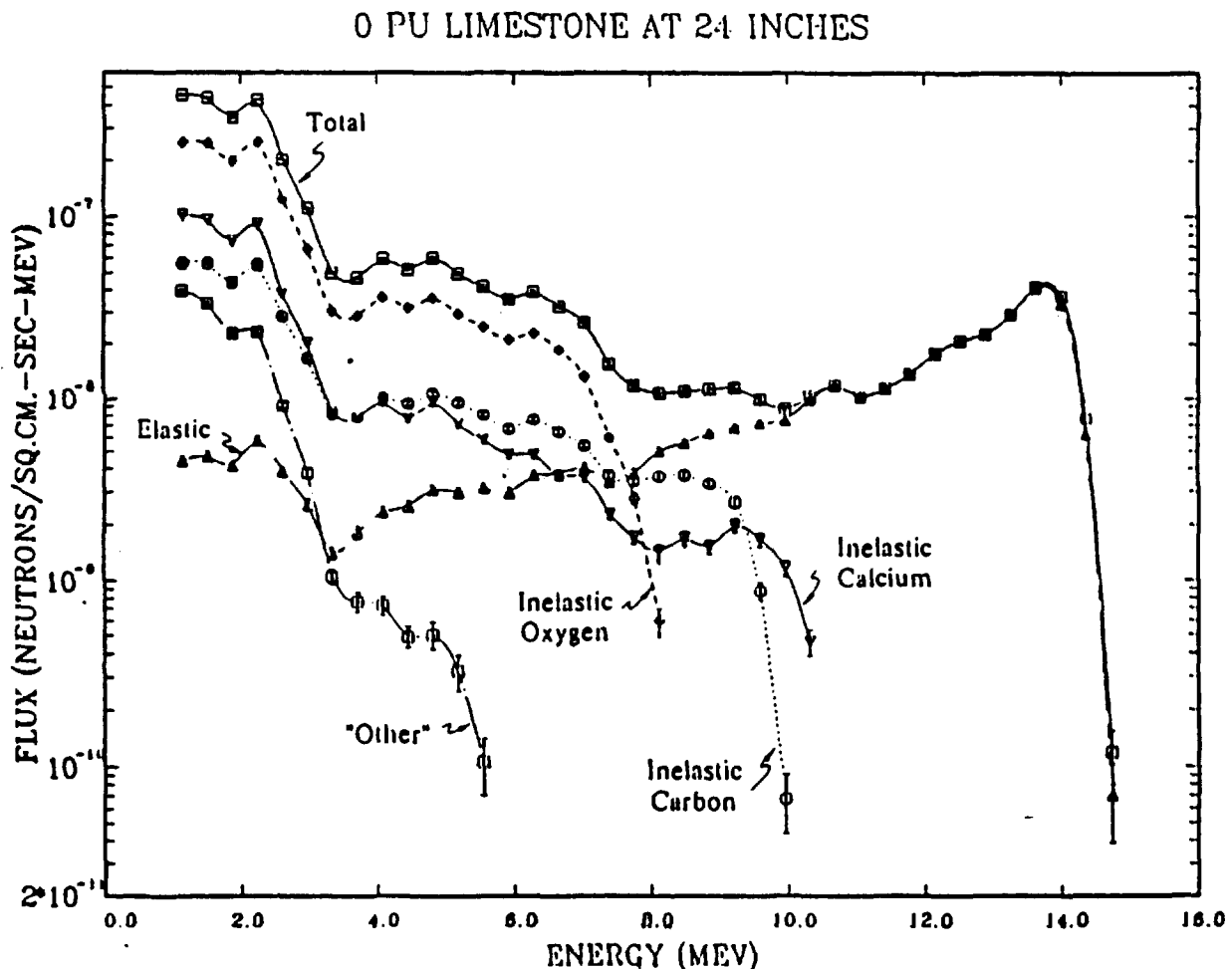


Figure 4. Typical neutron flux distribution showing the primary reaction mode governing each region of the spectrum.

Table 2. 2200 m/sec neutron scattering and capture cross sections.

Element or Isotope	Scattering Cross Section	Radiative Capture Cross Section
1-H-1	20.491 +/- 0.014 b	0.3326 +/- 0.0007 b
1-D-2	3.390 +/- 0.012 b	0.519 +/- 0.007 mb
1-T-3	1.70 +/- 0.03 b	< 0.006 mb
2-He	0.76 +/- 0.01 b	
2-He-3	3.10 +/- 0.13 b	0.031 +/- 0.009 mb
2-He-4	0.76 +/- 0.01 b	
3-Li	0.95 +/- 0.04 b	0.0448 +/- 0.0030 b
3-Li-6	0.75 +/- 0.02 b	0.0385 +/- 0.0030 b
3-Li-7	0.97 +/- 0.04 b	0.0454 +/- 0.003 b
4-Be-9	6.151 +/- 0.005 b	7.6 +/- 0.8 mb
5-B	4.27 +/- 0.07 b	0.10 +/- 0.04 b
5-B-10	2.23 +/- 0.06 b	0.5 +/- 0.2 b
5-B-11	4.84 +/- 0.04 b	5.5 +/- 3.3 mb
6-C-12	4.746 +/- 0.002 b	3.53 +/- 0.07 mb
7-N-14	10.05 +/- 0.12 b	75.0 +/- 7.5 mb
8-O-16	3.761 +/- 0.006 b	0.190 +/- 0.019 mb
9-F-19	3.641 +/- 0.010 b	9.6 +/- 0.5 mb
10-Ne	2.415 +/- 0.010 b	39 +/- 4 mb
11-Na-23	3.025 +/- 0.02 b	530 +/- 5 mb
12-Mg	3.4140 +/- 0.0024 b	0.063 +/- 0.003 b
13-Al-27	1.4134 +/- 0.0010 b	231 +/- 3 mb
14-Si	2.0437 +/- 0.0017 b	0.171 +/- 0.003 b
15-P-31	3.134 +/- 0.010 b	0.172 +/- 0.006 b
16-S	0.9787 +/- 0.050 b	0.52 +/- 0.01 b
17-Cl	15.8 +/- 0.2 b	33.1 +/- 0.3 b
18-Ar	0.647 +/- 0.003 b	0.675 +/- 0.009 b
19-K	2.04 +/- 0.10 b	2.1 +/- 0.1 b
20-Ca	2.93 +/- 0.04 b	0.43 +/- 0.02 b
21-Sc-45	22.4 +/- 0.4 b	27.2 +/- 0.2 b
22-Ti	4.09 +/- 0.03 b	6.09 +/- 0.13 b
23-V	4.8 +/- 0.1 b	5.08 +/- 0.04 b
24-Cr	3.38 +/- 0.01 b	3.07 +/- 0.08 b
25-Mn	2.2 +/- 0.2 b	13.3 +/- 0.2 b
26-Fe	11.35 +/- 0.03 b	2.56 +/- 0.03 b

and their corresponding experimental errors<sup>52)</sup> for several light elements. Examination of Table 2 shows that the experimental uncertainty is quite good for thermal data. It is possible to calculate the uncertainty in the thermal cross section data using the covariance information of ENDF/B-V. Table 3 is a subset of Table 2 which shows both the experimental and calculated uncertainties for a few geochemical elements of interest.

Unfortunately, there is very little evaluated nuclear dosimetry data and even less uncertainty data for those isotopes which do have evaluations. Table 4 shows 18 elements of geochemical interest; 15 of these elements have transport and some covariance data. However, in geochemical analysis isotopic cross section information is required. Table 5 depicts isotopes of interest along with the status of covariance information. Examination of the evaluated and experimental data<sup>54, 55)</sup> shows that the uncertainty is at best 30-50%. The number entries in the table refer to the notes below. Where data are found in ENDF/B-V transport or ENDL-85 transport, these data are used instead of tape 531, tape 532, or ACTL. In the column headed  $\sigma(n,n')$ , entries of  $\alpha$ ,  $p$ ,  $\alpha_1$ , or  $(3\alpha)$  refer to the existence also of  $\sigma(n,n'x)$  data, where  $x$  is given by the symbol shown.

Table 3. Partial list of geochemically important thermal cross sections and uncertainty estimates.

Elastic Scattering

Material	Cross Section (barns)	Uncertainty (%) COFILS-2 <sup>53)</sup>	Uncertainty (%) Experiment <sup>52)</sup>
6-C	4.739	0.2	0.04
8-O-16	3.748	1.4	0.16
11-Na-23	3.321	7.2	0.7
13-Al-27	1.348	1.03	0.07
14-Si	2.042	3.23	0.08
26-Fe	11.40	5.0	0.3

Radiative Capture

Material	Cross Section (barns)	Uncertainty (%) COFILS-2 <sup>53)</sup>	Uncertainty (%) Experiment <sup>52)</sup>
6-C	0.00336	6.0	2.0
8-O-16	0.00019	NA	10.0
11-Na-23	0.5272	2.0	0.9
13-Al-27	0.2317	4.2	1.3
14-Si	0.171	NA	1.8
26-Fe	2.556	2.0	1.2

Table 4. Elements of geochemical interest.

Material	Comments	Material	Comment
Ca	Table 5	Si	Table 5
H	No Competition	C	Table 5
Fe	Table 5	S	Table 5
K	Natural Activity	La	Table 5
Mg	Table 5	V	Table 5
Tb	Natural Activity	Hf	Not Detectable/No Competition
Al	Table 5	Zr	Not Detectable
Na	Table 5	U	Natural Activity
Sr	Not Detectable	Ti	Table 5

In the U.S. there are two public sources of dosimetry data: ENDF/B and ACTL. The ENDF/B data is from two sources: Tape 531 and Tape 532. The former data set contains 36 dosimetry reactions involving 26 target nuclei; however, only 11 target nuclei on Tape 531 have significant subsurface geochemical interest. Tape 532 contains 84 activation reactions involving 53 target nuclei; however, only 12 target nuclei on Tape 532 have significant geochemical interest. The evaluation techniques, format, and necessary preprocessing requirements<sup>53)</sup> are discussed elsewhere.

ACTL is an evaluated neutron activation cross-section library, from Lawrence Livermore National Laboratory. The evaluation techniques<sup>55)</sup> and the format of the

Table 5. Availability of dosimetry and uncertainty data.

Isotope	$\sigma(n,p)$	$\sigma(n,\alpha)$	$\sigma(n,\gamma)$	$\sigma(n,n')$	Covariance data
Ca-40	3	3	3	3 $\alpha,p$	N
Ca-42	3	3	3	3 $\alpha,p$	N
Ca-44	3	3	3	N	N
Ca-NAT	4,5	4,5	4,5	4,6	4,6
Fe-54	1,2,3	2,3	2,3	3 $\alpha,p$	N
Fe-56	1,3	1	3	3 $\alpha,p$	N
Fe-57	3	3	3	3 $\alpha,p$	N
Fe-58	3	3	1,2	3 $\alpha,p$	N
Fe-NAT	4,5	4,5	4,5	4,5	4,6
Mg-24	3	3	2,3	3p	N
Mg-25	3	3	3	N	N
Mg-26	3	3	3	N	N
Mg-NAT	4,5	4,5	4,5	4,5	4
Al-27	4,5	4,5	4,5	4,5	4
Na-23	4,5	4,5	4,5	4,5	4
Si-28	3	3	3	3 $\alpha,p$	N
Si-29	3,6	3	3	3 $\alpha,p$	N
Si-30	3,6	3	3	3 $\alpha,p$	N
Si-NAT	4,5	4,5	4,5	4,5	4,6
C-12	3	3	3	3(3 $\alpha$ )	N
C-13	3	3	3	3 $\alpha$	N
C-NAT	4,5	4,5	4,5	4,5	4
S-32	1,2,3	3	3	3p	N
S-33	3	3	3	3 $\alpha,p$	N
S-34	3	3	3	3 $\alpha,p$	N
S-36	3	3	3	3 $\alpha$	N
S-NAT	4,5	4,5	4,5	4,5	4
La-138	N	N	N	N	N
La-139*	N	N	2	N	N
V-50*	3	3	3	3 $\alpha,p$	N
V-51	3	3	3	3 $\alpha,p$	N
Ti-46	2	3	1	3 $\alpha,p$	N
Ti-47	1,2	3	3	3 $\alpha,p$	N
Ti-48	1,2	2	3	3p, $\alpha$ , $\alpha_1$	N
Ti-49	3	3	3	3 $\alpha,p$	N
Ti-50	3	3	3	3p, $\alpha$ , $\alpha_1$	N
Ti-NAT	4,5	4,5	4,5	4,5	4

\* Radioactive

## NOTES

- 1) ENDP/B Tape 531.
- 2) ENDF/B Tape 532.
- 3) ACTL.

- 4) ENDF/B-V Transport.
- 5) ENDL-85 Transport.
- 6) Evaluators have as private files.

library<sup>56)</sup> have been described in detail. A wealth of cross section data is available in the library, over 1800 activation reactions involving 373 target nuclei. The ACTL library is generally used for geochemical analysis and modeling.

Neither the ENDF nor the ACTL dosimetry data files contain covariance information. Clearly, there is an enormous effort involved in getting covariance or uncertainty data processed and available. Until such covariance data becomes available, other techniques<sup>57)</sup> will be used to assign uncertainty values to cross sections of geochemical interest. The availability of covariance data in dosimetry data is probably several years away.

## SUMMARY

The need for improved neutron induced reaction cross sections has been examined for elements that are important in subsurface geochemical analyses. Current spectroscopic systems that can be used in a borehole have the potential for providing a true multielement analysis, providing the elemental concentrations which can be used to provide geochemical descriptions of many properties of the geology. While prior emphasis had been on gross lithological descriptions or the location of ore-quality concentrations, current needs reflect the importance of many elements in smaller concentrations. This requires the separation of the effects from competing reactions populating the same nuclear state as well as spectral interferences that are not significant at higher elemental concentrations. These constraints place much greater weight on the neutron-induced cross section data and on the uncertainties with which they are determined. Currently, the cross section data and the evaluation of the cross section uncertainties are generally insufficient for geochemical applications. Substantial progress is needed to determine the neutron-induced reaction cross sections over a wide energy range (between 0 and 20 MeV) and improve the uncertainties on existing data. The importance of determining isotopic cross sections with good precision must receive increased attention to allow a proper evaluation of competing reaction mechanisms.

## ACKNOWLEDGMENTS

We are indebted to R. Little, R. Seamon, and D. Muir (LANL) for many useful discussions concerning the cross section data and uncertainties.

## REFERENCES

- [1] D. K. Keelan, *Jour. Can. Pet. Tech.* 42 April-June (1972).
- [2] S. S. Nargolwalla and H. Seigel, *Can. Min. Jour.* 98, 75 (1977).
- [3] D. K. Keelan, SPE 10011, Technical Symposium of the Society of Petroleum Engineers, Beijing (1982).
- [4] M. M. Herron, *Clays and Clay Minerals*, in press (1986).
- [5] M. M. Herron, Paper presented at I.A.E.A. meeting on nuclear data for applied nuclear geophysics. Vienna (1986).
- [6] R. V. Everett, M. Herron, G. Pirie, J. Schweitzer, and H. Edmundson, SPE 14176, Technical Symposium of the Society of Petroleum Engineers, Las Vegas (1985).

- [7] R. N. Anderson, *Nature* **316**, 486 (1985).
- [8] R. Everett, M. Herron, G. Pirie, J. Schweitzer, and H. Edmundson, *Studies in Geology* No. 23, American Association of Petroleum Geologists, in press (1986).
- [9] F. E. Senftle in *Short Course in Neutron Activation Analysis in the Geosciences* ed. by G. K. Muecke, Mineralogical Association of Canada (1980).
- [10] F. E. Senftle, A. B. Tanner, P. W. Philbin, G. R. Boynton, and C. W. Schram, *Mining Engineering (AIME)* **30**, 666 (1978).
- [11] M. R. Wormald and C. G. Clayton, *Int. J. Appl. Radiat. Isot.* **34**, 71 (1983).
- [12] R. Hertzog and R. Plasek, *IEEE Trans. Nucl. Sci.* **NS-26**, 1558 (1979).
- [13] R. C. Hertzog, *Soc. Pet. Eng. Jour.* **20**, 327 (1980).
- [14] C. G. Clayton, A. M. Hassan, and M. R. Wormald, *Int. J. Appl. Radiat. Isot.* **34**, 83 (1983).
- [15] A. Lauber and O. Landstrom, *Geophys. Prospect.* **20**, 800 (1972).
- [16] A. B. Tanner, R. M. Moxham, F. E. Senftle, and J. A. Baicker, *Nucl. Inst. and Meth.* **100**, 1 (1972).
- [17] F. E. Senftle, R. M. Moxham, A. B. Tanner, G. R. Boynton, P. W. Philbin, and J. A. Baicker, *Nucl. Inst. and Meth.* **138**, 371 (1976).
- [18] G. A. Nedostrup and F. N. Prokof'ev, *At. Energ.* **35**, 54 (1973).
- [19] D. W. Mellor and M. C. Underwood, SPWLA 26th Annual Logging Symposium, Paper FFF, 2 (1985).
- [20] J. S. Schweitzer, R. A. Manente, and R. C. Hertzog, *Jour. Pet. Tech.* **36**, 1527 (1984).
- [21] J. A. Grau, S. Antkiw, R. C. Hertzog, R. A. Manente, and J. S. Schweitzer, *AIP Conf. Proc.* **125**, 799 (1985).
- [22] B. A. Roscoe and J. A. Grau, SPE 14460, Technical Symposium of the Society of Petroleum Engineers, Las Vegas (1985).
- [23] J. A. Grau, B. A. Roscoe, and J. R. Tabanou, SPE 144620, Technical Symposium of the Society of Petroleum Engineers, Las Vegas (1985).
- [24] U. Fanger and R. Pepelnik, *Proc. of the Amer. Nucl. Soc., Topical Meeting, Austin, Rept. Conf-720902*, 245 (1972).
- [25] M. Sohrabpour and S. R. Bull, *Nucl. Inst. and Meth.* **161**, 281 (1979).
- [26] F. E. Senftle, R. M. Moxham, A. B. Tanner, P. W. Philbin, G. R. Boynton, and R. E. Wager, *Geoexploration* **15**, 121 (1977).
- [27] R. S. Caswell, *Neutron Sources and Applications, Proceedings of the American Nuclear Society National Topical Meeting, CONF-710402*, 1, I-53, (1971).
- [28] A. E. Profio, *Radiation Shielding and Dosimetry*, John Wiley and Sons (1979).
- [29] W. B. Nelligan and S. Antkiw, SPE 6156, Technical Symposium of the Society of Petroleum Engineers, New Orleans (1976).
- [30] R. R. Randall and E. C. Hopkinson, SPWLA 22nd Annual Logging Symposium, Paper JJ, 2, Mexico City (1981).

- [31] J. A. Czubek, K. Drozdowicz, E. Krynicka-Drozdowicz, A. Igielski, and U. Woznicka, SPWLA 22nd Annual Logging Symposium, Paper A, 1, Mexico City (1981).
- [32] P. Westaway, R. Hertzog, and R. E. Plasek, SPE 9461, Technical Symposium of the Society of Petroleum Engineers, Dallas (1980).
- [33] L. A. Haskin in *Short Course in Neutron Activation Analysis in the Geosciences* ed. by G. K. Muecke, Mineralogical Association of Canada (1980).
- [34] R. C. Hertzog, P. D. Soran, and J. S. Schweitzer, International Conference on Nuclear Data for Basic and Applied Science, Santa Fe (1985).
- [35] J. J. Ullo, Nucl. Sci. Eng. **92**, 228 (1986).
- [36] R. C. Hertzog, P. D. Soran, and J. S. Schweitzer, Paper presented at I.A.E.A. meeting on nuclear data for applied nuclear geophysics. Vienna (1986).
- [37] F. Senftle, R. Moxham, and A. Tanner, Nucl. Instr. Meth. **104**, 485 (1972).
- [38] S. L. Herron, SPWLA 27th Annual Logging Symposium, Houston (1986).
- [39] H. D. Scott and M. P. Smith, The Log Analyst **14**, 3 (1973).
- [40] R. Everett, M. Herron, and G. Pirie, SPWLA 24th Annual Logging Symposium, Paper OO, Calgary (1983).
- [41] O. Serra, J. Baldwin, and J. Quirein, SPWLA 21st Annual Logging Symposium, Paper Q, Lafayette (1980).
- [42] H. D. Smith, Jr., C. A. Robbins, D. M. Arnold, L. L. Gaden, and J. G. Deaton, SPE 12050, Technical Symposium of the Society of Petroleum Engineers, San Francisco (1983).
- [43] J. S. Schweitzer and R. A. Manente, AIP Conf. Proc. **125**, 824 (1985).
- [44] R. Pepelnik, B. Anders, and B. M. Bahal, International Conference on Nuclear Data for Basic and Applied Science, Santa Fe (1985).
- [45] A. H. Brownlow, *Geochemistry*, Prentice-Hall (1979).
- [46] M. A. Lone, R. A. Leavitt, and D. A. Harrison, At. Data and Nucl. Data Tables **26**, 511 (1981).
- [47] E. T. Jurney, in *Neutron Capture Gamma-Ray Spectroscopy*, eds. R. E. Chrien and W. R. Kane, Plenum Press (1979).
- [48] J. W. McKlveen, *Fast Neutron Activation Analysis*, Ann Arbor Science (1981).
- [49] W. Michaelis, NBS Special Publication 594, 615 (1980).
- [50] S. Antkiw, C. R. Case, and P. Albats, P., INDC(NDS)-151/L, 201 (1984).
- [51] B. A. Magurno, R. R. Kinsey, and F. M. Scheffel, EPRI Report NP-2510 (1982).
- [52] S. F. Mughabghab, M. Dwadeenam, and E. Holden, *Neutron Cross Sections*, **1**, Part A, Academic Press (1981).
- [53] D. W. Muir, LANL progress report LA-10288-PR, (1985).
- [54] B. A. Magurno, ed., BNL report BNL-NCS-50446, (1975).
- [55] R. J. Howerton, M. H. MacGregor, and S. T. Perkins, UCRL report UCRL-50400, **7**, Part A, Rev. 1 (1976).

- [56] M. A. Gardner and R. J. Howerton, UCRL report UCRL-50400, **18**, (1978).
- [57] R. J. Howerton, R. E. Dye, and S. T. Perkins, UCRL report UCRL-50400, **4**, Rev. 1 (1981).
- [58] S. A. W. Gerstl, D. J. Dudziak, and D. W. Muir, Nucl. Sci. Eng. **62**, 137 (1977).



Nuclear Ratio Technique Applied to Borehole Exploration  
for Industrial Metals and Coal

F. E. Senftle and J. L. Mikesell  
U.S. Geological Survey, Reston, VA 22092

Abstract

The nuclear characteristics of the thermal and fast neutron reactions for the important industrial metals and the major elements in coal have been examined to determine the most feasible neutron-induced reaction to use in exploration by borehole gamma-ray spectroscopy. The recommended reactions for each element are tabulated for quick reference.

A technique is presented in which the concentration of a minor element can be determined by measuring the ratio of its gamma-ray activity to that of a high-concentration common element in the rock matrix. The technique requires that the concentration of the common element be estimated using knowledge of the rock type. The method has been tried in the decay gamma ray mode to determine manganese in clay and in the prompt gamma ray mode to determine sulfur in coal. The results are very encouraging and point out the utility of the technique as a practical field method.

INTRODUCTION

The most expeditious method to obtain an elemental analysis of a subsurface ore deposit from a borehole is by gamma ray spectroscopy. This method can be a useful exploration technique to locate deposits of industrially important elements that may reside at considerable depths below the surface. Papers describing early attempts to make analyses of important industrial minerals from a borehole have been included in extensive bibliographies<sup>1-3</sup>, and the various state-of-the-art techniques have been discussed elsewhere<sup>4-6</sup>. The general direction of the research and development to date has been toward improving the accuracy and sensitivity of the in-hole

measurements. While this dual approach is important, there are many applications where a high level of accuracy is not required, but where good sensitivity is needed. Generally, high sensitivity is needed for mineral exploration or geologic mapping. Accuracy becomes more important than sensitivity where it is required to evaluate the value and extent of a known mineral deposit. In this paper we address several problems associated with the application of borehole gamma-ray spectroscopy to mineral exploration. Using sulfur in coal and manganese in clay as examples, we demonstrate the usefulness of an approximate technique for practical borehole gamma-ray spectroscopy.

#### PROBLEM OUTLINE

When faced with the problem of using borehole gamma-ray spectroscopy for exploration or mapping for a given element, several questions must be considered.

Most-suitable reaction: Most natural elements consist of several isotopes, each of which undergoes several possible nuclear reactions yielding gamma rays of specific energies and intensities. With regard to the need for high sensitivity rather than great accuracy, we have examined the multiplicity of reactions associated with the isotopes of the important industrial metals and the major elements in coal. Table 1 lists for each of these elements, the reactions, and the particular gamma ray which seems best suited for exploration work. In compiling this table, we assumed that a high-resolution detector is used in the borehole tool so that the selected photopeaks can be recorded with a resolution better than 10 keV. Under these conditions the gamma-ray photopeaks for each reaction have been selected so that the expected abundance of any interfering element in a typical mineral deposit of the desired element will yield an insignificant contribution ( $< 10\%$ ) to the measured photopeak.

Photopeak interferences noted in the table are of two kinds, exact and approximate. Exact interference of a photopeak takes place if the same nuclide is produced by two competing nuclear reactions and thus one cannot determine which reaction produced the photopeak. The photopeak interference is considered approximate if two different nuclides emit gamma rays whose energies are so close to each other as to be unresolved. If the most sensitive gamma ray for a given element is less than 10 keV from a gamma ray of a potential interfering element (approximate interference), the next most sensitive gamma ray is given in the table. Detection of an unresolved group of two or more gamma rays from the same element may be useful for exploration purposes, and thus several of the intense lines are shown in the table with the additional lines indicated in the footnote.

Not all industrial metals are amenable to measurement by borehole gamma-ray spectroscopy in typical economic concentrations. Platinum is not listed in the table because, as shown previously<sup>7</sup> its sensitivity is far too low for any practical application. The metals Zn, Cd, Sn and Au (marked with \*) have very marginal sensitivities and borehole gamma-ray spectroscopy is not recommended as an exploration method except in those situations where high concentrations are anticipated. Cu and Pb would be difficult to measure below concentrations of a few tenths to 1 percent. The nuclear parameters for the rest of the elements in the table are such that they could be measured at below ore-grade concentrations.

With the exception of the fast-neutron reactions listed for Au and Pb, the thermal neutron activation and capture reactions are the only reactions that have sufficient sensitivity to be considered for exploration purposes. For the metals of industrial interest the fast-neutron reaction cross sections are simply too small to yield the sensitivity needed for a practical exploration method using current state-of-the-art techniques.

Similar information is presented in the table for the major elements in coal. Most of these elements are best detected by thermal neutron capture,

TABLE 1. Recommended reactions for borehole exploration. Basic data taken from refs 15, 16, and 17.

Element/ Abundance	Recommended Reaction	$\sigma_{Th}$ ( $10^{-28}m^2$ )	$T^{1/2}$	E (keV)	I (**)	$\frac{\sigma I}{A}$	Interference footnote
<u>Industrial Metals</u>							
<u>Thermal Neutron Decay Reactions</u>							
Al-27/100	$^{27}Al(n, \gamma)^{28}Al$	0.232	2.246 m	1779	100	0.87	a
V-51/99.75	$^{51}V(n, \gamma)^{52}V$	4.88	3.755 m	1434	100	9.57	
Mn-55/100	$^{55}Mn(n, \gamma)^{56}Mn$	13.3	2.582 h	847	99	23.9	b
Cu-65/30.9	$^{65}Cu(n, \gamma)^{66}Cu$	2.17	5.10 m	1039	9.0	0.30	
Ag-109/48.17	$^{109}Ag(n, \gamma)^{110}Ag$	89	24.6 s	658	4.5	3.67	
*Sn-124/5.8	$^{124}Sn(n, \gamma)^{125}Sn$	0.13	9.2 m	332	99	0.10	
<u>Thermal Neutron Prompt Reactions</u>							
Ti-48/73.7	$^{48}Ti(n, \gamma)^{49}Ti$	7.8	prompt	1381	69.08	11.2	
Cr-53/9.5	$^{53}Cr(n, \gamma)^{54}Cr$	18.2	prompt	8884	26.97	9.26	
Fe-56/91.7	$^{56}Fe(n, \gamma)^{57}Fe$	2.63	prompt	7645	24.13	1.13	c
		2.63	prompt	7631	28.51	1.34	c
Co-59/100	$^{59}Co(n, \gamma)^{60}Co$	37.2	prompt	6877	8.21	5.18	d
			prompt	5660	7.20	4.55	
Ni-58/67.88	$^{58}Ni(n, \gamma)^{59}Ni$	4.6	prompt	8999	37.74	2.99	e
*Zn-64/48.9	$^{64}Zn(n, \gamma)^{65}Zn$	0.78	prompt	7863	10.58	0.13	
Mo-95/15.72	$^{95}Mo(n, \gamma)^{96}Mo$	14.5	prompt	778	36.92	5.63	
*Cd-144/28.8	$^{114}Cd(n, \gamma)^{115}Cd$	0.036	prompt	559	72.73	0.02	
Hg-200/23.1	$^{200}Hg(n, \gamma)^{201}Hg$	< 60	prompt	368	81.35	< 24.4	f
		< 60	prompt	1694	14.13	< 4.24	
Pb-207/22.1	$^{207}Pb(n, \gamma)^{208}Pb$	0.709	prompt	7368	94.06	0.32	g
<u>Fast Neutron Reactions</u>							
*Au-197/100	$^{197}Au(n, n' \gamma)^{197}Au$	1.4(3 Mev)	7.25 s	279	72.5	0.51	h
		0.29(14 Mev)	7.25 s	279	72.5	0.11	h
Pb-208/52.4	$^{208}Pb(n, 2n)^{207m}Pb$	1370	0.81 s	570	97.9	0.64	

<u>Thermal Neutron Capture Reactions</u>				<u>Coal</u>			
H-1/99.98	$^1\text{H}(n,\gamma)^2\text{H}$	0.332	prompt	2223	100.0	33.2	
C-12/98.89	$^{12}\text{C}(n,\gamma)^{13}\text{C}$	$3.4 \times 10^{-3}$	prompt	4945	67.64	0.019	i
			prompt	3684	32.10	0.009	
N-14/99.63	$^{14}\text{N}(n,\gamma)^{15}\text{N}$	0.075	prompt	5269	29.73	0.159	
S-32/95.0	$^{32}\text{S}(n,\gamma)^{33}\text{S}$	0.530	prompt	2380	44.50	0.737	
			prompt	3221	27.09	0.449	
Si-28/92.2	$^{28}\text{Si}(n,\gamma)^{29}\text{Si}$	0.170	prompt	3539	68.00	0.413	
Cl-35/75.77	$^{35}\text{Cl}(n,\gamma)^{36}\text{Cl}$	43	prompt	6111	20.00	24.57	j
		43	prompt	1165	19.93	24.48	k
		43	prompt	7414	10.42	12.80	
<u>Fast Neutron Reactions</u>							
C-12/98.89	$^{12}\text{C}(n,n'\gamma)^{12}\text{C}$	0.425	prompt	4439	100	1.5	l
O-16/99.76	$^{16}\text{O}(n,n'\gamma)^{16}\text{N}$	0.474	prompt	6129	100	0.9	m
	$^{16}\text{O}(n,p)^{16}\text{N}$	0.047	7.13 s	6129	68.8	0.2	m

\* Sensitivity too low for practical exploration use.

\*\* For decay reactions, I is in gammas/100 decays; for prompt reactions, I is in  $\gamma$ 's/100 neutrons absorbed.

a For high-energy neutrons  $^{28}\text{Si}(n,p)^{28}$  reaction interferes exactly.

b For high energy neutrons, Fe interferes exactly via the  $^{56}\text{Fe}(n,p)^{56}\text{Mn}$  reaction.

c Cu 7637-keV line is a possible approximate interference.

d V 6874-keV line interferes approximately.

e Cr 8884 keV line interferes approximately.

f Possible approximate interference from Fe at 366 keV.

g Cr 7366-keV line interferes approximately.

h Approximate interference from natural  $^{208}\text{Tl}$  decay.

i Good with high-resolution detector; Si line approximately interferes at 4934 keV.

j Approximate interference from single-escape lines from the 6618- and 6628-keV lines of Cl.

k Approximate interference from 1163-keV line of Cl.

l  $^{16}\text{O}(n,n'\alpha)^{12}\text{C}$  reaction interferes exactly; line is broad due to doppler shifting; must use pulsed neutron source to separate the neutron inelastic and thermal capture reactions.

m  $^{19}\text{F}(n,\alpha)^{16}\text{N}$  reaction interferes exactly.

with the exception of oxygen and carbon. Oxygen can be detected only by fast neutron reactions. Carbon is the only major element in coal for which a fast neutron reaction has a greater sensitivity than the thermal capture reaction.

Sonde calibration: It is generally recognized and has been demonstrated recently by Monte Carlo calculations<sup>8</sup> that for low gamma-ray energies, the sample detected in a borehole is a roughly symmetrical volume of wall rock in the vicinity of the detector. For higher energy gamma rays the location of the volume sampled becomes skewed in the direction of the neutron source because of the greater penetration of the gamma rays and because of the larger neutron fluence rate in the space between the neutron source and detector than on the far side of the detector. For either a neutron generator or an isotopic neutron source the neutrons are emitted at higher-than-thermal energies, and must be moderated within the rock between the source and the measured sample. For a monochromatic source of high-energy neutrons in a hydrogenous medium, the neutron fluence rate is highest at the emission and thermal energies, but is remarkably uniform and over an order of magnitude lower in the intermediate part of the energy distribution spectrum<sup>9,10,11</sup>. Although the total fluence rate drops off substantially with distance from the neutron source, the neutron energy distribution pattern does not change substantially with distance from the source. In non-hydrogenous rocks the situation is quite different. The neutron energy distribution curve shows dips at specific energies corresponding to inelastic scattering by the major elements present in the rock. At the thermal end of the distribution in either a hydrogenous or a non-hydrogenous matrix neutron depletion can be dramatic because of the high neutron absorption cross sections. If elements that have extraordinary large cross sections are present, even in relatively small concentrations, the thermal neutron fluence-rate depression can be significant. For this reason the neutron energy distribution, as well as the local thermal fluence rate will be dependent on the elemental composition of the sample. This effect has been demonstrated by the results of Underwood and

Petler<sup>8</sup> who have shown the effect of chlorine concentration in coal on the measurement of the intensity of the sulfur photopeak.

Proper calibration of the borehole gamma-ray spectrometer for quantitative analysis is a complex problem in light of this dependence of the neutron flux and energy distribution on sample composition. The proportionality constant between the counting rate in a specific gamma-ray photopeak and the concentration of the associated element in the wall rock is generally determined by calibration in a test pit or a borehole from which the core has been chemically analyzed. Such calibration techniques are not completely satisfactory. Although the sonde geometry and borehole size can be held constant from a test pit to an unknown borehole in the field, such variables as sample composition, water concentration, porosity and neutron poisons cannot be anticipated. All of these factors strongly influence the thermal and epithermal neutron flux densities. Several attempts have been made to eliminate the necessity of using a test pit by using analytical techniques that are independent of the neutron fluence rate<sup>12-14</sup>. These techniques require the activation of all the major elements in the rock matrix, which may not always be possible; oxygen is a typical example. Thus, these analytical techniques designed to eliminate the need to know the neutron fluence rate are limited in usefulness.

To circumvent the problem of calibration, we suggested an alternative approach<sup>7</sup> which has proved to have wider application than was at first thought. As sensitivity is more important than accuracy for an exploration technique, one may achieve adequate calibration in the following manner. Most geochemical exploration need not be a completely blind operation, as the rock type (e.g. limestone or sandstone) through which the hole is bored can generally be ascertained. The approximate concentrations of the major elements in different rock types are fairly well known. Consequently, the concentration of at least one of the major elements of the rock can often be estimated with a relative error of less than 20 percent. If that element can

be activated, its photopeak can be used with the method of ratios to determine the concentration of a minor element in the same rock matrix. Although the possible 20 percent error in estimating the major element may be unacceptable in exploration for that element, the same error applied to the minor element may be quite acceptable. Aluminum, for instance, is an obvious choice as a major element in many rocks and might be used to determine a minor element by decay gamma rays. Silicon may be a good choice for detection in the capture gamma ray mode. In coal, carbon can be estimated with sufficient accuracy to be used as a standard element.

The ratios of the mass fractions of any two elements as determined from their decay gamma ray photopeaks are given by equation (1)<sup>7</sup>. The subscripts a and b refer to the unknown element and the standard element, respectively.

Thus,

$$\frac{f_a}{f_b} = \frac{N_a A_a \lambda_a (\sigma_b + I_b/50) k_b I_{\gamma b} \epsilon_b S_b H(t_1, t_2, t_3)_b}{N_b A_b \lambda_b (\sigma_a + I_a/50) k_a I_{\gamma a} \epsilon_a S_a H(t_1, t_2, t_3)_a} \quad (1)$$

where f = mass fraction

N = integrated number of counts in the photopeak

A = atomic weight

$\lambda$  = decay constant of the activated nucleus

$\sigma$  = thermal-capture cross section

I = resonance integral

k = isotopic abundance

$I_{\gamma}$  = yield of the measured gamma ray, in photons per neutron absorbed

$\epsilon$  = relative efficiency of the detector at energy of measured gamma ray

S = source strength in neutrons per second.

$H(t_1, t_2, t_3)$  is the factor  $(e^{-\lambda t_1} - 1) \cdot (e^{-\lambda t_2} - e^{-\lambda t_3})$ , where  $t_1$  is the irradiation time,  $t_2 - t_1$  is the time lapse between the end of irradiation and the start of counting, and  $t_3 - t_2$  is the counting interval. The cross-section term,  $\sigma + I/50$ , assumes an epithermal-to-thermal flux ratio of 1:50, which is

a ratio valid for reactor neutrons. We have evaluated this ratio for a  $^{252}\text{Cf}$  source in a laboratory borehole in which there was 5-10 percent water in the material (concrete-simulated ore body) surrounding the casing<sup>7</sup>. Our data suggest the ratio to be about 1:50 and therefore an epithermal-to-thermal neutron ratio close to that observed for a reactor. It should also be noted that equation (1) assumes that the volume of the ore sampled is the same for the standard and the unknown element. If the gamma rays measured for the two elements do not differ widely in energy, this assumption is approximately true.

Choice of Neutron Source: The choice of neutron source is often dictated by factors such as shielding, licensing, safety, etc. However, something can be said solely on scientific grounds. Essentially all the reactions in Table 1 are based on thermal capture. The primary purpose of the source is thus to produce a high level of thermal neutron activation within the sample surrounding the detector, and this can be done with either an isotopic source or a generator. However, there are two facts that weigh against a 14-MeV generator. First, the high-energy neutron fluence rate from a generator is more likely to damage the detector crystal and thus the crystal will require more frequent annealing. Second, when using a generator in either a pulsing or continuous mode the background is generally higher due to other unwanted fast neutron reactions in both the sample and within the detector crystal<sup>18</sup>.

#### FIELD AND LABORATORY TESTS

We show two examples of the ratio technique where the concept was used: one for manganese in clay and the other for sulfur in coal.

Manganese in Clay: Decay gamma-ray experiments which are more fully described elsewhere<sup>19</sup> were carried out in a borehole cutting through a clay formation containing manganese-bearing siderite at specific horizons in the borehole. Measurements were made with a neutron source of about 100- $\mu\text{g}$   $^{252}\text{Cf}$ . A 50  $\text{cm}^3$  Ge(HP) crystal mounted in a melting cryogen detector provided high-resolution spectra. A 2"x2" NaI(Tl) crystal detector was used for comparison under the

same experimental conditions. Pulse-height spectra were recorded continuously as the sonde was raised or lowered in the borehole. Every 15 seconds a computer measured the net peak areas under the manganese 847-keV and the aluminum 1779-keV photopeaks. At the logging speed used, this represented a measurement every 10 cm along the borehole. Corrections for live time were made before the data were used in equation 1.

Measurements were made in both dry and wet boreholes at a logging speed of 0.5 cm/s. Because the compton-scattered gamma rays from the aluminum

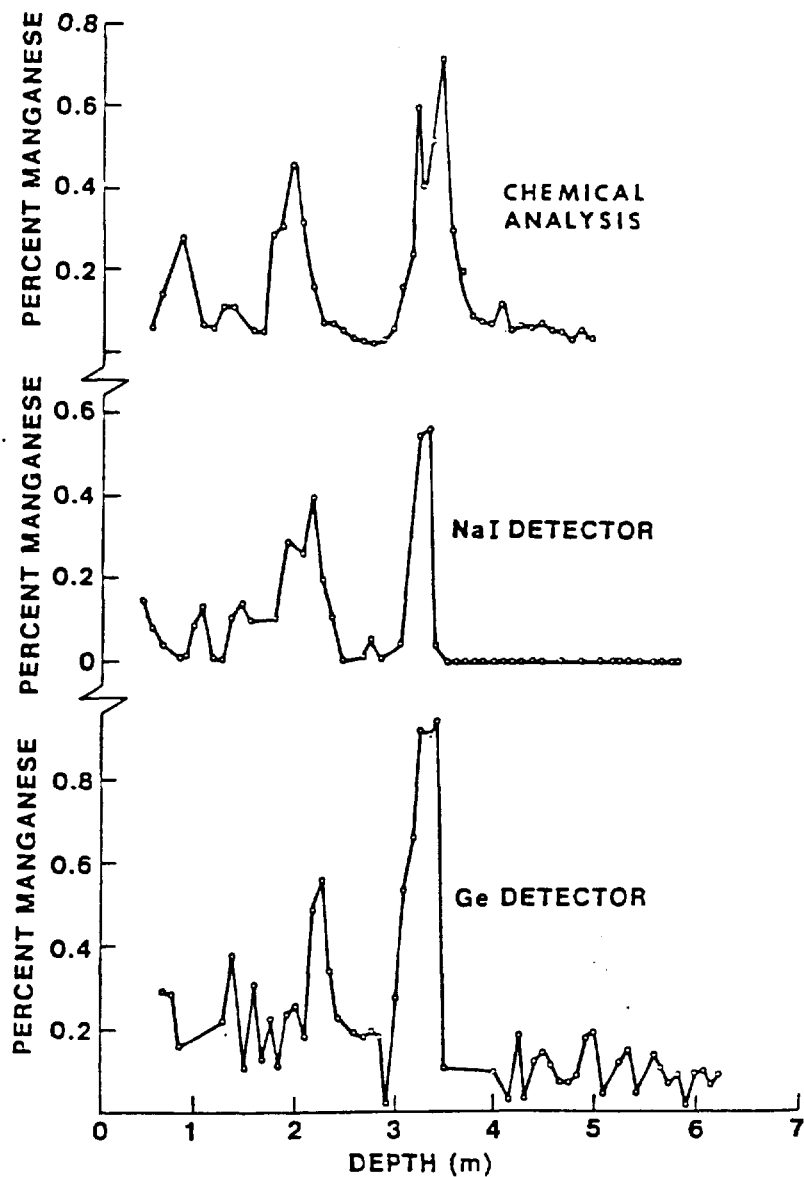


Fig. 1 - Manganese concentrations calculated from equation (1) for the NaI(Tl) and Ge(HP) detectors compared with data from chemical core analyses.

significantly interfered with the 847-keV photopeak of Mn, only aluminum was measured during the decent. The sonde was allowed to rest at the bottom of the hole for 20 minutes to allow the aluminum activity to die away. The longer-lived manganese was measured coming up the borehole. The double-pass procedure was necessary because of the low resolution of the scintillation detector, but both Al and Mn could be measured simultaneously on a single pass with the high-resolution Ge(HP) detector. After correcting for irradiation and decay times, and using the knowledge that the aluminum concentration in the clay formation averaged about 8.2 percent (data from the Maryland Clay Products Co. which uses the clay for fabricating bricks), we calculated the manganese concentration from equation (1). The data taken with both detectors (Figure 1) are comparable and yield the values for the manganese concentrations that compare well with the chemical core analyses. The accuracy is adequate for exploration purposes. Similar results (not shown) were obtained in both dry and water-filled boreholes.

Sulfur in Coal: If one knows the general rank of a coal seam, the carbon concentration can be estimated with reasonable accuracy. Thus, the concentration of a minor element such as sulfur can be estimated with acceptable accuracy by a ratio technique with carbon. Both sulfur and carbon can be determined simultaneously by thermal neutron capture, in which case equation (1) can be simplified to

$$\frac{f_S}{f_C} = \frac{N_S A_S (\sigma_C + I_C/50) k_C I_{\gamma C} \epsilon_C}{N_C A_C (\sigma_S + I_S/50) k_S I_{\gamma S} \epsilon_S} \quad (2)$$

where S and C refer to sulfur and carbon respectively and the rest of the symbols have their previous definitions.

To test the method a borehole in a coal seam was simulated by filling two steel casks, one with buckwheat-size bituminous coal (Illinois No. 6, Monterey No. 1 Mine) and one with anthracite coal (Pottsville, Pennsylvania) of similar size. The casks, described in more detail elsewhere<sup>20</sup>, were 1.2 m in diameter

and 1.5 m high, hermetically sealed, and had a 10-cm inside-diameter steel pipe welded along the axis to simulate the borehole. Neutron capture gamma ray spectra were collected using a 70- $\mu\text{g}$   $^{252}\text{Cf}$  neutron source. The efficiency curve used to determine  $\epsilon$  was found from the capture lines of iron or aluminum. Using the sulfur photopeaks at 2380 and 3221 keV and the carbon photopeaks at 3684 and 4945 keV the four possible ratios of the sulfur activity to that of carbon were used to determine the sulfur concentration. The bituminous coal (Monterey No. 1 mine, Carter Oil Co.), which had been used for a fluidized-bed coal combustion study, was reported to have an average carbon concentration of 62.1 percent (as received basis).<sup>21</sup> A typical carbon analysis of the anthracite, obtained from the coal company (Reading Anthracite Coal Co.) was 83 percent. The sulfur concentrations obtained from chemical analysis and as calculated from each of the photopeak ratios are given in Table 2. The results using any individual ratio are acceptable for exploration purposes, and the average value for the four ratios agrees well with the chemical analysis.

It should be pointed out that the sulfur analyses obtained by each of the ratios in Table 2 should theoretically be the same. The fact that they are not raises some questions about the possibility of the nuclear data being in error. For example, some values from the newer compilation<sup>15</sup> of the capture gamma-ray intensities are substantially different from those of the older compilation of Rasmussen et al<sup>22</sup>. However, the results are sufficiently accurate for field work where relative analyses from hole to hole in a given seam or where seam correlations are being made.

For the measurements of manganese in clay the good signal-to-noise ratio permitted the concentration to be measured every 15 seconds, which was sufficiently short to use the borehole sonde in a continuous logging mode. For the measurements of sulfur in coal, where a neutron capture technique was used, spectral accumulation times of 20-60 minutes and point-to-point measurements along the borehole were required to obtain high-quality spectra.

Table 2. Comparison of the sulfur concentration in coals as measured by chemical means with that determined by the approximate gamma-ray spectroscopy technique.

Sample	% S (chem)	Percent sulfur calculated from the photopeak area ratios				Average
		$\frac{2380}{3684}$	$\frac{3221}{3684}$	$\frac{2380}{4945}$	$\frac{3221}{4945}$	
Illinois No. 6 Bituminous Coal	3.44*	3.18	3.68	3.32	3.94	3.51
Pottsville, Pa. Anthracite	0.64	0.52	0.56	0.71	0.77	0.64

\* Average of six analyses

#### SUMMARY AND CONCLUSIONS

Borehole gamma-ray spectrometry is a practical exploration technique that can be very useful for exploration for specific metals and also for certain elements in coal. Most of the industrial metals and the major elements in coal can be measured satisfactorily by thermal neutron reactions. Isotopic neutron sources such as  $^{252}\text{Cf}$  are preferable to 14 MeV neutrons as a source of thermal neutrons. Fast neutrons are useful for detecting a few specific industrial metals and oxygen.

An exploration technique requires high sensitivity but only moderate accuracy. Those elements most amenable to exploration by gamma-ray spectrometry from the point of view of sensitivity are given in Table 1. Because there are many parameters that affect the neutron fluence rate through the sample and that are very difficult to evaluate, a ratio technique can be used to eliminate the need to know the neutron fluence rate. Such a method requires that the concentration of at least one element in the sample be known. One can, however, use the principle that the minor elements generally need not be known with the same accuracy as major elements. Thus, by estimating the concentration of a major element that also gives a good

spectral response, one can determine a minor element with sufficient accuracy for exploration purposes.

#### REFERENCES

1. Scott, J. and Tibbetts, B., 1974, Well-logging techniques for mineral deposit evaluation: A review: U. S. Bureau of Mines Information Circular IC-8677, Washington, D.C., USA.
2. Anonymous, 1976, Bibliography of borehole assay technology 1969-1975, Vol. II and III, Final Report on Contract No. J0255018: IRT Corp. San Diego, Cal. 92138, USA.
3. Senftle, F.E., 1980, Field studies of borehole gamma-ray spectrometer methods for mineral exploration: A selected bibliography: U. S. Geological Survey Open-File Report 80-503.
4. Nargowalla, S.S., Nguyen, N. D., and Rehman, A. U., 1977, Radioactivation Methods, Chap. 5 in Nuclear Methods in Mineral Exploration and Production, ed. J. G. Morse: Elsevier Sci. Pub. Co., New York, 113-200.
5. Senftle, F.E., 1980, Application of gamma-ray spectral analysis to subsurface mineral exploration, Chap. 8, in Mueike, G. W., ed., Short Course in Neutron Activation Analysis in the Geosciences: Mineral. Assoc. of Canada, Halifax, Nova Scotia, Canada, 211-254.
6. Clayton, C.G., 1983, Nuclear Geophysics: Pergamon press, New York.
7. Senftle, F.E., Mikesell, J.L., Tanner, A.B. and Lloyd, T.A., 1984, Sensitivity of in situ borehole neutron activation for the noble elements, in Proceed. IAEA Consultants Meeting on Nuclear Data for Borehole and Bulk Media Assay using Nucl. Techniques, Krakow, Poland Nov. 14-18, 1983: Int. Atom. Energy Agency, Rept. INDC(NDS)-151/L, 159-175.
8. Underwood, M.C., and Petler, J.S., 1986, High-resolution prompt (n, $\gamma$ ) spectroscopy using a down hole logging tool, in Proceed. of IAEA

Meeting on Nuclear Data for Applied Nuclear Geophysics, April 7-9, 1986  
Vienna, Int. Atomic Energy Agency, (in press).

9. Wormald, M. R., and Clayton, C. G., 1983, In-situ analysis of coal by measurement of neutron-induced prompt  $\gamma$ -rays: J. Appl. Radiat. Isotopes, 34, 71-82.
10. Antkiew, S., Case, C., and Albats, P., 1984, Measurements and calculations of neutron spectra in infinite media, in Proceed. IAEA Consultants Meeting on Nuclear Data for Borehole and Bulk Media Assay using Nuclear Techniques, Krakow, Poland, Nov 14-18, 1983: Int. Atomic Energy Agency, Report INDC(NDS)-151/L, 202-211.
11. Underwood, M.C. and Petler, J.S., 1986, Bulk material analysis using energetic neutrons, in Proceed. IAEA Consultants Meeting on Nuclear Data for App. Nucl. Geophysics, Vienna, Aust., April 7-9, 1986: Int. Atomic Energy Agency, (in press).
12. Fanger, U., Lubecki, A., Pepelnik, R., and Würz H., 1973, Borehole analysis by means of (n, $\gamma$ )- and XRF-technique demonstrated in a scheelite deposit near Mittersill: PACT-Bericht No. 37, Gesell. für Kernforschung mBH, Karlsruhe, Fed. Rep. of Germany, 80 p.
13. Senftle, F.E., Tanner, A.B., Philbin, P.W., Boynton, G.R. and Schram, C., 1978, In situ analysis of coal using a  $^{252}\text{Cf}$ -Ge(Li) borehole sonde: Mining Eng. (AIME) 30, 665-674.
14. Clayton, C.G., Hassan, A.M., and Wormald, M.R., 1983, Multi-element analysis of coal during borehole logging by measurement of prompt  $\gamma$ -rays from thermal neutron capture: Int. Appl. Rad. Isotopes 34, 83-93.
15. Lone, M., Leavitt, R. and Harrison, D., 1981, Prompt gamma rays from thermal neutron capture: Atomic Data and Nuclear Tables, 26, 511-559, Academic Press, N. Y.
16. Erdtmann, G., 1976, Neutron Activation Tables, Vol. 6: Verlag Chemie, New York.

17. Magurno, B.A., Kinsey, R.R., and Scheffel, F.M., 1982, Guidebook for the ENDF/B-V Nuclear Data Files, EPRI Report No. NP-2510: Brookhaven National Laboratory, N.Y.
18. Evans, L. G., Trombka, J. I., Jensen, D. H., Stephenson, W. A., Hoover, R. A., Mikesell, J. L., Tanner, A. B. and Senftle, F. E., 1984, Inter-pulse high-resolution gamma-ray spectra using a 14-MeV pulsed neutron generator: Nucl. Instr. and Methods, 219, 233-294.
19. Mikesell, J.L., Senftle, F.E., Lloyd, T.A., Tanner, A.B., Merritt, C.T. and Force, E.R., 1986, Borehole field calibration and measurement of low-concentration manganese by decay gamma-rays: Geophysics (in press).
20. Senftle, F.E., Mikesell, J.L., Doig, N.G. and Brown, F.W., 1983, Water analyses in salt deposits used for radioactive waste depositories: J. Appl. Radiat. Isotopes, 34, 389-96.
21. Hoke, R.C., Matulevicius, E.S., Ernst, M., Goodwin, J.L., Garabrant, A.R., Radovsky, I.B., Lescarret, A.S., Bertrand, R.R., Ruth, L.A., Siminski, V.J., Nutkis, M.S., Loughnane, M.D., Silakowski, H.R., Gregory, M.W., and Ichel, A., 1980, Miniplant and bench studies of pressurized fluidized-bed coal combustion: final report: Report EPA-600/7-80-013, U. S. Environmental Protection Agency, Research Triangle Park, N.C., USA
22. Rasmussen, N.C, Hakai, Y., Inouye, T. and Orphan, V.J., 1969, Thermal neutron capture gamma-ray spectra of the elements: Mass. Inst. of Tech Rept No. 2, MITNE-85 for the Air Force Cambridge Research Laboratory, Report AFCRL-69-0071.

Discrete  $\gamma$  ray production in  $(n,x\gamma)$  reactions for  
applied nuclear geophysics<sup>+</sup>

P. Obložinský and S. Hlaváč

Institute of Physics, Electro-Physical Research Centre of the  
Slovak Academy of Sciences, 842 28 Bratislava, Czechoslovakia

Abstract

The paper reviews the status of measurements and evaluation of microscopic cross sections for discrete  $\gamma$  ray production in reactions induced by neutrons below 20 MeV. Examined are the basic features of  $(n,x\gamma)$  reactions and their applicability to elemental analysis of bulk media. Discussed are experimental and theoretical methods for determining  $(n,x\gamma)$  cross sections. The status of these data is given. It is concluded that the situation in both measurements and evaluation of discrete  $\gamma$  ray production cross sections for nuclear geophysics/geochemistry applications is not satisfactory. Specialized effort should be undertaken to consolidate an appropriate data base in this important field.

1. Introduction

Methods of nuclear geophysics are well established in oil industry and their use in a wider field of mineral exploration, extraction and processing is increasing. Much of nuclear geophysics is concerned with the interactions of neutrons and subsequent emission of  $\gamma$  rays. Relevant techniques can be divided into 4 categories.

- (i) Detection of capture  $\gamma$  rays as used in pulsed neutron logging tools. The technique, based on neutron die away measurements developed for bore-hole logging, is in standard commercial use<sup>1)</sup>.

---

<sup>+</sup>) Invited talk delivered by P.O. at the IAEA Consultants Meeting on Nuclear Data for Applied Nuclear Geophysics, Vienna, April 7-9, 1986

- (ii) Delayed  $\gamma$  spectroscopy in neutron activation analysis<sup>2)</sup>. This well established technique is suitable for determining of about 30-40 elements in a typical geological sample<sup>3)</sup>.
- (iii) Prompt  $\gamma$  spectroscopy in neutron capture<sup>4)</sup>. The technique is in wider use for 5-10 years and in most geological samples 15-20 elements can be determined<sup>3)</sup>. In field applications one often uses neutrons from pulsed D+T source and adopt delay of about 100  $\mu$ s to allow for their thermalization<sup>5)</sup>.
- (iv) Prompt  $\gamma$  spectroscopy in fast neutron reactions<sup>6)</sup>. This technique is based on observing truly prompt discrete  $\gamma$  rays from  $(n, x\gamma)$  reactions (x means any particle, often it is inelastically scattered neutron, though for light elements charged particle emission may dominate, thus,  $x = n', p, d, t, \alpha, np, 2n, \dots$ ). As suggested in ref.<sup>7)</sup> fast timing is clearly advantageous here since majority of  $\gamma$  rays can be effectively emitted within time windows as narrow as  $\sim 10$  ns after neutron hits large sample.

Our main concern is the last technique, which is rather new, still needs a great deal of development and assesment. Certain exception to this is the carbon/oxygen logging based on  $\gamma$  ray spectroscopy following inelastic scattering of 14 MeV neutrons<sup>1)</sup>. Quantitative analysis of prompt  $\gamma$  spectra requires knowledge of discrete  $\gamma$  production cross sections from the incident neutron energy, often 14 MeV, down to the threshold. Surveys, reviews or catalogues of this type of data useful for applied nuclear geophysics are virtually nonexistent.

So far,  $(n, x\gamma)$  studies were largely motivated by two objectives. First, nuclear physics was primarily interested in  $(n, n'\gamma)$  spectra at a few MeV of incident neutron energy carrying important information on nuclear structure and level schemes. To much lesser extent,  $(n, n')$  cross sections were measured indirectly via  $(n, n'\gamma)$  ones, and  $(n, x\gamma)$  cross sections were used in reaction mechanisms studies. Second, nuclear energy industry was interested in data related to nuclear heating and shielding. To date, total  $\gamma$  ray production cross sections and  $\gamma$  spectra with modest resolution induced by neutrons below 20 MeV were measured for nearly 30 elements. Thus, discrete  $\gamma$  ray production cross sections in the above region were neither of pri-

mary importance for nuclear physics nor for nuclear energy industry. Not surprisingly, it was acknowledged at the Krakov'83 meeting on nuclear data for bore-hole and bulk-media assay<sup>8)</sup> that these cross sections are scarce and one of the most pressing requirements is to catalogue discrete  $\gamma$  ray production cross sections in  $(n, x\gamma)$  reactions from threshold energies to 20 MeV.

The objective of this paper is to review the status of measurements and evaluation of microscopic cross sections for discrete  $\gamma$  ray production in  $(n, x\gamma)$  reactions below 20 MeV. In sect. 2 we examine the basic features of  $(n, x\gamma)$  reactions together with their analytical sensitivities. In sect. 3 we discuss experimental and theoretical methods for obtaining  $(n, x\gamma)$  cross sections. The status of the data is examined and summarized in sect.4. We stress that we do not pretend to give a complete survey of the data, rather we focus on general situation in the field. Conclusions are drawn in sect.5.

## 2. Reactions $(n, x\gamma)$ and their analytical sensitivities

For practical reasons the single most important incident neutron energy available for nuclear geophysics seems to be 14 MeV. It is, therefore, natural to demonstrate some important features of  $(n, x\gamma)$  reactions just at this energy point.

Shown in fig.1 taken from ref.<sup>9)</sup> is typical total  $\gamma$  ray production spectrum for the target mass  $A \approx 60$ . Dominant is the smooth component originating in statistical  $(n, n'\gamma)$  transitions. Superimposed on this component, well pronounced in low energy region,  $E_\gamma \lesssim 3$  MeV, are discrete  $\gamma$  rays. High energy component,  $E_\gamma \gtrsim 14$  MeV, which is very weak and unimportant for our discussion, is due to capture. It is important to realize that, generally, continuous (energetically unresolved) statistical  $\gamma$  rays produce natural background for observation of discrete  $\gamma$  rays we are interested in.

The above picture changes with incident neutron energy and with the mass number. At low incident neutron energies,  $E_n \gtrsim 1$  MeV, the spectra contain but discrete  $\gamma$  rays. With increasing incident neutron energy production of  $\gamma$  rays increases. As new reaction channels open up, production of a specific discrete  $\gamma$  ray can, however, be sharply reduced.

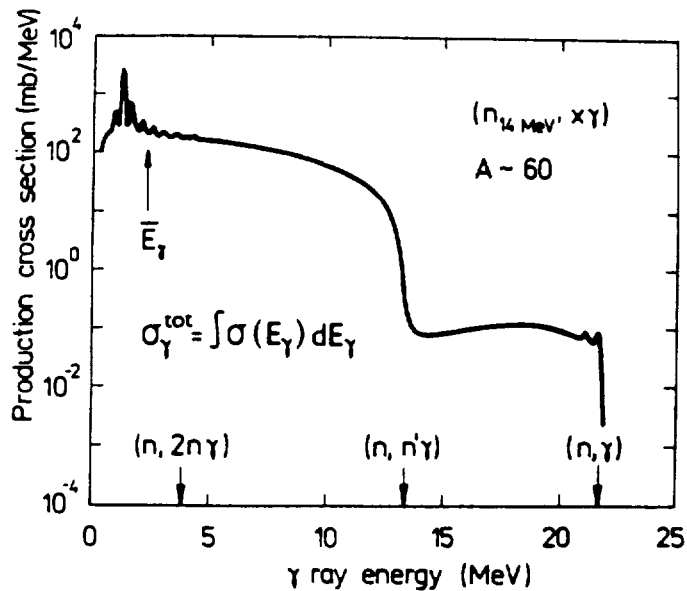


Fig.1. Typical  $\gamma$  ray production spectrum induced by 14 MeV neutrons.

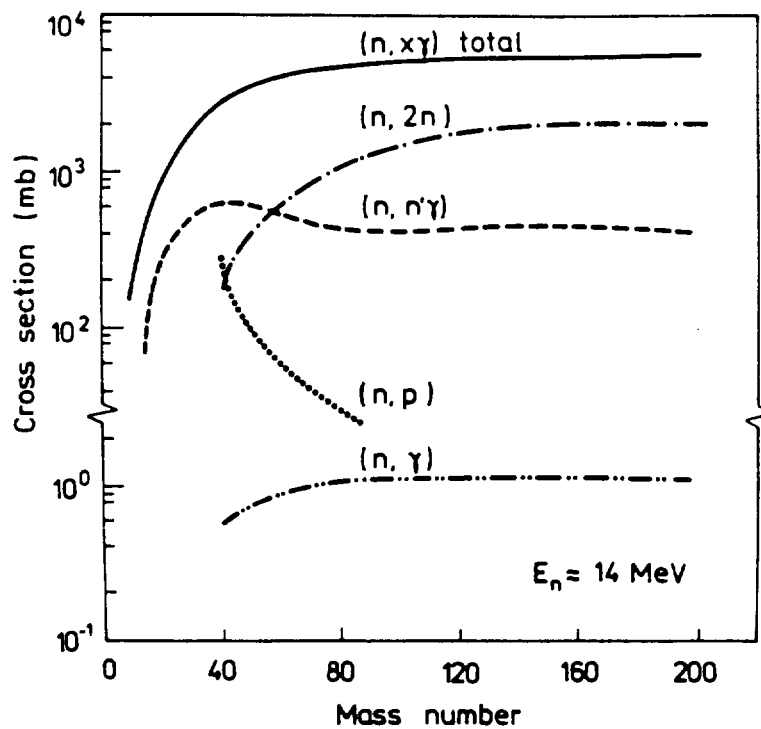


Fig.2. Gross trend in  $(n, x\gamma)$  total production cross section at 14 MeV as a function of the mass number. Shown for comparison are gross trends of some other reaction channels. (Taken from ref.9, cfr. also ref.34 and fig.5.)

As demonstrated experimentally in ref.<sup>10)</sup> discrete  $\gamma$  ray component prevails in light elements, with increasing mass number discrete  $\gamma$  rays become less prominent due to increasing statistical component and, eventually, they may be virtually absorbed into unresolved  $\gamma$  rays. This latter point is partly demonstrated in fig.2 displaying gross trend in total  $\gamma$  ray production cross section at 14 MeV as a function of the mass number.

The prompt  $\gamma$  ray technique consists in irradiating a sample by a beam of fast neutrons and in taking a high resolution  $\gamma$  ray spectrum due to  $(n, x\gamma)$  reactions on the elements/ isotopes of the sample. Intensities of  $\gamma$  lines contain information about elemental composition of the sample. It seems useful to introduce sensitivity factors characterizing analytical capability of the method for various elements of interest. In analogy to ref.<sup>11)</sup> dealing with thermal neutron capture we define the sensitivity factor as

$$S = 100 \sigma \alpha / A, \quad (1)$$

where  $\sigma$  is the (isotopic rather than elemental) cross section for production of discrete  $\gamma$  line in  $(n, x\gamma)$  reaction given in barns,  $\alpha$  is the isotopic abundance in the element and A is the mass number. Thus, S represents a number of specific discrete  $\gamma$  rays created by 100 incident neutrons in a weight unit.

Sensitivity factors at 14 MeV neutron incident energy for several elements are given in tab.1. Shown for comparison are the sensitivity factors for thermal neutron capture on these elements<sup>11)</sup>. From this comparison and by considering the minimum detection limits for  $(n_{th}, \gamma)$  as quoted in ref.<sup>4)</sup>, it can be concluded that  $(n, x\gamma)$  reactions should provide sufficient

Tab.1. Sensitivity factors of  $(n, x\gamma)$  reactions at 14 MeV for selected elements. Given in the last column are sensitivity factors for thermal neutron capture.

Element	Reaction	$E_{\gamma}$ (MeV)	$\sigma$ (b)	S	$S_{th}$
C	12-C( $n, n'\gamma$ )	4.443	.180(25)	1.5	.02
O	16-O( $n, n'\gamma$ )	6.130	.144(21)	.9	<.01
Si	28-Si( $n, n'\gamma$ )	1.779	.410(45)	1.3	.45
Fe	56-Fe( $n, n'\gamma$ )	.847	.550(70)	.9	1.3
In	115-In( $n, 2n\gamma$ )	.451	.088(10)	.07	20.
Pb	208-Pb( $n, n'\gamma$ )	2.613	.400(50)	.10	.08

sensitivity for all major ( $\geq 1\%$ ) geological elements and probably partly also for minor elements ( $\sim 0.01 - 1\%$ ). The method is unsuitable for trace geological elements.

### 3. Methods for determining discrete $\gamma$ production cross sections

The methods to be discussed are experimental and theoretical. Importance of the theoretical methods is underlined by the fact that many cross sections are not available and one has often resort on theoretical calculations to obtain the data of interest.

#### 3.1. EXPERIMENTAL METHODS

Experimental methods are those of in-beam  $\gamma$  ray spectroscopy<sup>12)</sup>. Schematic view of experimental arrangement for  $(n, \gamma)$  cross section measurement is shown in fig.3. A beam of charged particles is converted by appropriate target into neutrons which irradiate a sample.  $\gamma$  rays are measured by a spectrometer, in recent years usually a large Ge(Li) diode, located under the angle  $\vartheta$  towards the neutron beam and heavily shielded from the beam of primary neutrons. Neutron fluence is determined by means of the external monitor.

Important questions in such experiment concern neutron source, geometry of the experiment, sample and its size, choice of  $\gamma$  spectrometer, its shielding, timing, neutron monitor, data reduction, corrections to be applied and uncertainties of measured cross sections. Below we briefly touches on some of these points.

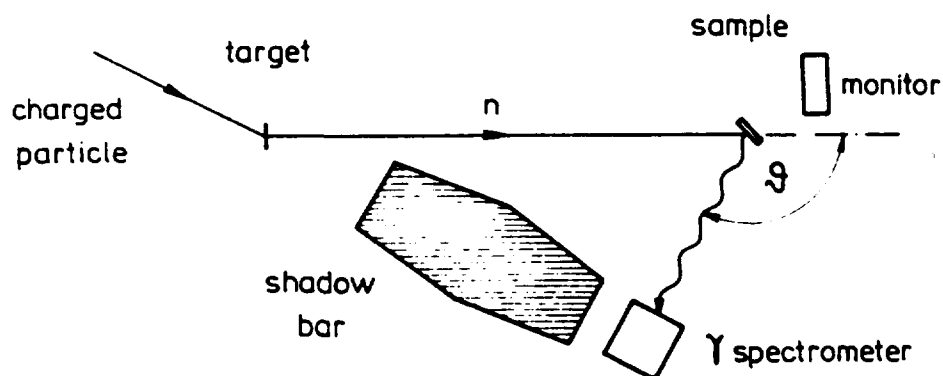


Fig.3. Schematic view of experimental arrangement for  $(n, \gamma)$  cross sections measurements.

Sources producing neutrons with energies in the region 1-20 MeV are monoenergetic and pulsed white neutron sources<sup>13)</sup>. Monoenergetic sources, based on p+T, D+D and D+T reactions, are relatively cheap and they cover the energy ranges 1-6 MeV and around 14 MeV. As a consequence, many data in the region from 6 to 14 MeV are missing. White neutron sources, covering the whole energy region of interest, ususally convert beam of energetic electrons into bremsstrahlung radiation which is subsequently converted into neutron beam by means of ( $\gamma, n$ ) reactions. Neutron energy has to be determined by the time-of-flight technique. Probably the only pulsed white neutron source presently used for ( $n, x\gamma$ ) cross section measurements is the ORELA (Oak Ridge Electron Linear Accelerator) facility at Oak Ridge.

Geometry of the experiment should be considered carefully because of the angular distribution of the  $\gamma$  production cross section. It can be expressed via the sum of the Legendre polynomials as

$$\frac{d\sigma(\vartheta)}{d\omega} = a_0 + a_2 P_2(\cos\vartheta) + a_4 P_4(\cos\vartheta), \quad (2)$$

where  $a_0, a_2, a_4$  are the coefficients to be determined experimentally. Important for the present application are the angle-integrated cross sections given as

$$\sigma = \int_{4\pi} \frac{d\sigma(\vartheta)}{d\omega} d\omega = 4\pi a_0. \quad (3)$$

Usually  $P_4$  represents a small contribution and

$$\sigma \approx 4\pi \frac{d\sigma(125^\circ)}{d\omega} \quad (4)$$

because of  $P_2(\cos\vartheta) = 0$  at  $125^\circ$  and also at  $55^\circ$ . The approximation (4) is usually well valid, there are cases, however, when up to 15% discrepancies between (3) and (4) were observed<sup>14)</sup>. Traditionally, many measurements were done at  $\vartheta = 90^\circ$  and one should take angle-integrated cross sections based on such single-angle values with care.

Another important point is fast timing. Since the processes involved are very fast, it is advisable to apply fast timing techniques to reduce background radiation substantially in the observed  $\gamma$  spectra. With Ge(Li) spectrometers the timing resolution of about 5-6 ns can be achieved.

Uncertainties in measured cross sections are due to contributions from various effects. Among them are Ge(Li) absolute photopeak efficiency, neutron fluence, statistics of peak intensity, corrections for multiple scattering and attenuation, and already discussed geometry. In best cases the uncertainties of about 5% are achieved, though typical values are 10-20%.

### 3.2. THEORETICAL METHODS

Generally,  $(n, x\gamma)$  reactions below 20 MeV are governed by slow statistical processes and one should apply the statistical model of nuclear reactions to calculate  $\gamma$  ray production cross sections. In recent versions of this model one already accounts for semi-fast preequilibrium or multi-step compound particle emission. Fast processes which are best accounted for by direct reaction theories are of much less importance and they are commonly neglected. One should keep in mind that although direct contribution to lowest excited levels via  $(n, n')$  scattering is often important, the  $\gamma$  ray production itself is still essentially statistical because of feeding from higher levels via complicated  $\gamma$  cascades.

The  $\gamma$  ray production cross section is expressed in the statistical model as a product of 3 terms

$$\sigma_{(n, x\gamma)} = \text{compound nucleus} \otimes \text{particle emission} \otimes \gamma \text{ cascade. (5)}$$

The first term, compound nucleus cross section, is calculated by means of the optical potential. The second term, representing the probability to emit a particle  $x$ , is treated within the standard Hauser-Feshbach formalism as well as the preequilibrium nuclear reaction theory. The third term describes the

cascade which is treated statistically at higher excitations and realistically between low lying discrete levels.

Pictorial presentation of the statistical description of  $(n, n'\gamma)$  reaction is given in fig.4. In the first step the compound nucleus  $(Z, A+1)$  is formed. This is followed by inelastically emitted neutron giving rise to a spectrum of excited

compound  $\times$  particle emission  $\times$   $\gamma$  cascade

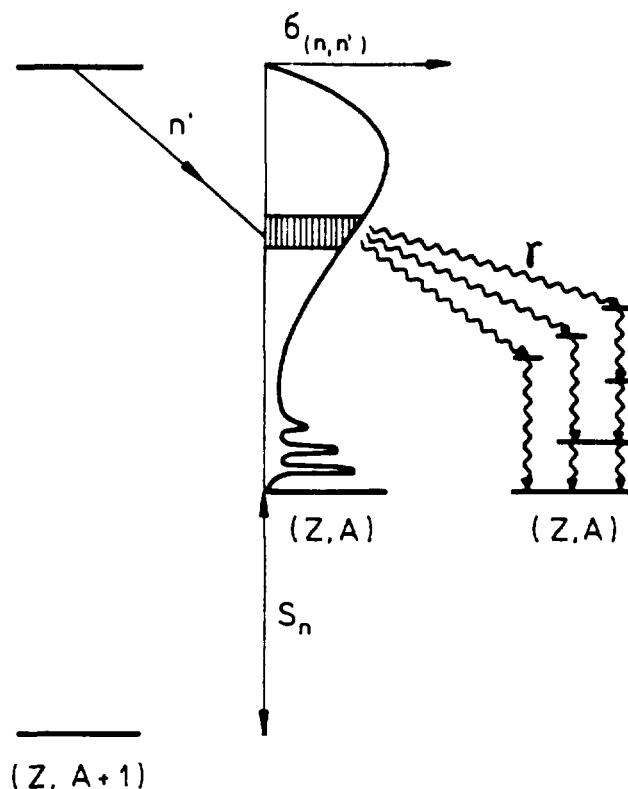


Fig.4. Pictorial presentation of the statistical description of  $(n, n'\gamma)$  reactions.

levels in a nucleus  $(Z, A)$ . Each of these excited states decays by a cascade composed of several  $\gamma$  transitions. The  $\gamma$  rays involve continuum-continuum transitions, continuum-discrete levels transitions and finally transitions between discrete levels. Resulting intensity of a specific discrete  $\gamma$  ray is obtained by summing up all ways of its population.

A set of parameters needed for the statistical model calculation include optical potential, level densities, preequilibrium decay,  $\gamma$  ray strength functions and decay schemes. Each of these points represents a field in its own being in permanent development<sup>15-19</sup>).

Presently, several useful statistical model codes for discrete  $\gamma$  production are available. They are listed in tab. 2 (see refs.<sup>20-22</sup>).

Important in these calculations is their accuracy. This is a very difficult question, where simple answer is impossible. Still, as a guideline, we make the following comments.

(i) Present application seems to be limited to common elements/isotopes and respective strong  $\gamma$  lines. This implies

Tab.2. Statistical model codes for discrete production.

Program	Authors	Laboratory	Year	Formalism
GNASH	E.D.Arthur P.Young	Los Alamos	1977	Hauser-Feshbach Preeq. exciton & cascade
HAUSER 5	F.Mann	Hanford	1978	- " -
STAPRE	M.Uhl B.Strohmaier	Vienna	1976	- " -
TNG	C.Y.Fu	Oak Ridge	1977	- " -
EMPIRE	M.Herman A.Marcinkowski	Warsaw	1984	Hauser-Feshbach Preeq. hybrid & cascade

that parameters needed for calculations should be available in a rather reasonable shape. (ii) Total  $(n,n')$  cross section, which is probably of most interest here, can be calculated with accuracy about 20%. This can be inferred from the optical model parametrization, the Hauser-Feshbach and preequilibrium decay. There are cases, however, where direct contribution to collective levels even at low incident energies is substantial (confer  $\sim 30\%$  contribution to  $2_1^+$  levels in a number of even-even nuclei as observed in ref.23). (iii)  $\gamma$  cascade causes another uncertainty which probably may add additional  $\sim 20-50\%$ . (iv) Total uncertainty in calculated discrete  $\gamma$  ray production cross sections may be thus  $\sim 30-50\%$  or even more. Only in best cases one should reasonably expect  $\sim 20\%$  accuracy.

#### 4. Status of measurement and evaluation

In this section we outline the status of measurement and evaluation of discrete  $\gamma$  ray production cross sections in  $(n,\gamma)$  reactions below 20 MeV. We focus on essential features in the field rather than on many details involved. We note that the activity in the field, as can be inferred from several representative sources<sup>24-26</sup>, is limited to a few groups worldwide. This suggests that one should often rely on measurements of an older vintage while evaluations and systematics are very limited in both scope and aim.

First, we discuss the status of experimental data and follow two useful classifications - according to neutron in-

cident energy  $E_n$  and according to atomic number  $Z$ . Second, we discuss the status of evaluated data. Finally, we illustrate the present state of these data on several examples.

#### 4.1. STATUS OF MEASUREMENT

Three major neutron energy groups can be distinguished. Low energy group from about 1 MeV to 3 MeV or even up to 6 MeV, 14 MeV neutron group, and 1-20 MeV group as covered by pulsed white neutron sources. Number of elements studied is summarized in tab.3.

Tab.3. Summary of discrete  $\gamma$  ray production cross sections as measured for 3 neutron energy groups.

Neutron energy	1 - 3 (6) MeV	14 MeV	1 - 20 MeV
Number of elements	many	35	13

Data in low neutron energy region are available practically for all elements/isotopes of interest. Useful guidance is provided by the Gamma atlas<sup>27)</sup>. Given there is rather comprehensive set of high resolution  $\gamma$  ray spectra and reference cross sections as integrated over fission spectrum of fast neutrons,  $E_n \geq 1$  MeV, from the reactor. More systematical surveys are not available. Extensive list of references can be found in CINDA<sup>28)</sup>. A lot of early cross section measurements was carried out with NaI(Tl) spectrometers (initiated in ref. 29)), they are still valuable since the  $\gamma$  ray spectra at a few MeV of neutron energy are relatively simple.

The 14 MeV data are available for about 35 elements. A number of discrete  $\gamma$  ray cross sections was measured with NaI(Tl) spectrometers. Such works, though still useful, report only several strongest  $\gamma$  lines (e.g., ref.<sup>30)</sup>) or groups of strongest lines only. Of more interest are careful high resolution measurements carried out with Ge(Li) spectrometers as initiated in ref.<sup>31)</sup>. Some recent measurements are reported in ref.<sup>32)</sup>. Surveys of 14 MeV data are not available. Based on literature sources, referred to in CINDA, we have found that for all elements from Li up to Zn,  $3 \leq Z \leq 30$ , with the exception of Ne and Ar, the cross sections of interest were measured. Often, several measurements are available. As a guidance we collected

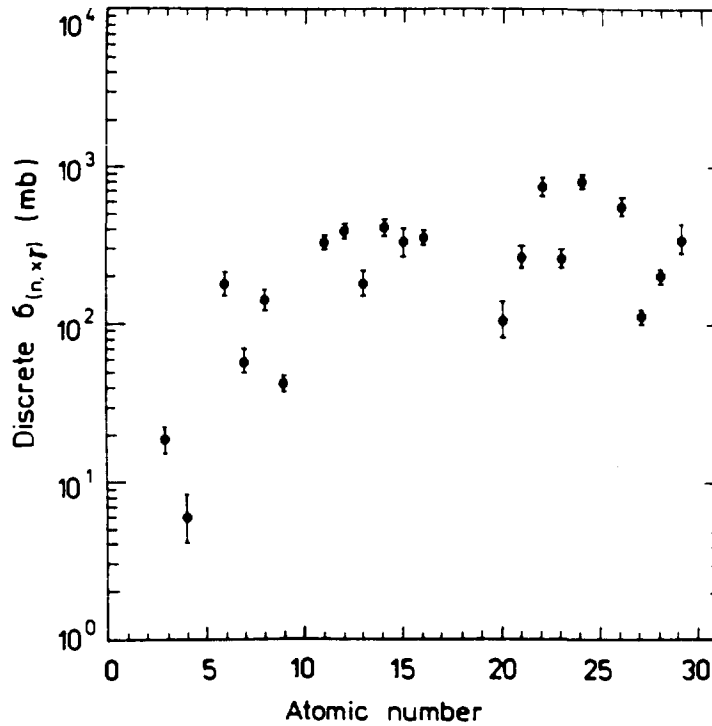


Fig.5. Production cross sections for strongest  $\gamma$  lines induced by 14 MeV neutrons as a function of the atomic number. (Taken from from refs. quoted as 33).

the strongest  $\gamma$  lines, probably of most importance for geophysical applications, for these elements. They are shown in fig.5.

The last neutron energy group, from 1 to 20 MeV, actually covers the whole energy region of interest. The  $\gamma$  ray production cross section measurements in this group are systematically carried out only with the Oak Ridge pulsed white neutron source. The motivation, however, is the fusion reactor program, therefore, simplified energy spectra rather than high resolution ones are of primary interest. Still, some useful sets of data were collected and for about 13 elements discrete  $\gamma$  ray production cross sections are available in this energy region.

Since fusion reactor requirements represent important objectives for  $\gamma$  production cross section measurements we show in tab.4 an overview of 2 representative sets of data. Experimental data as supplied for 23 elements by the Soviet Kurchatov Atomic Energy Institute concentrate on 14 MeV region<sup>34)</sup>. These data, with perhaps a very few exceptions, can not be used for present application. Oak Ridge supplied 1-20 MeV data for 26 elements<sup>35)</sup>. Most of them are NaI(Tl) spectra, only

Tab.4. Elements measured by 2 major suppliers of production data for nuclear energy industry. Further given is the list of evaluated  $\sigma$  production cross sections.

Z	Element	E x p e r. data		E v a l. in ENDF			Geophys. importance
		Kurchatov	Oak Ridge	Version	(n,n $\gamma$ )	(n,x $\gamma$ )	
		14 MeV	1-20 MeV				
3	Li		x	B5	x		
4	Be			B4		x	
5	B	x		B5	x	x	
6	C	x	x	B5	x		oil
7	N	x	x	B4	x	x	
8	O	x	x	B4	x	x	major
9	F		x	B4	x	x	
11	Na		x	B4	x		major
12	Mg	x	x	B4	x	x	major
13	Al	x	x	B4	x	x	major
14	Si	x	x	B4	x	x	major
15	P	x					major
16	S	x					
17	Cl			B4	x		sea
19	K			B4	x	x	major
20	Ca		x	B4	x	x	major
21	Sc						
22	Ti	x	x				major
23	V		x	B4	x		
24	Cr		x	B5	x		
25	Mn		x	B4	x		
26	Fe	x	x	B4	x		major
27	Co						
28	Ni		x	B5	x	x	
29	Cu	x	x	B5	x		
30	Zn	x	x				
40	Zr	x					
41	Nb		x				
42	Mo	x	x				
47	Ag		x				
48	Cd	x					
49	In	x					
50	Sn	x	x				
73	Ta	x	x	B5	x		
74	W	x	x	B5	x		
79	Au		x				
80	Hg	x					
82	Pb	x	x	B5	x		
83	Bi	x					
	Sum	23	26	23	22	11	

recently systematic measurements of Ge(Li) spectra are reported (Cu, Cr, Fe, Ni, see refs.<sup>36,37</sup>). The NaI(Tl) data for light elements, up to about Al, are valuable for present application, in a few other cases only most prominent  $\gamma$  line can be extracted (e.g, Si). Discrete  $\gamma$  ray production cross sections for 12 elements were collected in the Japanese compilation study<sup>38</sup>).

Table 4 suggests that one should classify the data according to the atomic number and 2 broad categories of elements can be identified. While for  $Z \leq 30$  many results are available (confer also 14 MeV data collected in fig.5), the  $Z > 30$  elements were studied in several cases only. For present application, however, this circumstance does not seem disadvantageous. Majority of geophysically important elements as well as those where the prompt  $\gamma$  ray technique with fast neutrons seems to be applicable falls just into the  $Z \leq 30$  category.

#### 4.2. STATUS OF EVALUATION

It turns out that the evaluated nuclear data libraries provide rather limited information about discrete  $\gamma$  ray production cross sections. The reason is that these libraries do serve nuclear energy programs. Moreover, even total  $\gamma$  ray production spectra were not given high priority. An overview of elements, <sup>where</sup> evaluations from 1 to 20 MeV incident neutrons were done, is shown in the second half of tab.4. Here, we quote ENDF/B4 and B5 data files. It is seen, that the total number of elements is 23. As can be inferred from the recent paper by Clayton<sup>39</sup>), other evaluated libraries such as JENDL and ENDL do not provide much more information. Thus, only for light nuclei one can find in these files useful data we are interested in.

Another view of the problem of evaluated data can be made by looking on recent activities in the field. From the 3 very recent evaluations of various elements<sup>40-42</sup>), no one deals with the discrete  $\gamma$  production. This suggests that little changes concerning discrete  $\gamma$  ray cross sections are to be expected in the evaluated data files in near future. Only in a few cases discrete  $\gamma$  ray production was evaluated explicitly (e.g., Si for the Soviet library SOKRATOR, see ref.<sup>43</sup>).

### 4.3. ILLUSTRATIVE EXAMPLES

Here, we demonstrate some of the points (together with some interesting details), made so far, on several illustrative examples. We briefly discuss O, Si, Ca, Fe, Ni, Nb and Pb.

Oxygen, shown in fig.6, is a representative of light nuclei. Threshold energies of  $^{16}\text{O}(n, x\gamma)$  reactions are high and

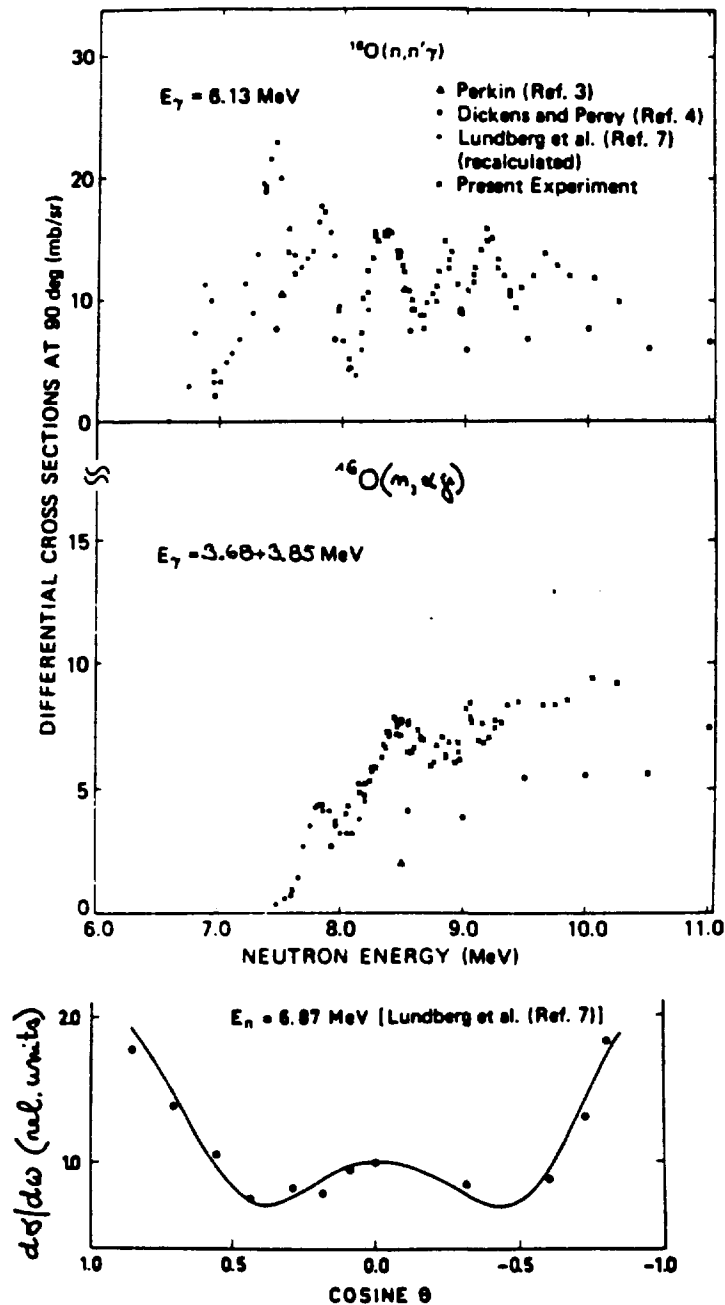


Fig.6. Discrete  $\gamma$  ray production in the  $^{16}\text{O}(n, x\gamma)$  reactions. Shown from top to bottom is the excitation function for the 6.13 MeV  $\gamma$  line in  $(n, n'\gamma)$ , the excitation function for the 3.68 MeV + 3.85 MeV  $\gamma$  lines in  $(n, \alpha\gamma)$ , and the angular distribution of the 6.13 MeV  $\gamma$  line at 6.87 MeV of neutron energy. (Taken from ref. 45.)

the excitation functions of discrete  $\gamma$  ray production cross sections reveal resonance structure. The dominant transition is the 6.13 MeV  $\gamma$  line in  $(n,n'\gamma)$ . Charged particle channels, due to low Coulomb barriers, are rather strong, too. Production of the 6.13 MeV  $\gamma$  line displays strong angular dependence providing an example of the angular distribution which should be probably explicitly included into the data base rather than mere angle-integrated values.

Silicon is a major geophysical element and it plays an important role in shielding due to concrete. The most prominent  $\gamma$  line is the 1.78 MeV transition in the  $^{28}\text{Si}(n,n'\gamma)$  reaction. As shown in fig.7 there are several measurements up to about 8 MeV and 4 measurements at 14 MeV. The spread of data at low energies is appreciable, which seems to be true also for many other elements. Evaluated data files, e.g., ENDF/B4 and B5, do not quote explicitly cross sections for this line. Rather, they give total  $\gamma$  spectra, where from such information, in favourable cases, can be extracted. The results of such a procedure, which certainly is not without difficulties, are displayed in fig.7, too. Explicit calculations carried out with the statistical code STAPRE<sup>21)</sup> seems perform better than both the ENDL-2 and ENDF/B4 evaluations.

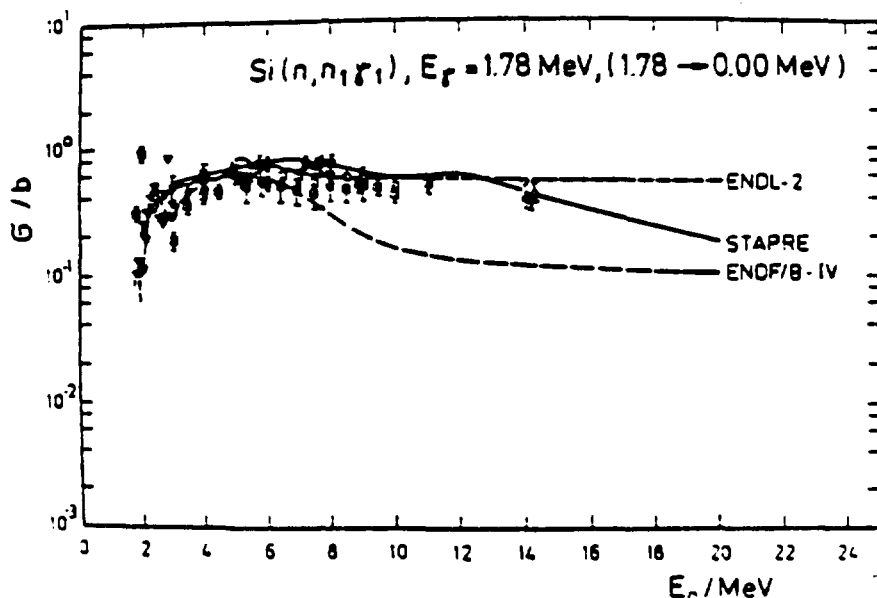


Fig.7. Excitation function for the 1.78 MeV  $\gamma$  line in the  $^{28}\text{Si}(n,n'\gamma)$  reaction. Data are compared with the ENDL-2 and ENDF/B4 files as well as with the statistical calculations using the code STAPRE. (Taken from ref.43).

Calcium is an example of relatively heavier nucleus where the NaI(Tl) spectra as taken at ORELA can be used for extracting production of the strongest  $\gamma$  lines only. Shown in fig.8 (top) is the unfolded  $\gamma$  spectrum which displays a strong bump at about 3.8 MeV composed of the 3.737 MeV and 3.904 MeV  $\gamma$  lines. Overall accord between evaluated and measured spectrum for  $E_n = 10 - 12$  MeV seems to be good. Explicit measurements of the above discrete lines are limited to low neutron energies and to the 14 MeV region (fig.8, bottom), and the excitation functions have to be completed by theoretical calculations.

Two further examples of typical excitation curves are shown in figs. 9,10. Iron is an example of element where very many measurements were done. This is especially valid for the strong 847 keV  $\gamma$  line in the  $^{56}\text{Fe}(n,n'\gamma)$  reaction. There are more than 20 different cross sections at 14 MeV itself with the spread within the factor of 2 (cfr. ref.<sup>9</sup>). The situation at lower energies as illustrated in fig.9 seems to be very much the same. Theoretical analysis should be used to decide which set of experimental data is more reliable.

Nickel was studied at Oak Ridge<sup>36)</sup> from 1 to 25 MeV. Dominant is the 1454 keV  $\gamma$  line due to  $^{58}\text{Ni}(n,n'\gamma)$  reaction. As seen in fig.10, the maximum production is at about 4 MeV, while at 14 MeV it is already down to  $\sim 1/3$  due to competing reaction channels. At still higher energies the  $(n,n'\gamma)$  channel is even weaker than the  $(n,np\gamma)$ . We note that the  $(n,2n\gamma)$  is extremely weak because of the magic number of neutrons. Accord with calculated cross sections is fairly good.

Our final example concerns two  $Z > 30$  elements. Shown in fig.11 are excitation functions for dominant  $\gamma$  lines produced in niobium and lead. Here, experimental data are essentially limited to low neutron energy region. In fact, the excitation functions are based on theoretical calculations.

## 5. Conclusions

We reviewed the status of measurements and evaluation of microscopic cross sections for discrete  $\gamma$  ray production in reactions induced by neutrons from threshold energies to 20 MeV. These data are of interest for nuclear geophysics/geoche-

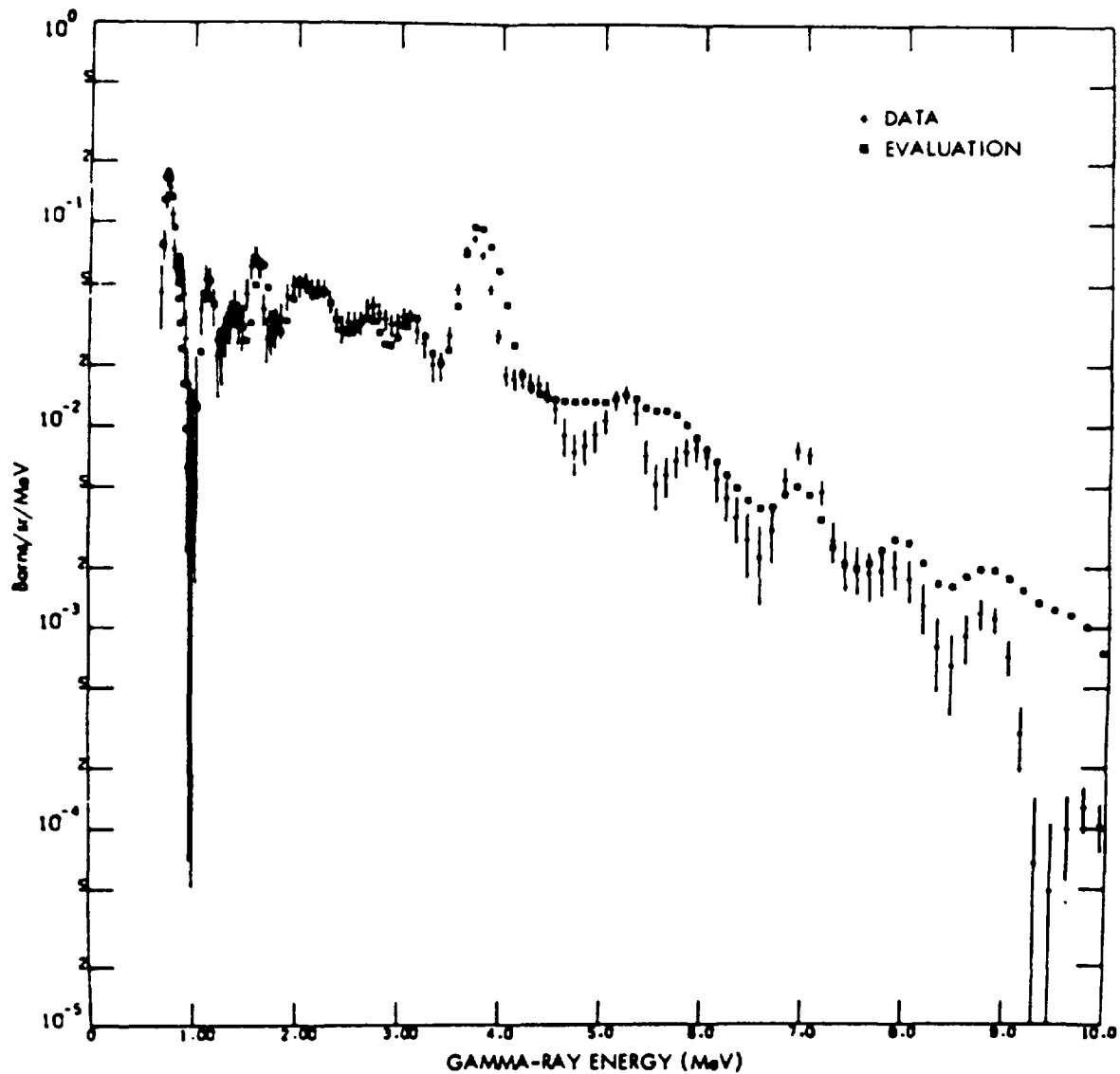
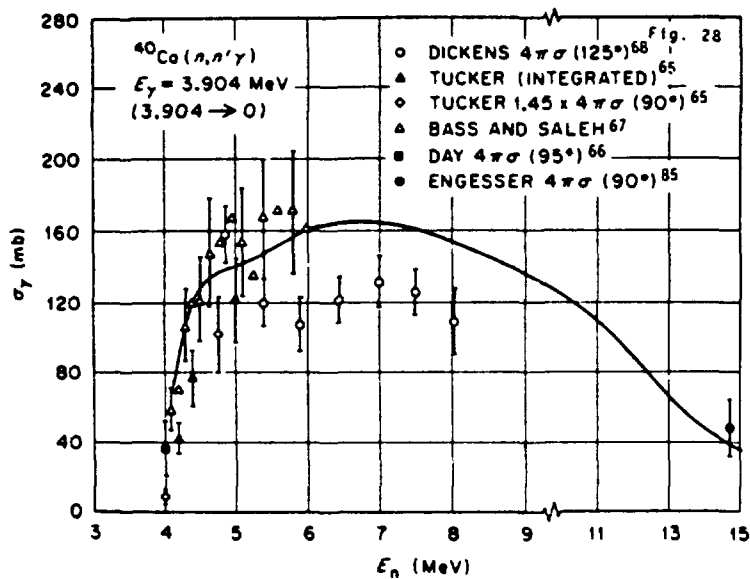


Fig.8.



γ-ray production in Ca (n,xγ) reactions. Shown above is the total γ-ray spectrum for  $10 \text{ MeV} \leq E_n \leq 12 \text{ MeV}$ . Shown below is the excitation function for the strong 3.904 MeV γ line in  $^{40}\text{Ca}(n,n'\gamma)$ . (Taken from ref.46.)

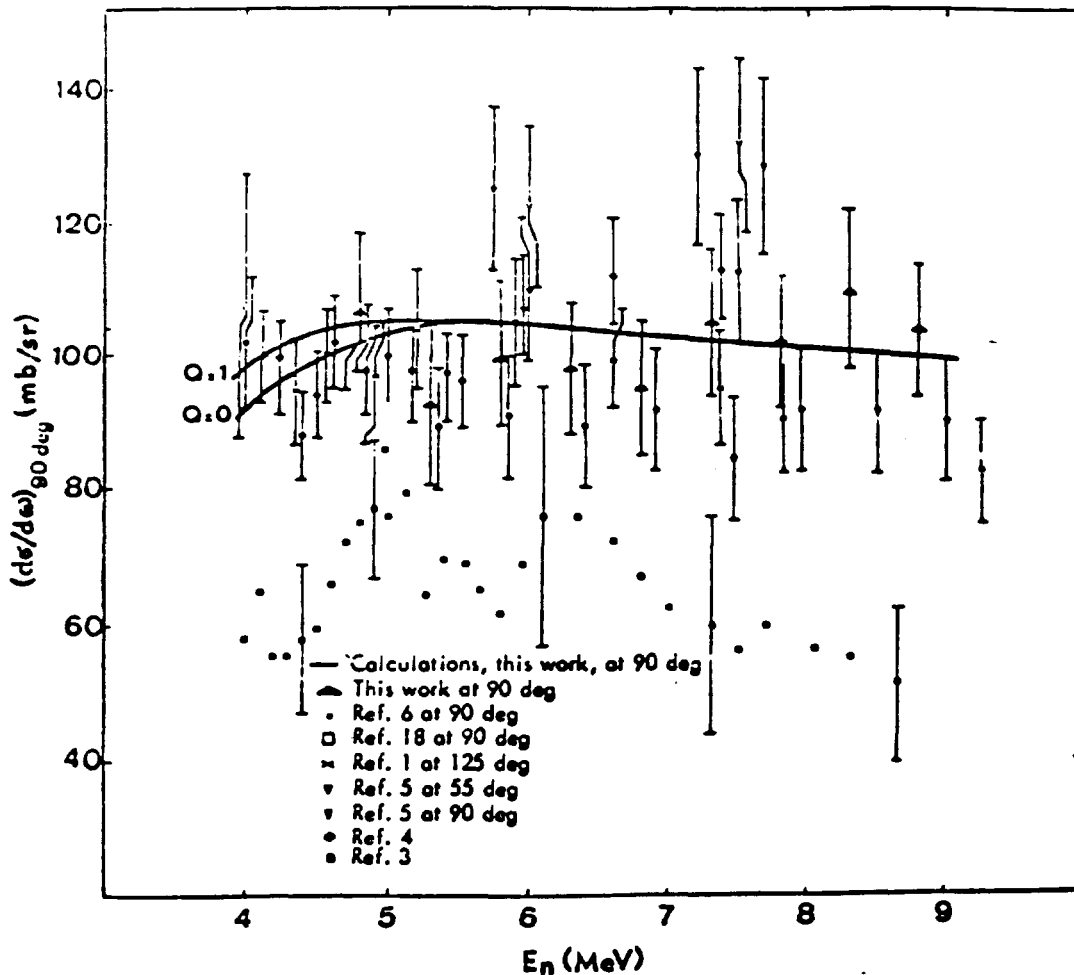


Fig.9. Excitation function for the dominant 847 keV  $\gamma$  line in the  $^{56}\text{Fe}(n, n'\gamma)$  reaction. (Taken from ref.47.)

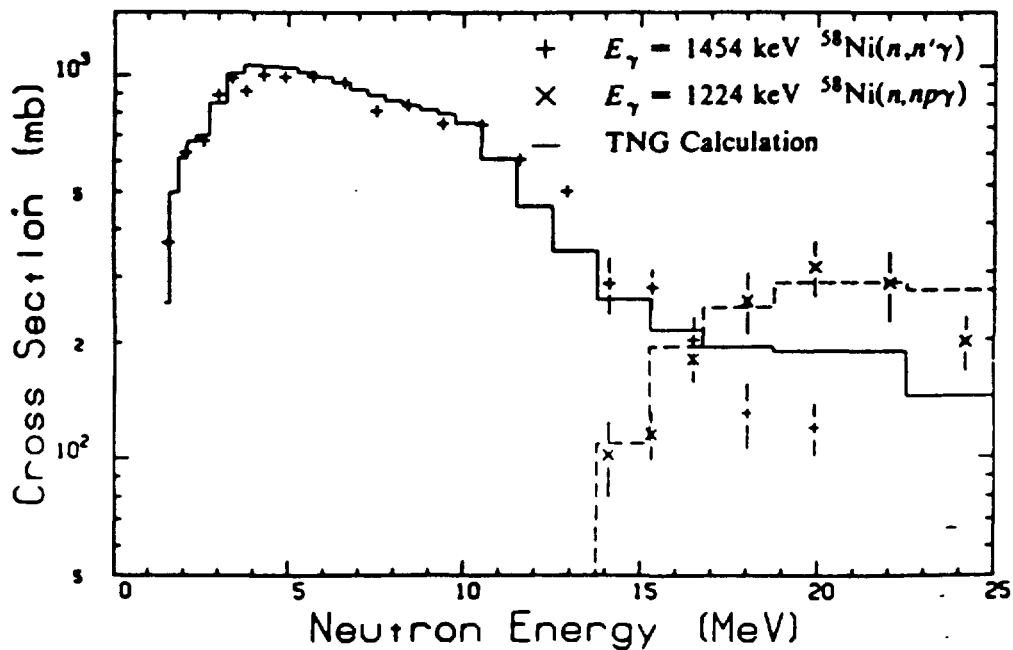


Fig.10. Excitation functions for the 1454 keV  $\gamma$  line in the  $^{58}\text{Ni}(n, n'\gamma)$  reaction and for the 1224 keV  $\gamma$  line in the  $(n, np\gamma)$  channel. (Taken from ref.36.)

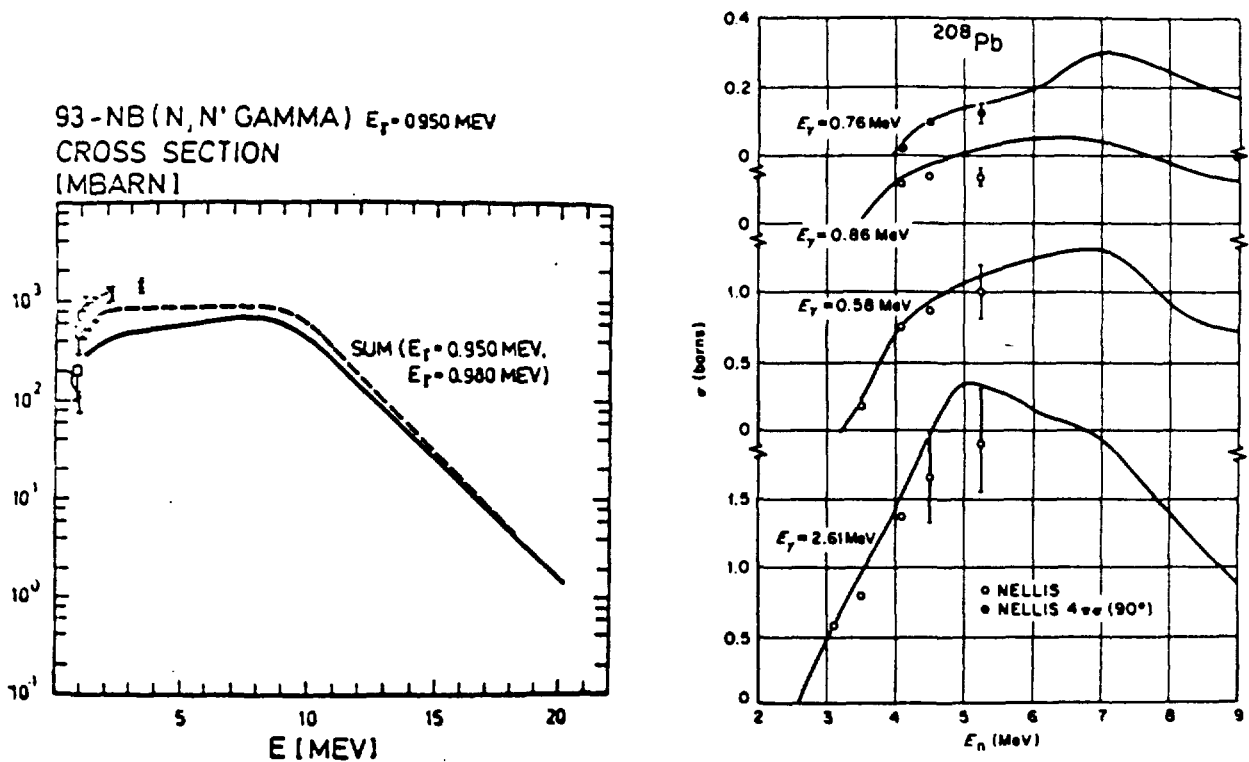


Fig.11. Excitation functions for dominant  $\gamma$  lines produced in Nb and Pb. Shown above is the 0.950 MeV  $\gamma$  line in the  $^{93}\text{Nb}(n,n'\gamma)$  reaction. Shown below are four  $\gamma$  lines in the  $^{208}\text{Pb}(n,n'\gamma)$  reaction. (Taken from refs. 44, 48.)

mistry applications employing the prompt  $\gamma$  ray technique via  $(n,x\gamma)$  reactions with fast neutrons.

We have found that the situation in both measurements and evaluation of angle-integrated production cross sections of discrete  $\gamma$  rays is not satisfactory. Often, measurements are confined only to a few MeV and to 14 MeV neutron energy regions. Systematics of data are virtually non-existing. Evaluated nuclear data files basically omit this type of information.

Specialized effort should be undertaken to create/consolidate an appropriate data base for application of  $(n,x\gamma)$  reactions in nuclear geophysics.

## References

1. R.R. Randall: Application of accelerator sources for pulsed neutron logging of oil and gas wells, Nucl.Instr. Meth. B10(1985)1028
2. J.C. Laul: Neutron activation analysis of geological materials, Atomic Energy Review (IAEA) 17(1979)603

3. M.D. Glascock et al.: Geochemical applications for prompt gamma neutron activation, Nucl.Instr.Meth. B10(1985)1024
4. R.E. Chrien: Practical uses of neutron capture gamma-ray spectroscopy, in Neutron Radiative Capture, ed. R.E. Chrien (Pergamon Press, Oxford 1984) p. 187
5. J.A. Grau, S. Antkiw, R.C. Hertzog, R.A. Manente and J.S. Schweitzer: In situ neutron capture spectroscopy of geological formations, in Capture Gamma-Ray Spectroscopy and Related Topics-1985, ed. S. Raman (Amer.Inst.Phys., New York 1985) p. 799
6. L.G. Evans et al.: Determination of elemental composition in geochemical exploration using a 14-MeV neutron generator, IEEE Trans.Nucl.Sci. 28(1981)1626
7. S. Hlaváč and P. Obložinský: Fast-neutron induced prompt  $\gamma$  ray analysis, to be published
8. Proceedings of the IAEA Consultants' Meeting on Nuclear Data for Bore-Hole and Bulk-Media Assay Using Nuclear Techniques, Krakow 1983, ed.K. Okamoto (IAEA, Vienna 1984) pp.1,5
9. P. Obložinský: Measurements of cross sections and spectra by in-beam  $\gamma$  ray spectroscopy, Inter.Symp.Fast Neut.Phys., Gaussig 1983, in Report INDC(NDS)-173/GI (IAEA,Vienna 1985) p. 62
10. J.K. Dickens et al.: Cross sections for gamma-ray production by fast neutrons for 22 elements, Nucl.Sci.Eng. 62(1977)515
11. D.Duffey, A. El-Kady and F.E. Senftle: Analytical sensitivities and energies of thermal-neutron-capture  $\gamma$  rays, Nucl.Instr.Meth. 80(1970)149
12. H. Morinaga and T. Yamazaki: In-Beam  $\gamma$  Ray Spectroscopy (North-Holland, Amsterdam 1976)
13. Neutron Sources for Basic and Applications, ed.S. Cierjacks (Pergamon Press, Oxford 1983)
14. Z.W. Bell et al.: Neutron induced  $\gamma$  ray production in  $^{57}\text{Fe}$  for incident neutron energies between 0.16 and 21 MeV, Nucl. Sci.Eng. 84(1983)12
15. NEANDC Specialists' Meeting on the Optical Model for Calculations of Neutron Cross Sections below 20 MeV, Paris, November 13-15, 1985
16. IAEA Advisory Group Meeting on Basic and Applied Problems of Nuclear Level Densities, Brookhaven 1983, ed.M.R. Bhat, Report BNL-NCS-51694 (Brookhaven 1983)
17. M. Blann: Preequilibrium decay, Ann.Rev.Nucl.Sci. 25(1975) 127
18. D.G. Gardner: Methods for calculating neutron capture cross sections and  $\gamma$  ray energy spectra, in Neutron Radiative Capture, ed. R.E. Chrien (Pergamon Press, Oxford 1984)p. 62

19. Eds. C.M. Lederer and V.S. Shirley: Table of Isotopes (Wiley, New York 1978)
20. P.G. Young: Nuclear model codes and data evaluation, Symp. Neut. Cross Sect. from 10 to 50 MeV, Brookhaven 1980, see Report BNL-NCS-51245 (Brookhaven 1980) p. 43
21. M. Uhl and B. Strohmaier: Statistical model code STAPRE, Report IRK 76/01 (IRK, Vienna 1976)
22. M. Herman et al.: Statistical model code EMPIRE, Comp. Phys. Comm. 33 (1984)373
23. L.I. Govor et al.: On cross sections of excited levels in  $(n, n'\gamma)$  reactions on even-even spherical nuclei with  $28 \leq A \leq 152$ , Yad. Phys. 29(1979)1425, in Russian
24. Eds. M.R. Bhat and P.F. Rose: Fast-Neutron Cross-Section Newsletter No. 1-10 (Brookhaven 1981-1986)
25. Ed. K.H. Böckhoff: Nuclear Data for Science and Technology, Proc. Inter. Symp., Antwerp 1982 (Reidel, Dordrecht 1983)
26. Co-ordinated Research Programme on Measurement and Analysis of 14 MeV Neutron Nuclear Data (dir. M.K. Mehta, IAEA, Vienna 1983-1986)
27. A.M. Demidov et al.: Atlas of  $\gamma$ -Ray Spectra from the Inelastic Scattering of Reactor Neutrons (Atomizdat, Moscow 1978), also IAEA Report INDC(CCP)-120
28. CINDA = Computer Index of Neutron Data, vol.1,2 (1935-1976) and Suppl. 83 (1977-1983) (IAEA, Vienna)
29. R.B. Day: Gamma rays from neutron inelastic scattering, Phys. Rev. 102(1956)767
30. D.M. Drake: More 14 MeV neutron induced  $\gamma$  ray production cross sections, Report LA-5893-MS (Los Alamos 1975)
31. B. Jönsson et al.: High resolution measurements of  $\gamma$  rays produced by 15 MeV neutrons, Reports NP 6803(1968), NP 6902(1969) (University of Lund)
32. S. Hlaváč and P. Obložinský:  $\gamma$  ray production cross sections and  $\gamma$  ray multiplicities from Fe and Ni bombarded with 14.6 MeV neutrons, in Report INDC(CSR)-5/GI (IAEA, Vienna 1983)
33. Bezotosnyj 1975 = Li, Hino 1980 = Be, Asami 1979 = C, Jönsson 1969 = N, O, Mg and Al, Corcalciuc 1978 = F and Co, Degtiarev 1977 = Na, Bezotosnyj 1980 = Si, P, S and Ti, Grenier 1973 = Ca and Sc, Larson 1985 = Cr, Hlaváč 1982 = Fe, Hlaváč 1983 = Ni, Slaughter 1983 = Cu, Hlaváč 1980 = Zn
34. V.M. Bezotosnyj et al.: Group and total gamma ray production cross sections in inelastic scattering of 14 MeV neutrons on various nuclei, Atomnaja Energija 49(1980)239, in Russian

35. D.C. Larson: ORELA measurements to meet fusion cross sections needs, in Symp. Neut. Cross-Sect. from 10 to 50 MeV, Brookhaven 1980 (eds. M.R. Bhat and S. Perlstein, Report-NCS-51245, Brookhaven 1980) p. 277
36. D.C. Larson: High-resolution structural material (n,x<sub>g</sub>) production cross sections for  $0.2 \leq E_n \leq 40$  MeV, Inter. Conf. Nucl. Data for Basic and Applied Science, Sanata Fe, May 13-17, 1985, to be published
37. G.G. Slaughter and J.K. Dickens: Gamma-ray production due to neutron interactions with copper for neutron energies between 0.7 and 10.5 MeV, Nucl. Sci. Eng. 84(1983)395
38. Eds. T. Asami and S. Tanaka: Graphs of neutron cross section data for fusion reactor development, Report JAERI-M 8136 (Japan Atomic Energy Res. Inst., 1979)
39. C.G. Clayton et al.: Some comments on the requirement for nuclear data in earth sciences, in Proc. IAEA Cons. Meet. Nucl. Data for Bore-Hole and Bulk-Media Assay, Krakow 1983 (ed. K. Okamoto, IAEA, Vienna 1984) p. 17
40. H. Kitazawa et al.: Calculation of gamma-ray production cross sections at neutron energies of 1~20 MeV, J. Nucl. Sci. Tech. 20 1983 273
41. P.G. Young and E.D. Arthur: Analysis of n + <sup>197</sup>Au cross sections for E = 0.01-20 MeV, in Capture Gamma-Ray Spectroscopy and Related Topics, Knoxville 1984 (ed. S. Raman, Amer. Inst. Phys., New York 1985) p. 530
42. A. Mengoni et al.: Evaluation of gamma-ray production cross sections and spectra for neutron induced reactions on chromium, REport ENEA, RT/TIB/86 (Bologna 1986)
43. D. Hermsdorf: Theoretical models and computer codes for 14 MeV neutron nuclear data calculation, in Report INDC(NDS)-173/GI (IAEA, Vienna 1985) p. 79
44. D. Hermsdorf, in Report ZfK (TU Dresden 1983)
45. C. Nordborg et al.: Gamma-ray production cross sections of neutron-induced reactions in oxygen, Nucl. Sci. Eng. 66(1978) 75
46. C.Y. Fu: Consistent calculation of (n,x) and (n,x<sub>g</sub>) cross sections for 40-Ca, E<sub>n</sub> = 1-20 MeV, Atomic Data and Nucl. Data Tables 17(1976)127
47. J. Lachkar et al.:  $\gamma$  ray production cross sections for the <sup>56</sup>-Fe(n,n'<sub>g</sub>) reaction from 2.5 to 14.1 MeV, Nucl. Sci. Eng. (1978)
48. C.Y. Fu and F.G. Perey: An evaluation of neutron and  $\gamma$  ray production cross-section data for lead, Atom. Data and Nucl. Data Tables 16(1975)409



# NUCLEAR DATA FOR ELEMENTAL ANALYSIS OF GEOLOGICAL SAMPLES WITH 14 MEV NEUTRONS

R. Pepelnik  
Institut für Physik, GKSS-Forschungszentrum Geesthacht GmbH  
D-2054 Geesthacht, Federal Republic of Germany

## INTRODUCTION

In comparison to other analytical techniques for geological samples, 14 MeV neutron activation analysis has the advantage that all elements of the main and minor components are detectable within a rather short time. In particular, light elements such as B, F, O, Si and P - which have good analytical sensitivities for fast neutrons - cannot be detected by X-ray fluorescence or thermal neutron activation analysis. In the past, accuracy in fast neutron activation analysis (FNAA) was often insufficient because of uncertainties in the distribution of neutron energy and flux, or in 14 MeV neutron reaction cross-sections. Another important source of error in FNAA is the frequent occurrence of elemental interferences: neighbouring elements may produce the same isotope via different reaction channels. To reduce systematic errors due to such interferences, many 14 MeV neutron activation cross-sections have been remeasured at the GKSS facility.

## NEUTRON ACTIVATION AND ANALYSIS SYSTEM

At the GKSS Research Center Geesthacht a high intensity 14 MeV neutron generator with an integrated rabbit system, named KORONA, has been used for NAA since 1981 [1]. The samples, encapsulated in polyethylene containers, are activated in the center of a cylindrical neutron target. Cyclic irradiation and measurement are feasible with a minimum transfer time of 140 ms and a minimum cycle period of 5 s. Due to the high neutron flux of more than  $3 \cdot 10^{10}$  n/cm<sup>2</sup> s, the induced initial activities of short-lived isotopes often exceed 10<sup>6</sup> Bq. To handle such high counting rates, the  $\gamma$ -ray spectroscopy system has been improved by a novel method for real-time correction of counting losses [2].

The neutron flux variations within the dimensions of the sample container (10 mm diameter, 7 mm height) were determined to be  $\pm 5\%$  [3]. The neutron energy distribution was investigated by experimental [4] and theoretical [5, 6] methods, yielding a median at 14.7 MeV with a FWHM of 600 keV. The contribution of thermal neutrons to the total neutron flux was measured to be less than 0.5%.

## MEASUREMENTS OF 14 MEV NEUTRON ACTIVATION CROSS-SECTIONS

To achieve accurate results in FNAA many cross-sections have been investigated. Therefore, cyclic and conventional activation technique have been applied. The measured reaction cross-sections used for the analysis of geological samples are summarized in Table I. More details about the measurements as well as a comparison with literature values are given in Ref. [7, 8, 9, 10].

The neutron energy spectrum within the cylindrical target of KORONA also contains contributions from elastically and inelastically scattered neutrons. These contributions have been calculated [5, 11] to be 26 and 9% of

Table I: Activation Cross-Sections at  $14.7 \pm 0.3$  MeV

Reaction	$\sigma$ (mb)	Ref.	Reaction	$\sigma$ (mb)	Ref.
$^{23}\text{Na}(n,\alpha)^{20}\text{F}$	$123 \pm 4$	[10]	$^{46}\text{Ti}(n,p)^{46}\text{Sc}^*$	$304^+ \pm 10$	[10]
$^{23}\text{Na}(n,p)^{23}\text{Ne}$	$47 \pm 2$	[10]	$^{47}\text{Ti}(n,d)^{46}\text{Sc}^*$		
$^{26}\text{Mg}(n,\alpha)^{23}\text{Ne}$	$52.0 \pm 1.3$	[9]	$^{50}\text{Ti}(n,\alpha)^{47}\text{Ca}$	$8.5 \pm 0.5$	[10]
$^{25}\text{Mg}(n,p)^{25}\text{Na}$	$63^+ \pm 4$	[10]	$^{55}\text{Mn}(n,\alpha)^{52}\text{V}$	$23.3 \pm 0.7$	[8]
$^{26}\text{Mg}(n,d)^{25}\text{Na}$			$^{55}\text{Mn}(n,2n)^{54}\text{Mn}$	$741 \pm 22$	[8]
$^{27}\text{Al}(n,p)^{27}\text{Mg}$	$69.0 \pm 1.7$	[9]	$^{56}\text{Fe}(n,p)^{56}\text{Mn}$	$110.0^+ \pm 5.5$	[8]
$^{28}\text{Si}(n,p)^{28}\text{Al}$	$265^+ \pm 11$	[10]	$^{57}\text{Fe}(n,np)^{56}\text{Mn}$		
$^{28}\text{Si}(n,d)^{28}\text{Al}$			$^{54}\text{Fe}(n,2n)^{53}\text{Fe}^*$	$7.9 \pm 0.7$	[8]
$^{29}\text{Si}(n,p)^{29}\text{Al}$	$138 \pm 6$	[10]	$^{57}\text{Fe}(n,p)^{57}\text{Mn}$	$89^+ \pm 5$	[8]
$^{30}\text{Si}(n,d)^{29}\text{Al}$			$^{58}\text{Fe}(n,np)^{57}\text{Mn}$		
$^{35}\text{Cl}(n,2n)^{34\text{m}}\text{Cl}$	$7.2 \pm 0.3$	[10]	$^{85}\text{Rb}(n,2n)^{84\text{m}}\text{Rb}$	$474 \pm 13$	[10]
$^{39}\text{K}(n,2n)^{38}\text{K}^*$	$3.6 \pm 0.2$	[9]	$^{87}\text{Rb}(n,2n)^{86\text{m}}\text{Rb}$	$559 \pm 17$	[9]
$^{41}\text{K}(n,p)^{41}\text{K}$	$50.7 \pm 1.3$	[9]	$^{85}\text{Rb}(n,2n)^{84}\text{Rb}^*$	$1140 \pm 35$	[10]
$^{41}\text{K}(n,\alpha)^{38}\text{Cl}$	$33.0 \pm 1.3$	[9]	$^{88}\text{Sr}(n,2n)^{87\text{m}}\text{Sr}$	$268^+ \pm 8$	[10]
$^{40}\text{Ca}(n,p)^{40}\text{K}$	$44.0 \pm 7.5$	[9]	$^{86}\text{Sr}(n,\gamma)^{87\text{m}}\text{Sr}$		
$^{40}\text{Ca}(n,\alpha)^{37}\text{Ar}$	$29.0 \pm 1.2$	[9]	$^{86}\text{Sr}(n,2n)^{85\text{m}}\text{Sr}$	$225^+ \pm 7$	[10]
$^{40}\text{Ca}(n,p)^{39}\text{K}$	$150.0^+ \pm 8.2$	[9]	$^{86}\text{Sr}(n,\gamma)^{85\text{m}}\text{Sr}$		
$^{40}\text{Ca}(n,np)^{39}\text{K}$			$^{90}\text{Zr}(n,2n)^{89\text{m}}\text{Zr}$	$75 \pm 12$	[7]
$^{40}\text{Ca}(n,2n)^{39}\text{Ca}$	$850 \pm 35$	[9]	$^{90}\text{Zr}(n,p)^{89\text{m}}\text{Y}$	$12.4 \pm 0.8$	[9]
$^{46}\text{Ti}(n,p)^{46}\text{Sc}$	$62.6 \pm 3.0$	[9]	$^{90}\text{Zr}(n,2n)^{89}\text{Zr}^*$	$754 \pm 29$	[9]
$^{47}\text{Ti}(n,p)^{46}\text{Sc}$	$68.7^+ \pm 2.1$	[10]	$^{135}\text{Ba}(n,2n)^{134\text{m}}\text{Ba}$	$1043^+ \pm 73$	[9]
$^{47}\text{Ti}(n,d)^{46}\text{Sc}$			$^{136}\text{Ba}(n,\gamma)^{135\text{m}}\text{Ba}$		
$^{47}\text{Ti}(n,p)^{47}\text{Sc}$	$257^+ \pm 12$	[10]	$^{136}\text{Ba}(n,2n)^{135\text{m}}\text{Ba}$	$1180 \pm 79$	[10]
$^{47}\text{Ti}(n,d)^{47}\text{Sc}$					

\* If a cumulative decay of parent and daughter nuclide is observed, the total cross-section is presented.

+ Cross-section normalized to the isotopic abundance of the first mentioned isotope.

the total neutron flux, respectively. If the scattered neutrons of lower energy lead to increased activation during the irradiation, the effective cross-section might differ from that related to 14.7 MeV, depending on the ratio of this contribution to monitor and sample reaction. Fortunately most of the reactions have thresholds above the energy of inelastically scattered neutrons, so the majority of the measured activation cross-sections can be used for FNAA at similar neutron generator facilities.

The utilization of reaction cross-sections measured at the same facility eliminates uncertainties in fast neutron activation analysis. Errors in literature values not only of energy dependent cross-sections but also of nuclear decay data have no effect on the results.

Many reactions with 14 MeV neutrons of neighbouring elements lead to the same radioisotope. These elemental interferences can only be corrected successfully, if the contributing elements are accurately detected by different reaction channels. Therefore the activation cross-sections have to be measured with high accuracy. An example of interferences related to the

Table II: Interferences of 14 MeV neutron induced reactions

IAEA-Sediment SD-N-1/2

Reaktion	Ab. [%]	$\sigma$ [mb]	$T_{1/2}$	$E_{\gamma}$ [keV]	$I_{\gamma}$ [%]	$\frac{Ab. \cdot \sigma}{A}$ [mb/g]	Cum. Conc. [mg/g]	Conc. [mg/g]
$^{16}\text{O}(n,p)^{16}\text{N}$	100	37	7.1 s	6129	69	2.31	564	564 ± 17
$^{19}\text{F}(n,p)^{19}\text{F}$	100	21				1.11	1240	0 ± 0
$^{19}\text{F}(n,p)^{18}\text{O}$	100	19	27 s	197	96	1.00	0	0 ± 0
$^{23}\text{Na}(n,\alpha)^{20}\text{F}$	100	125	11 s	1634	100	5.43	10.5	10.5 ± 1.0
$^{19}\text{F}(n,\gamma)^{20}\text{F}$	100	0.05				0.003	21700	0 ± 0
$^{24}\text{Mg}(n,p)^{24}\text{Na}$	79	180	15 h	1369	100	5.85	36.2	8.2 ± 0.9
$^{27}\text{Al}(n,\alpha)^{24}\text{Na}$	100	114				4.23	50.1	38.8 ± 1.8
$^{23}\text{Na}(n,\gamma)^{24}\text{Na}$	100	2.9				0.13	1680	10.5 ± 1.0
$^{27}\text{Al}(n,p)^{27}\text{Mg}$	100	69	9.5 min	844	72	2.56	47.3	38.8 ± 1.8
$^{30}\text{Si}(n,\alpha)^{27}\text{Mg}$	3.1	70				0.077	1560	285 ± 11
$^{24}\text{Mg}(n,\gamma)^{27}\text{Mg}$	11	0.4				0.002	66600	8.2 ± 0.9
$^{28}\text{Si}(n,p)^{28}\text{Al}$	92	265	2.2 min	1779	100	8.70	285	285 ± 11
$^{31}\text{P}(n,\alpha)^{28}\text{Al}$	100	118				3.81	652	0 ± 0
$^{27}\text{Al}(n,\gamma)^{28}\text{Al}$	100	1.6				0.06	42700	38.8 ± 1.8
$^{28}\text{Si}(n,p)^{29}\text{Al}$	4.7	131	6.6 min	1273	91	0.218	290	290 ± 30

analysis of geological samples is illustrated in Table II. For an exact determination of Mg, Al and Si the detection of Si via the reaction  $^{29}\text{Si}(n,p)^{29}\text{Al}$  is necessary.

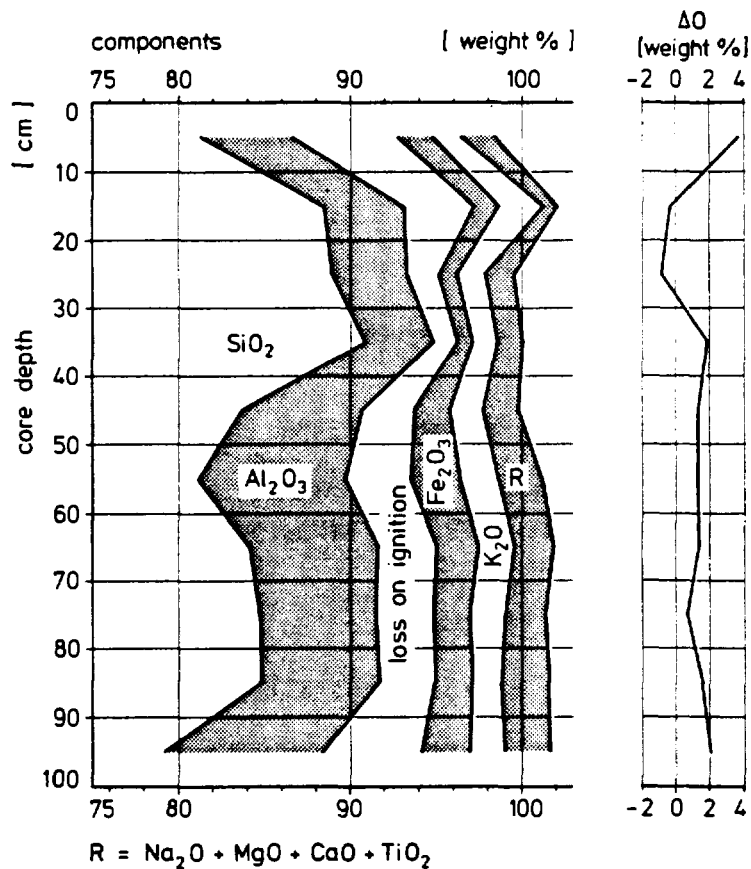


Fig. 1: Sums of measured concentrations as a function of depths. Comparison of measured oxygen contents with oxygen complements of all elements forming oxides.

For characterization of the river sediment strata [12], cores were taken from the Elbe river with a length of about 1 m. The frozen sediment cores were divided into small discs. Samples of the total sediment and of the fraction with grain sizes  $< 63 \mu\text{m}$  were analyzed by FNAA [13]. The concentrations of the elements O, Na, Al, Si and Ba were determined using cyclic activation and measurement. For the analysis of Mg, K, Ca, Mn, Fe and Rb a second irradiation of 16 min with subsequent measurement of 20 min was performed. In a third measurement of 16 h or longer the elements Ti, As, Sr and Zr were detected.

The completeness of analyses was tested by summing up all element concentrations found plus the losses of ignition. As a result, these sums equal 100 % with deviations less than 2 %. An additional check of consistency is to compare the measured oxygen content of the sample with the summed oxygen complements of all elements (as they usually occur as oxides). These comparisons also result in small deviations of about 2 % (see Fig. 1).

## DISCUSSION

In prompt  $\gamma$ -ray spectroscopy at thermal neutron capture as well as in X-ray fluorescence analysis of geological samples, there always arises a lack of information with respect to the 100 % test. The reason is that the main component oxygen is not detectable.

If thermal NAA of delayed  $\gamma$ -rays is applied, even the second main constituent silicon is usually not detected because of its low neutron-capture cross-section and the very low  $\gamma$ -ray emission probability of  $^{31}\text{Si}$ , the radionuclide produced. In FNAA generally all important elements are determined. With the exception of hydrogen and carbon all light elements can be analyzed. In combination with X-ray powder diffractometry information on the mineralogical composition of geological samples is provided.

## REFERENCES

- [1] H.-U. Fanger, R. Pepelnik, W. Michaelis, J. Radioanal. Chem. 61 (1981) 147.
- [2] R. Pepelnik, G.P. Westphal, B. Anders, Nucl. Inst. and Meth. Phys. Res. 226 (1984) 411.
- [3] B. Anders, E. Bössow, GKSS 83/E/23, 1983, Geesthacht.
- [4] B. Anders, R. Pepelnik, H.-U. Fanger, Int. Conf. Nucl. Data for Science and Technology, K.H. Böckhoff (Ed.), 1982, Antwerp, p. 859.
- [5] B.M. Bahal, H.-U. Fanger, Nucl. Instr. and Meth. 211 (1983) 469.
- [6] B.M. Bahal, H.-U. Fanger, Nucl. Instr. and Meth. Phys. Res. 220 (1984) 517.
- [7] J.L. Barreira Filho, H.-U. Fanger, GKSS 82/E/8, 1982, Geesthacht.
- [8] B.M. Bahal, R. Pepelnik, GKSS 85/E/11, 1985, Geesthacht.
- [9] B. Anders, B.M. Bahal, R. Pepelnik, GKSS 85/E/24, 1985, Geesthacht.

- [10] B.M. Bahal, E. Bössow, M. Farooq, R. Pepelnik, GKSS 86/E/..., 1986, Geesthacht, to be published.
- [11] A. Pavlik, G. Winkler, Inst. f. Radiumforschungs- und Kernphysik der Universität Wien, to be published.
- [12] B. Anders, W. Junge, J. Knoth, W. Michaelis, R. Pepelnik, H. Schwenke, Vth Int. Conf. on Nucl. Meth. in Environmental and Energy Research, 1984, Mayaguez, Puerto Rico. GKSS 84/E/20.
- [13] B. Anders, R. Pepelnik, GKSS 85/E/41.



# Detection of Na, Mg, Al, and Si in Wells With Reactions Generated By 14 MeV Neutrons

R.C. Hertzog and P.D. Soran  
Schlumberger Well Services, Houston, TX 77210-4594, and

J.S. Schweitzer  
Schlumberger-Doll Research, Ridgefield, CT 06877-4108.

## ABSTRACT

Geochemical analyses of potential oil bearing formations, based on gamma ray spectroscopy following neutron-induced reactions, are often limited by the current level of uncertainties on neutron reaction cross section data. Four elements which are commonly present and are coupled through  $(n,\gamma)$ ,  $(n,p)$ , and  $(n,\alpha)$  reactions are Na, Mg, Al, and Si. To obtain data as rapidly as possible, it is necessary to use a 14 MeV neutron source; the use of high energy neutrons results, however, in delayed activation gamma rays whose intensities cannot be simply related to original elemental concentrations, as would be the case for a purely thermal source. The relationship between the final activation gamma ray intensities and the derived initial elemental concentrations has been examined in light of the currently available cross section uncertainties for typical concentrations of each of these four elements. This analysis shows the critical areas where improved uncertainties on the reaction cross sections are needed to result in geochemically useful elemental analyses.

## Introduction

Significant interest has recently been generated<sup>1,2)</sup> for describing the properties of geological formations through a geochemical analysis which is based on the knowledge of the elemental concentrations and the ability to generate a description of the mineralogy of the rock. From the mineralogy, many important properties<sup>2)</sup> of the rock and fluid can be described. For some time techniques for obtaining information on elemental concentrations in rock and fluid have existed through neutron-induced gamma ray spectroscopy in a borehole.<sup>3-6)</sup> With the introduction of gamma-ray spectrometers using germanium detectors,<sup>7-13)</sup> the potential for extended multielement analysis can be realized in practice. However, relating observed gamma ray yields to elemental concentrations requires an accurate knowledge of both the spatial dependence of the energy-dependent neutron flux and the energy-dependent reaction cross sections for the particular gamma rays used in the analysis. Without this information a prohibitive calibration problem can occur. The neutron cross sections are particularly critical when the neutrons are produced by a d,t accelerator, which is desirable to generate a much larger neutron flux than is practical with chemical neutron sources. The 14 MeV neutrons produced by this accelerator result in a neutron energy distribution<sup>14)</sup> in the geological formation having all energies between thermal and 14 MeV. Previous work has described the needed improvements in cross section data for the detection of aluminum by delayed activity in the presence of silicon.<sup>15)</sup> Now, a geologically realistic situation is examined in which the attempt is made to detect the elemental concentrations of Na, Mg, Al, and Si when they are present in typical concentrations for sedimentary environments. These four elements are all geochemically interesting and the sequence illustrates the demands placed on cross section data to resolve the contributions from competing reactions.

## Detection of Na, Mg, Al, and Si

The main elements of interest for a geochemical analysis are the dominant elements in the earth's crust as well as a few of the trace elements. In a typical situation, the elements can be directly related to specific minerals or to the fluids contained in the rock. We will focus on the analysis of delayed activity, but similar considerations apply for prompt gamma ray analysis. At typical geological concentrations, Na, Mg, Al, and Si can all be detected in a delayed activation measurement. Na occurs as salt, both crystalline and dissolved in water and in feldspar and some clays. Mg is contained in some clays and in dolomite ( $\text{CaMg}(\text{CO}_3)_2$ ). Al is common in all clay minerals, and Si is present in quartz and all clays. The significant role of these four elements in deriving the mineralogy<sup>1)</sup> and determining other geological properties<sup>2)</sup> has been discussed elsewhere.

While Si can easily be detected in thermal capture spectroscopy, the other elements would be difficult to detect in a short time, especially at the lower end of their concentration ranges. The relationship between the delayed gamma ray yield and the element which caused its production is straightforward when using a thermal neutron source. However, the use of a higher energy source, such as 14 MeV neutrons from the d,t reaction, leads to the observed gamma ray peak being populated by reactions involving at least two of these four elements. The possible reactions involving these four elements or populating the same delayed activities are shown in Table 1. Of the possible reactions shown in this table, the  $^{31}\text{P}(n,\alpha)^{28}\text{Al}$  reaction can be ignored, since the yield from this reaction will almost always be insignificant as the P/Si atomic ratio is very small<sup>16)</sup> in most sedimentary rocks. The  $^{23}\text{Na}(n,\alpha)^{20}\text{F}$  reaction, because of its

Table 1. Reactions involved in the detection of Na, Mg, Al and Si from delayed activity. Delayed gamma ray energies are shown in keV.

Number	Initial Isotope	Reaction	Delayed Activity	Half-life
1	$^{23}\text{Na}$	(n,γ)	$^{24}\text{Na}$ (2754, 1368)	15 hrs.
2	$^{23}\text{Na}$	(n,α)	$^{20}\text{F}$ (1633)	11 secs.
3	$^{24}\text{Mg}$	(n,p)	$^{24}\text{Na}$ (2754, 1368)	15 hrs.
4	$^{26}\text{Mg}$	(n,γ)	$^{27}\text{Mg}$ (844, 1014)	9.45 mins.
5	$^{27}\text{Al}$	(n,α)	$^{24}\text{Na}$ (2754, 1368)	15 hrs.
6	$^{27}\text{Al}$	(n,p)	$^{27}\text{Mg}$ (844, 1014)	9.45 mins.
7	$^{27}\text{Al}$	(n,γ)	$^{28}\text{Al}$ (1779)	2.25 mins.
8	$^{28}\text{Si}$	(n,p)	$^{28}\text{Al}$ (1779)	2.25 mins.
9	$^{29}\text{Si}$	(n,p)	$^{29}\text{Al}$ (1273)	6.52 mins.
10	$^{30}\text{Si}$	(n,α)	$^{27}\text{Mg}$ (844, 1014)	9.45 mins.
11	$^{31}\text{P}$	(n,α)	$^{28}\text{Al}$ (1779)	2.25 mins.

short half life, is very difficult to detect with sufficient statistical precision at the normal Na concentrations. Thus, there are 9 remaining reactions with 4 different delayed activities ( $^{29}\text{Al}$ ,  $^{28}\text{Al}$ ,  $^{27}\text{Mg}$ , and  $^{24}\text{Na}$ ) which must be understood to determine the original elemental concentrations of Na, Mg, Al, and Si.

The extraction of the elemental concentrations from the observed delayed activities is mathematically straightforward. The Si concentration,  $\eta_{\text{Si}}$ , can be determined from the  $^{29}\text{Al}$  activity. Then, the  $^{28}\text{Al}$  activity can be used to find the Al concentration<sup>15)</sup> after correcting for the  $^{28}\text{Al}$  activity produced by the Si in the rock. Similarly, the Mg concentration can be determined from the  $^{27}\text{Mg}$  activity, after correcting for the Si and Al contributions to this activity. Finally, the Na concentration can be determined from the  $^{24}\text{Na}$  activity after correcting for the contribution from Mg and Al. The final Na concentration can be written as:

$$\eta_{\text{Na}} = [Y_{\text{Na}} - [Y_{\text{Mg}} - (Y_{\text{Al}} - Y_{\text{Si}} \frac{R_{28n,p}}{R_{29n,p}}) \frac{R_{27n,p}}{R_{27n,\gamma}} - Y_{\text{Si}} \frac{R_{30n,\alpha}}{R_{29n,p}}] \frac{R_{24n,p}}{R_{26n,\gamma}} - (Y_{\text{Al}} - Y_{\text{Si}} \frac{R_{28n,p}}{R_{29n,p}}) \frac{R_{27n,\alpha}}{R_{27n,\gamma}}] \frac{1}{R_{23n,\gamma}}$$

where we have ignored the relative detection efficiencies for the different delayed gamma rays.  $Y_{\text{Na}}$ ,  $Y_{\text{Mg}}$ ,  $Y_{\text{Al}}$ , and  $Y_{\text{Si}}$  are the time corrected gamma ray intensities from the  $^{24}\text{Na}$ ,  $^{27}\text{Mg}$ ,  $^{28}\text{Al}$ , and  $^{29}\text{Al}$  decays. The  $R_{\text{Nn},x}$  are the reaction rates for the reaction from the stable nucleus  $^{\text{N}}\text{Z}$  given by:

$$R_{\text{Nn},x} = \int_V \int_E \sigma_{n,x}(E) \Phi(E, \mathbf{r}) dE dV$$

with  $\Phi(E, \mathbf{r})$  describing the neutron flux distribution. From this relationship, the uncertainty on the Na concentration will depend on the uncertainties in the  $R_{\text{Nn},x}$  uncertainties since the statistics on the observed gamma ray intensities can generally be made to be very small. An important point to notice from the above equation for the concentration of Na is that to reduce the uncertainties it is not necessary to know the absolute uncertainties on all the cross sections, but rather that the uncertainty that governs the final uncertainty in the elemental concentration is frequently the uncertainty in the relative cross sections for two reactions and only a small number of cross sections need to be known with good absolute uncertainty. Naturally, this ignores the uncertainty in the neutron flux distributions, which also depend on all neutron cross sections.

To evaluate the effects of statistical uncertainties in the cross section data, irradiations have been performed in a laboratory formation that has typical concentrations of these four elements ( $\text{Na}_2\text{CO}_3$  0.49 wt %,  $\text{MgO}$  1.22 wt %,  $\text{Al}_2\text{O}_3$  4.76 wt %, and  $\text{SiO}_2$  77.1 wt %, with the balance  $\text{H}_2\text{O}$ ). The formation was contained in a cylindrical tank (56 cm diameter x 61 cm high) with a 9 cm hole along the axis. Delayed activity was monitored following a ten minute irradiation with a  $^{252}\text{Cf}$  source ( $\sim 10^8$  n/sec) and also following an irradiation with a d,t source of  $\sim 8 \times 10^8$  n/sec. The spectra from these two irradiations are shown in Figures 1 and 2. Both spectra are accumulated for four minutes following delays of 4.63 minutes for the  $^{252}\text{Cf}$  irradiation and 5.5 minutes for the 14 MeV irradiation. The  $^{252}\text{Cf}$  irradiation shows a majority of peak intensities that are primarily due to (n, $\gamma$ ) reactions. However, the presence of the  $^{29}\text{Al}$  peak at 1273 keV confirms that even with the  $^{252}\text{Cf}$  source high energy

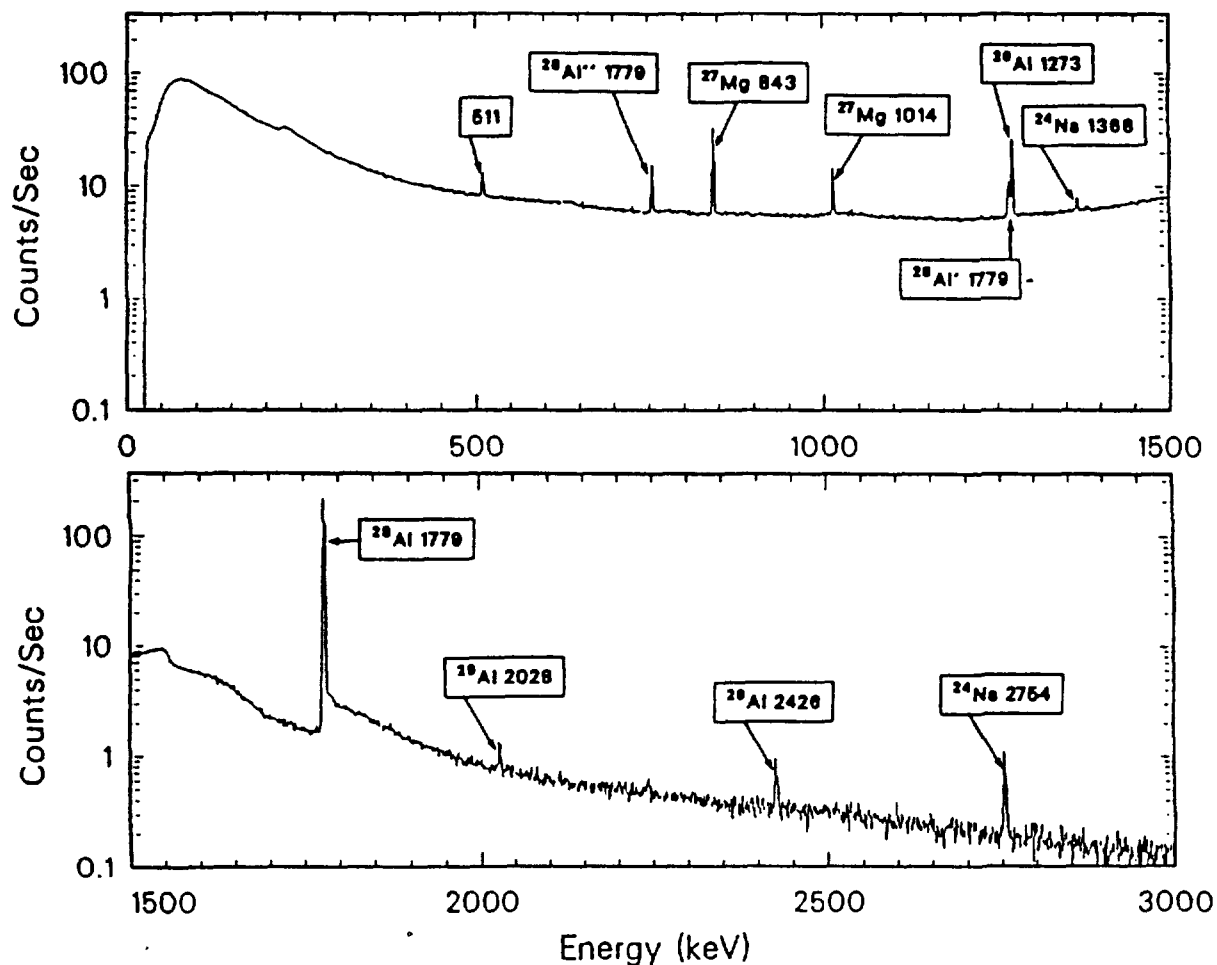


FIGURE 1 Delayed activation spectrum following irradiation with a  $^{252}\text{Cf}$  source.

neutron-induced reactions cannot be ignored. The 14 MeV spectrum illustrates the increased count rate from the increased source strength and the added contributions to the delayed activities from the (n,p) and (n, $\alpha$ ) reactions. This can most easily be seen by noting that the  $^{24}\text{Na}$  activity is increased by a factor of  $5.1 \pm 0.9$  which is mostly accounted for by the increase in neutron flux. Most of this activity is produced by the  $^{23}\text{Na}(n,\gamma)^{24}\text{Na}$  reaction. In contrast, the  $^{29}\text{Al}$  activity is only produced by a high energy reaction and is increased by a factor of  $73.7 \pm 13.7$ . The  $^{28}\text{Al}$  and the  $^{27}\text{Mg}$  activities are intermediate cases with increases in activity of  $14.0 \pm 0.1$  and  $34.4 \pm 2.9$ , respectively.

### Calculation of Reaction Rate Sensitivities

The calculated results were generated using the Los Alamos National Laboratory's Monte Carlo code MCNP.<sup>17)</sup> MCNP is a general purpose, continuous-energy, generalized geometry, time dependent, coupled neutron-photon Monte Carlo transport code. The code uses pointwise cross section data on energy grids<sup>18)</sup> that are tailored to reproduce the salient features of each isotope to within a few percent of the ENDF/B-V cross sections.<sup>19)</sup>

To illustrate the error propagation in the cross section data, a calculation has been performed to determine  $\eta_{\text{Na}}$ ,  $\eta_{\text{Mg}}$ ,  $\eta_{\text{Al}}$ , and  $\eta_{\text{Si}}$  when all of these elements are present. The experiment described earlier and a 50 cm sphere containing the same elemental concentrations as the experiment with a point 14 MeV neutron source and a  $^{252}\text{Cf}$  neutron source at the center has been examined using MCNP. The 50 cm sphere

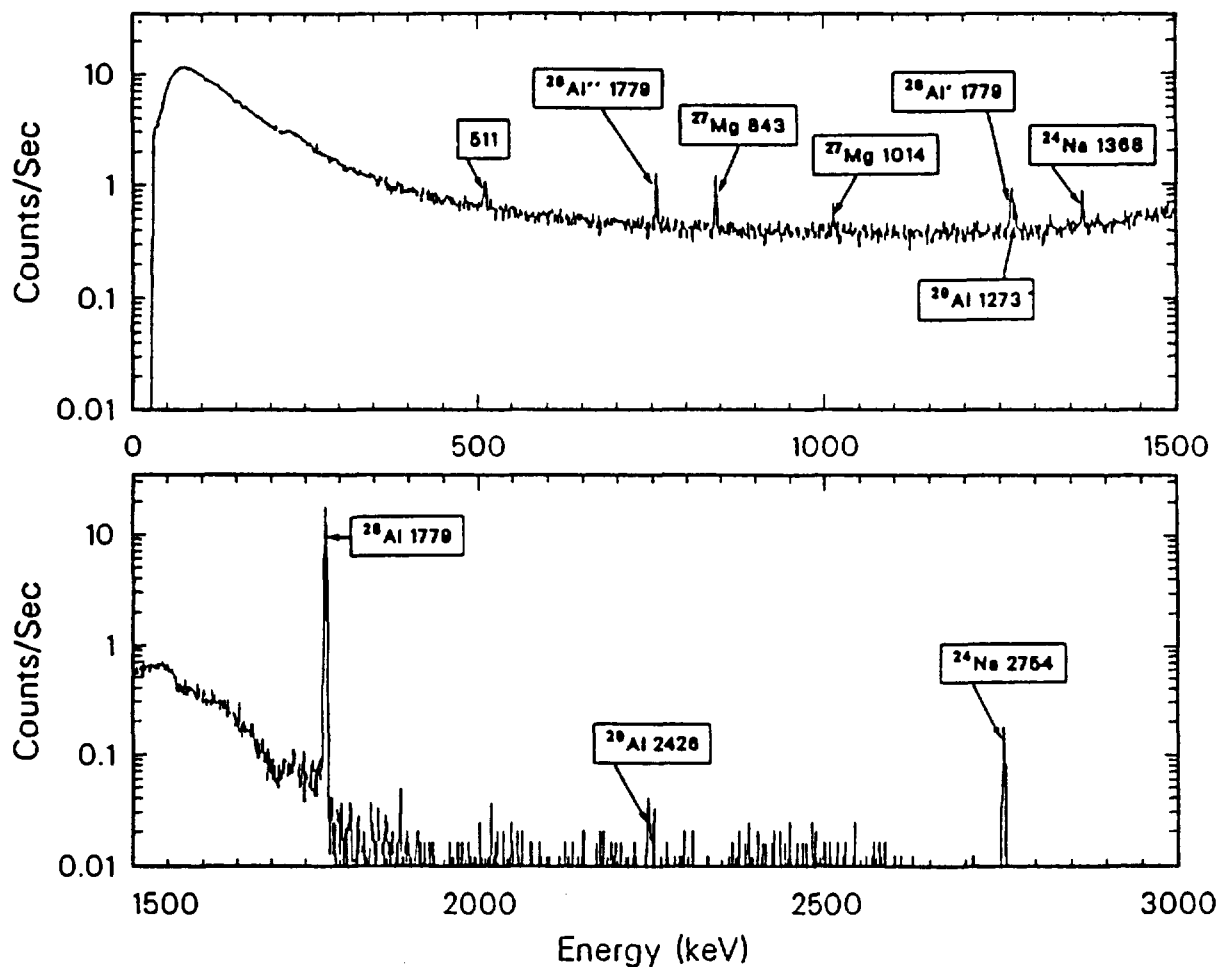


FIGURE 2 Delayed activation spectrum following irradiation with a source of 14 MeV neutrons.

calculation can be used to determine the sensitivity of the elemental concentrations to uncertainties in the neutron cross sections that is representative of a borehole measurement. The loss to capture in the four systems is shown in Table 2. Production rates of the gamma rays (averaged over each system) are given in Table 3. However, the reaction rates are given for 100% loading of the isotope, thus to convert to yield it is necessary to multiply each reaction rate by the appropriate atomic concentration, isotopic abundance, and gamma-ray conversion efficiencies. The values in Table 3 are reaction rate/volume/source neutron. Comparison of the relative rates for a 14 MeV source to the  $^{252}\text{Cf}$  source shows that the relative rates in the two systems are comparable. The average neutron flux in the sphere is distributed over all energies below 14 MeV as shown in Figure 3. The total reaction rates for the production of the delayed activities, the product of the neutron flux and the respective cross sections, are shown in Figure 4 for the spherical system with a 14 MeV source (The reaction rates for the other two (n,p) reactions have been shown previously<sup>15</sup>). The regions on the four curves where these reaction rates are large or are strongly varying correspond to the regions where the uncertainties in the cross sections most significantly affect the uncertainty on the total reaction rate.

In general, the uncertainties on these cross sections are not well determined. However, if we assign an arbitrary uncertainty of  $\pm 20\%$  for each of the threshold reactions, and assume there is negligible uncertainty on the thermal neutron capture cross sections, we can calculate the resultant uncertainties on elemental concentrations. Such a calculation has been performed for the 14 MeV source in the

Table 2. Loss to capture.

GEOMETRY	SPHERE		CYLINDER		
	SOURCE:	14 MeV	Cf-252	14 MeV	Cf-252
H		$3.78 \times 10^{-1}$	$6.50 \times 10^{-1}$	$1.15 \times 10^{-1}$	$3.16 \times 10^{-1}$
C		$1.01 \times 10^{-4}$	$1.49 \times 10^{-5}$	$7.98 \times 10^{-5}$	$7.56 \times 10^{-6}$
O		$1.64 \times 10^{-1}$	$9.65 \times 10^{-3}$	$1.30 \times 10^{-1}$	$7.96 \times 10^{-3}$
Na		$3.19 \times 10^{-3}$	$4.95 \times 10^{-3}$	$1.20 \times 10^{-3}$	$2.49 \times 10^{-3}$
Mg		$3.49 \times 10^{-3}$	$2.11 \times 10^{-3}$	$2.34 \times 10^{-3}$	$1.03 \times 10^{-3}$
Al		$1.85 \times 10^{-2}$	$2.34 \times 10^{-2}$	$8.02 \times 10^{-3}$	$1.36 \times 10^{-2}$
Si		$2.59 \times 10^{-1}$	$2.29 \times 10^{-1}$	$1.43 \times 10^{-1}$	$1.13 \times 10^{-1}$
Total		0.826	0.918	0.400	0.452
Leakage		0.183	0.082	0.453 Side 0.073 Bottom 0.074 Top	0.418 Side 0.067 Bottom 0.068 Top

Table 3. System average reaction rates (reactions/cm<sup>3</sup>/neutron).

GEOMETRY	SPHERE		CYLINDER		GAMMA RAY (keV)	
	SOURCE:	14 MeV	<sup>252</sup> Cf	14 MeV		<sup>252</sup> Cf
<sup>31</sup> P(n,α)		$4.09 \times 10^{-6}$	$8.49 \times 10^{-8}$	$1.43 \times 10^{-5}$	$3.05 \times 10^{-7}$	1779
<sup>28</sup> Si(n,p)		$1.03 \times 10^{-5}$	$2.50 \times 10^{-7}$	$3.61 \times 10^{-5}$	$8.93 \times 10^{-7}$	1779
<sup>29</sup> Si(n,p)		$9.75 \times 10^{-6}$	$2.45 \times 10^{-7}$	$3.39 \times 10^{-5}$	$1.36 \times 10^{-6}$	1273
<sup>30</sup> Si(n,α)		$2.61 \times 10^{-6}$	$3.99 \times 10^{-9}$	$9.42 \times 10^{-6}$	$1.88 \times 10^{-8}$	844/1014
<sup>27</sup> Al(n,γ)		$2.23 \times 10^{-5}$	$3.84 \times 10^{-5}$	$3.01 \times 10^{-5}$	$8.15 \times 10^{-5}$	1779
<sup>27</sup> Al(n,p)		$3.09 \times 10^{-6}$	$1.72 \times 10^{-7}$	$1.09 \times 10^{-5}$	$6.19 \times 10^{-7}$	844/1010
<sup>27</sup> Al(n,α)		$3.94 \times 10^{-6}$	$3.08 \times 10^{-8}$	$1.40 \times 10^{-5}$	$1.15 \times 10^{-7}$	2754/1368
<sup>23</sup> Na(n,γ)		$5.11 \times 10^{-5}$	$8.81 \times 10^{-5}$	$6.89 \times 10^{-5}$	$1.87 \times 10^{-4}$	2754/1368
<sup>23</sup> Na(n,α)		$4.91 \times 10^{-6}$	$2.03 \times 10^{-8}$	$1.78 \times 10^{-5}$	$7.73 \times 10^{-8}$	1233
<sup>24</sup> Mg(n,p)		$5.81 \times 10^{-6}$	$6.14 \times 10^{-8}$	$2.05 \times 10^{-5}$	$2.26 \times 10^{-7}$	2754/1368
<sup>26</sup> Mg(n,γ)		$3.63 \times 10^{-6}$	$6.24 \times 10^{-6}$	$4.91 \times 10^{-6}$	$1.33 \times 10^{-5}$	844/1014
Total		$1.21 \times 10^{-4}$	$1.34 \times 10^{-4}$	$2.61 \times 10^{-4}$	$2.85^{-4}$	

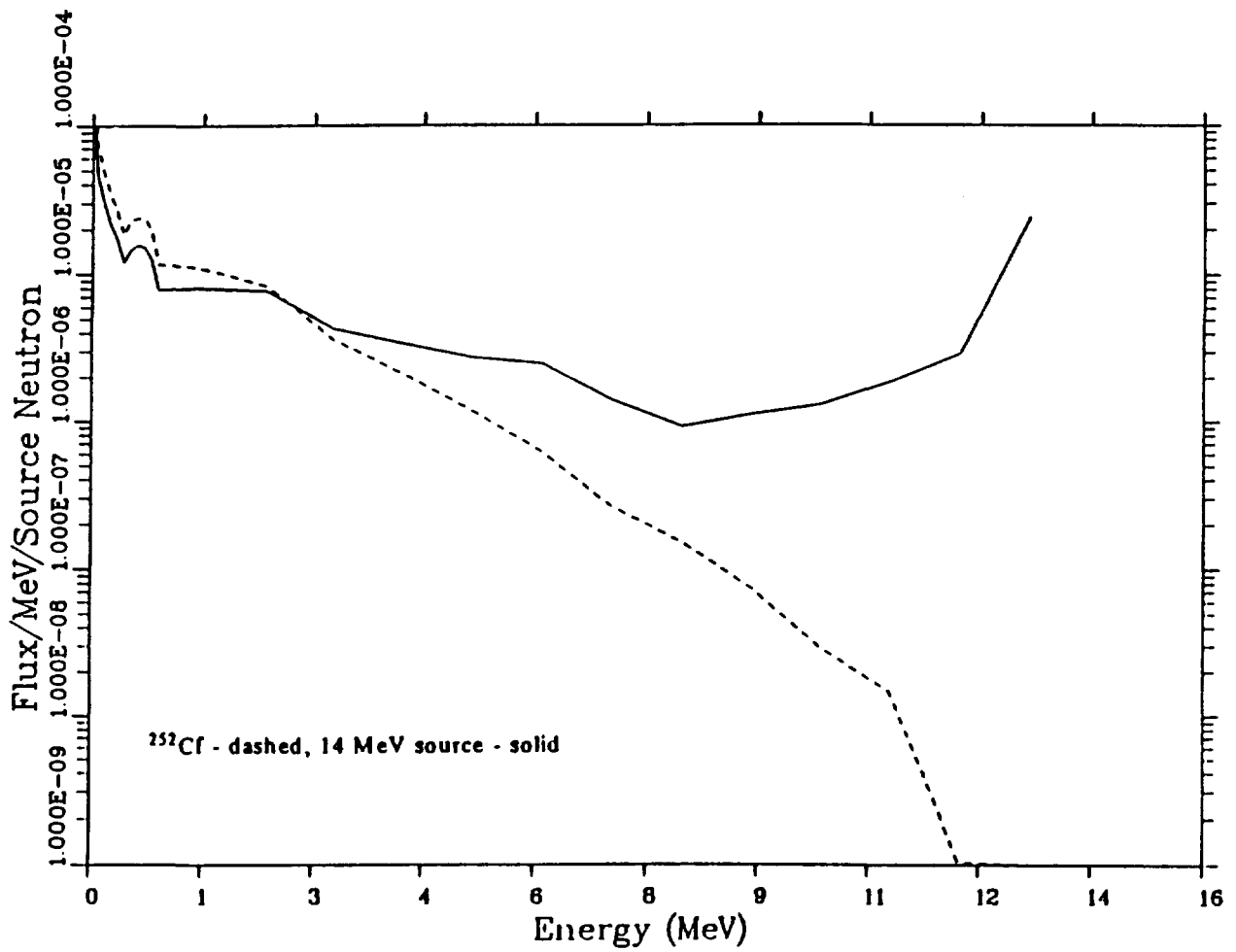


FIGURE 3 Neutron Flux in the Sphere.

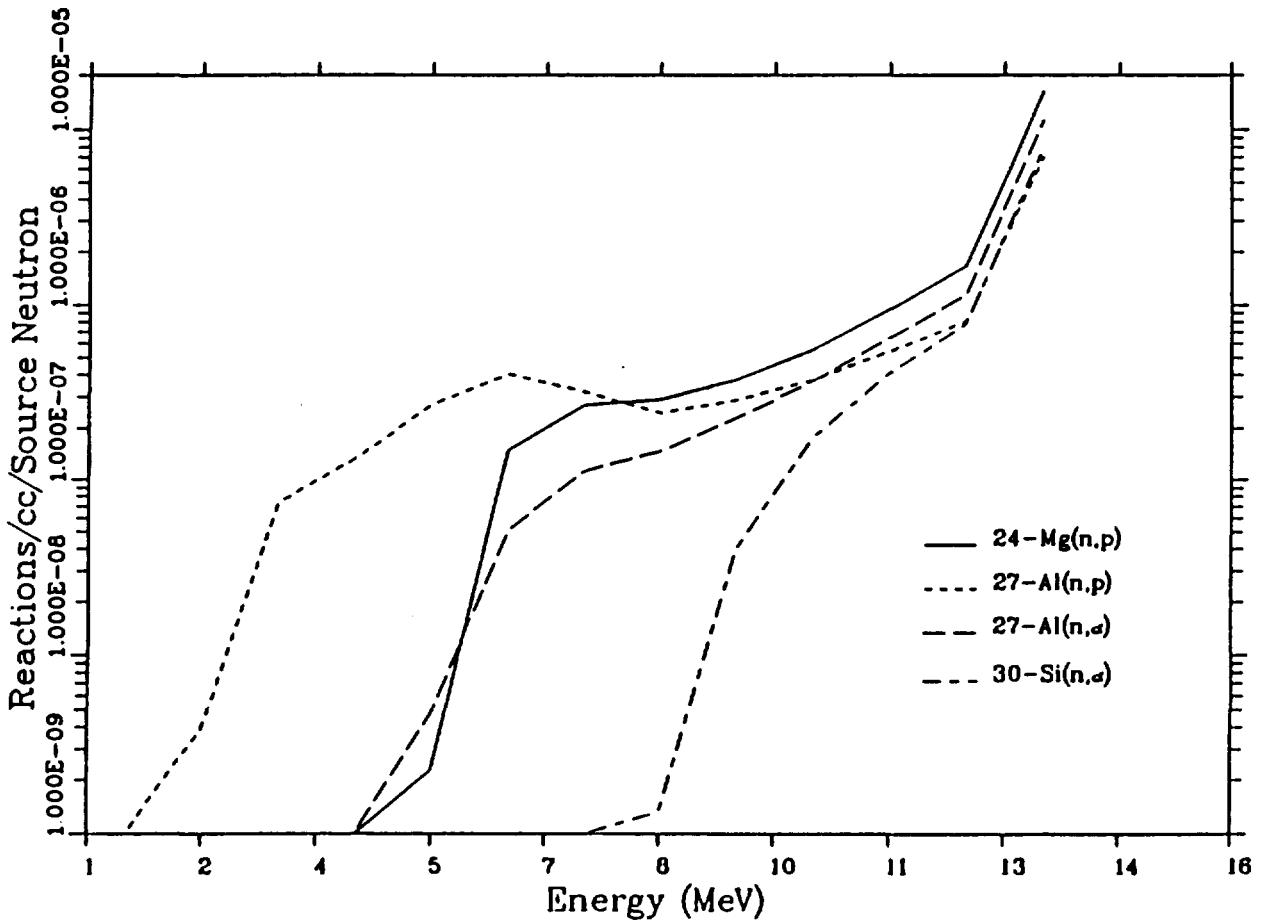


FIGURE 4 Energy-Dependent Reaction Rates and the Cumulative Reaction Rates from 14 MeV to Threshold.

50 cm sphere. The results, also assuming no statistical error in the gamma ray peak intensities, are  $\eta_{Al} \pm 150\%$ ,  $\eta_{Mg} \pm 4000\%$ , and  $\eta_{Na} \pm 120\%$ . Improvements in the cross section uncertainties would provide a corresponding improvement in the uncertainties for the elemental concentrations. For example, if all cross sections become known to  $\pm 2\%$ , the resultant concentrations are  $\eta_{Al} \pm 15\%$ ,  $\eta_{Mg} \pm 400\%$ , and  $\eta_{Na} \pm 12\%$ . Clearly, significantly better knowledge of the cross section uncertainties are needed to use this type of spectroscopic analysis for geochemical applications.

### Summary

The need for improved neutron induced reaction cross sections has been examined for four elements that are important in subsurface geochemical analyses. Overall precision must clearly be improved for certain reactions and certain energy ranges in  $\sigma(E_n)$  are of particular importance. In a typical situation, we have shown that a  $\pm 20\%$  error in certain (n,p) and (n, $\alpha$ ) reactions cross sections can result in  $\pm 4000\%$  and  $\pm 120\%$  errors in determining the concentrations of Mg and Na. Because of the creation of Al activity from both Al and Si,  $\pm 20\%$  uncertainties for the Si(n,p) cross sections can result in a  $\pm 150\%$  uncertainty in the concentration of Al. If the cross section uncertainties could be reduced to a few percent, the uncertainties on the elemental concentrations would become reasonable for geochemical applications. Only when these fundamental nuclear data are improved can the true potential for subsurface geochemical analysis be realized.

### Acknowledgements

The authors are grateful for the assistance of R. Manente and C. Peterson (SDR) in acquiring the experimental data and to R. Little and R. Seamon (LANL) for providing the dosimetry data.

### References

- [1] M. M. Herron, Clays and Clay Minerals, in press (1986).
- [2] M. M. Herron, Paper presented at I.A.E.A. meeting on nuclear data for applied nuclear geophysics. Vienna, Austria (1986).
- [3] R. B. Culver, E. C. Hopkinson, and A. H. Youmans, Soc. Pet. Eng. Jour. **14**, 463 (1974).
- [4] R. Hertzog and R. Plasek, IEEE Trans. Nucl. Sci. **NS-26**, 1558 (1979).
- [5] R. C. Hertzog, Soc. Pet. Eng. Jour. **20**, 327 (1980).
- [6] J. S. Schweitzer, R. A. Manente, and R. C. Hertzog, Jour. Pet. Tech. **36**, 1527 (1984).
- [7] A. Tanner, R. Moxham, F. Senftle, and J. Baicker, Nucl. Instr. Meth. **100**, 1 (1972).
- [8] F. Senftle, R. Moxham, and A. Tanner, Nucl. Instr. Meth. **104**, 485 (1972)
- [9] R. Everett, M. Herron, and G. Pirie, SPWLA Twenty-Fourth Annual Logging Symposium, Calgary, (1983).

- [10] J. S. Schweitzer and R. A. Manente, AIP Conf. Proc. **125**, 824 (1985).
- [11] G. A. Nedostup and F. N. Prokof'ev, At. Energ. **35**, 54 (1973).
- [12] F. E. Senftle in *Short Course in Neutron Activation Analysis in the Geosciences* ed. by G. K. Muecke, Mineralogical Association of Canada (1980).
- [13] D. W. Mellor and M. C. Underwood, SPWLA 26th Annual Logging Symposium, Paper FFF, **2** (1985).
- [14] S. Antkiw, C. R. Case, and P. Albats, P., INDC(NDS)-151/L, 201 (1984).
- [15] R. C. Hertzog, P. D. Soran, and J. S. Schweitzer, International Conference on Nuclear Data For Basic and Applied Science, Santa Fe (1985).
- [16] A. H. Brownlow, *Geochemistry*, Prentice-Hall (1979).
- [17] MCNP - A General Purpose Monte Carlo Code for Neutron and Photon Transport, LA-7396-M (rev.) Version 2B, Los Alamos National Laboratory (1981).
- [18] R. E. MacFarlane, R. J. Barrett, D. W. Muir, and R. M. Barcourt, "The NJOY Nuclear Data Processing System: User's Manual," LA-7584-M (1978).
- [19] R. Kinsey, compiler, "ENDF-201: ENDF/B Summary Documentation," BNL-NCS-17541, 3rd ed. (1979).



AN EXAMPLE OF NUCLEAR DATA CENTER SERVICES  
FOR GEOPHYSICS APPLICATIONS

P. Rose, T. Burrows, and J. Tuli

National Nuclear Data Center  
Brookhaven National Laboratory  
Upton, New York 11973

Abstract

A bibliographic survey of the available experimental data on neutron induced gamma-ray production has been made. Use was made of Data Center on-line search and retrieval capabilities. CINDA was searched for prompt gamma-ray production data covering a large incident neutron energy range, and where possible, EXFOR was used to scan the data and select representative works. From the survey it appears that many measurements will have to be supplemented by theoretical calculations.

INTRODUCTION

Applications of nuclear techniques in the earth sciences are becoming increasingly more important. These applications require more and more accurate nuclear data. Nuclear data centers can play an active and vital role in supplying these needs. Data centers collate and evaluate nuclear data of interest to both the basic and applied researcher. Virtually the entire range of low-energy nuclear physics is addressed, including nuclear structure and decay data and nuclear reaction data. The files maintained by the various centers include bibliographies, compilations of experimental data, and evaluations. Data centers maintain evaluated data files such as ENDF/B<sup>(1)</sup> which contain neutron induced  $\gamma$ -ray production in a format that is application oriented. From these files, the centers provide specialized retrievals on request, on-line access, and timely publications. As a specific example, a survey of neutron-induced prompt gamma ray production has been made and the results are discussed.

BIBLIOGRAPHIC SEARCH

A bibliographic survey of the available experimental data on neutron induced prompt gamma-ray production was carried out. The experimental instead of evaluated data were studied since (1) the range of elements covered is probably more complete; (2) the data may be more current; and (3) the experimental data probably reflect the limits and accuracies of the evaluated data. We relied primarily on data center on-line search and retrieval capabilities which allowed us easy access to CINDA and EXFOR.

CINDA, a Computer Index of Neutron Data, contains bibliographic reference to measurements, calculations reviews, and evaluations of neutron cross sections and other microscopic neutron data; it also includes index references to computer libraries of numerical neutron data (EXFOR) exchanged between the four world-wide regional data centers. The contents of CINDA are periodically published in book form by the International Atomic Energy Agency (IAEA).

CINDA was searched for gamma-ray production data covering a large incident neutron energy range (at least 10 MeV) and at about 14 MeV. Where possible, EXFOR was then used to scan the data and select representative works.

## 1. 0.2- to 20-MeV Neutron Induced Prompt Gamma-Ray Production Measurements

Table 1 summarizes the data available. This table is not inclusive in that only one or two representative measurements are given for each element or isotope. Contained in this table are the element studied, neutron energy range, detector, gamma energy range, angles, reference, indication of use in ENDF/B-V, and explanatory comments. The EXFOR accession number has also been given when the data have been compiled. The data are dominated by work from the Oak Ridge Electron Linear Accelerator (ORELA) and this work spanning better than a decade has been reviewed by Larson<sup>(2)</sup>, among others.

Most of the work has used sodium iodide detectors (NaI) which have poorer energy resolution than lithium-drifted germanium detectors Ge(Li). However, many of the measurements have an energy resolution or bin size of 10 to 20 keV for the lower-energy gammas. This may be adequate for nuclear geophysics since Clayton, et al.<sup>(3)</sup> note that a bin size of 50 keV was adequate for silicon. Sodium iodide measurements have the advantage of including many weak transitions as a continuum.<sup>(2)</sup> New measurements planned or under way at ORELA for structural and other materials using Ge(Li)'s,<sup>(4,5)</sup> at the Los Alamos White Neutron Source using bismuth germanate (BGO),<sup>(5)</sup> and by a collaboration providing data for the Mars Geoscience Climatology Observer<sup>(7)</sup>, should improve the situation over the next few years.

There seems to be a practical lower limit of 200-keV neutron energy for these experiments. Therefore, data below this limit will have to come from other experiments or calculations. Also note that there appear to be two large areas where no measurements have been made. These are from Ga through Sr and Sb through Hf.

Cross section uncertainties have not been included in Table 1 but are roughly comparable to those given in Table 2.

## 2. 14-MeV Neutron Induced Gamma-Ray Production Measurements

Table 2 summarizes the data available. Only one or two representative measurements are given for each element or isotope. Contained in this table are the element studied, detector, angles, cross section uncertainties, reference, and explanatory comments.

While there are more Ge(Li) data available at this energy, NaI measurements still dominate. The resolution of these NaI data also seem poorer than above, typically 100-500 KeV. The large gaps of no data, Ga through Sr, and Sb through Hf, are also evident here.

## CONCLUSIONS

Evaluated  $\gamma$ -production files can readily be used by geophysicists in Monte Carlo calculations of neutron induced prompt  $\gamma$  spectra<sup>(8)</sup>. From the survey above, it appears that measurements will have to be supplemented by theoretical calculations. Nuclear model codes are becoming increasingly sophisticated and appear capable for reproducing the experimental data well within the experimental uncertainties.<sup>(9,10,11)</sup> Another approach is to employ semiempirical formalisms. One of these formalisms, relevant to gamma ray production, is the R-parameter formalism developed by Howerton and Plechaty.<sup>(12,13)</sup> Although this technique is limited in scope, it has the great advantage of simplicity.

## REFERENCES

1. R. Kinsey. ENDF/B Summary Documentation, BNL-NCS-17541 (ENDF-201), (ENDF/B-V), 3rd Edition. (1979).
2. D. C. Larson. Symposium on Neutron Cross-Sections from 10 to 50 MeV, BNL-NCS-51245, Vol. I, 277 (1984).
3. C. G. Clayton, B. H. Patrick, L. G. Sanders, and M. G. Sowerby. Proceedings of the IAEA Consultants' Meeting on Nuclear Data for Bore-hole and Bulk-Media Assay using Nuclear Techniques, INDC(NDS)-151, 17 (1984).
4. D. C. Larson. International Conference on Nuclear Data for Basic and Applied Science (Santa Fe, 1985), AB02 (to be published), DOE-NDC-36, 130 (1985).
5. D. C. Larson and J. K. Dickens. DOE-NDC-33, 144 (1984).
6. C. R. Gould, J. Dave, G. E. Mitchell, P. Ramakrishnan, G. F. Auchampaugh, R. C. Little, and S. A. Wender. International Conference on Nuclear Data for Basic and Applied Science (Santa Fe, 1985), AD04 (to be published).
7. R. C. Reedy, J. R. Arnold, A. U. Khan, P. Englehart, J. Bruckner, H. Wanke, and A. E. Metzger. DOE-NDC-36, 91 (1985).
8. Eldon Schmidt and Philip F. Rose. Int. J. Appl. Radiat. Isot. 35, 796 (1984).
9. D. G. Gardner. Symposium on Neutron Cross-Sections from 10 to 50 MeV. BNL-NCS-51245, Volume II, 641 (1984).
10. C. Y. Fu. *ibid.* 675.
11. E. D. Arthur and P. G. Young. *ibid.* 731.
12. R. J. Howerton and E. P. Plechaty. Nuclear Science Eng. 32, 178 (1968).
13. S. T. Perkins, R. C. Haight, and R. J. Howerton. UCRL-75640 (1974).

Table 1. 0.2- to 20-MeV Prompt Gamma Production Measurements\*

Element Isotope	En(MeV)			Detector	E $\gamma$ (MeV)			Angles	Ref	ENDF B-V	Comments
	E <sub>min</sub>	E <sub>max</sub>	$\Delta E$		E <sub>min</sub>	E <sub>max</sub>	$\Delta E$				
H											
He											
Li	0.5	20.6	0.01-1.1	NaI	0.48			125	1	Y	
7	0.2	40.		Ge(Li)	0.2	10			2		92.5%. In progress.
	0.5	19.8	0.007-0.2	NE213	0.48			125	3		
Be 9	2	25		BGO	1	20		45-140	4		5 angles. No data.
B 10	0.2	40.		Ge(Li)					5		19.9%. Planned.
11	0.2	40.		Ge(Li)					5		80.1%. Planned.
C 12	4.8	20.7	0.25-3.5	Ge(Li)	4.43			4 $\pi$	6		98.90%.
N	6.2	15.9	1.0-2.5	Ge(Li)	0.73	7.03		4 $\pi$	7		Discrete $\gamma$ 's.
	2.0	20.0	1.0-3.0	NaI	1.85	10.6	0.06-0.3	90,125	8	Y	
14	6.0	20.0	1.0-3.0	Ge(Li)	0.57	10.2	0.3-0.5	4 $\pi$	6		99.634%.
O	6.5	20.0	0.5-3.0	NaI	1.6	10.6	0.03-0.15	125	9	Y	
F 19	1.3	20.0	0.23-3.0	NaI	0.91	10.6	0.02-0.3	125	1	Y	
Ne											
Na 23	0.2	20.1	0.2-3.0	NaI	0.35	10.6	0.02-0.25	125	10	Y	
Mg	1.0	19.9	0.25-0.5	NaI	0.69	10.3	$\approx 0.1$	90,125	11	Y	
Al 27	0.9	16.7	0.4-4.2	Ge(Li)	0.47	7.6	0.25	125	12		Also discrete $\gamma$ 's.
	0.85	20.0	0.2-3.0	NaI	0.69	10.6	0.02-0.2	90,125	13	Y	
Si	1.0	20.0	0.24-3.0	NaI	0.69	10.4	$\approx 0.1$	90,125	14		
P 31											
S											
Cl											
Ar											
K											
Ca	0.7	20.1	0.5-3.0	NaI	0.69	10.6	0.02-0.2	125	15	Y	
Sc 45											
Ti	0.4	19.9	0.3-3.0	NaI	0.31	20.5	0.02-1.0	125	16		
V 51	0.2	20.1	0.27-10.6	NaI	0.27	10.6	0.02-0.2	125	17	Y	99.750%.
Cr	0.2	20.0	0.4-3.0	NaI	0.30	10.3	0.01-0.1	125	18	Y	
	0.2	40.		Ge(Li)	0.2	10			19		Some data.
53	0.2	40.		Ge(Li)	0.2	10			19		9.501%. Some data.



Table 1. 0.2- to 20-MeV Prompt Gamma Production Measurements (continued)\*

Element Isotope	E <sub>n</sub> (MeV)			Detector	E <sub>γ</sub> (MeV)			Angles	Ref	ENDF B-V	Comments
	E <sub>min</sub>	E <sub>max</sub>	ΔE		E <sub>min</sub>	E <sub>max</sub>	ΔE				
La											
Ce											
Pr141											
Nd											
Sm											
Eu											
Gd											
Tb159											
Dy											
Ho165											
Er											
Tm169											
Yb											
Lu											
Hf											
Ta	0.4	20.2	0.1-5.0	NaI	1.0	10.4	0.04-0.2	90	30	Y	
181	2	25		BGO	1	20		45-140	31		99.988%. 5 angles. Some data.
W	1.0	20.0	0.5-3.0	NaI	0.69	10.6	0.02-0.2	125	32	Y	
Re	1.2	10.8	0.15-1.2	Scin	1.0	5.0	0.25	4π	33		
Os											
Ir											
Pt											
Au197	0.2	20.1	0.4-3.0	NaI	0.30	10.6	0.02-0.2	125	34		
Hg											
Tl											
Pb	0.6	20.0	0.4-2.5	???	0.3	10.6	0.02-0.2	125	35	Y	
Bi209											
Th232	0.3	20.0	0.2-3.0	NaI	0.31	10.6	0.02-0.2	125	36	Y	
U											

\* Excluding Tc and Pm and the daughters of actinide decay, Po, At, Rn, Fr, Ra, Ac, and Pa which do not occur naturally. No data were found for these nuclides.

References:

1. J.K. Dickens, *et al.* ORNL-TM-4538 (1974). EXFOR10502.
2. D.C. Larson. DOE-NDC-36, 130 (1985).
3. G.L. Morgan. ORNL-TM-6247 (1978). EXFOR10788.
4. C.R. Gould, *et al.* Int. Conf. Nucl. Data for Basic and Applied Sci (Santa Fe, 1985) AD04 (to be published).
5. D.C. Larson and J.K. Dickens. DOE-NDC-33, 144 (1984).
6. V.C. Rogers, *et al.* DNA-3495F (1974). EXFOR10490.
7. V.J. Orphan and C.G. Hoot. GA-8006 (1969). EXFOR10471.
8. J.K. Dickens, *et al.* ORNL-4864 (1973). EXFOR10351.
9. G.L. Morgan and G.T. Chapman. ORNL-5575 (1979). EXFOR10847.
10. D.C. Larson and G.L. Morgan. ORNL-TM-6281 (1978). EXFOR10926.
11. J.K. Dickens, *et al.* ORNL-TM-4544 (1974). EXFOR10582.
12. C.G. Hoot, *et al.* Nucl. Sci. Eng. 57, 309 (1975) and GULF-RT-A-10743 (1971). EXFOR10219.
13. J.K. Morgan, *et al.* ORNL-TM-4232 (1973). EXFOR10352.
14. J.K. Dickens, *et al.* Phys. Rev. C10, 958 (1974). EXFOR10397.
15. J.K. Dickens, *et al.* ORNL-TM-4252 (1973). EXFOR10350.
16. G.L. Morgan and D.C. Larson. ORNL-TM-6323 (1978). EXFOR10790.
17. E. Newman and G.L. Morgan. ORNL-TM-5299 (1976). EXFOR10657.
18. G.L. Morgan and E. Newman. ORNL-TM-5098 (1976). EXFOR10581.
19. D.C. Larson. Int. Conf. Nucl. Data for Basic and Applied Sci (Santa Fe, 1985) AB02 (to be published).
20. G.L. Morgan. ORNL-TM-5531 (1976). EXFOR10656.
21. G.T. Chapman, *et al.* ORNL-TM-5416 (1976). EXFOR10585.
22. J.K. Dickens, *et al.* ORNL-TM-4379 (1973). EXFOR10402.
23. G.T. Chapman. ORNL-TM-5215 (1976). EXFOR10585.
24. G.L. Morgan. ORNL-5499 (1979). EXFOR10977.
25. J.K. Dickens, *et al.* ORNL-TM-4464 (1972). EXFOR10398.
26. J.K. Dickens, *et al.* ORNL-TM-4972 (1975). EXFOR10553.
27. G.L. Morgan, *et al.* ORNL-TM-5097 (1975). EXFOR10584.
28. J.K. Dickens, *et al.* ORNL-TM-5081 (1975). EXFOR10400.
29. J.K. Dickens, *et al.* ORNL-TM-4406 (1973). EXFOR10396.
30. J.K. Dickens, *et al.* ORNL-TM-3702 (1972). EXFOR10399.
31. Z.W. Bell, *et al.* Nucl. Sci. Eng. 84, 12 (1983).
32. J.K. Dickens, *et al.* ORNL-4847 (1973). EXFOR10353.
33. M.V. Savin, *et al.* At. Energiya 49(4), 236 (1980). EXFOR40508.
34. G.L. Morgan and E. Newman. ORNL-TM-4973 (1975). EXFOR10551.
35. G.T. Chapman, *et al.* ORNL-TM-4822 (1975). EXFOR10586.
36. G.L. Morgan. ORNL-TM-6758 (1979). EXFOR10883.

Table 2.  $\approx 14$ -MeV Prompt Gamma Production Measurements\*

Element Isotope	Detector	Angles	$\Delta I\gamma(\%)$	Ref	Comments ( $E\gamma$ in MeV)
H					
He					
Li 6	NaI	$4\pi$	36	1	7.5%. 3.56 $\gamma$ .
7	NaI	$4\pi$	15	1	92.5%. 0.48 $\gamma$ .
Be 9	NaI	$4\pi$	20-42	1	0.48, 2.45 $\gamma$ 's.
B 10	NaI	$4\pi$	12-50	1	19.9%. 12 $\gamma$ 's (0.48-6.1).
11	NaI	$4\pi$	10-33	1	80.1%. 10 $\gamma$ 's (1.1-9.3).
C	NaI	45-130	14	2	4.4 $\gamma$ . 6 angles.
N 14	NaI	$4\pi$	10-50	1	99.634%. 13 $\gamma$ 's (0.73-7.0).
O 16	NaI	$4\pi$	10-50	1	99.762%. 13 $\gamma$ 's (0.74-7.1).
F 19	NaI	$4\pi$	11-25	3	5 $\gamma$ 's (1.39-5.20).
Ne					
Na23	Ge(Li)	$4\pi$	11-14	4	7 $\gamma$ 's (0.440-2.641).
Mg	NaI	$4\pi$	10-20	3	4 $\gamma$ 's. (1.37-4.00).
Al27	NaI	90, 110, 130	6-15	2	6 $\gamma$ 's (0.84-3.0).
	Ge(Li)	125	11-68	5	18 $\gamma$ 's (0.631-3.203).
Si	NaI	$4\pi$	14-50	1	Binned. 0.5-12.0; 0.5.
	NaI	90, 110, 130	12	2	1.78 $\gamma$ .
28	NaI	$4\pi$	10-32	3	92.23%. 4 $\gamma$ 's (1.02-2.76).
P 31	NaI	$4\pi$	14-25	3	1.26, 2.23, 2.96 $\gamma$ 's.
S	NaI	$4\pi$	16-200	1	Binned. 0.5-12.0; 0.5.
32	NaI	$4\pi$	11-20	3	95.02%. 5 $\gamma$ 's (1.27-3.95).
Cl	NaI	$4\pi$	15-32	3	1.30, 2.19, 2.99 $\gamma$ 's.
35	Ge(Li)	125	24-27	5	75.77%. 1.769, 2.132 $\gamma$ 's.
37	Ge(Li)	125	31	5	24.23%. 1.730 $\gamma$ .
Ar					
K					
Ca	NaI	90, 110, 130	10-36	2	Binned. 0.4-8.5; 0.1 to 0.5.
40	NaI	$4\pi$	35	3	96.941%. 3.9 $\gamma$ .
Sc45					
Ti	NaI	90, 110, 130	10-24	2	Binned. 0.2-8.5; 0.1 to 0.5.
48	NaI	$4\pi$	9-18	6	73.8%. 0.99, 1.31 $\gamma$ 's.

V	NaI	90, 110, 130	10-23	2	Binned. 0.2-8.5; 0.1 to 0.5.
Cr	Ge(Li)	125	17-28	5	1.811, 1.946 $\gamma$ 's.
52	Ge(Li)	125	7-33	5	83.789%. 7 $\gamma$ 's (0.744-1.783).
Mn55					
Fe	Ge(Li)	90	10-50	4	30 $\gamma$ 's (0.412-3.602).
	Ge(Li)		0.8-57	7	43 $\gamma$ 's (0.438-8.80). Relative
Co59					
Ni	Ge(Li)	90	7-10	8	37 $\gamma$ 's (0.230-1.919).
Cu	Ge(Li)	80	9-43	9	13 $\gamma$ 's (0.365-1.863).
	Ge(Li)	55	8-50	10	29 $\gamma$ 's (0.344-1.861).
63	Ge(Li)	125	9-154	5	69.17%. 10 $\gamma$ 's (0.670-1.866).
65	Ge(Li)	125	11-48	5	30.83%. 6 $\gamma$ 's (0.470-1.482).
Zn	NaI	4 $\pi$	16-100	1	Binned. 0.5-12.0; 0.5.
Ga					
Ge					
As75					
Se					
Br					
Kr					
Rb					
Sr					
Y 89	Ge(Li)	90	11-30	11	19 $\gamma$ 's (0.1276-1.5064).
Zr	NaI	4 $\pi$	19-140	1	Binned. 0.5-12.0; 0.5.
Nb93	NaI	90, 110, 130	10-100	2	Binned. 0.2-8.5; 0.1 to 0.5.
Mo	NaI	4 $\pi$	2-100	1	Binned. 0.5-12.0; 0.5.
Ru					
Rh103					
Pd					
Ag					
Cd	NaI	4 $\pi$	16-100	1	Binned. 0.5-12.0; 0.5.
In	NaI	4 $\pi$	16-200	1	Binned. 0.5-12.0; 0.5.
Sn	NaI	4 $\pi$	16-100	1	Binned. 0.5-12.0; 0.5.

Table 2.  $\approx 14$ -MeV Prompt Gamma Production Measurements (continued)\*

<u>Element Isotope</u>	<u>Detector</u>	<u>Angles</u>	<u><math>\Delta I\gamma(\%)</math></u>	<u>Ref</u>	<u>Comments (<math>E_\gamma</math> in MeV)</u>
Sb					
Te					
I 127					
Xe					
Cs 133					
Ba					
La					
Ce					
Pr 141					
Nd					
Sm					
Eu					
Gd					
Tb 159					
Dy					
Ho 165					
Er					
Tm 169					
Yb					
Lu					
Hf					
Ta	NaI	120	10-80	2	Binned. 0.3-8.5; 0.1 to 0.5.
W	NaI	$4\pi$	20-100	1	Binned. 0.5-7.0. 0.5.
Re					
Os					
Ir					
Pt	NaI	90, 130	10-88	2	Binned. 0.4-8.5; 0.1 to 0.5.
Au 197					
Hg	NaI	$4\pi$	17-100	1	Binned. 0.5-12.0; 0.5.
Tl					

Pb	Ge(Li)	80	6-50	8	12 $\gamma$ 's (0.538-4.089).
206	Ge(Li)	125	11-20	5	24.1%. 4 $\gamma$ 's (0.537-0.987).
207	Ge(Li)	125	11-27	5	22.1%. 6 $\gamma$ 's (0.569-1.777).
208	Ge(Li)	125	13-22	5	52.4%. 1.042, 2.614 $\gamma$ 's.
Bi209	Ge(Li)	80	6-20	8	5 $\gamma$ 's (0.896-2.741).
	Ge(Li)	4 $\pi$	$\geq 15$	11	30 $\gamma$ 's (0.2853-1.938). Energy resolution=30-80 keV.
Th232	NaI	90,130	10-270	2	Binned. 0.4-8.5; 0.1 to 0.5.
U 235	NaI	120	10-67	2	0.7200%. Binned. 0.4-8.5; 0.1 to 0.5.
238	NaI	90,130	10-67	2	99.2745%. Binned. 0.4-8.5; 0.1 to 0.5.

\* Does not include Tc or Pm which are not naturally occurring or the daughters of actinide decay, Po, At, Rn, Fr, Ra, Ac, and Ac. No data were found for these nuclides.

#### References:

1. V.M. Bezotosnyj, *et al.* 3<sup>rd</sup> All-Union Conf. on Neutron Physics 4, 133 (1975). EXFOR40516.
2. D.M. Drake, *et al.* Nucl. Sc. Eng. 65, 49 (1978). EXFOR10684.
3. J. Roturier. Thesis. U. Bordeaux (1968). EXFOR20599.
4. A.P. Degtjarjov, *et al.* 4<sup>th</sup> All-Union Conf. on Neutron Physics 2, 3 (1977). EXFOR40575.
5. T. Yamamoto, *et al.* Nucl. Sci. Tech. 15, 797 (1978). EXFOR21304.
6. U. Abbondanno, *et al.* J. Nucl. Energy 27, 227 (1973). EXFOR20493.
7. K. Gul, *et al.* INDC(PAK)-5, 13 (1984).
8. S. Hlavac and P. Oblozinsky. INDC(CSR)-5 (1983). EXFOR30801.
9. B. Joensson, *et al.* Ark. Fiz. 39, 295 (1969). EXFOR20164.
10. X. Shi, *et al.* Chinese J. Nucl. Phys. 4, 120 (1982).
11. F.S. Dietrich, *et al.* Phys. Rev. C9, 973 (1974). EXFOR10392.
12. E.J. Feicht and H. Goebel. Z. Phys. 245, 13 (1971). EXFOR20982.



# FAST NEUTRON ACTIVATION ANALYSIS: AN ELEMENTAL DATA BASE

John W. McKlveen  
Radiation Measurement Facility  
College of Engineering and Applied Sciences  
Arizona State University, Tempe, Arizona 85287

## Summary

Fast neutron activation analysis (FNAA) is an excellent non-destructive assay technique for selected nuclides such as Al, Cu, F, N, O, P, and Si and may be used to identify other trace elements such as Ag, Ba, Ca, Cd, Fe, Ga, Mg, Nd, Pd, Rb, Se, Sr, Th, U, Zn, and Ar when other, more sensitive methods are not available or whenever interference reactions render the preferred method useless. FNAA has considerable potential for increased usage in undergraduate and graduate educational experiments, industrial applications and a variety of research pursuits. However, multiple trace element identification is often difficult because there is a dearth of publications which organize and present FNAA data in a format suitable for this type of research effort. Whereas considerable amounts of general information and specific applications are described in the published literature, it is often difficult as well as tedious to consolidate the data and facts into a format suitable for general experiments or multi-element analysis. Furthermore, theoretical reactions may not be observed during experimental activation or unreported gamma radiations may impede element identification. To rectify the situation a literature survey was conducted and existing information on FNAA cross-sections, reactions, half-lives and decay energies was assembled for every nuclide. Then all nuclides which exist in solid form were activated for representative times and resulting gamma-ray emissions plotted to show characteristic short and long half-life decay spectra. Also, new tables were generated which show (i) nuclides having the highest FNAA sensitivity and the preferred reaction, (ii) interference nuclides, and (iii) nuclides arranged according to decay energy. The information is now available in a book designed for laboratories interested in deciphering individual elements from unknown samples or performing multiple element analysis.<sup>1</sup>

## Introduction

Neutron activation is a nuclear reaction process in which free neutrons are used to induce changes in atomic structure and energy. All atoms exist in preferred energy states and exhibit some affinity for neutrons. Depending on the possible excitation states of atoms, preference will be shown for neutrons with energies comparable to that needed for excitation; this preferred absorption is known as resonance absorption and is characteristic of the nuclide involved. Upon absorption of a neutron, the interaction forms a compound nucleus in an excited state of high internal energy. The de-excitation ( $\sim 10^{-13}$  to  $10^{-15}$  s) modes of particular importance in neutron activation are particle emission, radiative capture, and fission, and each has a certain probability of occurrence.

Particle emission reactions such as  $(n,p)$ ,  $(n,\alpha)$ , and  $(n,2n)$  are generally endothermic. Reaction cross sections tend to be small ( $\sim$  mb), even when the incident neutron kinetic energy is above the necessary threshold energy. Capture cross sections  $(n,\gamma) \sim b$  are common at thermal neutron energies and generally decrease as a function of increasing neutron kinetic energy. Fission results in the splitting of the compound nucleus into two (or more) nuclei with the accompanying release of neutrons. This process is restricted to a few elements of high atomic number ( $\geq 90$ ) and may require a threshold energy. In general, each of these prompt decay modes leaves the nucleus, or fission products, in an excited state. It is at this point that the nuclei are termed radioactive and decay occurs with a specific probability which is characteristic of the radionuclide. By analysis of the radioactive decay products from neutron activation and a knowledge of the prompt decay schemes and cross sections, it is possible to identify and quantify a specific element.

Unlike thermal neutron facilities (*vis-à-vis* reactors) where the neutron capture reaction  $(n,\gamma)$  predominates almost to the exclusion of other interactions, FNAA elicits several particle reactions, particularly  $(n,2n)$ , and the capture reaction occurs primarily as a result of thermalized neutrons. For inexperienced investigators, or organizations electing to pursue FNAA the numbers of possible interactions and products may become extremely complicated and difficult to decipher, particularly in situations where the sample contains more than one nuclide. Interfering reactions, or situations where particle

reactions produce an identical radionuclide from different stable elements [i.e.,  $Mg^{27}$  from  $Mg^{26}(n,\gamma)$ ,  $Al^{27}(n,0)$ , or  $Si^{30}(n,\alpha)$ ] may add to the confusion. In an attempt to improve the data base for FNAA a literature survey was conducted to determine as much information about known or reported reactions, cross sections and gamma spectra. All theoretical reactions for every element were tabulated. Then, all elements, other than noble gasses or naturally radioactive samples with large specific activities were activated in a 14 MeV neutron generator and the spectra plotted. Finally, the observed spectra were correlated with reported reactions. All information was then tabulated into several categories to permit (i) a summary of each element, its sensitivity to FNAA and the predominant reaction, (ii) a summary of theoretical reactions, cross sections, and experimentally observed spectra, (iii) a listing of all reactions as a function of increasing gamma decay energy with the observed reactions identified, and (iv) a listing of the observed interference reactions. A summary of the experimental collection techniques and the data formats are presented herein.

#### Neutron Generator Facility

A continuous source of 14 MeV neutrons is provided by a Kaman Sciences A-711 accelerator located in a down-hole mount. This system has a sealed-tube generator utilizing the  $H^3(d,n)He^4$  reaction to produce a prolific neutron source which is nearly isotropic. Ionized deuterium and tritium gas molecules are accelerated at 160kV and 3mA to bombard a 15 Ci target of mixed deuterium and tritium. The output yield of the accelerator head is rated at approximately  $10^{11}$  n/s and produces a flux  $\sim 3(10^8)$  n/cm<sup>2</sup>-s based on Cu foil activation. Thermal flux is  $\sim 1\%$  of fast.

A 1-1/4-in. dual tube pneumatic transfer system operated at 45 psig, with dual axis rotating terminal, automatically programs sample irradiation and counting evolutions. A BF<sub>3</sub> proportional counter is mounted in the hole to monitor flux variations during accelerator operation.

The system has an automatic sample counting station which is programmable. The station is located at a bank of five He-3 filled proportional counters immersed in a 20-in. cube of paraffin (hydrogenous moderator). Also in the paraffin is a NaI(Tl)

scintillation detector. The five He-3 counters are used to measure delayed neutron emissions from Uranium, Thorium, and Oxygen-17. The NaI(Tl) crystal provides detection of the gamma spectrum, and in particular the gammas from the  $O^{16}(n,p)N^{16}$  reaction.

There are two other supporting gamma spectroscopy systems. The first consists of a well-type NaI(Tl) crystal housed within a 3-ton lead shield. This is used to measure short half-life radionuclides or samples containing a few elements. This system usually requires manual sample transfer but may be modified for automatic sample counting as needed. The second system is strictly manual and consists of a shielded GeLi system. This is used whenever high resolution gamma spectroscopy is warranted. Additional details on the facility have been published elsewhere.<sup>2</sup>

### Results and Documentation

A complete listing of the theoretically possible reactions was prepared for each stable nuclide and includes half-lives and gamma decay characteristics. Cross section data or graphs were included for information purposes as no attempt was made to assess the accuracy or errors associated with these data. Exhibit 1 provides an example of the information tabulated for each element.

Observed reactions and spectral plots were made for each stable element other than noble gasses. The observed gamma emissions are tabulated from low to high energy and are normalized to the predominant peak. Frequently more than one plot is provided and depicts the spectra observed after different decay and count times. The spectral information for Titanium is shown in Exhibit 2.

Using the theoretical reactions for each nuclide, a table was created which lists all gamma emissions as a function of increasing energy. Observed reactions are noted for ease in identification. Table I is an example of the format.

Finally a table was prepared which serves as a quick reference for each element. Table II is a portion of this table. Only information on the most prominent reactions (if any) is listed here. The physical transfer time between irradiation and detection precluded observation of extremely short half-lived products which, in selected situations, might provide improved detection sensitivity. Because of the excessive numbers of positron emitters, representative energies other than 0.511

TITANIUM (22)

TITANIUM - CROSS SECTION DATA

	All Possible Reactions	$T_{1/2}$	$E_{\gamma}$	
(73.7%)	$Ti^{48}(n,\gamma)Ti^{49}$	1.83 d	0.175 (6%)	
	$Ti^{48}(n,2n)Ti^{47}$		0.983 (100%)	
	$Ti^{48}(n,p)Sc^{48}$		1.040 (100%)	
			1.314 (100%)	
(8.0%)	$Ti^{48}(n,\alpha)Ca^{45}$	3.08 h	0.718 (0.4%)	
	$Ti^{46}(n,\gamma)Ti^{47}$		1.408 (0.3%)	
	$Ti^{46}(n,2n)Ti^{45}$	84 d	0.889 (100%)	
	$Ti^{46}(n,p)Sc^{46}$		1.120 (100%)	
	$Ti^{46}(n,p)Sc^{46m}$		20 s	0.142
	$Ti^{46}(n,\alpha)Ca^{43}$			
(7.5%)	$Ti^{47}(n,\gamma)Ti^{48}$	3.4 d	0.16 (73%)	
	$Ti^{47}(n,2n)Ti^{46}$			
	$Ti^{47}(n,p)Sc^{47}$			
	$Ti^{47}(n,\alpha)Ca^{44}$			
(5.5%)	$Ti^{49}(n,\gamma)Ti^{50}$	57 m	1.76 (0.03%)	
	$Ti^{49}(n,2n)Ti^{48}$			
	$Ti^{49}(n,p)Sc^{49}$			
(5.3%)	$Ti^{50}(n,\gamma)Ti^{51}$	5.8 m	0.32 (95%)	
			0.605 (1.5%)	
			0.928 (5%)	
	$Ti^{50}(n,2n)Ti^{49}$	1.71 m	0.52 (100%)	
	$Ti^{50}(n,p)Sc^{50}$		1.12 (100%)	
			1.55 (100%)	
	$Ti^{50}(n,\alpha)Ca^{47}$		4.83 d	0.49 (5%)
			0.815 (5%)	
	1.308 (74%)			

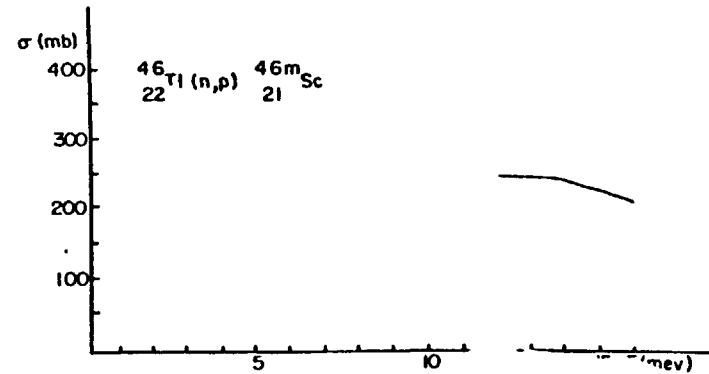
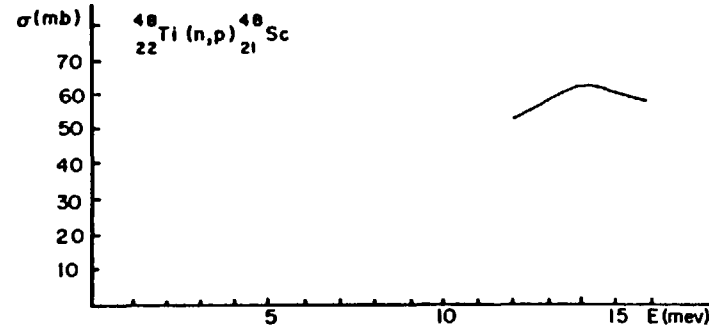


Exhibit 1. Theoretical reactions and reported cross sections for a typical nuclide.

Peak No.	E <sub>Mev</sub>	Reaction	% Abun	T <sub>1/2</sub>	γ Yield	Counts/g
1	.140	Ti <sup>46</sup> (n,p)Sc <sup>46m</sup>	7.95	20 s	100%	10,000
2	.320	Ti <sup>50</sup> (n,γ)Ti <sup>51</sup>	5.3	5.8 m	95%	
3	.511	?	-	-	-	
4-a	.520	Ti <sup>50</sup> (n,p)Sc <sup>50</sup>	5.25	1.72 m	100%	
4-b	1.120	"	"	"	"	
4-c	1.550	"	"	"	"	
5	1.760	Ti <sup>49</sup> (n,p)Sc <sup>49m</sup>	5.51	57.5 m	<1%	
6	.160	Ti <sup>47</sup> (n,p)Sc <sup>47</sup>	7.5	3.4 d	73%	150
7-a	.175	Ti <sup>48</sup> (n,p)Sc <sup>48</sup>	73.45	1.83 d	6%	
7-b	.983	"	"	"	100%	
7-c	1.040	"	"	"	"	
7-d	1.314	"	"	"	"	

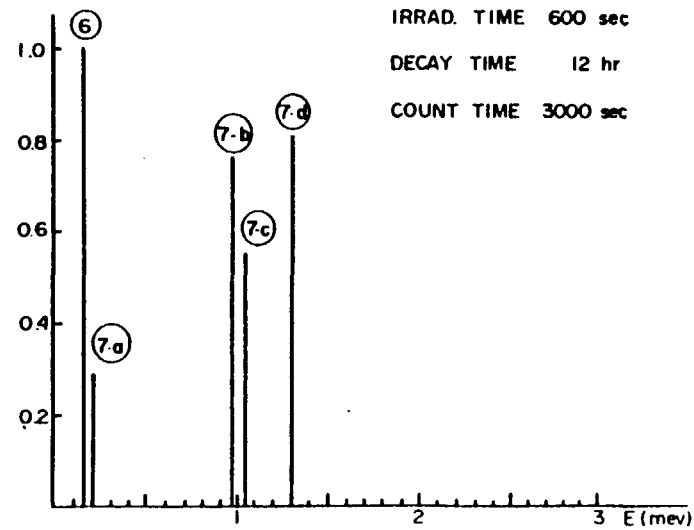
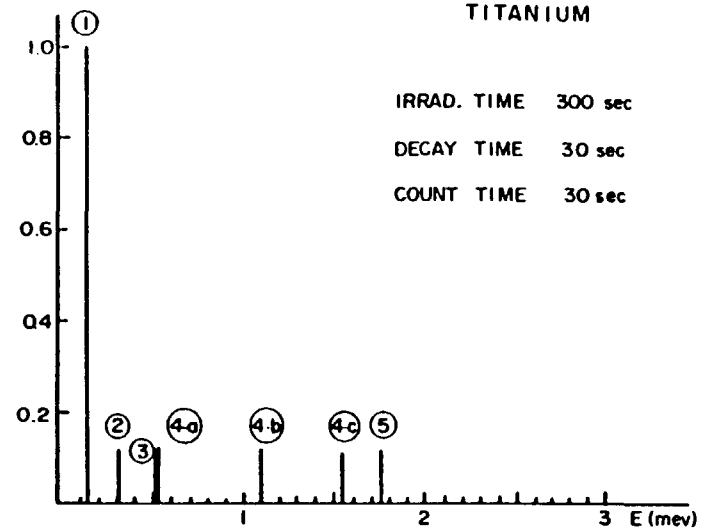


Exhibit 2. Observed reactions for Titanium.

Table I. Fast Neutron Reactions by Increasing Energy.

Energy MeV	% Gamma Emission	Theoretical Reactions (* Observed Reactions)	Half Life	% Natural Abundance	Multiple Decay (MeV)
0.170	100	W186(n,2n)W185m	1.67m	28.6	
0.171	0.7	Th232(n, $\gamma$ )Th233	22.3 m	100	
0.172	40	Re185(n, $\alpha$ )Ta182m	16.3 m	37.5	
0.172	40	Ta181(n, $\gamma$ )Ta182m	16.3 m	99.988	
0.173	0.10	Gd69(n, $\gamma$ )Ga70	20.5 m	.60	
0.173	0.16	Ge70(n,p)Ga70	20.5 m	20.5	
0.174	13	Hf177(n,p)Lu177m	155d	18.5	
0.174	16	Hf176(n, $\gamma$ )Hf177	1.1 s	5.2	
0.174	10	Nd150(n, $\gamma$ )Nd151	12 m	5.6	
0.174	10	Sm154(n, $\alpha$ )Nd151	12 m	22.8	
0.175	6	* Ti48(n,p)Sc48	1.83d	73.7	0.983, 1.040, 1.314
0.175	6	V51(n, $\alpha$ )Sc48	1.83d	99.75	
0.176	-	Lu175(n,2n)Lu174	145d	97.4	
0.176	67	* Yb174(n,p)Tm174	5.2 m	31.8	.273, .366, .500, .990
0.177	22	Yb170(n,2n)Yb169	31.8 d	3	
0.177	22	Yb170(n,2n)Yb169	31.8 d	3	
0.178	13	Os192(n, $\alpha$ )W189	11.3 m	41	
0.180	0.7	* Al27(n,p)Mg27	9.48m	100	.840, 1.013
0.180	-	Dy163(n,p)Tb163m	7 m	24.9	
0.180	26	Ho165(n, $\alpha$ )Tb162	7.48m	100	
0.180	0.7	Mg26(n, $\gamma$ )Mg27	9.5 m	11.01	
0.180	0.7	Si30(n, $\alpha$ )Mg27	9.5 m	3.1	
0.180	-	Yb176(n,p)Tm126	2 m	12.7	
0.180	-	Yb176(n,p)Tm176	2 m	12.7	
0.181	2.2	Lu175(n, $\alpha$ )Tm172	63.5 h	97.4	
0.181	7	Mo198(n, $\gamma$ )Mo99	66.6 h	24.4	
0.181	7	Ho100(n,2n)Mo91	66.6 h	7.6	
0.181	7	Ru102(n, $\alpha$ )Mo99	66.6 h	31.6	
0.181	2.2	Yb172(n,p)Tm172	63.6 h	21.9	
0.181	2.2	Yb172(n,p)Tm172	63.6 h	21.9	
0.182	-	Gd158(n,p)Eu158	53 m	24.7	
0.184	20	Re185(n, $\alpha$ )Ta182m	16.3 m	37.5	
0.184	20	Ta181(n, $\gamma$ )Ta182m	16.3 m	99.988	
0.184	40	* Zn67(n,p)Cu67	58.5 h	4.1	Single Emission
0.187	51	* Ir191(n,2n)Ir190	11.65d	37.4	.370, .403, .518, .560, .604
0.187	66	* Ir191(n,2n)In190m	3.1 h	37.4	.361, .502, .616

Table II. Quick Reference - Predominant Reactions and Maximum Sensitivity

Element	Z	Reaction	Half Life	Irrad. Time	Decay Time	Count Time	Gamma Radiation	Sensitivity $\mu\text{g}$
Titanium	22	$\text{Ti}^{46}(\text{n},\text{p})\text{Sc}^{46\text{m}}$	20 s	300 s	30 s	30 s	0.14(100%)	9800
		$\text{Ti}^{47}(\text{n},\text{p})\text{Sc}^{47}$	3.4 d	600 s	1.0 h	10000	0.16(73%)	17000
Tungsten	74	$\text{W}^{184}(\text{n},\gamma)\text{W}^{185\text{m}}$	1.67 m	600 s	60 s	200 s	0.13(70%)	23500
		$\text{W}^{186}(\text{n},2\text{n})\text{W}^{185\text{m}}$	23.9 h	600 s	1.0 h	10000 s	0.48(81%) 0.686(27%)	15000
		$\text{W}^{186}(\text{n},\gamma)\text{W}^{187}$						10500
Uranium	92	Fission	delayed neutrons	60 s	4 s	40 s	--	50
Vanadium	23	$\text{V}^{51}(\text{n},\gamma)\text{V}^{52}$	3.75 m	600 s	60 s	200 s	1.434(100%)	750
		$\text{V}^{51}(\text{n},\text{p})\text{Ti}^{51}$	5.8 m	600 s	60 s	200 s	0.32(95%)	200
Xenon	54	--	--	--	--	--	--	Not Irradiated
Ytterbium	70	$\text{Yb}^{174}(\text{n},\text{p})\text{Tm}^{174}$	5.2 m	600 s	60 s	200 s	0.176(67%)	32600
		$\text{Yb}^{174}(\text{n},\gamma)\text{Yb}^{175}$	101 h	600 s	1.0 h	10000 s	0.395(6%)	4350
Yttrium	39	$\text{Y}^{89}(\text{n},\text{n}'\gamma)\text{Y}^{89\text{m}}$	16 s	600 s	30 s	100 s	0.91(100%)	1800
Zinc	30	$\text{Zn}^{64}(\text{n},2\text{n})\text{Zn}^{63}$	38.2 m	600 s	60 s	1000 s	0.511(186%)	5600
Zirconium	40	$\text{Zr}^{90}(\text{n},2\text{n})\text{Zr}^{89\text{m}}$	4.34 m	600 s	60 s	200 s	0.588(87%)	290
		$\text{Zr}^{90}(\text{n},2\text{n})\text{Zr}^{89}$	78.9 h	600 s	1.0 h	10000 s	0.91(99%)	550

MeV were selected whenever possible. A minimum sensitivity was calculated by using the activation equation and comparing the data collected for the standard against a hypothetical sample which yielded 100 counts above background for the principal identification peak. Exact sensitivities are a function of the specific counting system being used, so the values presented here should be considered representative for a shielded 3X3 in NaI(Tl) detector.

#### Acknowledgements

I wish to express my sincere appreciation to Messrs. Charles Stevens, Kent Faris and Thomas Perry for assisting with the data collection and interpretation of the spectral information and to Ms. Elinor Lindenberger and her staff for preparing the final documents.

#### References

1. J. W. McKlveen, Fast Neutron Activation Analysis: An Elemental Data Base. (ISBN 0-250-40406-0), Ann Arbor Science, Ann Arbor, MI. (1981).\*
2. J. W. McKlveen, "Fast Neutron Activation Analysis in Multidisciplinary Studies," IEEE Transactions on Nucl. Sci., 26, 1, 1614 (1979).

\* Available after January, 1981 from;

Ann Arbor Science Publishers, Inc.  
10 Tower Office Park  
Woburn, Mass. 01801



# BULK MATERIAL ANALYSIS USING

## ENERGETIC NEUTRONS

M.C. UNDERWOOD and J.S. PETLER

Nuclear Geophysics Section, BP Research Centre,  
Sunbury-on-Thames, Middlesex, England.

### ABSTRACT

There is considerable interest in bulk material analysis using energetic neutrons, e.g. on-line coal analysis and down-hole logging. Recent work has indicated that an in-situ analysis of all the major elements of coal, using prompt capture and inelastic neutron scattering reactions may be an operational possibility. A down-hole logging tool is described utilising a 5 Ci  $^{241}\text{Am}$ -Be neutron source and intrinsic germanium gamma-ray detector. Measurements are reported upon 4 well characterised coal samples and the sulphur concentration correlated with the intensity of the 2380 keV gamma-ray line arising from the  $(n,\gamma)$  reaction. Gamma-ray spectra are also presented arising from 14 MeV neutron bombardment of the same coal samples. Neutron transport modelling is described that evaluates the effects of variations in material content and the presence of trace quantities of "neutron poisons" upon induced gamma-ray response. Thus, the feasibility of a multi-element analysis using neutron induced reactions is assessed.

### 1. INTRODUCTION

The use of neutron induced gamma-ray spectroscopy for bulk material analysis is a well established technique and has been adapted for down-hole logging in both the coal and oil industries. Pulsed 14 MeV neutron sources are used together with sodium iodide, i.e. NaI(Tl) detectors to obtain gamma-ray spectra from both inelastic neutron

scattering and capture reactions (1,2). There is, however, growing interest in using high resolution i.e. solid state detectors and multi-element analyses of coal have been reported using isotopic neutron sources (3-5). The use of high resolution detectors offers the promise of an improved elemental analysis, due to enhanced spectral resolution, but suffers from some potential disadvantages including the requirements of a low temperature environment and modest gamma-ray detection efficiency (when compared with sodium iodide). However, developments in cryogenic technology now allow the use of solid state detectors in hostile environments and so the usefulness of such measurements should be assessed (6). In this paper a logging tool is described comprising an intrinsic n-type gamma-ray detector and  $^{241}\text{Am-Be}$  neutron source. In addition, measurements are reported using a 14 MeV neutron source to give an enhanced response from inelastic scattering reactions. Neutron transport modelling is used to evaluate the effects of variations in material content and the presence of "neutron poisons" upon induced gamma-ray emission. These investigations allow the feasibility of multi-element analysis to be assessed.

## 2. EXPERIMENTAL PROCEDURE AND RESULTS

A schematic representation of the logging tool is shown in Figure 1. The neutron source comprises 5 Ci of  $^{241}\text{Am-Be}$  with an output of  $1.1 \times 10^7 \text{ n/s}$  mounted approximately 35cm below an intrinsic n-type detector (diameter 48mm and length 48mm) of efficiency 20.1%. The detector is housed within a pressure case inside which there is a vacuum insulated pressure vessel containing propane. The propane is frozen by connecting the vessel to a closed-cycle helium cooler. A typical cooling cycle is shown in Figure 2. When the propane is frozen the head from the cooler is removed and the tool assembled. An operating period (at ambient

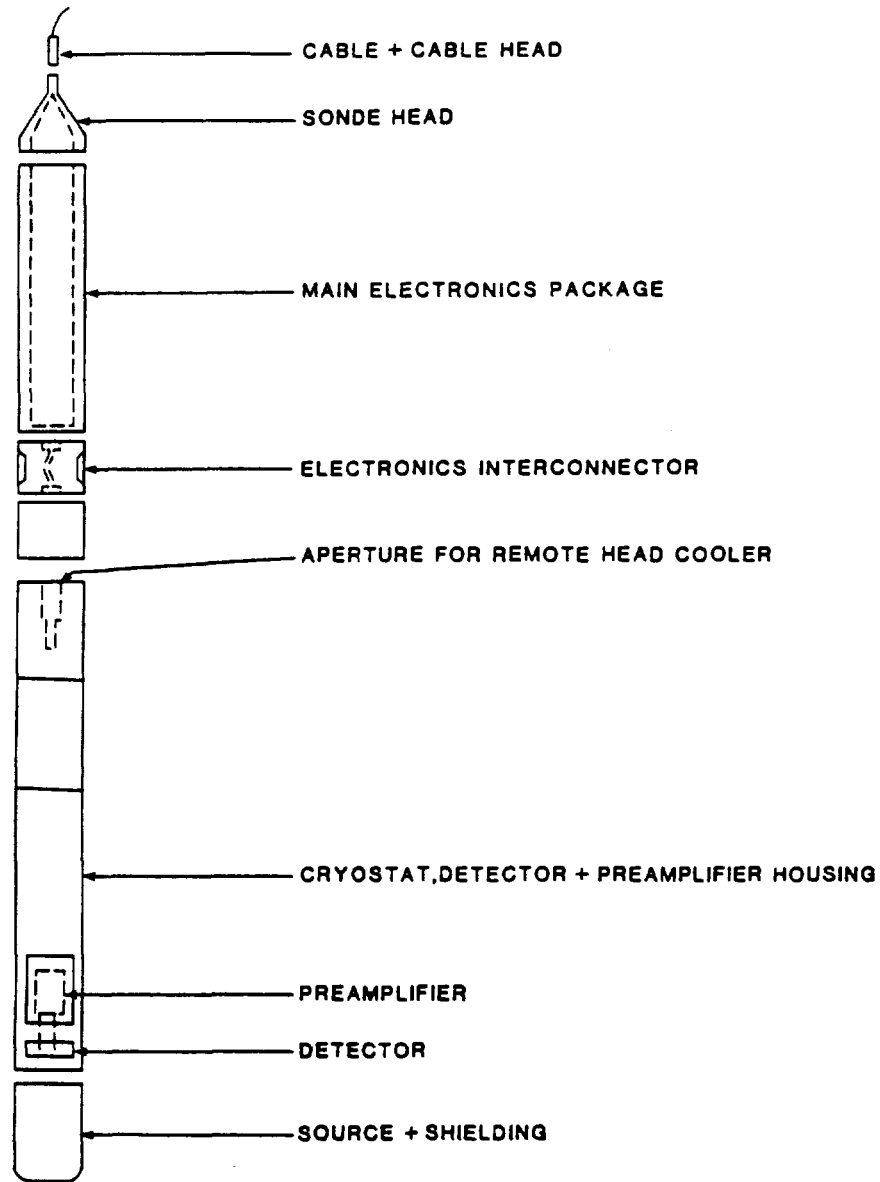


Figure 1. Schematic representation of logging tool.

temperature and pressure) in excess of twenty hours is obtained. The detector is connected to a charge sensitive (warm F.E.T.) pre-amplifier and conventional signal amplification and pulse shaping is achieved in the upper half of the logging tool. High voltage biasing of the detector is produced in the tool by a Cockcroft-Walton voltage multiplier comprising 8 stages and developing about 4kV. Pulse height spectra were acquired on a conventional 4k Multi Channel Analyser.

Four calibration pits were constructed containing different grades of coal as listed in Table I. Each calibration tank was

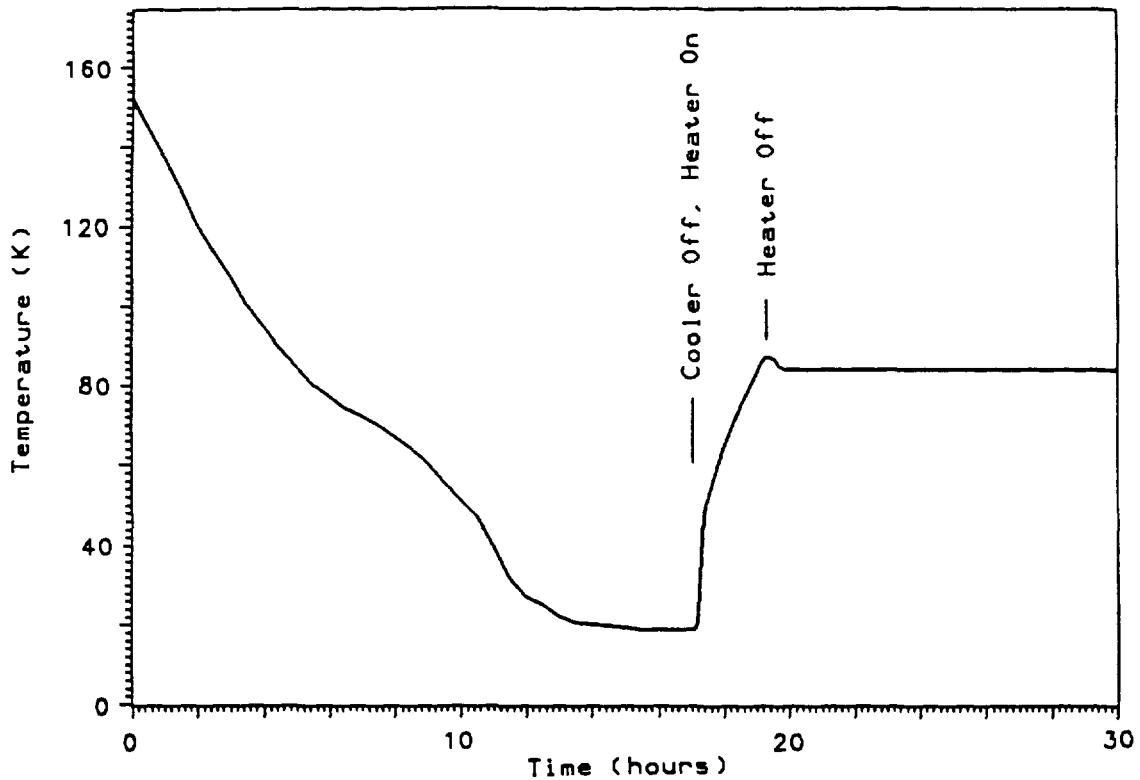


Figure 2. Logging tool cooling cycle.

**ELEMENTAL ANALYSIS (% BY WEIGHT) OF MAJOR COMPONENTS  
IN THE CALIBRATION PITS**

	PIT A	PIT B	PIT C	PIT D
CARBON	70.2	72.7	66.4	56.6
SULPHUR	0.54	0.92	3.0	2.2
CHLORINE	0.01	0.55	0.09	0.17
HYDROGEN	4.89	5.46	5.39	4.7
OXYGEN (TOTAL)	19.0	18.2	23.1	27.3
NITROGEN	1.7	1.3	0.9	0.8
SiO <sub>2</sub>	2.43	0.77	1.06	4.91
Al <sub>2</sub> O <sub>3</sub>	1.55	0.52	0.79	3.01

constructed from glass reinforced plastic with a central copper tube in which the logging tool was located. The sulphur line occurring at 2380 keV is shown in Figure 3. In Figure 4 is plotted the correlation between the count-rate into the sulphur peak and the sulphur concentration, as given by chemical analysis, indicating a count-rate of about 12 counts/min per 1% (weight) sulphur concentration. Of the other elements giving rise to gamma-ray emission following neutron capture only hydrogen, iron and chlorine give rise to significant emission. There is measurable gamma-ray emission from carbon and silicon but no usable emission from aluminium and nitrogen. The iron content of a coal would be difficult to quantify as the response is dominated by the gamma-ray emission from the tool itself.

The 14 MeV neutron irradiations were performed upon material packed into fibreglass cubes ( $60 \times 60 \times 60 \text{ cm}^3$ ) with an indentation in one side to allow the tritium target of the accelerator to be positioned such

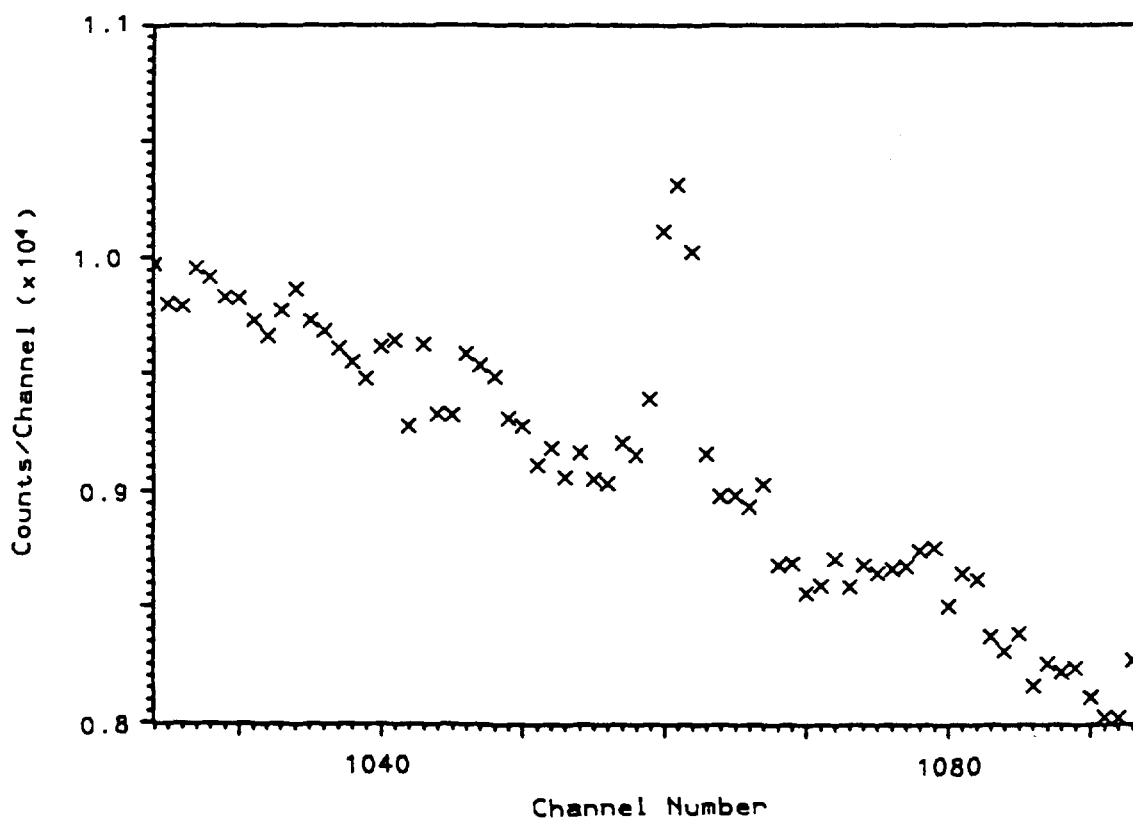


Figure 3. Portion of gamma-ray spectrum showing sulphur peak.

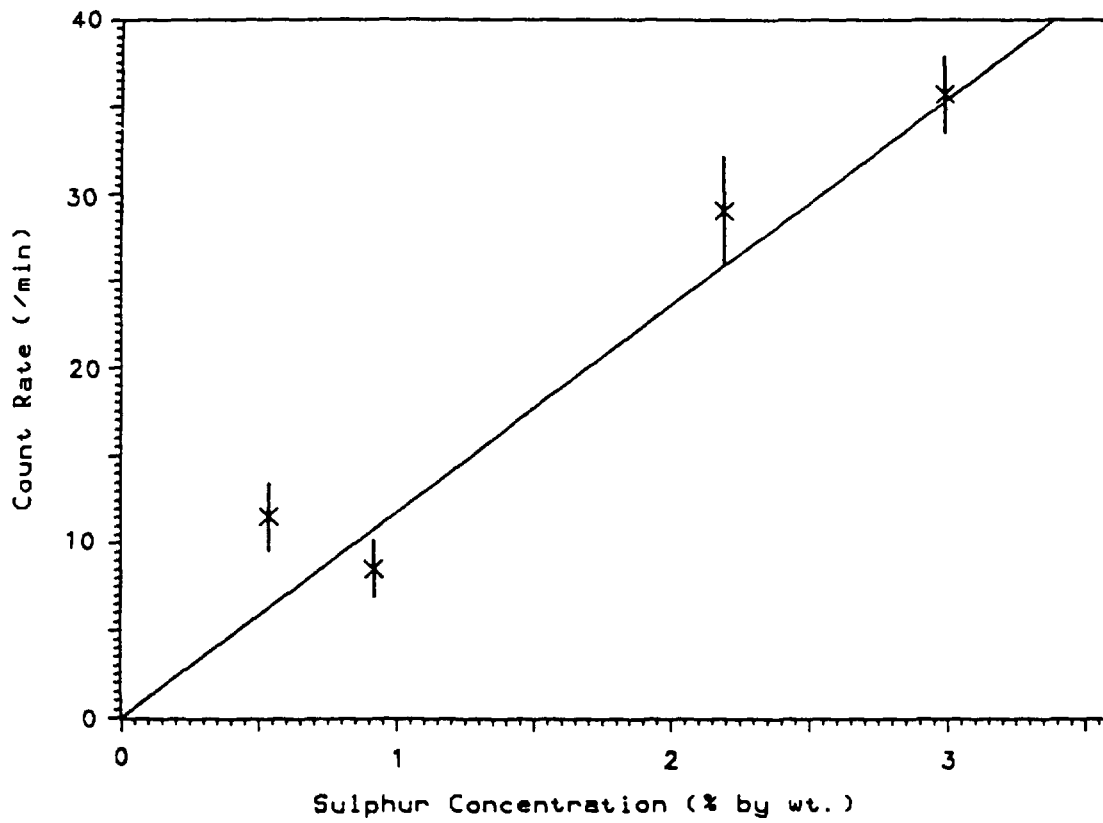


Figure 4. Correlation between count rate and sulphur concentration.

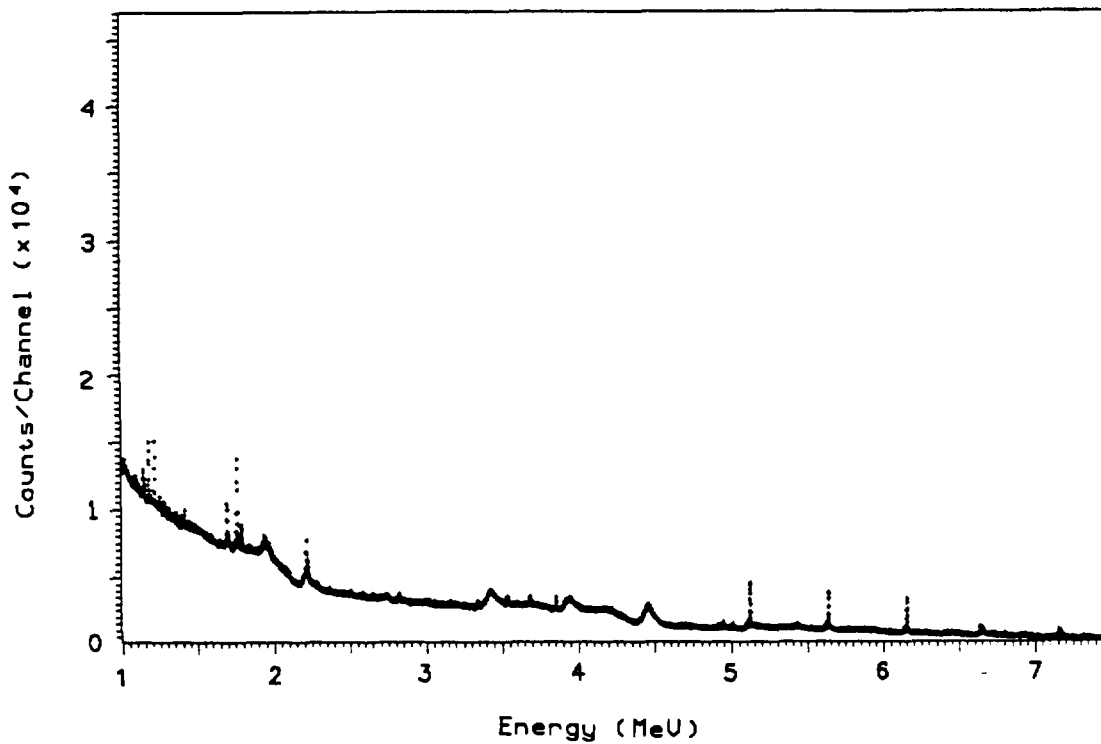


Figure 5. Gamma-ray spectrum arising from 14 MeV neutron irradiation of coal D.

that samples were irradiated from approximately the centre. All irradiations were using a continuous source output. A typical spectrum is shown in Figure 5 with a dominant hydrogen peak at 2.22 MeV, with its associated Compton edge, and inelastic scattering peaks (and associated single and double escape peaks) from carbon and oxygen at 4.437 and 6.129 MeV respectively. Capture peaks are also evident from Si, Fe, Al and the  $^{28}\text{Si}$  ( $n, n' \gamma$ ) peak at 1.78 MeV. The peak at 4.437 MeV arising from the  $^{12}\text{C}$  ( $n, n' \gamma$ ) reaction is Doppler broadened as the lifetime of the  $2^+$  excited state in  $^{12}\text{C}$  is  $4.2 \times 10^{-14}\text{s}$ , which is considerably shorter than the slowing down time of the recoiling nucleus (7).

### 3. NEUTRON FLUX MODELLING AND PREDICTED GAMMA RESPONSE

The response of a detector,  $R_{ij}$ , to gammas,  $\gamma_i$ , from element  $j$  is given by:

$$R_{ij} = \int_V \int_{E_n} \phi(E_n, r) \sigma_{ij}(E_n) v_j(r) G(E_i, r) dE_n dV \quad (1)$$

where:

$\phi(E_n, r)$  is the flux of neutrons of energy  $E_n$  at position  $r$ .

$\sigma_{ij}(E_n)$  is the microscopic reaction cross-section for producing  $\gamma_i$  with neutrons of energy  $E_n$  from element  $j$ .

$v_j$  is the number density of element  $j$  per unit volume at  $r$ .

$V$  is the total volume of material under investigation.

and

$G(E_i, r)$  is the detection probability for gammas of energy  $E_i$  emitted at a point  $r$ . This factor takes into account the detection efficiency as well as geometrical and attenuation factors.

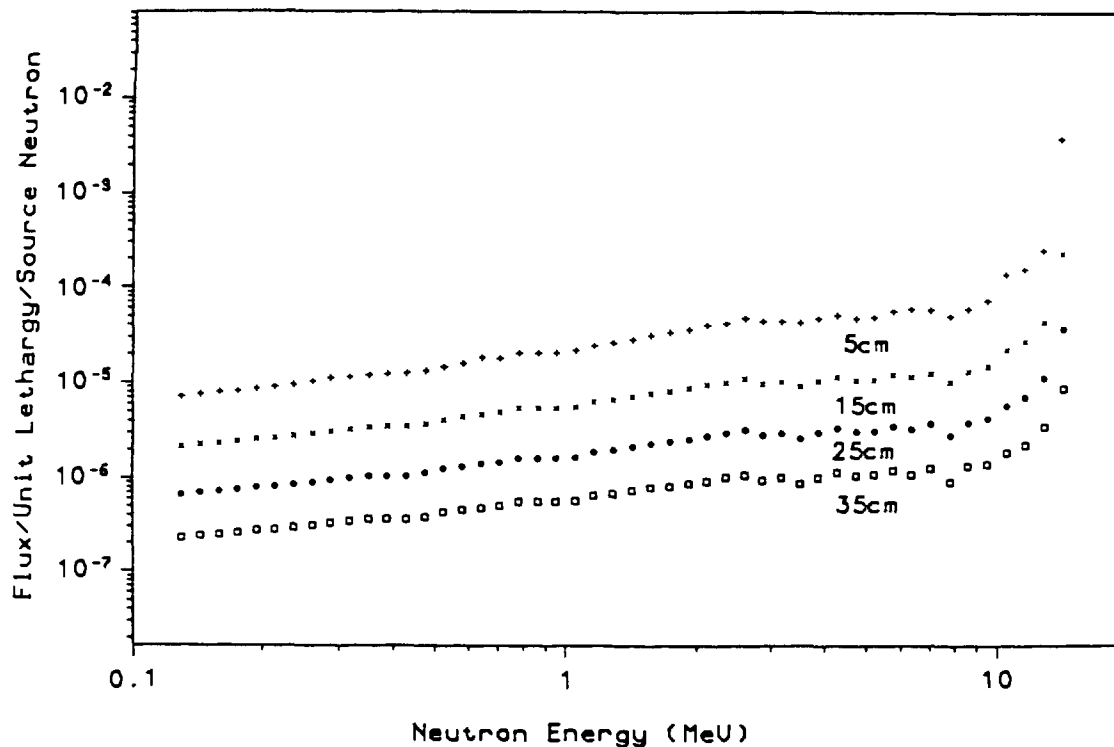


Figure 6. Predicted fast neutron distributions in coal.

In the present calculations the determination of the neutron distribution was decoupled from the gamma response, in that the neutron transport calculations were performed independently of the determination of gamma production and the calculation of gamma attenuation within the sample.

The one dimensional discrete ordinate transport code ANISN was used to determine the neutron flux distribution within the irradiated cubes. Spherical symmetry was assumed with a point 14 MeV source surrounded by a void of 10cm radius and then a sphere of coal to a radius of 30cm. It was found that the predicted fast flux distribution within a sample was only weakly dependent on the size of modelling space and hence the assumption of spherical geometry is reasonable for the determination of inelastic scattering response throughout the cube. However, the thermal flux distribution is affected by the size of the modelling space and the boundary conditions applied (reflection/no reflection) and hence predictions of the capture responses are expected to be qualitative rather

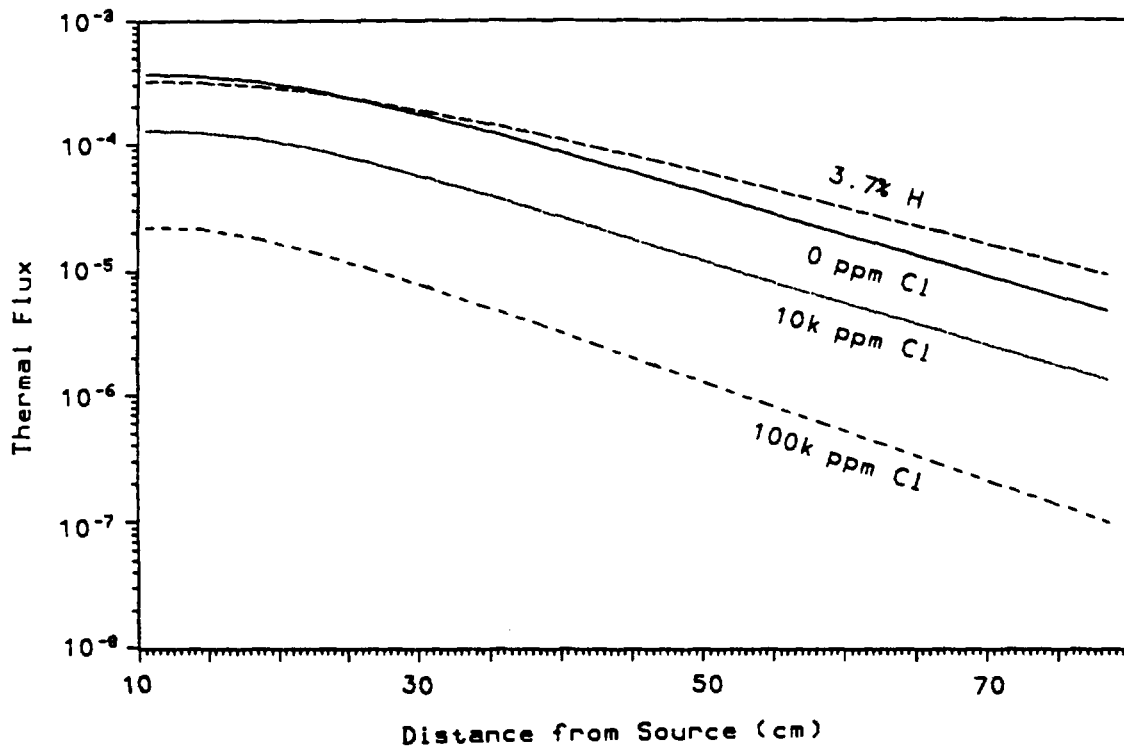


Figure 7. Predicted thermal neutron distributions in coals of differing hydrogen and chlorine concentration.

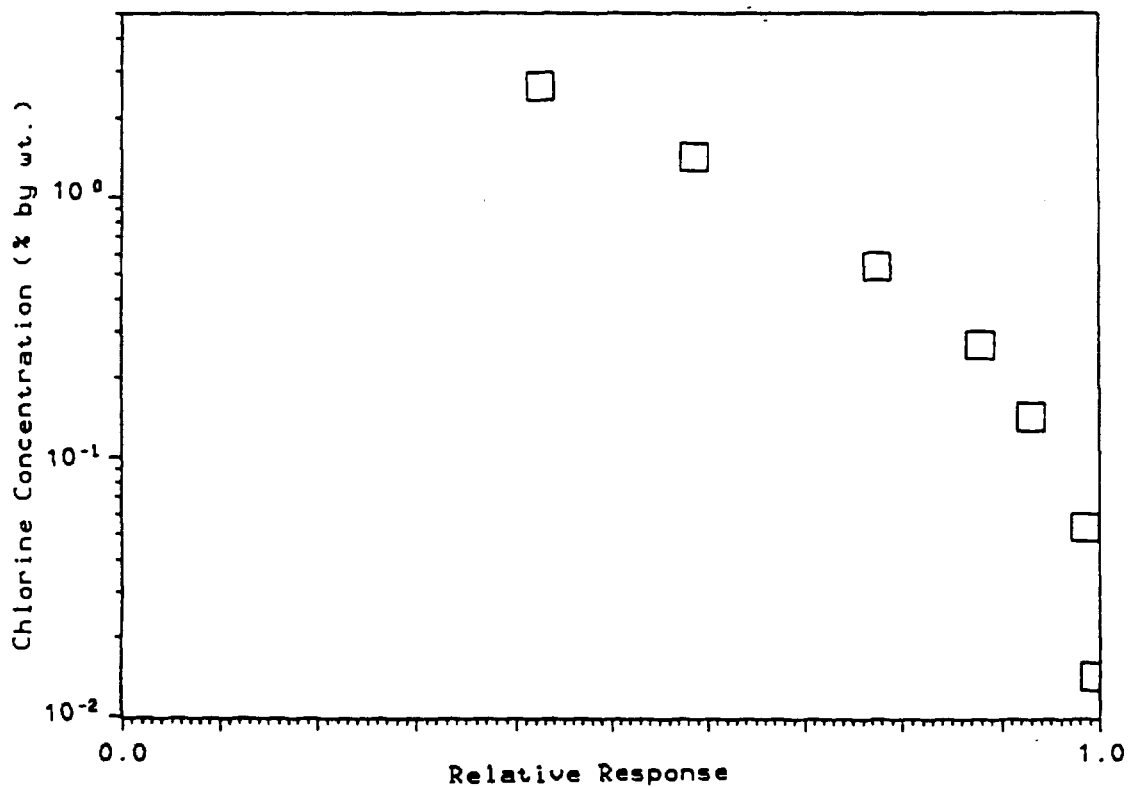


Figure 8. Predicted count rate into sulphur peak as a function of chlorine content.

than quantitative. But modelling can give an insight into the likely dependence of the thermal flux distribution in borehole environments.

The response of the detector to gammas produced within the sample and the shielding was calculated by numerical techniques using equation 1 in 1cm steps. The neutron flux distribution at each distance from the source was calculated using ANISN, with 100 energy groups between thermal energies and 14 MeV. The probability of inelastic scattering from a particular nuclear level for each neutron energy group was calculated using data obtained from ENDF/B-IV. The experimental geometry was modelled exactly. The distances from the gamma production site to the detector were calculated and the attenuation of gammas of a particular energy through the sample and shielding explicitly taken into account.

The neutron energy distribution is spatially dependent, becoming progressively softer away from the 14 MeV source. Figure 6 shows the predicted flux distributions at 4 different radii for neutron energies above 0.1 MeV for a coal sample. The progressive decrease in flux density at increasing radii and the softening of the spectrum shows coal to be an extremely efficient moderating material. It was found that for the 4 coals investigated, the neutron flux distribution at  $E_n > \sim 1$  MeV (i.e. all neutrons energies of interest for  $(n,n'\gamma)$  reactions) is the same to within  $\pm 5\%$ . The effect of widely different hydrogen concentrations was investigated by reducing the hydrogen number density by a factor of 1.5. Although the 14 MeV contribution is increased there is a reduction in the lower energy contribution and hence only small changes in  $(n,n'\gamma)$  response will be observed. However, changes in material composition have a much greater effect on the thermal flux distribution. Figure 7 shows the predicted thermal flux distributions for coals with 5.5% and 3.7% hydrogen concentrations. Even larger effects can be induced by the presence of nuclei with significant thermal capture cross sections (neutron poisons),

of which Cl, B and Gd are good examples having cross section of 33.2, 752 and 39,100 barns respectively. Also in Figure 7 is shown the effect of adding 10,000 ppm and 100,000 ppm of chlorine. In each case the fast flux distribution is not significantly changed. These effects mean that any correlation of results from capture and scatter must take into account the presence of neutron poisons and the hydrogen content.

## DISCUSSION

The easiest approach to elemental analysis is simply to correlate the intensity of a given gamma-ray arising from the element of interest with the elemental concentration (given typically by chemical analysis). An example is shown in Figure 4, for the case of sulphur, but the presence of "neutron poisons" (elements with high thermal neutron capture cross-sections) within the material of interest will influence such a correlation. This is illustrated by a depression in the count rate for coal B that has a comparatively large chlorine content (~ 0.55% by weight). Using the transport code ANISN the influence of varying chlorine concentrations upon count rate into the sulphur peak was determined and is shown in Figure 8. The count rate into the sulphur peak decreases significantly for chlorine concentrations above about 0.1% (by weight).

An alternative approach to multi-element analysis has been given by Wormald and Clayton (5). The suggestion has been made that gamma-rays arising from  $(n, \gamma)$  reactions upon elements of interest can be linked quantitatively to gamma-rays arising from  $(n, n' \gamma)$  reactions. This linking is through the measured gamma-ray responses from those elements that undergo both reactions, e.g. silicon. Thus, the oxygen concentration of a given material can be determined by measuring the 6.129 MeV gamma-ray response arising from the  $(n, n' \gamma)$  reaction and linking this with the  $(n, \gamma)$  gamma-ray responses from elements such as H, C, Si, Al, Cl etc.

(oxygen having a negligible capture cross-section). However, this analysis is subject to potential errors (at least for a steady state flux of fast neutrons). The thermal flux is very sensitive to the material composition, i.e. hydrogen content and the presence of strongly absorbing nuclei. However, it has been shown that above about 1 MeV the fast neutron flux distributions for the 4 coal samples investigated here are the same to within  $\pm 5\%$ . Hence, the simple analytical model outlined is sensitive to material composition.

The preceding discussion highlights some problems that will be encountered using 14 MeV neutron sources and high resolution detectors in logging tools. Pulsing of the neutron source enables contributions from the  $(n, \gamma)$  and  $(n, n' \gamma)$  reactions to be more easily distinguished and gamma-rays arising from activation reactions to be measured. However, a more accurate determination of the characteristic gamma-rays of interest does not in itself entail a more accurate measurement of elemental concentrations. The problems discussed concerning the sensitivity of the thermal neutron flux to material composition need to be addressed. This problem can be investigated by monitoring characteristic gamma-ray emissions from strongly absorbing nuclei, and using models of the effects upon the thermal neutron flux to determine the influence upon the measured elemental concentrations. However, even if a reliable elemental description is available, the problem then remains of extracting useful petrophysical or geochemical information.

## CONCLUSIONS

It has been shown that energetic neutron bombardment of bulk material can give measurable gamma-ray responses from a variety of elements of interest. However, even if the gamma-rays are easily resolved and the intensities can be determined with confidence (by using solid

state detectors) the problem remains of correlating a gamma-ray intensity with an elemental concentration. Simple interpretational models assume that the energy variation in the neutron flux within the sample is insensitive to material composition. This is not the case for the thermal neutron flux component of the neutron energy distribution within the material. Hence, a more careful analysis of the spatial and energy variation of the neutron flux within bulk samples is required as a function of changing material composition.

#### REFERENCES

1. R.B. Culver, E.C. Hopkinson and A.H. Youmans, J. Petr. Technol. 14 (1974) 463.
2. R.C. Hertzog, SPE of AIME, SPE 7430 (1978).
3. F.E. Senftle, A.B. Tanner, P.W. Philbin, G.R. Boynton and C.W. Schram, Mining Engineering (AIME) 30 (1978) 666.
4. J.L. Mikesell, D.W. Dotson, F.E. Senftle, R.S. Zych, J. Kroger and L. Goldman, Nucl. Inst. Meth. 215 (1983) 561.
5. M.R. Wormald and C.G. Clayton, Int. J. App. Rad. Isot. 34 (1983) 71.
6. D.W. Mellor, Int. J. App. Rad. Isot 36 (1985) 295.
7. M.C. Underwood, Int. J. App. Rad. Isot in press.



# FAST NEUTRON INDUCED PROMPT $\gamma$ RAY ANALYSIS

S. Hlaváč and P. Obložinský

Institute of Physics EPRC SAS, 842 28 Bratislava  
CZECHOSLOVAKIA

Time and energy spectra of  $\gamma$  rays emitted after interaction of 14.6 MeV neutrons in the bulk sample of concrete were observed. Time spectrum shows that most of the  $\gamma$  rays of interest for prompt  $\gamma$  ray analysis are emitted within 20 ns after neutron hits the sample. In the  $\gamma$  ray energy spectrum measured in this time window all major components of the sample were identified.

In recent years there was a growing interest in employing neutron induced  $\gamma$  rays for analytical purposes in geosciences<sup>1)</sup>. Pulsed 14 MeV neutron generators with high resolution  $\gamma$  spectrometers are used for this purposes. Apart from neutron capture  $\gamma$  rays, measured in delayed time windows, attempts were made to use also prompt  $\gamma$  rays from  $(n, x\gamma)$  reactions. These were measured in coincidence with neutron pulse, typically of some 10  $\mu$ s width.

Sensitivity figures of  $(n, x\gamma)$  reactions for a number of common elements are comparable or even higher than for neutron capture, the most prominent examples being carbon and oxygen<sup>2)</sup>.

Contrary to the advantageous sensitivity figures, the prompt  $\gamma$  ray analysis is plagued with difficulties, mainly due to low signal/background ratio. This is nicely demonstrated for example by prompt and delayed spectra in ref.<sup>3)</sup>.

To analyze possible reasons, we measured  $\gamma$  ray spectra from a bulk sample - concrete wall of our laboratory. We utilized slightly modified system, based on the time-correlated associated particle method<sup>4)</sup>, outlined in fig. 1.

The time spectrum measured with the  $\gamma$  detector versus the associated  $\alpha$  particle detector should give insight into the nature of neutron interaction with bulk media. The spectrum is influenced by the finite neutron velocity, complexity of the neutron - nucleus interaction and the neutron as well as  $\gamma$  ray absorption. However, with relatively poor time resolution of the Ge(Li) detector ( $\sim 10$  ns) we were not able to distinguish between the influence of the large sample and the instrumental

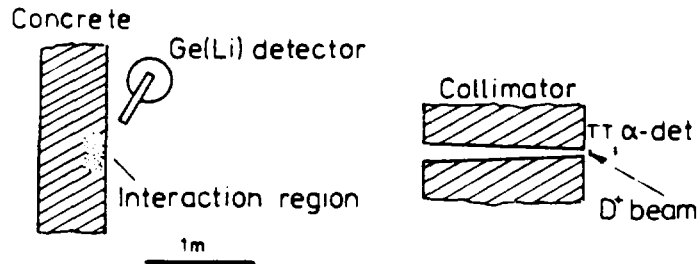


Fig. 1. Simplified drawing of the experimental arrangement. In the time studies the Ge(Li) detector was replaced by the fast scintillation counter.

effects. Therefore, we used fast scintillation detector NE213, equipped with XP2041 photomultiplier and neutron/gamma pulse shape discrimination to study the structure of the time spectrum.

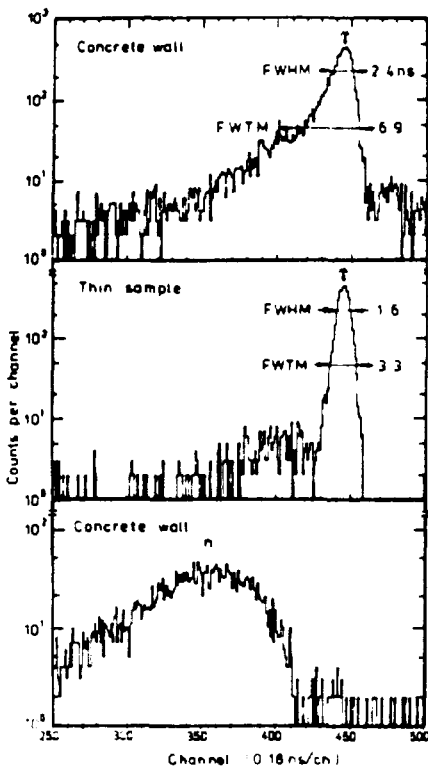


Fig. 2. Time spectra of  $\gamma$  rays and neutrons emitted from the concrete wall and the thin sample.

The time spectrum of  $\gamma$  rays originating in the neutron interactions in the concrete wall is given in fig. 2. Shown for comparison is the time resolution function as measured with a thin sample as well as the time spectrum of neutrons backscattered from the concrete wall. Majority of  $\gamma$  rays from the concrete wall are emitted in a very narrow time interval, giving rise to the prompt  $\gamma$  peak. FWHM and FWTM of this peak are 2.4 and 6.9 ns, respectively. They are significantly higher than the corresponding figures 1.6 and 3.3 ns, respectively, observed in the thin sample time spectrum. Shape of the neutron time spectrum indicates negligible contribution of neutrons to the prompt  $\gamma$  ray peak.

Increased width of the prompt  $\gamma$  ray peak observed in the concrete wall spectrum is caused mainly by changed slope of its left-hand side. This proves that some of the  $\gamma$  rays are emitted later in time, i. e., from greater depth. Rough estimate of the characteristic emission time made from the tail leads to value 2 - 4.5 ns. These figures together with the velocity of 14.6 MeV neutrons (18.9 ns/m) sug-

gest, that detected  $\gamma$  rays are emitted effectively from material depth up to 0.11 - 0.25 m.  $\gamma$  rays originating from greater depths are practically lost because of too small solid angle and tremendous selfabsorption.

The prompt  $\gamma$  peak is superimposed on essentially flat random background. Slow exponential decay observed in the delayed (n, $\gamma$ ) spectroscopy is not visible here because of very short time interval covered (45 ns). Total width of the  $\gamma$  ray peak is  $\sim 20$  ns. In this time interval practically all of the prompt  $\gamma$  rays of interest for analytical purposes are emitted.

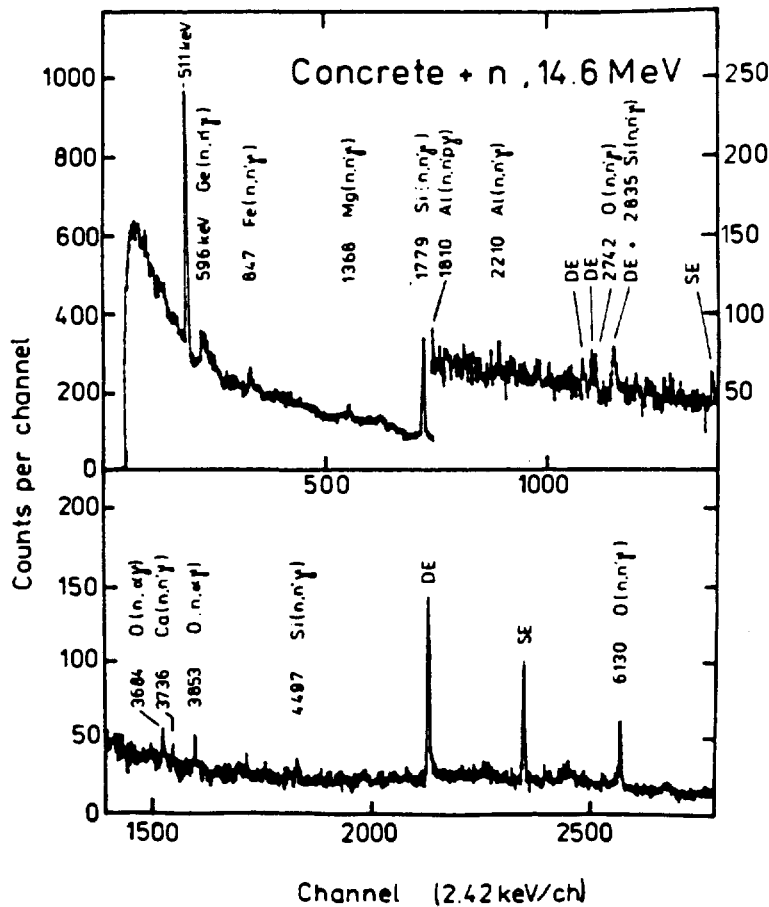


Fig. 3. Energy spectrum of  $\gamma$  rays observed by the Ge(Li) spectrometer within prompt time window ( $\sim 20$  ns)

Later on, essentially background  $\gamma$  rays from different sources are detected. Significantly improved signal/background ratio in the  $\gamma$  ray energy spectrum can be therefore achieved using prompt time window of the comparable width.

Energy spectrum of  $\gamma$  rays observed with the 70 cm<sup>3</sup> Ge(Li) spectrometer in the prompt time window ( $\sim 20$  ns) is given in fig. 3. Total number of neutrons incident on the concrete wall

was intentionally kept rather low  $\sim 5 \cdot 10^9$ . The spectrum shows prominent peaks of all major concrete components (H 6.8%, O 57.7%, Mg 3.2%, Al 4.7%, Si 16.1%, Ca 6.8%, and Fe 2.7%)<sup>5)</sup>, except of hydrogen. Most prominent lines are 6 130 keV of  $^{16}\text{O}$  and 1779 keV of  $^{28}\text{Si}$ .

Prompt  $\gamma$  ray spectrum, measured in the true prompt time window improves substantially signal/background ratio and allows for more accurate analytical conclusions.

#### References

- 1) Proc. of the IAEA consultants' meeting on nuclear data for bore-hole and bulk-media assay, Krakow 1983, INDC(NDS)-151/L, IAEA Vienna 1984.
- 2) P. Obložinský, S. Hlaváč, Discrete  $\gamma$  ray production in  $(n, x\gamma)$  reactions for applied nuclear geophysics, Invited talk at the IAEA consultants' meeting on nuclear data for applied nuclear geophysics, Vienna 1986.
- 3) L. G. Evans et al., Determination of elemental composition of geochemical exploration using a 14 MeV neutron generator, IEEE Trans. Nucl. Sci. NS-28(1981) 1626.
- 4) S. Hlaváč, P. Obložinský, Multidetector setup for  $(n, xn\gamma)$  studies at 14 MeV, Nucl. Instr. Meth. 206 (1983) 127.
- 5) L. L. Carter et al., Nuclear data relevant to shield design of FMIT facility, Proc. Symp. on neutron cross-sections from 10 to 50 MeV, BNL-NCS-51245, Vol.II, page 431, BNL July 1980.

# SHORT TIME ACTIVATION ANALYSIS IN GEOSCIENCE

F.Grass, G.P.Westphal, T.Kasa

Atominstitut der Österreichischen Universitäten, Schüttelstraße 115

A-1020 Wien, Austria

## ABSTRACT

In short time activation analysis elements having nuclides with half lives down to the subsecond range are analyzed measuring their gamma spectra or the decay curves, applying in addition to a Ge(Li) or an HP-Ge detector a Cerenkov and/or a neutron counter. To meet the demands for quantitative pulse height analysis with rapidly varying count rates and spectra, a real time correction of counting losses was unavoidable. The principles of the "Loss Free Counting System" in the virtual pulse generator version are presented. Tests for the stability of count rates down from 780 kc/s were made by the two source method, showing that the method is in perfect statistical control. For the main elements of geochemical applications, sensitivities obtained with a prototype system are listed. The Table gives the total activities obtained with our system for activation analysis with short lived nuclides up to 20 s half life. Application in phosphorite analysis by  $\gamma$ -spectrum- and decay curve analysis as well as to analysis of NBS 1648 urban particulates by pulse activation demonstrate the usefulness of the method.

## INTRODUCTION

With the aid of activity-, gamma- and neutron logging systems, geochemical insitu analyses will provide a more detailed knowledge of rock mineralogy in geological formations. Especially, the use of high resolution gamma spectroscopy of neutron induced activities in multielement analysis delivers data on a number of elemental concentrations in the well.

Neutron logs are usually obtained from ( $\alpha, n$ )- or Cf-252-sources, both of which have a rather low neutron intensity of  $>1E8/s$  (Hertzog 1985). Only very recently the preparation of a 50 mg Cf-252 source was announced (Bigelow 1987).

In the last decade neutron sources depending on the D,T-reaction have been introduced. They constitute highly intensive sources of 14 MeV neutrons (see e.g. Pepelnik 1986) which are moderated down to thermal neutron energies depending on the moderation properties of the surrounding.

For the evaluation of the measured data it is necessary to know the spatial- and energy dependence of the neutron flux and the energy dependence of the cross section for the respective elements. These subjects will be discussed in more detail in this volume by other authors. The findings are very promising for the in situ analyses in well logging.

Moreover conventional neutron activation analysis is already widely used in main, minor and trace element analysis in the geosciences. Many problems have been solved by this method and its usefulness is convincingly demonstrated by the analysis of extra-terrestrial matter, e.g. moon samples and meteorites. Likewise a number of problems in geoscience have been solved by studying rare earth distributions in various minerals and brines to demonstrate processes in the course of geological evolution (Haskin 1966 and Stosch 1986).

One major disadvantage of conventional neutron activation analysis, however, is the long delay between the arrival of the sample and the obtaining of results, largely due to the long half lives of many commonly applied nuclides. As some of the latter elements also have shorter lived nuclides or isomeric states, we studied their applicability with a view to increasing the rate of analysis. In the past, large efforts were undertaken at various laboratories e.g. General Atomic, University of California Irvine, Reactor Center London University, Riso National Laboratory, Texas A.M. University, our Institute and many others, to extend the useful range of half lives for activation analysis down to the second and the subsecond range.

At a meeting at the International Atomic Energy Agency in Vienna 1986, it was suggested that nuclides or isomeric states with half lives of less than 1 minute be termed short lived. From a more pragmatic point of view, we prefer the term Short Time Activation Analysis to Activation Analysis with Short Lived Nuclides because a number of elements may be determined by a short neutron activation though the nuclides produced in the activation process have half lives up to the day range because they have large cross sections, as in the analysis of rare earth minerals by Grass 1986.

Activation analysis using subsecond nuclides is only possible if extremely high countrates can be handled, as the information is condensed in the short time interval of a few half lives. Moreover, the countrates and the spectral distribution change rapidly, so that corrections have to be made in real time. These problems are accumulated if activation is performed with a reactor pulse where the flux is drastically enhanced, in our TRIGA Mark II reactor up to 1200 fold.

Thus nuclides activated with a short irradiation may give valuable information in well logging provided intensive neutron sources are available, preferably pulsed 14 MeV sources as short activation favours the shorter lived nuclides in the subsecond range. A time dependent registration would then provide maximal information on prompt and delayed activities.

In the following we will describe only work performed in our institute.

## EXPERIMENTAL

The experimental setup and data processing in our Fast Irradiation and Measurement System (FIMS) are shown schematically in Fig. 1a.

The fast irradiation system was originally described in Brandstädter 1972. We use a 14% Ge(Li) detector coaxially drifted with a basis resolution of 2.8 keV and a liquid nitrogen container surrounded by a rubberfoam sound shield to suppress the sound waves accompanying expulsion which would disturb the measurements by a microphonic noise. Next follows the preamplifier modified by Westphal 1977 for high rate operation by using an additional circuit which prevents the preamplifier from leaving its dynamic range. A fast and a slow signal are fed into the LFC-System in the virtual pulse generator version (see below) which delivers the original and the deadtime and pile-up corrected signals. These are fed into a Direct Memory Access Processor designed and constructed by Popp 1981 or, alternatively, into a  $\mu$ -processor based multichannel analyzer system (Westphal 1984). The DMA-Processor enables registration of the original and the corrected  $\gamma$ -spectrum together with 4 time channels for multiscaling operations. Two of them are used to register the total count rate of the corrected and the uncorrected  $\gamma$ -spectrum. Instead of the latter, the analysis of fissionable material may be carried out by a neutron counter. The third time channel enables the Cerenkov counting of

# FAST IRRADIATION AND MEASUREMENT SYSTEM

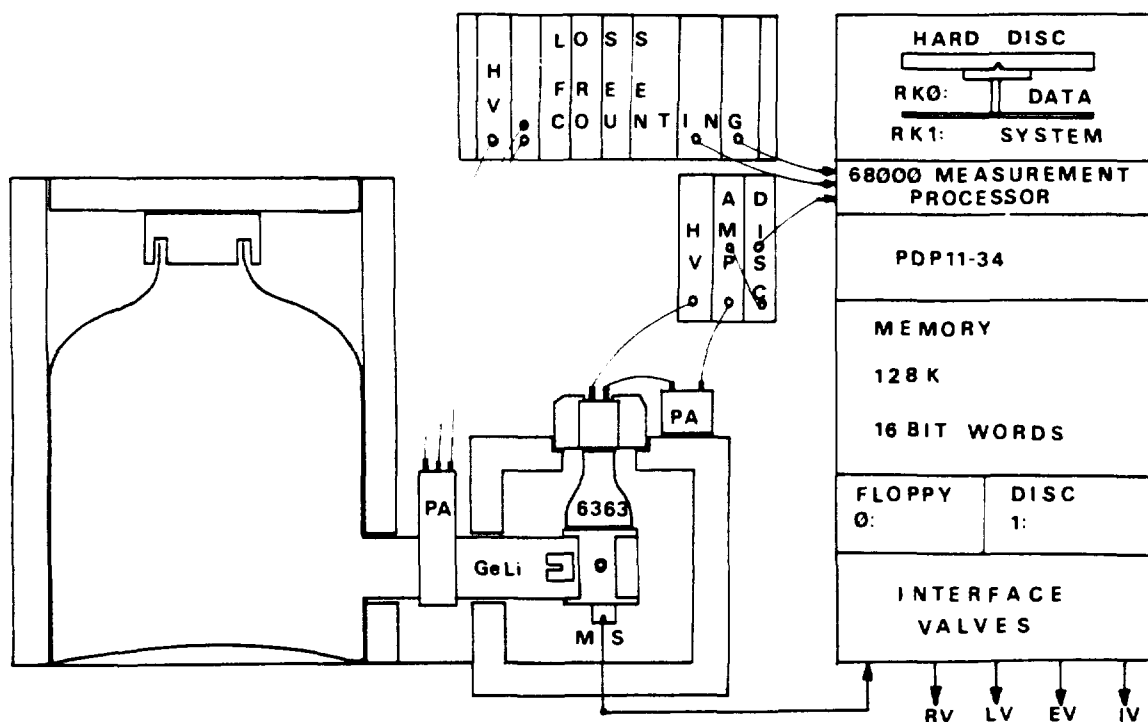


Fig. 1 HV high voltage  
 AMP amplifier  
 DIS discriminator  
 PA preamplifier  
 MS micro switch  
 RV release valve  
 LV loading valve  
 EV ejection valve  
 IV injection valve

hard  $\beta$ -emitters e.g. B-12 or Li-8. The fourth time channel is used as counter for the pulse operation. Fig. 2 shows the construction of the sample catcher in detail. The main part of the sample catcher is constructed from plexiglass which acts as Cerenkov radiator. A light proof lead shielding case is used to protect the RCA 6363 photomultiplier tube from damage by light. Irradiated polythylene emits light, a phenomenon which Nikolski 1971 calls radiothermoluminescence. So the slightly conically shaped slowing down pipe (details see Fig. 2.4), fabricated from plexiglass, which discriminates the weaker  $\beta$ -rays by absorption in about  $470 \text{ mg/cm}^2$ , was blackened on the outside to prevent direct light from reaching the photomultiplier so that only hard  $\beta$ -emitters penetrating the slowing down pipe produce the Cerenkov radiation.

As an alternative, we have recently been using an electronic system consisting of a gated integrator with a semigaussian amplifier-prefilter (Fig.2). On the one hand, this combination prevents the deterioration of the resolution caused by the ballistic losses of the gauss filter and the

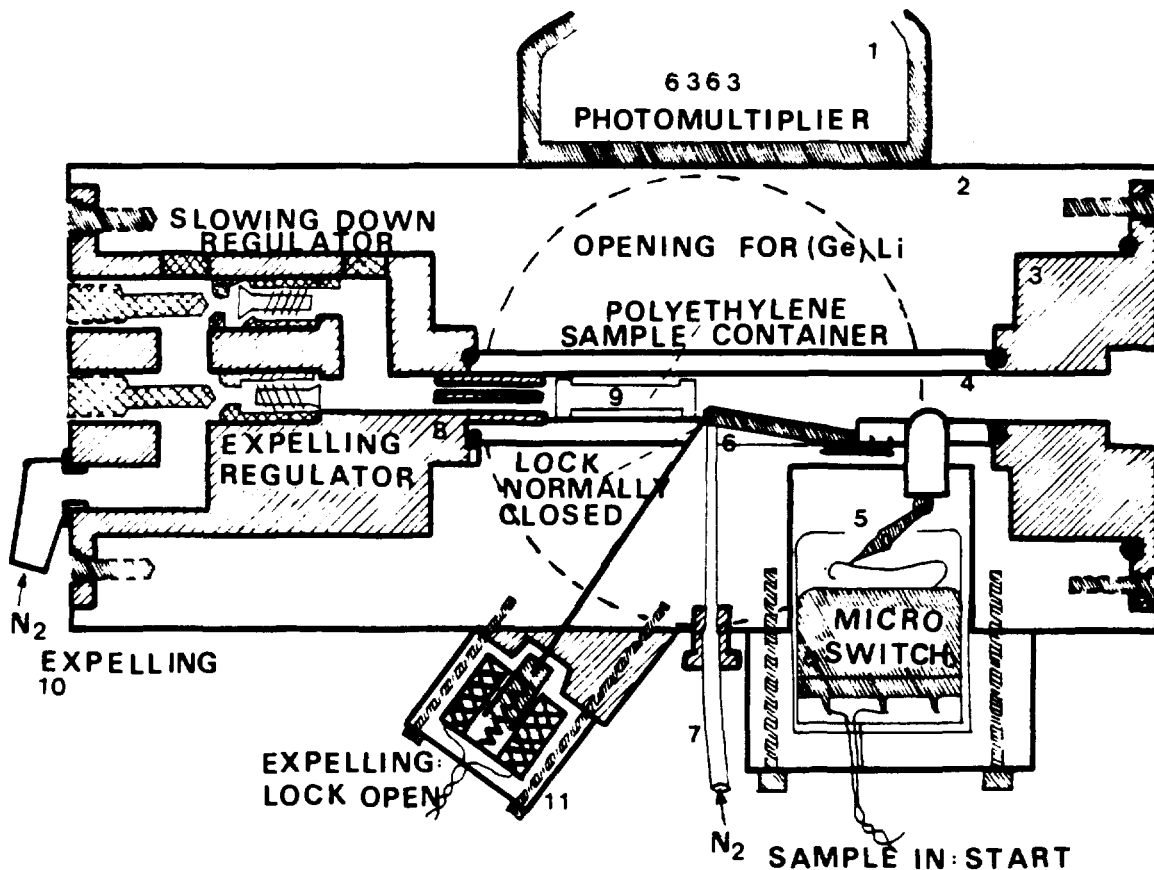


Fig. 1b: Sample catching device and Cerenkov-counter

- 1) Photomultiplier RCA 6363, optical contact with high viscosity silicone grease
- 2) Cerenkov radiator, plexiglass
- 3) Pipe connector, brass with O-ring seal
- 4) Slighters conically shaped slowing down pipe, plexiglass blackened on the outside
- 5) Micro switch trigger system
- 6) Spring loaded lock for arresting the sample, opened magnetically in the expelling phase only
- 7) Nitrogen inlet for sample slow down
- 8) Unit (brass) containing slowing down- and expelling regulator with O-ring seals
- 9) Sample container in measuring position
- 10) Nitrogen expelling inlet
- 11) Electromagnetically operated spring loaded catching lock

scatter of the charge collecting time in a detector of large volume and on the other hand minimizes the influence of pulse overlapping at high countrates, as the pulse shaping time is short. The best detectors for this purpose are n-type HP-Ge detectors. The preamplifier works with a FET included in the cooled part of the detector. To enable a high charge throughput, the preamplifier is furnished with a resetting circuit, based on a proposal of Landis 1982. Data are fed via the LFC correction system

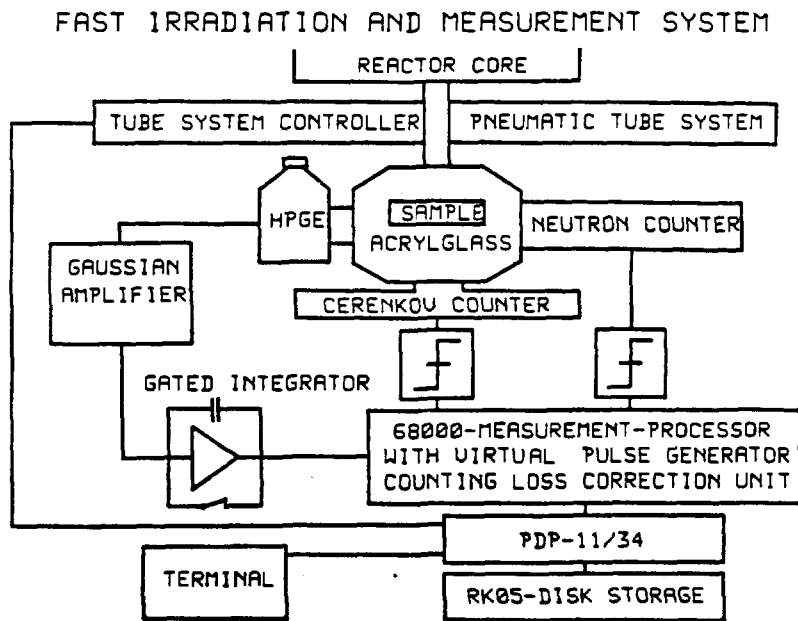


Fig. 2: Blockdiagramm of the microprocessor version of FIMS

in the virtual pulse generator version to a modified 68000  $\mu\text{P}$ , adapted as multichannel analyzer and double multiscaler (Westphal 1984).

The DMA-processor or the 68000  $\mu\text{P}$  in connection with the PDP 11/34 are used to store spectra and decay curves on the removable hard disc system RK0. To handle the irradiation system, an interface controls the four valves used in our fast transportation system (Brandstädter 1972). The programmes for valve control and data processing are stored on RK1.

The original construction of the sample catcher was changed to meet the requirements of higher reliability and allows measurements with three detectors simultaneously. The sample lock was spring loaded and therefore closed in the normal position as shown in Fig.2.6. The spring load was removed electromagnetically only for expelling the sample from the catching device. A sample could now only pass the catching lock when the expelling valve was activated leading the expelling nitrogen Fig. 2.10 in direction to the core. The stopping- and the expelling-force within the catching device are regulated by the respective regulator (a type of needle valve) which has to be carefully adjusted to maintain an exact transportation time and a proper stopping position. Measurement is started by triggering the microswitch.

The main advantage of our electronic measurement system over conventional setups is the "Loss Free Counting System in the Virtual Pulse Generator

Version". As the paper has only been published very recently, we shall outline the principles and verification of the deadtime correction with the decaying source method, referring the interested reader to the papers of Westphal.

#### PRINCIPLES OF THE "LOSS FREE COUNTING SYSTEM IN THE VIRTUAL PULSE GENERATOR VERSION"

In the course of work we invested to promote analysis with short lived nuclides, several real time corrections were developed at our institute (Westphal 1977 and 1979, Harms 1967). They all have in common that the channels which are addressed by the analog to digital converter are incremented by a variable integer weighting factor depending on the instant counting loss situation, instead of being incremented by one only, as in conventional multichannel analyzers. Westphal 1977 and 1979 introduced the LFC-method in which the weighting factors are derived by a real time processor from the true integral counting rate. The successive weighting factors are computed from the dead time and the counting rate of a discriminator set slightly above the noise level of the system. A further improvement was the introduction of the "Virtual Pulse Generator" version by Westphal 1981, which from a statistical point of view is completely equivalent to the classical pulse generator method without its drawbacks. By the latter method, a statistically relevant counting loss correction for rapidly changing spectra could only have been achieved by means of a test pulse generator frequency in the megacycle range resulting in a prohibitive increase in dead time. The "Virtual Pulse Generator Method" has no limit in test frequency as weighting factors are determined parallel to the analyzer system thus avoiding deadtime losses in the latter. The test frequency is only limited by the speed of the digital logic and well suited for real time corrections of rapidly changing spectra.

#### RESULTS

Fig. 3 shows the results of a reliability test with the decaying source method using the 1173 keV line of a fixed Co-60 source and the 90s Dy-165 m as the decaying source. The non-corrected and the loss corrected peak

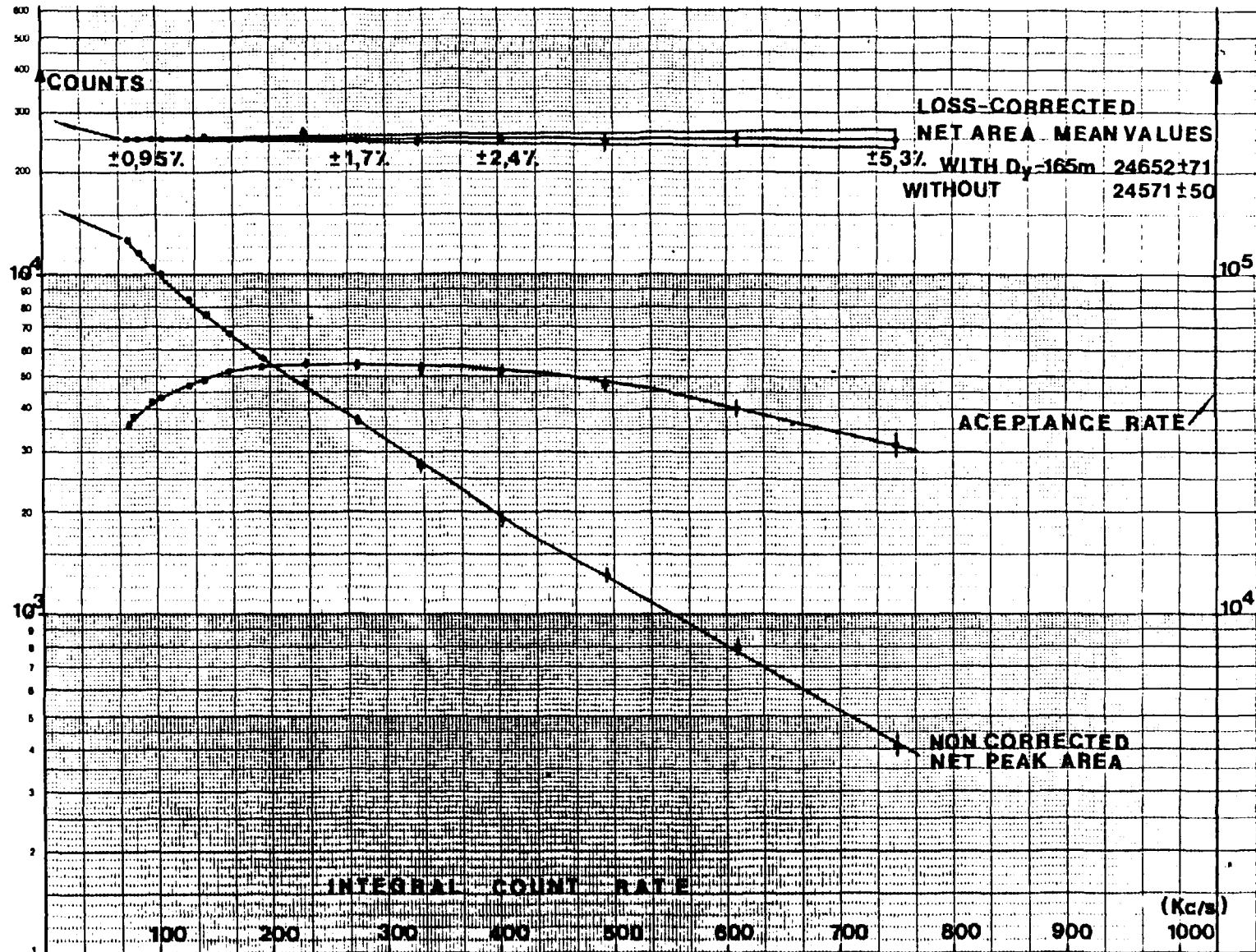


Fig. 3: High rate test of the LFC-system in the virtual pulse generator  
Version

Table 1: Preliminary total activities obtained with FIMS

Element	Nuclide	keV	t1/2 (s)	Activities cts/ $\mu\text{g}^{\dagger}$	EF*
As	75 m	279	0.016	3E-2	700
Na	24 m	472	0.020	1.66	640
Ge	71 m	175	0.020	0.2	640
Ga	72 m	102	0.039	0.14	460
Yb	175 m	514	0.068	18.4	320
Ba	136 m	164	0.308	4E-2	76
Ge	73 m	54	0.530	3.2	46
Cl	38 m	671	0.740	2.0	33
Pb	207 m	570	0.800	0.15	30
In	116 m <sup>2</sup>	164	2.2	12.1E3	11
Er	167 m	208	2.3	470	10
Hf	178 m	213	4.3	9.7E3	5.7
Br	79 m	207	4.8	32.4	5
Yb	177 m	150	6.4	8.8E3	3.8
F	20	1633	11	13.5	2.3
Y	89 m	909	15.7	64	1.6
Se	77 m	162	17.5	4.9E3	1.5
Sc	46 m	143	18.7	88.2E3	1.4
Hf	179 m	215	18.7	38.8E3	1.4
B	12	§	0.02	0.4	640
Li	8	§	0.840	950	26

<sup>†</sup>Total activities = activated to saturation, decay of 20 ms, 10 t1/2 measured with a 14% coaxially drifted Ge(Li) detector (distance between sample and detector window 22 mm, 20 mm of which are acrylic glass), activated at a flux of 1.3E12/cm<sup>2</sup>s and a Cd-ratio of 12 at 250 kW in steady state operation

\*Enhancement factor by pulse activation at 300 MW peak power and 28 ms FWHM

§beta 13 MeV

areas of the Co-60 line (left scale) and the acceptance rate (right scale) are plotted versus integral countrate. Mean values of the 1173 keV, 24652  $\pm$  71 cts and 24571  $\pm$  60 cts, obtained with and without the Dy-165 m activity, respectively, are in perfect statistical control. The error increases towards higher integral countrates as it depends on the non-corrected peak area. The optimum of the acceptance rate of the setup in Fig. 1 is at 250 kc/s.

The total activities and the enhancement factors calculated from the experimental results obtained with FIMS are listed in Table 1, measuring the nuclides with a 14% coaxially drifted Ge(Li) detector at a sample-to-

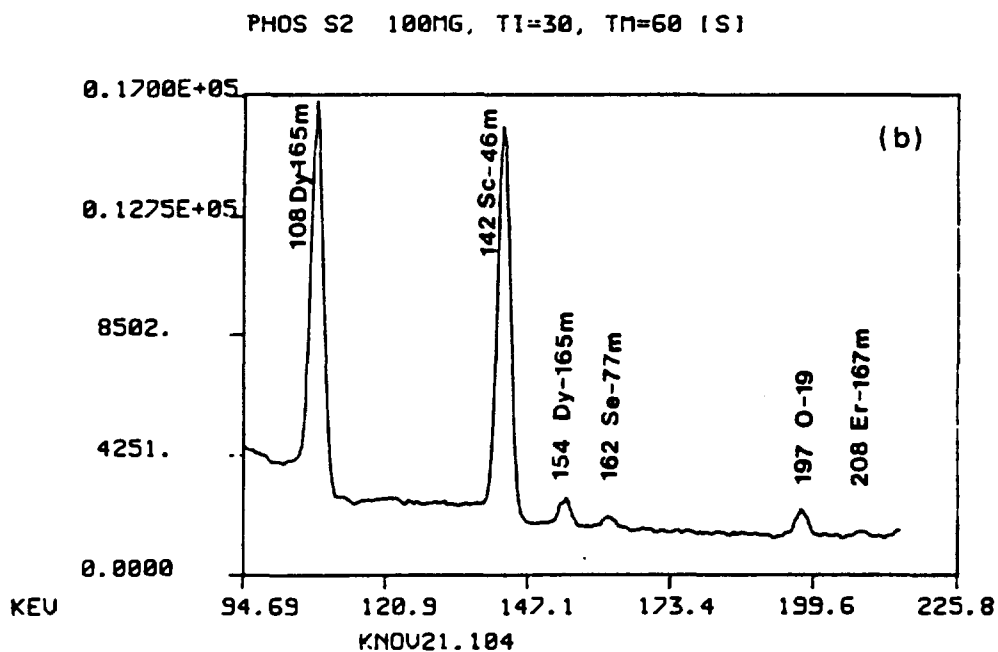
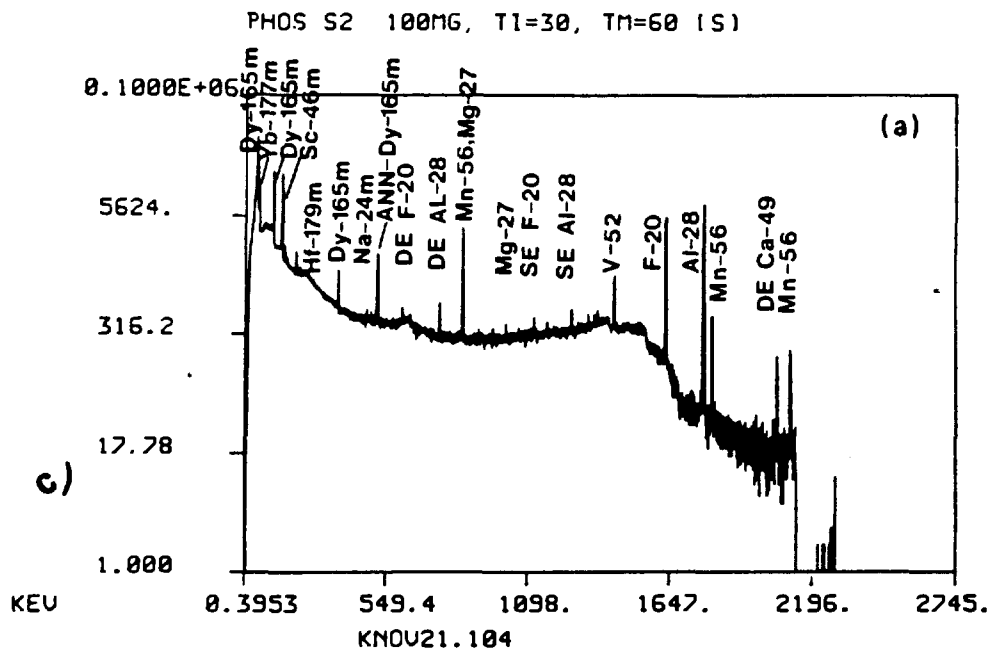


Fig. 4: Gamma spectra of a 100 mg phosphorite sample obtained after steady state activation,  $T_i = 30s$ ,  $T_m = 60s$   
 a) total range    b) 150 keV range

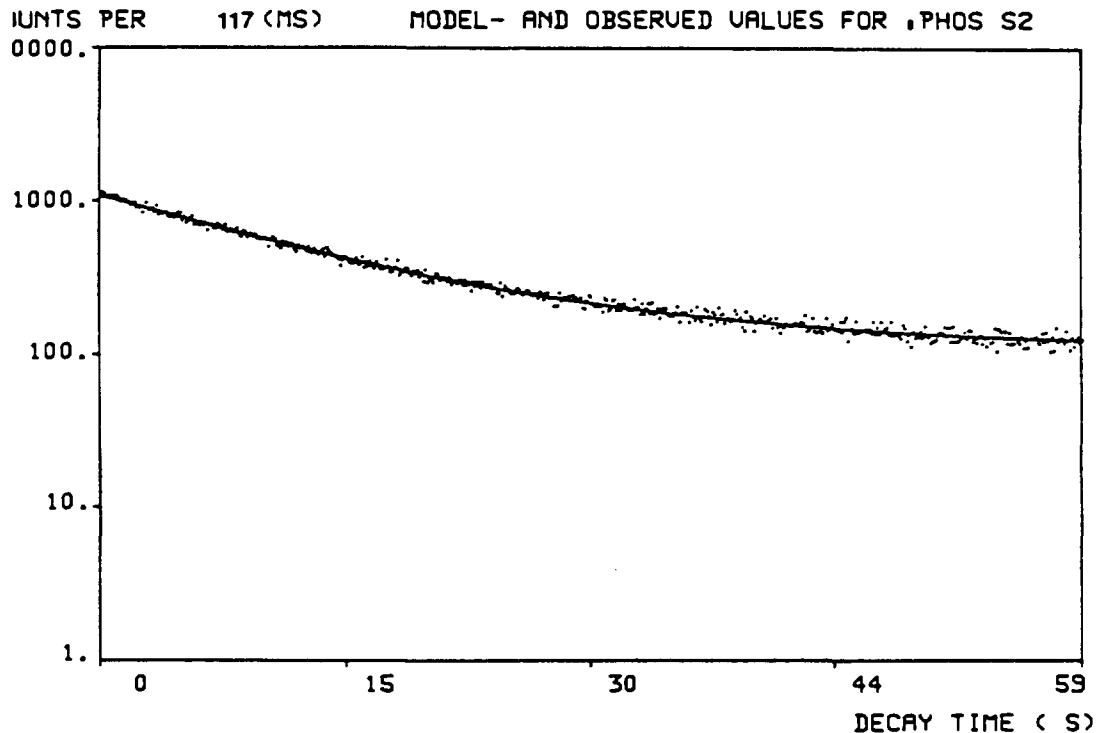
detector-window distance of 22 mm, 20 mm of which were acrylic glass. The irradiation was performed in our TRIGA Mark II reactor operated at 250 kW at a neutron flux of  $1.3E12/cm^2s$  and a Cd ratio of 12. The enhancement factors EF refer to a gaussian shaped reactor pulse of 300 MW peak power and 28 ms full width at half maximum. Total activities data being available for nuclides with half lives longer than 20 s, only nuclides with shorter half lives are listed in this table.

A recent application of FIMS in geosciences is the analysis of a phosphorite sample from Egypt (Saad El Din 1987). Fig. 4a demonstrates how rapidly the results may be obtained, using short time activation analysis with an irradiation time of 30 s and a counting time of 60 s. Fig. 4b shows a detail of this spectrum in the region of 150 keV, where Se-77 m and Er-167 m are semiquantitatively detected. To determine these elements the summing up of 10 spectra or pulse activation would yield more accurate data.

A decay curve analysis of the measurement of the same phosphorite sample with our Cerenkov counter using the RINAA programs (Schmidt 1983) is seen in Fig. 5a-d. In Fig. 5a the observed data and their least square fit with the half lives blank = infinite, N-16 7.13 s and F-20 11.3 s are shown. The quality of the fit is assured by Figs. 5b-d where in 5b the residuals between measured and calculated data are plotted versus the decay time. In this representation a summation of the deviation is introduced, which should show an ideal standard normal distribution. The  $\pm 2$  sigma lines should cover 95% of the data. Fig. 5c and d represent quantil-quantil grafics which compare the residuals found with a normal- or chi squared distribution, respectively. The grafics include the Komolgorof-Smirnov test band that allows a quick decision whether the assumed distribution is accepted or not.

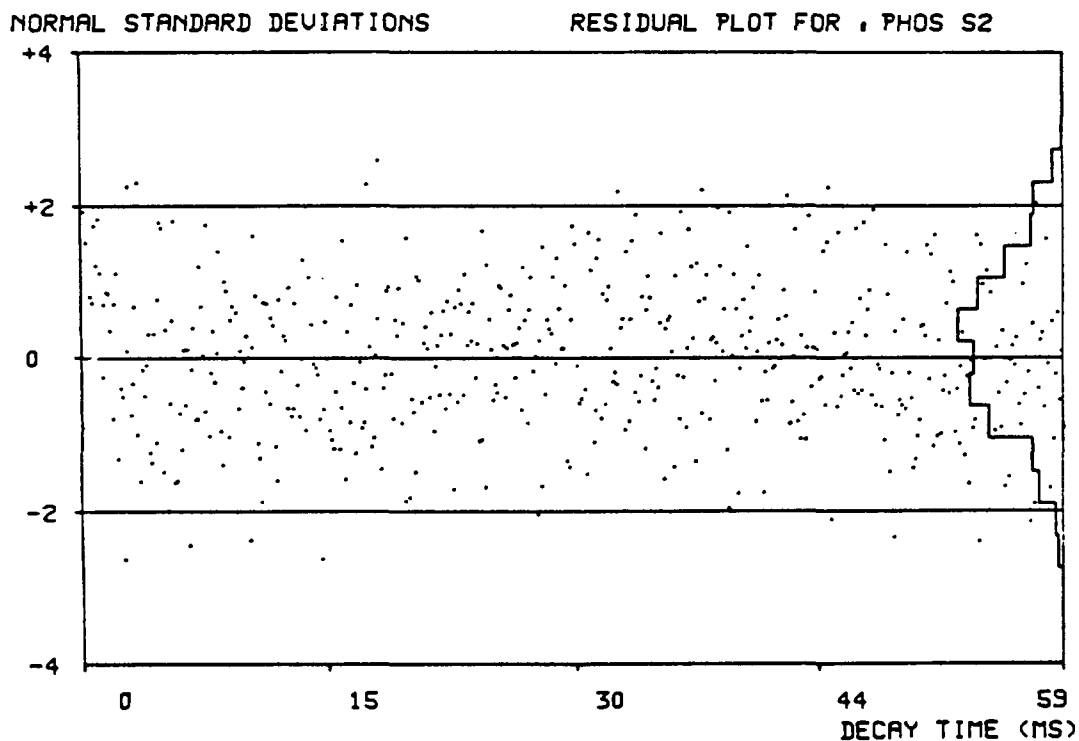
By means of these programs it is possible to compare data obtained from gamma spectra with those from decay curve analysis.

Pulse activation with progressively prolonged measuring times collects the entire information available in short time activation analysis as seen from Fig. 6. Three spectra of a 15 mg sample of NBS 1648 urban particulates were obtained after activation with a 140 MW pulse measuring 2, 20 and 200 s. This enables the measurement of the nuclides with subsecond and second half lives in the 2 s measurement, while the nuclides with half lives in the 20 s range are best measured in the next spectrum and the nuclides with minute half lives are determined favourably in the 200 s measurement.



SPECTRUM , MNOU19.127 NUMBER OF OBSERVATIONS = 496

- a) least square fit of the observed data with the half-lives  
 blank = infinite, N-16 = 7.13s, F-20 = 11.3s

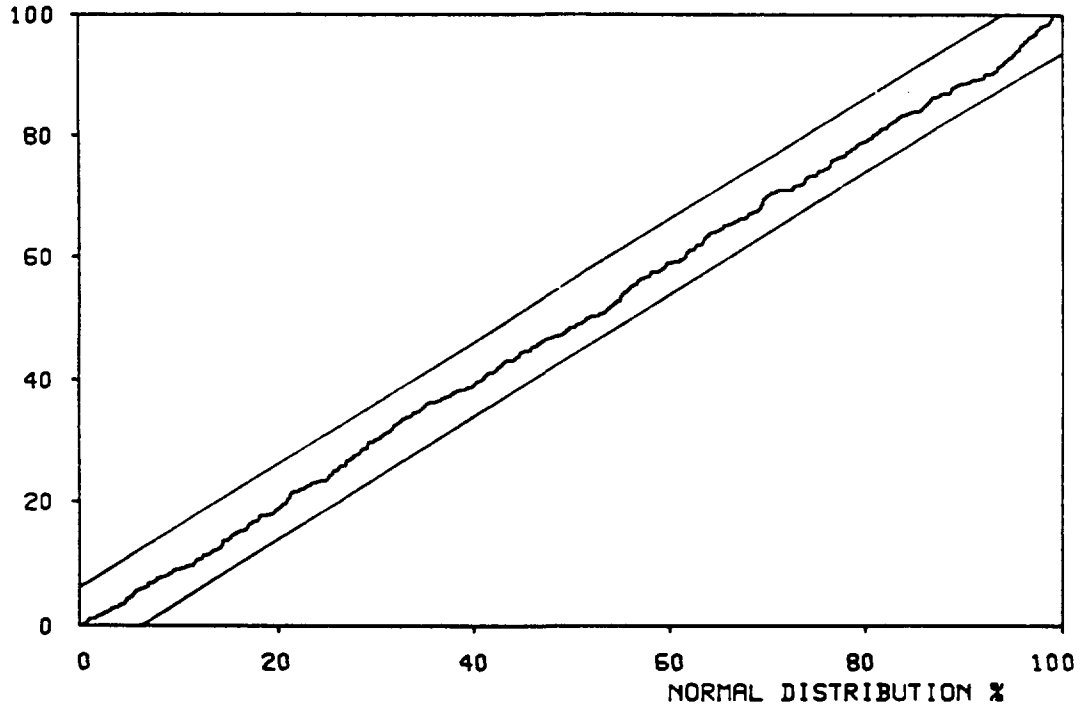


SPECTRUM , MNOU19.127 NUMBER OF OBSERVATIONS = 496

- b) Residual Plot (difference between calculated and observed data) versus decay-time

Fig. 5: Decay curve analysis of phosphorite data obtained by the Cerenkov counter; conditions as in Fig. 4 evaluated by RINNA (Schmidt 1983)

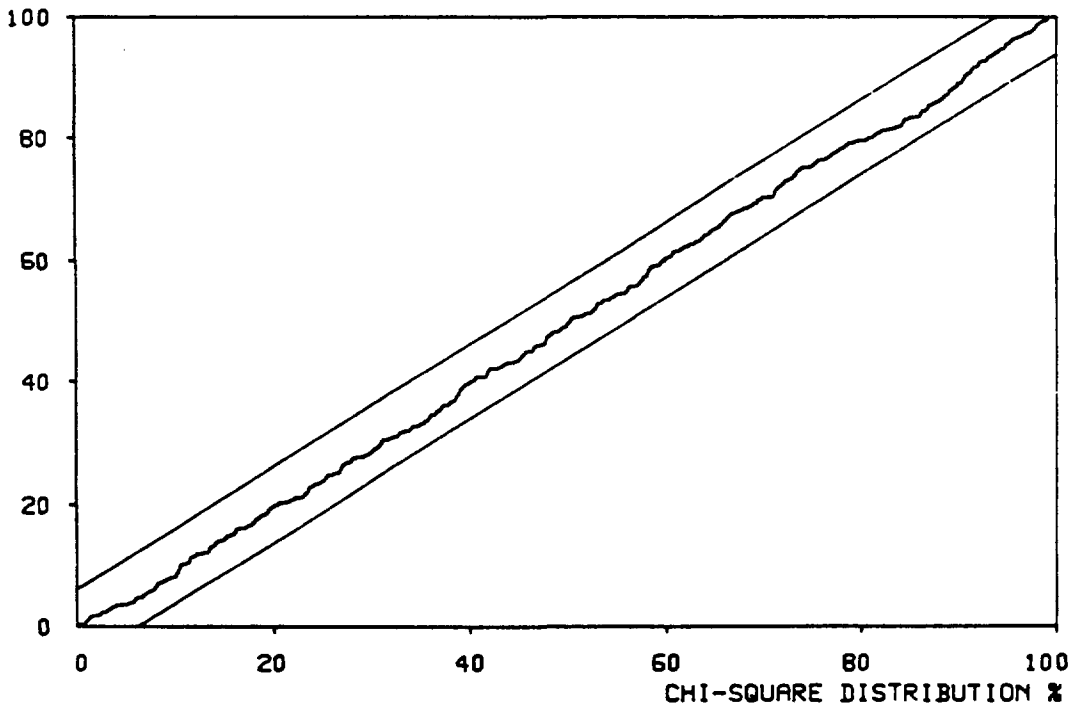
EMPIRICAL DISTRIBUTION % QUANTILE-QUANTILE PLOT FOR , PHOS S2



SPECTRUM, MNOU19.127 NUMBER OF OBSERVATIONS = 496.

c) Quantil-quantil plot: Distribution of the residuals versus normal distribution

EMPIRICAL DISTRIBUTION % QUANTILE-QUANTILE PLOT FOR , PHOS S2



SPECTRUM, MNOU19.127 NUMBER OF OBSERVATIONS = 496

d) Quantil-quantil plot: Distribution of the residuals versus chi-squared distribution

The graphic c) and d) includes the Komolgorof-Smirnov test band

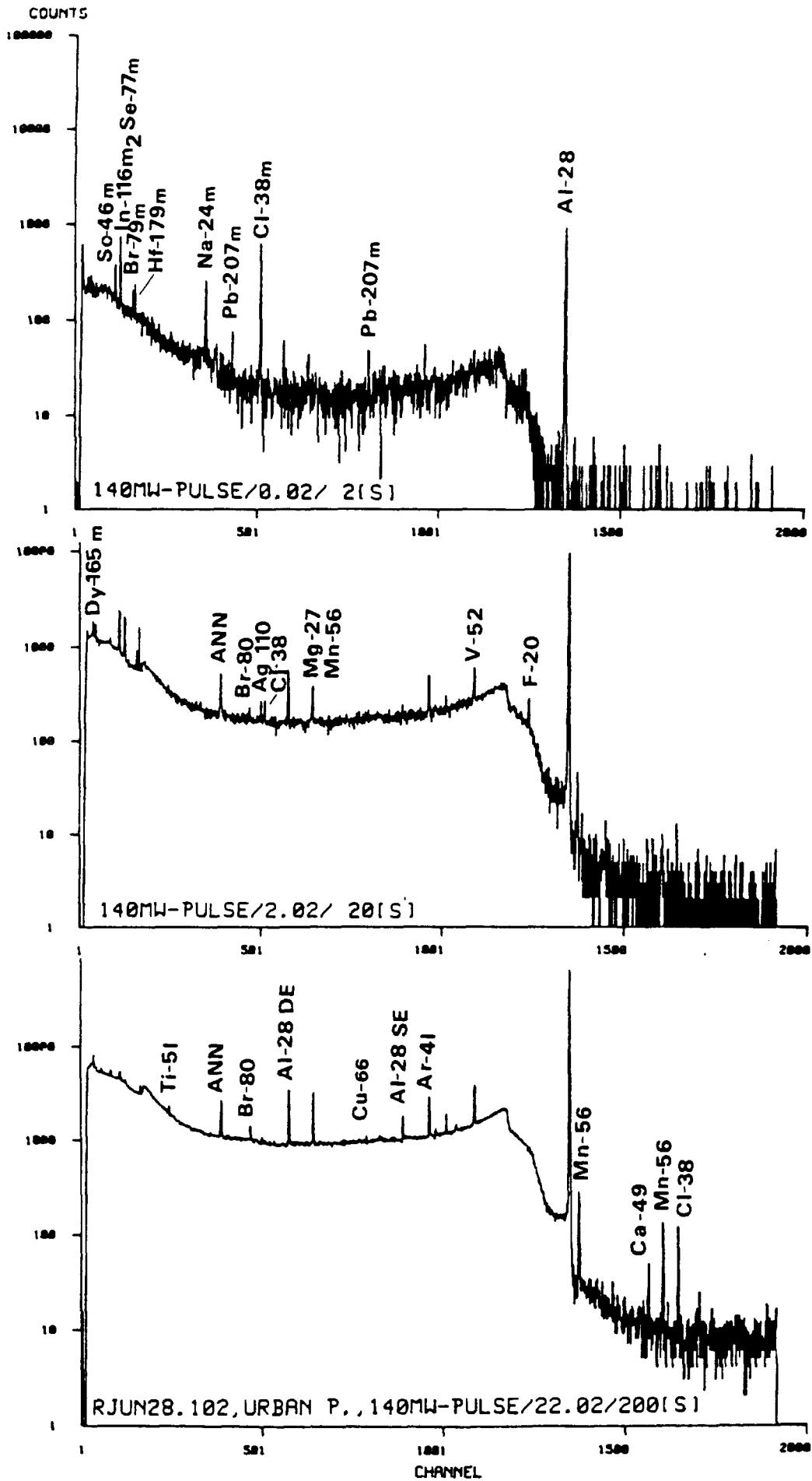


Fig. 6: Gamma spectra of a 15 mg NBS-1648 urban particulates sample after a 140 MW pulse activation,  $T_m = 2, 20$  and  $200$ s taken from Grass 1986

## CONCLUSION

The results discussed in this paper demonstrate the applicability of short time activation analysis to the analysis of a number of elements which are interesting in geosciences (Heron 1985), e.g. Na, Cl, Hf, Sc, besides the longer lived Ca, Al, Dy, Mg, Ti.

In in-situ analysis of geological structures, the information obtained through prompt and the usual delayed activities could be enhanced by means of short lived nuclides produced by using cyclic activation analysis with a large number of cycles together with intensive pulsed 14 MeV neutron sources, as suggested by Givens 1969.

## REFERENCES

- BRANDSTATTER 1972 O., GIRSIG F., GRASS F., KLENK R., Eine schnelle Transportautomatik zur Untersuchung kurzlebiger Kernzustände bis in den Millisekundenbereich, Nucl.Instr.Methods 104, 45
- GIVENS 1969 W.W., MILLS W.R.Jr., CALDWELL R.L., Cyclic Activation Analysis Modern Trends in Activation Analysis, US Dept. of Commerce, special publ. 312, Vol.2
- GRASS 1986 F., Short Time Activation Analysis with Steady State and Pulse Irradiation, 7th Internat.Conf.MTAA, Copenhagen, p.255
- HARMS 1967 J., Automatic Dead-Time Correction for Multichannel Pulse-Height Analyzers at Variable Counting Rates, Nucl.Instr.Methods 53, 192
- HASKIN 1966 L.A.R., FREY F.A., SCHMITT A., SMITH N., Researchers in Geochemistry, J.Wiley & Son Inc., 234-260
- HERRON 1986 M.M., Subsurface Geochemistry: I Future Applications of Geochemical Data, Research Note, Schlumberger-Doll Res, March 1986
- HERTZOG 1985 R.C., SORAN P.D., SCHWEITZER J.S., Application of Cross Section Data for Nuclear Geochemical Well Logging, Internat.Conf.on Nuclear Data for Basic and Applied Sciences, Santa Fe, New Mexico, USA, May 1985
- LANDIS 1982 D.A., CORK C.P., MADDEN N.W., GOULDING F.S., IEEE Trans.Nucl. Sci, NS-29, No 1, 619
- NIKOLSKI 1971 W., Radiothermolumineszenz Ideen des exakten Wissens, 555 DVA-Stuttgart
- PEPELNIK 1986 R., Capability of the 14 MeV Neutron Activation Analysis of  $3 \times 10^{10}$  n/cm<sup>2</sup>s with Respect to Sensitivities and Interferences of all useful Reactions, 7th Internat.Conf. MTAA, Copenhagen, p.367
- POPP 1981 R., A Fast Event Processor for Counting Loss Corrected Gamma Spectrometry, J.Radioanalyt.Chem. 61, 361
- SAAD EL DIN 1987 M., GRASS F., Short Time Activation of Phosphorites from Egypt, in preparation
- SCHMIDT 1983 J.O., A FORTRAN-IV-Plus Program Package for Rapid Instrumental Neutron Activation Analysis (RINAA), AIAU 83510, Atom-institut Report, July 1983
- STOSCH 1986 H.G., HERPERS U., KÖTZ J., Neutron AA of the Rare Earth Elements in Rocks from the Earth'Upper Mantle and Deep Crust, 7th Internat.Conf. MTAA, Copenhagen, p.455

- WESTPHAL 1977 G.P., Loss-Free Counting - a Concept for Real-Time Compensation of Dead-Time and Pile-Up Losses in Nuclear Pulse Spectroscopy, Nucl.Instr.Methods 176, 605
- WESTPHAL 1979 G.P., On the Performance of Loss-Free Counting - a Method for Real-Time Compensation of Dead-Time and Pile-Up Losses in Nuclear Pulse Spectroscopy, Nucl.Instr.Methods 163, 189
- WESTPHAL 1981 G.P., High Rate Gamma-Spectrometry and Related Problems, J.Radioanalyt.Chem. 61, 111
- WESTPHAL 1982 G.P., Real-Time Correction of Counting Losses in Nuclear Pulse Spectroscopy, J.Radioanalyt.Chem. 70, 387, Austrian Patent 368291, US-Patent 4476384
- WESTPHAL 1984 G.P., KASA T., A Multichannel Analyzer with Real Time Correction of Counting Losses Based on a Fast 16/32 Bit Microprocessor, Proc. 5th Internat.Conf. on Nucl. Methods in Environmental & Energy Res. April 1984, Mayaguez Conf-840408

V. PIKSAIKIN, V. GOULO, O. SCHWERER  
(IAEA, Nuclear Data Section)

ABSTRACT. An approach for the production of a catalogue of microscopic nuclear data for specific use in nuclear geology and generation of an associated computerized data base is proposed. Availability of experimental and evaluated data and their comparison for Al and Si is demonstrated.

-----

Current spectroscopic systems that can be used in a borehole have the potential for providing a true multi-element analysis, yielding element concentrations which can be used to describe geochemical compositions of rocks.

While prior emphasis had been on gross lithological descriptions on the location of ore-quantity concentrations, current needs reflect the importance of many elements in smaller concentrations. This requires the separation of the effects from competing reactions populating the same nuclear state as well as spectral interferences that are not significant at higher elemental concentrations. These constraints place much greater weight on the neutron-induced cross section data and on the uncertainties with which they are determined.

Currently, the cross section data and their uncertainties are generally insufficient for geochemical applications (excluding maybe the thermal radiative capture cross sections).

Table 1 shows availability of some neutron-induced reaction cross sections and their uncertainties in the evaluated nuclear data libraries for isotopes of geochemical interest. Examination of the evaluated and experimental data shows that the accuracy is at 30-50%. This value often limits the accuracy of original elemental concentrations analyses in case

of 14 MeV neutron sources. Detection of Na, Mg, Al and Si in wells with 14 MeV neutron-induced reactions carried out by R.C. Herzog, P.D. Soran and J.S. Schweitzer showed that a  $\pm 20\%$  error in certain (n,p) and (n, $\alpha$ ) reactions cross sections can result in  $\pm 4000\%$  and  $\pm 120\%$  error in determining the concentrations of Mg and Na respectively. Because of the production of Mg activity from both Al and Si,  $\pm 20\%$  uncertainties for the Si(n,p) cross section can result in a  $\pm 150\%$  uncertainty in the concentration of Al. If the cross section uncertainties could be reduced to a few percent, the uncertainties on the elemental concentrations would become reasonable for geochemical applications. Only when these fundamental nuclear data are improved, can the true potential for subsurface geochemical analysis be realized.

Currently, the Nuclear Data Section has started activities which are focussed on the assessment of availability and status of microscopic nuclear cross sections needed for an effective implementation of those nuclear geophysics methods which are based mainly on neutron induced gamma-ray (prompt and delayed) spectrometry and applied to the exploration, exploitation and processing of mineral resources.

As an example, Table II represents the availability of experimental data related to microscopic nuclear cross sections for the production of particular prompt gamma-rays from (n, $\gamma$ ) reactions in the neutron energy range from threshold to 20 MeV for Al and Mg.

In addition, experimental information on gamma-ray production cross sections for Al available in the EXFOR file of experimental nuclear data was compared with the evaluated nuclear data from ENDF/B-4 (see Figures in the Appendix). Total cross sections for the emission of specific gamma-rays were obtained by multiplying the differential cross sections at  $125^\circ$  by  $4\pi$ .

The above examples illustrate the approach which will be used in the identification of gaps and discrepancies in existing experimental data files and major evaluated data libraries aiming at the production of a catalogue of microscopic nuclear data for specific use in nuclear geology and generation of an associated computerized data base.

Table Availability of dosimetry and uncertainty data.

Isotope	$\sigma(n,p)$	$\sigma(n,\alpha)$	$\sigma(n,\gamma)$	$\sigma(n,n')$	Covariance data
Ca-40	3	3	3	3	N
Ca-42	3	3	3	3	N
Ca-44	3	3	3	N	N
Ca-NAT	4,5	4,5	4,5	4,6	4,6
Fe-54	1,2,3	2,3	2,3	3	N
Fe-56	1,3	1	3	3	N
Fe-57	3	3	3	3	N
Fe-58	3	3	1,2	3	N
Fe-NAT	4,5	4,5	4,5	4,5	4,6
Mg-24	3	3	2,3	3	N
Mg-25	3	3	3	N	N
Mg-26	3	3	3	N	N
Mg-NAT	4,5	4,5	4,5	4,5	4
Al-27	4,5	4,5	4,5	4,5	4
Na-23	4,5	4,5	4,5	4,5	4
Si-28	3	3	3	3	N
Si-29	3,6	3	3	3	N
Si-30	3,6	3	3	3	N
Si-NAT	4,5	4,5	4,5	4,5	4,6
C-12	3	3	3	3	N
C-13	3	3	3	3	N
C-NAT	4,5	4,5	4,5	4,5	4
S-32	1,2,3	3	3	3	N
S-33	3	3	3	3	N
S-34	3	3	3	3	N
S-36	3	3	3	3	N
S-NAT	4,5	4,5	4,5	4,5	4
La-138	N	N	N	N	N
La-139*	N	N	2	N	N
V-50*	3	3	3	3	N
V-51	3	3	3	3	N
Ti-46	2	3	1	3	N
Ti-47	1,2	3	3	3	N
Ti-48	1,2	2	3	3	N
Ti-49	3	3	3	3	N
Ti-50	3	3	3	3	N
Ti-NAT	4,5	4,5	4,5	4,5	4

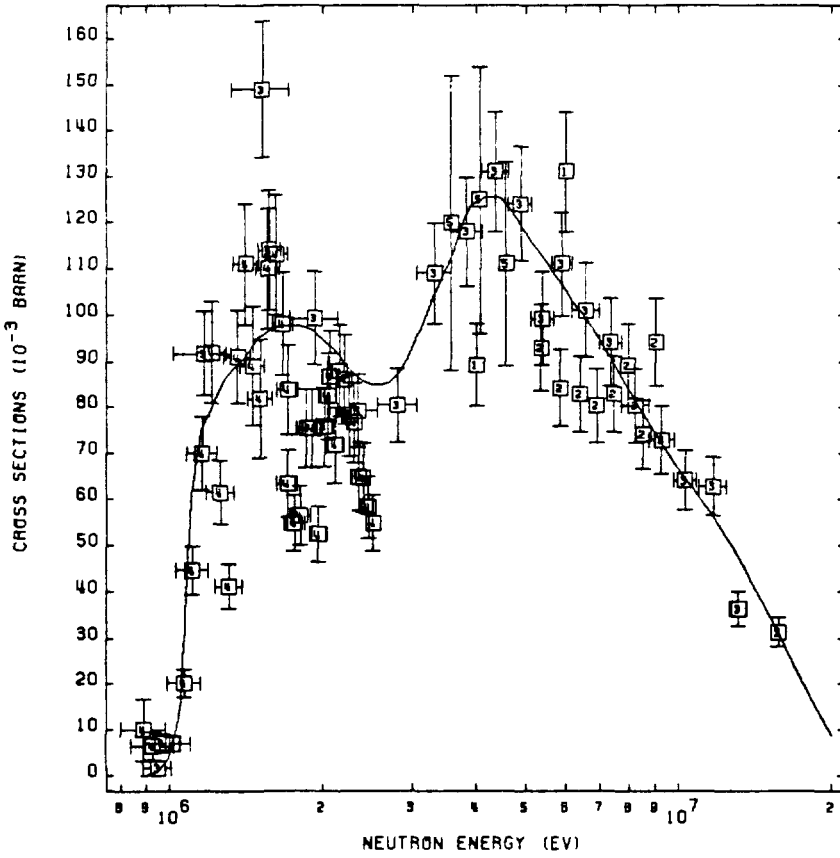
\* Radioactive

NOTES

- 1) ENDP/B Tape 531.
- 2) ENDF/B Tape 532.
- 3) ACTL.

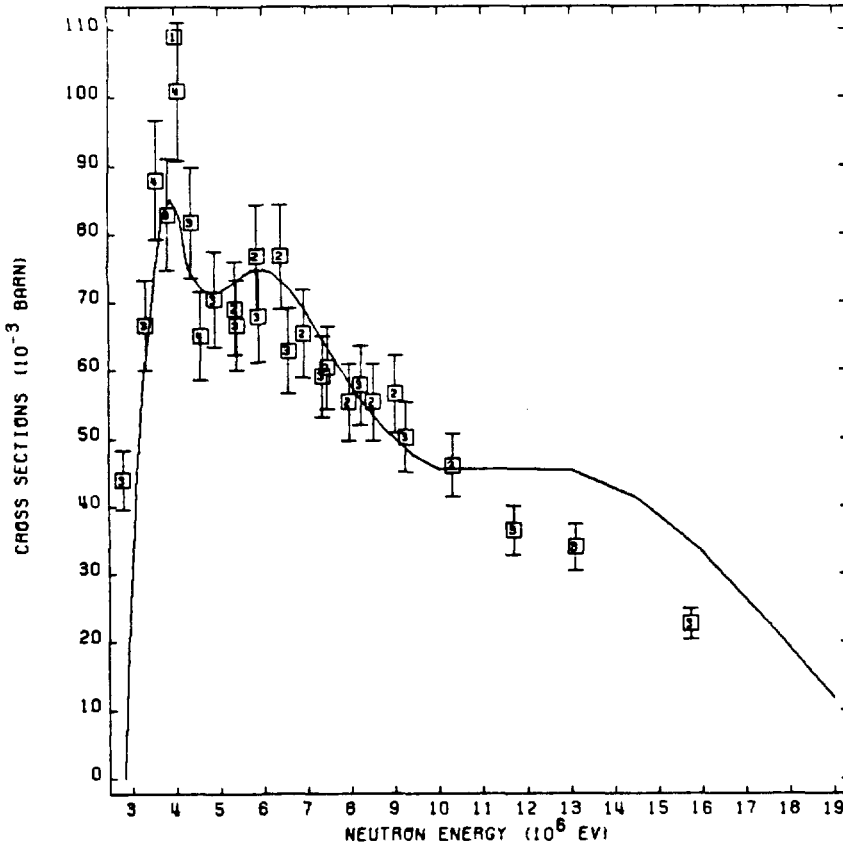
- 4) ENDF/B-V Transport.
- 5) ENDL-85 Transport.
- 6) Evaluators have as private files.

GAMMA PRODUCTION AL-27  
 CROSS SECTIONS (GAMMA-RAY ENERGY 0.843KEV)



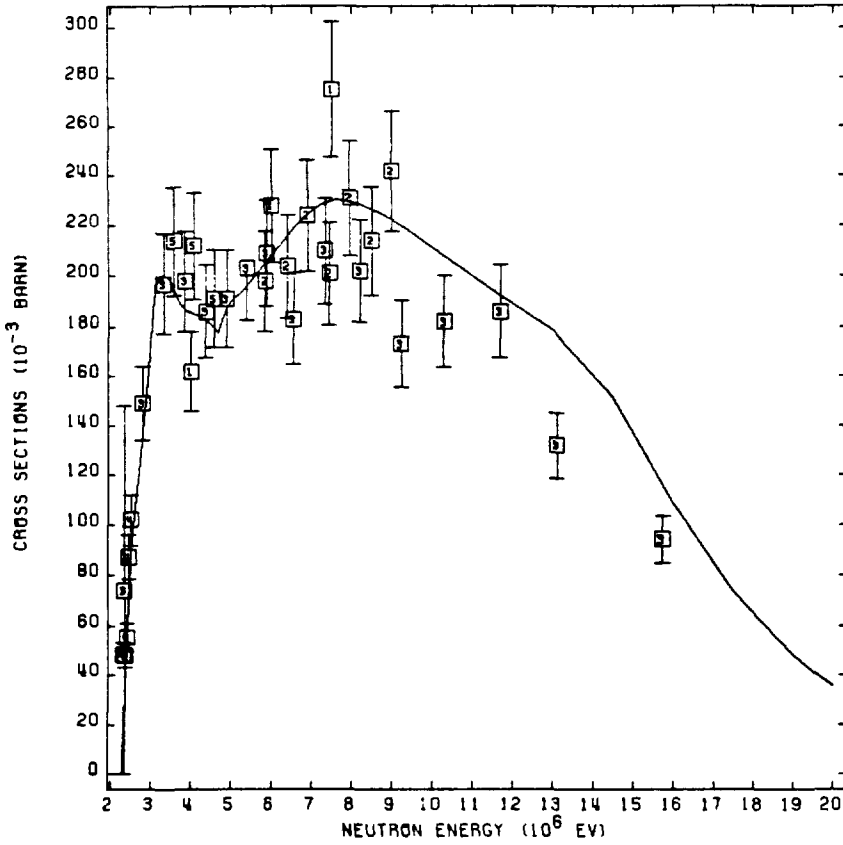
CURVES	
—	ENDF/B-4
POINTS	
1	D.M. DRAKE (70) ANGLE 55
2	J.K. DICKENS (72) ANGLE 55
3	C.G. HOOT (71) ANGLE 125
4	D.L. SMITH (79)
5	S.C. MATHUR (65)

GAMMA PRODUCTION AL-27  
 CROSS SECTIONS (GAMMA-RAY ENERGY 1.719KEV)



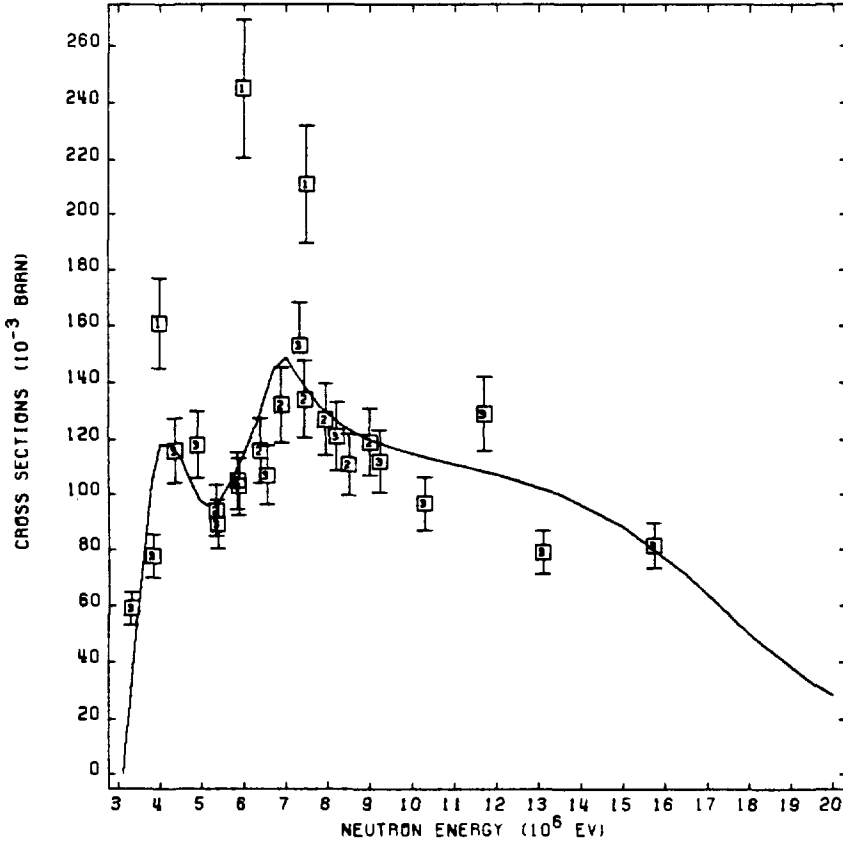
CURVES	
—	ENDF/B-4
POINTS	
1	DRAKE-70 EX4 10025 55°
2	DICKENS-72 EX4 10201 55°
3	HOOT-71 EX4 10219
4	MATHUR-65 EX4 11466

GAMMA PRODUCTION AL-27  
 CROSS SECTIONS (GAMMA-RAY ENERGY 2.210KEV)



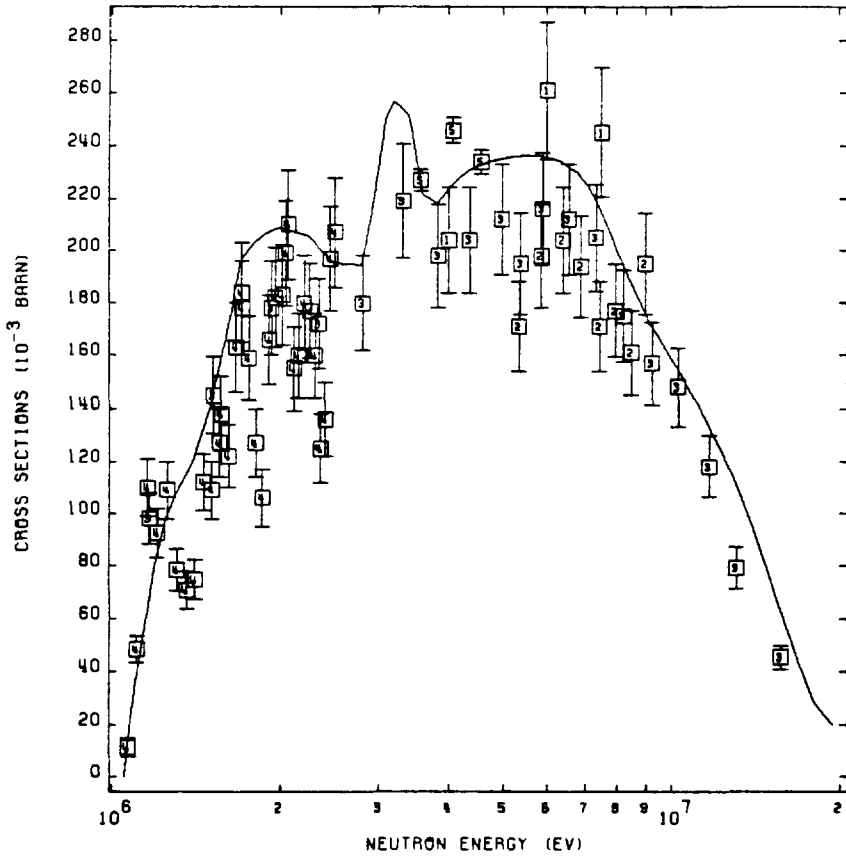
CURVES	
—	ENDF/B-4
POINTS	
1	DRAKE-70 EX4 10025 55
2	DICKENS-72 EX4 10201 55
3	HOOT-1971 EXFOR 10219
4	SMITH-79 EX4 10777
5	MATHUR-65 EX4 11466

GAMMA PRODUCTION AL-27  
 CROSS SECTIONS (GAMMA-RAY ENERGY 3.001KEV)



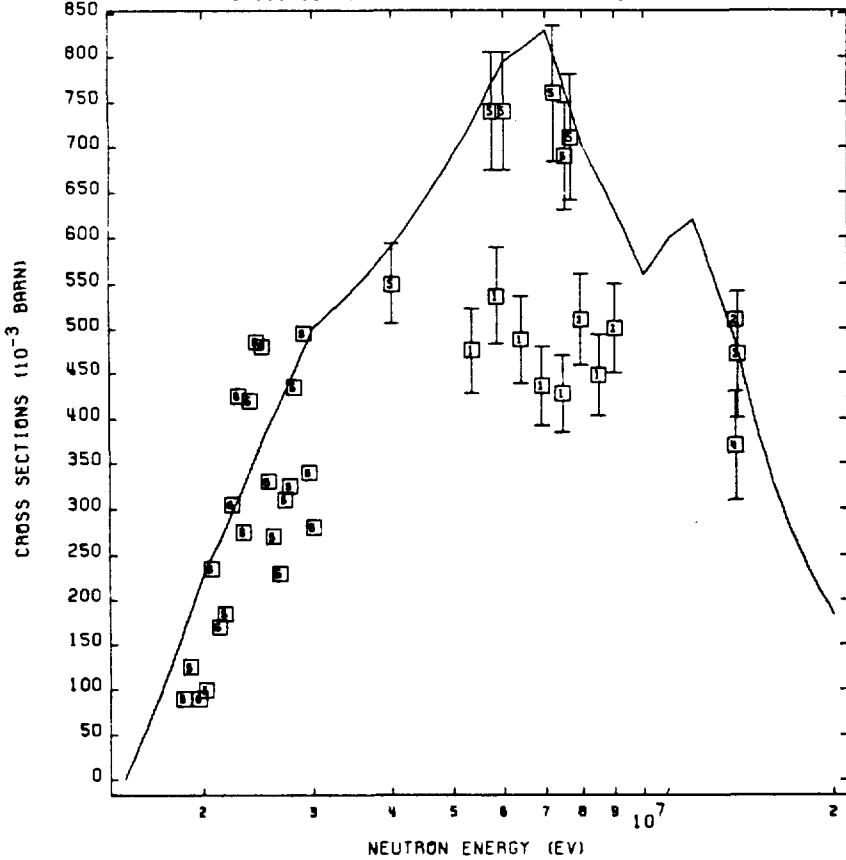
CURVES	
—	ENDF/B-4
POINTS	
1	DRAKE-70 EX4 10025 55'
2	DICKENS-72 EX4 10201 55'
3	HOOT-71 EX4 10219 ANG 125

GAMMA PRODUCTION AL-27  
 CROSS SECTIONS (GAMMA-RAY ENERGY 1.013KEV)



CURVES	
—	ENDF/B-4
POINTS	
1	DRAKE-70 EX4 10025 55°
2	DICKENS-72 EX4 10201 55°
3	HOOT-71 EX4 10219 125°
4	SMITH-79 EX4 10777 55°
5	MATHUR-65 EX4 11466

GAMMA PRODUCTION 14-SI  
 CROSS SECTIONS (GAMMA-RAY ENERGY 1.779KEV)



CURVES	
—	HEERMSOORF 1981
POINTS	
1	DICKENS 70 EX4 10094.002
2	BENVENISTE 63 EX4 11537.5
3	MARTIN 65 EX4 21191.007
4	BENECKIJ 65 EX4 40802.003
5	DRAKE 70 EX4 10025.007
6	LIND 61 EX4 11188.004



Dr. Soran, P.D.

Schlumberger Well Services  
Houston, Texas 77210-4594  
U.S.A.

Dr. Underwood, M.C.

British Petroleum Research Centre  
Sunbury-on-Thames  
Middlesex  
U.K.